Discontinuous Galerkin approximation of flows in fractured porous media on polygonal and polyhedral grids

Doctoral Dissertation of

Chiara Facciolà

Politecnico di Milano
Department of Mathematics

Advisor:
Prof.ssa Paola Francesca Antonietti

Co-advisor:
Prof. Marco Verani

Chair of the Doctoral Programme:
Prof.ssa Irene Sabadini

Doctoral programme in
MATHEMATICAL MODELS AND
METHODS IN ENGINEERING

2019 - Cycle XXXII

Contents

Acknowledgements

I would like to express my deepest gratitude to my PhD advisors Prof. Paola Antonietti and Prof. Marco Verani for their guidance throughout this journey. I am particularly grateful for their constant support and confidence in me, which have encouraged me to overstep every difficulty and were fundamental for my growth as a person and as a researcher. I would also like to thank Prof. Fabio Nobile for hosting me as a visiting PhD student at Ećole Polytechnique Fédérale de Lausanne (EPFL), giving me the possibility to experience research in such an inspiring environment.
I acknowledge the financial support given by MIUR via my PhD scholarship and via the SIR Starting grant n. RBSI14VT0S "PolyPDEs: Non-conforming polyhedral finite element methods for the approximation of partial differential equations". I also acknowledge the financial support given by INdAM-GNCS.

Abstract

In this thesis, we present a numerical approximation of Darcy's flow through a fractured porous medium which employs discontinuous Galerkin methods on polytopic grids. Our method is very flexible from the geometrical point of view, being able to handle meshes made of arbitrarily shaped elements, with edges/faces that may be in arbitrary number (potentially unlimited) and whose measure may be arbitrarily small. Our approach is then very well suited to tame the geometrical complexity featured by most of applications in the computational geoscience field. We adopt a model for single-phase flows that treats fractures as a $(d-1)$-dimensional interfaces between two d-dimensional subdomains, $d = 2, 3$. In the model, the flow in the porous medium (bulk) is assumed to be governed by Darcy's law and a suitable reduced version of the law is formulated on the surface modelling the fracture. The two problems are then coupled through physically consistent conditions. For simplicity, in the first part of the thesis, we consider the case where the porous medium is cut by a single, non-immersed fracture. We take into account all the possible combinations of primal/primal, mixed/primal, primal/mixed and mixed/mixed formulations for the Darcy's law describing the flow in the bulk and fracture problems, respectively. In particular, the primal discretizations are obtained using the Symmetric Interior Penalty DG method, and the mixed discretizations using the Local DG method, both in their generalization to polytopic grids. We perform a unified analysis, based on the flux formulation, of all the derived combinations of DG discretizations, where the coupling conditions between bulk and fracture are imposed through a suitable definition of the numerical fluxes on the fracture faces. We prove well-posedness and derive a priori hp-error estimates in a suitable (mesh-dependent) energy norm. Next, we extend the primal-primal formulation to the case of networks of intersecting fractures, supplementing the model with conditions prescribing pressure continuity and flux conservation along the intersections. Both the bulk and fracture discretizations are obtained employing the SIPDG method

extended to the polytopic setting, the key point to obtain a DG discretization being the generalization of the concepts of jump and average at the intersection. We prove the well-posedness of the discrete formulation and perform an error analysis obtaining a priori *hp*-error estimates. All our theoretical results are validated performing numerical tests with known analytical solution. Moreover, we consider more realistic configurations involving totally immersed networks of fractures. Finally, we briefly explore the case where the position of the fractures is uncertain and may be described by a stochastic parameter. We present some preliminary numerical results that employ a stochastic collocation approach.

Sommario

In questa tesi presentiamo un'approssimazione numerica per il flusso di Darcy attraverso un mezzo poroso fratturato, che utilizza i metodi discontinuous Galerkin su griglie poligonali. Il nostro metodo è molto flessibile dal punto di vista geometrico, essendo in grado di gestire griglie composte da elementi di forma arbitraria, con un numero qualsiasi (potenzialmente illimitato) di lati/facce, la cui misura può essere arbitrariamente piccola. Il nostro approccio risulta quindi molto efficace nel gestire la complessità geometrica che caratterizza la maggior parte delle applicazioni nell'ambito delle geoscienze. Il modello per flussi monofase adottato considera le fratture come interfacce $(d-1)$-dimensionali tra due sottodomini d-dimensionali, $d = 2, 3$. Il modello assume che il flusso nel mezzo poroso (bulk) sia governato dalla legge di Darcy e che una opportuna versione ridotta della legge sia formulata sulla superficie che descrive la frattura. I due problemi sono poi accoppiati tramite condizioni fisicamente consistenti. Per semplicità, nella prima parte della tesi, consideriamo il caso in cui il mezzo poroso è tagliato da una singola frattura non immersa. Prendiamo in considerazione tutte le possibili combinazioni di formulazioni per il problema di Darcy che descrive il flusso nel mezzo poroso e lungo la frattura, cioè primale/primale, mista/primale, primale/mista e mista/mista. In particolare, le discretizzazioni primali sono ottenute con il metodo DG Symmetric Interior Penalty e le discretizzazioni miste con il metodo Local DG, entrambi nella loro generalizzazione a griglie poligonali/poliedriche. Svolgiamo un'analisi unificata di tutte le combinazioni di discretizzazioni DG derivate, nella quale le condizioni di accoppiamento tra bulk e frattura sono imposte tramite una opportuna definizione dei flussi numerici sulle facce di frattura. Proviamo la loro buona posizione e deriviamo stime *hp* dell'errore a priori in una norma dell'energia opportuna (dipendente dalla mesh). Successivamente, estendiamo la formulazione primale-primale al caso di network di fratture che si intersecano tra loro. A tal fine estendiamo il modello fisico aggiungendo delle condizioni che impongono la continuità

della pressione e la conservazione del flusso lungo le intersezioni. Sia la discretizzazione del problema nel bulk, che quella del problema lungo le fratture sono ottenute utilizzando il metodo SIPDG esteso al setting poligonale. Il punto fondamentale per ottenere una discretizzazione DG del problema risiede nella opportuna generalizzazione dei concetti di salto e media alle intersezioni. Dimostriamo la buona posizione della formulazione discreta e svolgiamo un'analisi dell'errore ottenendo stime a priori *hp*. Tutti i nostri risultati teorici sono validati tramite test numerici con soluzione analitica nota. Inoltre consideriamo anche configurazioni più realistiche che coinvolgono network di fratture che presentano intersezioni e sono totalmente immersi nel dominio computazionale. Infine, esploriamo brevemente il caso in cui la posizione delle fratture è affetta da incertezza e può essere descritta tramite un parametro stocastico. In particolare presentiamo alcuni risultati numerici preliminari dove utilizziamo un approccio di tipo collocazione stocastica.

Introduction

Many Geophysical and Engineering applications, including, for example, fluid-structure interaction, crack and wave propagation problems, and flow in fractured porous media, are characterized by a strong complexity of the physical domain, possibly involving thousands of fault/fractures, heterogeneous media, moving geometries/interfaces and complex stratigraphies and topographies. Whenever classical Finite-Element-based approaches are employed to discretize the underlying differential model, the process of mesh generation can represent the bottleneck of the whole simulation, as classical finite elements only support computational grids composed by tetrahedral/hexahedral/prismatic elements. To overcome this limitation, in the last decade a wide strand of literature focused on the design of numerical methods that support computational meshes composed of general polygonal and polyhedral (polytopic, for short) elements. In the conforming setting, we mention for example the Composite Finite Element Method that was developed in [94, 93]; the Polygonal Finite Element Method [115] and the eXtended Finite Element Method (XFEM) [81, 116, 88], which achieve conformity by enriching/modifying the standard polynomial finite element spaces; the Mimetic Finite Difference (MFD) method [96, 56, 54, 55, 39] and its evolution, the Virtual Element Method (VEM), introduced in [38, 40, 7, 8] (see also [107, 102, 104, 103] for some recent applications), which overcome the difficulty in handling non-standard shape functions and the resulting increase in computational effort by only using the degrees of freedom of the added non-polynomial functions; and the Hybrid High-Order (HHO) method [79, 77, 78, 80], which is formulated in terms of discrete unknowns attached to mesh faces and cells employing local reconstruction operators and a local stabilization term. In the setting of non-conforming/discontinuos polygonal methods, we mention, for example, Composite Discontinuous Finite Element methods [16, 17], which exploit general meshes consisting of agglomerated elements; Hybridizable Discontinuous Galerkin methods [68, 69, 70, 71],

where additional unknowns are introduced on the boundary of each element so that the solution may be recovered solving many local problems; non-conforming VEM [22, 28, 62], which, unlike the conforming case, provides in one-shot a nonconforming approximation of any degree for any spatial dimension and any element shape; Gradient Schemes [83] and the polytopic Discontinuous Galerkin (polyDG) method[5, 34, 35, 33, 61, 59, 58, 19, 6, 60], which will be introduced below.

Within this framework, this thesis focuses on the problem of modelling the flow in a fractured porous medium. This problem has received increasing attention in the past decades, being fundamental in many energy or environmental Engineering applications, such as water resources management, oil migration tracing, isolation of radioactive waste and groundwater contamination, for example. In all these applications, the porous medium often features regions, typically called *fractures*, that are characterized both by a different porous structure and by a very small width compared to their length and to the size of the domain. The first feature implies that fractures have a very strong impact on the flow, since they can possibly act as barriers for the fluid (when they are filled with low permeable material), or as preferential paths (when their permeability is higher than that of the surrounding medium). The second feature entails the need for a very large number of elements for the discretization of the fracture layer and, consequently, a high computational cost. For this reason, the task of effectively modelling the interaction between the system of fractures and the porous matrix is particularly challenging. One popular modelling choice consists in a reduction strategy, so that fractures are treated as $(d-1)$-dimensional interfaces between d-dimensional porous matrices, $d = 2, 3$. The development of this kind of reduced models, which can be justified in case of fractures with very small width, has been addressed for single-phase flows in several works, see e.g. [2, 1, 101, 89]. In the first part of the thesis we will refer mainly to the model described in [101], see also [74, 15], which considers the simplified case of a single, non-immersed fracture. Here, the flow in the porous medium (bulk) is assumed to be governed by Darcy's law and a suitable reduced version of the law is formulated also on the surface modelling the fracture. Physically consistent coupling conditions are then added to account for the exchange of fluid between the fracture and the porous medium. We remark that this model is able to handle both fractures with low and large permeability. The first version of this model has been introduced in [2, 1] under the assumption of large

permeability in the fracture. In [101] it has been generalised to handle also fractures with low permeability. Moreover, its extension to the case of two-phase flows has been addressed in [91, 97], while the case where the porous medium is cut by a totally immersed fracture has been considered in [3]. Finally, the model may be generalized in order to handle network of intersecting fractures. In this case, some physical conditions need to be added to describe the behaviour of the flow at the intersection points/lines. A possible choice is to impose pressure continuity and balance of fluxes as in [87, 51]. Other, more general conditions, where the angle between fractures is taken into account and jumps of pressure across the intersection are allowed, can be found, for example, in [86, 112].

Even if the use of this kind of dimensionally reduced models avoids the need for extremely refined grids inside the fracture domains, in realistic cases, the construction of a computational grid aligned with the fractures is still a major issue. For example, a fractured oil reservoir can be cut by several thousands of fractures, which often intersect, create small angles or are nearly coincident [87]. Various numerical methods have been employed in the literature for the approximation of this coupled bulk-fracture model. Roughly speaking, they can be classified depending on the interaction between the bulk and the fracture meshes: the computational grid can be either aligned or not-aligned with the fracture network. In more traditional approaches the bulk meshes are usually chosen to be aligned with the fractures and to be made of simplicial elements. Some examples can be found in [2, 89, 101], where mixed finite element schemes have been employed for the discretization. However, in realistic cases, the geometrical conformity of the bulk mesh to the fracture can either lead to low-quality elements or to very fine grids, and the process of grid generation might become unaffordable from the computational view point, especially in three-dimensions. An alternative strategy consists in the use of not-aligned discretizations, where the fractures are allowed to arbitrarily cut the bulk grid. This allows for the choice of a fairly regular mesh in the bulk. We refer in particular to [74, 91, 85], where an approximation employing XFEM has been proposed and to the recent work [57], where the use of the cut Finite Element Method has been explored. We also mention the promising framework, based on an optimization procedure, to treat flows in systems of fracture networks introduced in [46, 47, 48, 49].

A good compromise with respect to the above issues is represented by methods based on computational meshes consisting of general polytopic elements (polygons in two dimensions and polyhedra in three dimensions). First a (possibly structured) bulk grid is

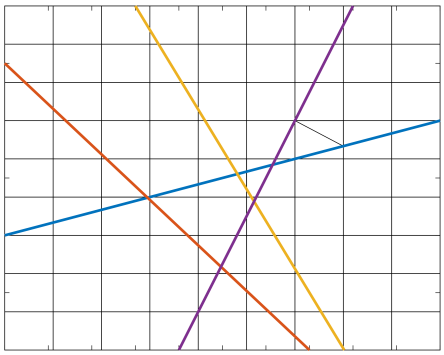

Figure 1: A two-dimensional example of fracture network cutting a Cartesian grid

generated independently of the fracture networks, secondly the elements are cut according to the fracture geometry see Figure 1 for a representative example in $2D$. The above approach leads to a grid that

(i) is aligned with the fracture network;

(ii) contains possibly arbitrarily shaped elements in the surrounding of fractures;

(iii) is regular far from fractures.

Beyond the simplicity of generating the computational grid based on employing the previously described approach, one of the main advantages of polytopal decompositions over standard simplicial grids is that, even on relatively simple geometries, the average number of elements needed to discretize complicated domains is lower [16, 17], without enforcing any domain approximation. This advantage becomes even more evident whenever the domain presents complex geometrical features (large number of fractures, fractures intersecting with small angles, etc.) and the bulk grid is chosen to be matching with the interfaces. In line with the previous discussion, various numerical methods supporting polytopic elements have been employed in the literature for the approximation of the coupled bulk-fracture problem. For example, a mixed approximation based on the use of MFD method has been explored in [15] and generalized to networks of fractures in [87]; in [44, 45, 43] a framework for treating flows in Discrete Fracture Networks based on VEM has been introduced, and in [65] the HHO method has been employed.

In this thesis we aim at employing Discontinuous Galerkin (DG) finite elements on polytopic grids to discretize the coupled bulk-fracture problem stemming from the

modelling of flows in fractured porous media. The inherited flexibility of DG methods in handling arbitrarily shaped, non-necessarily matching, grids and elementwise variable polynomial orders represents, in fact, the ideal setting to handle such kind of problems that typically feature a high-level of geometrical complexity. Discontinuous Galerkin methods were first introduced by Reed and Hill in the early 1970s for the discretization of hyperbolic problems [110]. Right afterward they were successfully proposed for dealing with the approximation of elliptic and parabolic problems. We refer in particular to the early works by Baker [32], Douglas [82], Wheeler [119] and Arnold [26], which contributed to the development of the interior penalty method. DG methods were then employed for the approximation of problems arising from a wide range of applications: various examples can be found, for example, in [36, 64, 67, 52, 95, 111, 76]. Over the last 20 years, alongside the development of High Performance Computing technologies, tremendous progress has been made on the study of both the analytical and computational aspects of DG methods [60]. In particular, since they employ local polynomial spaces defined elementwise without any continuity constraint, DG methods feature a high-level of intrinsic parallelism. Moreover, the local nature of the test spaces allows elementwise variable polynomial orders (p-refinement), which, together with h-refinement, enables more accurate approximation of solutions that vary in character from one part of the domain to another (hp-adaptivity). Furthermore, the lack of continuity between neighbouring elements allows for the employment of extremely broad families of meshes, featuring hanging nodes or made of general polygons or polyhedra. The first effort to extend DG methods to polytopic meshes can be found in [5]. The key idea for dealing with arbitrarily shaped elements is to construct a basis in the physical frame without resorting to the use of local element mappings to a given reference element. The local polynomial discrete space can then be defined, for example, making use of a bounding box of each element, so that, spaces of polynomials of total degree p may be employed, irrespective of the shape of the element [61]. In particular, this implies that the dimension of the local polynomial space and thus the order of convergence of the method is independent of the element shape [60]. This strategy has been first proposed by Cangiani et al. in [61, 59], extending the techniques developed by Bassi et al. in [35] and by Antonietti, Giani and Houston in [16, 17]. In [35], Bassi et al. applyed DG methods to meshes consisting of general agglomerated elements, while in [16, 17], Antonietti, Giani and Houston proposed the so-called composite DG methods, which

are a DG discretization of elliptic problems posed on domains featuring a very large number of local geometrical components or microstructures. The interior penalty DG method proposed by Cangiani et al. in [61, 59] (see also [6] for a review) is characterized by a careful choice of the discontinuity penalization parameter, which allows for the use of meshes made of polytopic elements whose edges/faces may have arbitrarily small measure compared to their diameter. In this thesis we will employ a further generalization of this scheme, described in [58, 19, 60] (see also [23, 4] for an application to elastodynamics and elasto-acoustic problems and [10] for a review on geophysical applications), which allows elements to possess faces not only with degenerating measure, but also in unlimited number. Note that this is made possible by an assumption that may be seen as the generalization of the standard shape-regularity property to polytopic domains. Finally, we mention that the capability of DG methods of handling general polytopic meshes provides great advantages also in the context of multilevel linear solvers, such as Schwarz-based domain decomposition preconditioners and multigrid schemes. Indeed, the key issue of constructing a hierarchy of coarser meshes, starting from a given fine mesh, may be naturally solved by agglomerating fine elements into coarser polytopes. Regarding Schwarz-based domain decomposition preconditioners, we refer in particular to [18, 84, 100, 98] and to the recent work [21]. In the multigrid context, we mention [19, 25] in the case of nested polytopic grids, and [24] for the non-nested case.

Finally, we conclude remarking that the intrinsic geometric flexibility of DG methods illustrated above is not the only motivation to employ DG methods for addressing the problem of approximating the flow in a fractured porous medium. In fact, the choice of employing them arises quite spontaneously in view of the discontinuous nature of the solution at the matrix-fracture interface. Moreover, as previously described, the differential model that we adopt, which comes from [101], is based on Darcy's equations for the bulk and fracture flows, together with suitable conditions that couple the two problems at the interface. We will show that these coupling conditions can be naturally reformulated using jump and average operators, which are one of the basic tools for the construction of DG methods. This will enable us to efficiently handle the coupling of the two problems, which will be indeed naturally embedded in the variational formulation.

In the following we provide a brief description of the contents of each chapter of the thesis.

- In Chapter 1 we introduce the notation and all the basic tools needed for dealing with the development and the analysis of polytopic DG approximations. In particular, we summarize the main theoretical results concerning this class of methods, see [61, 59, 6, 58, 60], for example. Following [58, 60], we start from the generalization of the standard shape-regularity property to polytopic elements and we introduce suitable trace and inverse inequalities and polynomial approximation properties of the underlying discrete spaces. These results, together with a specific choice of the interior penalty parameter, represent the main tools for handling elements with an unlimited number of faces/edges, which may also have arbitrarily small measure compared to the diameter of the element. The content of this chapter form the basis for the theoretical analysis of the discretization schemes for the flow in fractured porous media presented in the rest of the thesis.

- In Chapter 2 we start addressing the problem of discretizing the flow in a fractured porous medium by considering the simplest case, where one single non-immersed fracture divides the porous medium in two halves. We consider the *primal* formulation of Darcy's law for modelling the flow both in the bulk and along the fracture, and we propose a discretization that combines a DG approximation for the problem in the bulk, with a *conforming* finite element approximation in the fracture. For the DG approximation in the bulk we employ the Symmetric Interior Penalty discontinuous Galerkin (SIPDG) method [119, 26], generalized to the polytopic setting that we have introduced in Chapter 1 taking as a reference [61, 59, 6, 58, 19, 60]. Regarding the problem in the fracture, the use of standard conforming finite elements is made here just for the sake of simplicity, so that we can put better focus on the polyDG-discretization of the problem in the bulk and on the coupling of the two problems. A polyDG-based discretization of the fracture problem will be considered in the next chapters. Here, we analyse the resulting method, prove its well-posedness and derive a priori *hp*-error estimates in a suitable (mesh-dependent) energy norm. Moreover, we present some numerical experiments in a two-dimensional setting, with the aim of validating the theoretical error estimates. Finally, we test the capability of the method of handling more complicated geometries, including networks of partially immersed fractures.

  The results of this chapter are original, and have been published in [12].

- In Chapter 3 we extend the results obtained in Chapter 2 (see also [12]), where the mathematical model (and the corresponding discretization based on PolyDG methods) was in a primal setting for both the bulk and fracture problems. Indeed, when dealing with the approximation of Darcy's flow there are two possible approaches: primal and mixed. The primal approach considers a single-field formulation with the pressure field of the fluid as only unknown. The mixed approach describes the flow not only through the pressure field, but also through an additional unknown representing Darcy's velocity, which is of primary interest in many Engineering applications. The primal setting has the advantage of featuring less degrees of freedom and leads to a symmetric positive definite system algebraic system of equations that can be efficiently solved based on employing multigrid techniques. In this case, Darcy's velocity is afterwards reconstructed taking the gradient of the computed pressure and multiplying it by the permeability tensor. However, this process usually entails a loss of accuracy and does not guarantee mass conservation [105, 53]. For this reason, the mixed setting is sometimes preferred. In this case Darcy's velocity is directly computed, so that a higher degree of accuracy is achieved, together with local and global mass conservation. However, the drawback of this approach is the complexity of the resulting scheme, which leads to a generalized saddle point algebraic system of equations.

  From the above discussion we may infer that, according to the desired approximation properties of the model, one may resort to either a primal or mixed approximation for the problem in the bulk, as well as to a primal or mixed approximation for the problem in the fracture. For this reason, the aim of Chapter 3 is to design and analyze, in the *unified* framework of [27] based on the *flux-formulation*, all the possible combinations of primal-primal, mixed-primal, primal-mixed and mixed-mixed formulations for the bulk and fracture problems, respectively. In particular, the primal discretizations are obtained using the Symmetric Interior Penalty discontinuous Galerkin method [119, 26], whereas the mixed discretizations are based on employing the local DG (LDG) method of [72], both in their generalization to polytopic grids [61, 59, 6, 58, 60]. Moreover, the coupling conditions between bulk and fracture are imposed through a suitable definition of the numerical fluxes on the fracture faces. Such an abstract setting allows to analyse theoretically at the same time all the possible formulations. We perform a unified analysis of

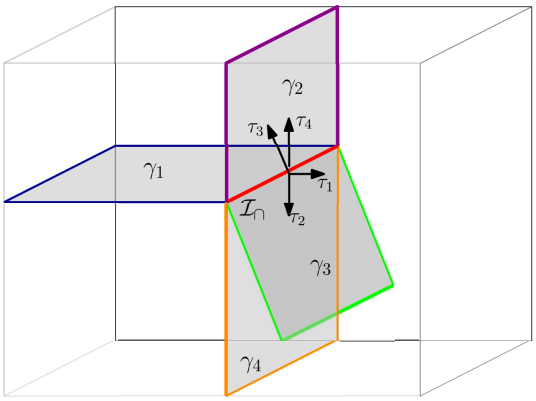

Figure 2: Example of network of intersecting fractures and corresponding normal vectors for $d = 3$.

all the derived combinations of DG discretizations for the bulk-fracture problem. We prove their well-posedness and derive a priori *hp*-version error estimates in a suitable (mesh-dependent) energy norm. Finally, we present numerical experiments assessing the validity of the theoretical error estimates and testing and comparing the practical performance of the proposed formulations.

All the results presented in this chapter are original and are contained in [14].

- In Chapter 4, we consider again the primal-primal setting and we focus on extending our formulation to the case of networks of *intersecting* fractures. To this aim, we supplement our mathematical model [101] with some suitable physical conditions at the intersections, prescribing the behaviour of the fluid. In particular, following [87, 51, 45], we impose pressure continuity across fractures and flux conservation, the latter condition implying that no exchange of fluid between bulk and fracture network takes place along the intersections. From the DG-discretization point of view, the key instrument for dealing with intersections is the generalization of the concepts of jump and average. If we assume that the fracture network may be approximated by the union of N_Γ fractures γ_k, each of which is a one co-dimensional planar manifold, i.e. $\Gamma = \bigcup_{k=1}^{N_\Gamma} \gamma_k$, the intersections correspond to lines when $d = 3$ and to points when $d = 2$. Let us focus for simplicity on the case $d = 3$, see Figure 2 for an example. Here, the intersection line is denoted by $\mathcal{I}_\cap$ and each fracture γ_k, $k = 1, 2, 3, 4$, is characterised by the outward normal vector $\boldsymbol{\tau}_k$ at the intersection, which belongs to the plane containing the fracture. In order to describe the pressure field in all the network, we employ the global variable $p_\Gamma = (p_\Gamma^1, \ldots, p_\Gamma^{N_\Gamma})$, defined in a suitable product space of all the local fracture spaces. Our aim is to introduce

some operators that are able to capture the behaviour of the function p_Γ across the intersection line, taking into account the contribution from all the fractures, similarly to how classic jump and average operators [27] describe the discontinuity of a piecewise-continuous function across elemental interfaces. The main difference with respect to the standard case is that the normal vectors, contained into the definition of the operators, are not aligned. This is related to the linear DG approximation of elliptic PDEs on surfaces presented in [75], then extended to high order in [9]. Here, the surface is approximated by a piecewise linear surface composed of planar triangles, so that a new definition of jump and average operators is needed, to take into account the fact that the outward normal vectors of two neighbouring triangles are not, in general, opposite. Our definition is a further generalization, since it considers the intersection of an arbitrary number of planar surfaces.

Using the newly defined jump and average operators we are able to define a DG approximation for the problem in the bulk combined with a DG approximation for the problem in the fracture network, where the conditions at the intersection are imposed "in the spirit of DG methods ". In particular, this means that continuity is enforced *penalizing the jump* of the pressure (after a suitable definition of the penalization coefficient at the intersection), while balance of fluxes is imposed *naturally*, similarly to how homogeneous Neumann boundary conditions are usually enforced. Both the bulk and fracture discretizations are obtained employing the SIPDG method extended to the polytopic setting. In this chapter we also prove the well-posedness of the method and derive a priori *hp*-version error estimates in a suitable (mesh-dependent) energy norm. Finally, we present some preliminary numerical experiments with known analytical solution assessing the validity of the theoretical error estimates and a more realistic configuration involving a totally immersed network of fractures.

All the results presented in this chapter are original and are contained in [13].

- In Chapter 5 we briefly explore the case where the position of the fractures is uncertain and may be described by stochastic parameters. The characterization of fluid dynamics in geological media is, indeed, a classical field for the application of Uncertainty Quantification (UQ) methodologies, due to the difficulty in obtaining precise measurements. In the context of fractured porous media, typical quantities

that may be affected by uncertainty are the actual position and geometry of the fractures, so that a description of these features is usually only available in the form of probabilistic distributions. We start from the observation that, due to the discontinuous nature of the solution at the bulk-fracture interface, the state variables (pressure or Darcy's velocity) may undergo discontinuities also in their dependence on the stochastic parameters describing the fracture position. Since the accuracy of standard UQ techniques (in particular, we will consider the stochastic collocation method of [29]) typically deteriorates in the presence of discontinuities with respect to the random variables, we take inspiration from the approach of [73] to propose a technique to avoid this drawback. In particular, we introduce a mapping to a reference domain, where all fractures are aligned, so that continuity with respect to the random variables may be recovered. We present some preliminary results showing that, applied to a simple test case, where the position of the fracture is determined by a single stochastic parameter, our technique is effective to recover the convergence properties of the stochastic collocation method of [29].

The preliminary results presented in this chapter are original and are contained in [11].

1 | hp-version Polytopic Discontinuous Galerkin methods

In this chapter we introduce the notation and all the theoretical tools needed for dealing with polytopic Discontinuous Galerkin approximations. In particular, we summarize the main theoretical results concerning this class of methods contained in [61, 59, 6, 58, 60], where an hp-version interior penalty DG method for the numerical solution of elliptic problems on polytopic meshes has been proposed and analysed. The use of grids made of general polytopic elements presents challenges on a number of points. Indeed, in contrast to the case when standard-shaped elements are employed, polytopes may admit an arbitrary number of faces/edges and the measure of the faces/edges may potentially be much smaller than the measure of the element itself. In [61, 59, 6] it is assumed that the number of edges/faces of each mesh element is uniformly bounded. In [58, 60] this assumption is no longer required (i.e., elements with an arbitrary number of possibly degenerating faces/edges are admitted). However, this comes at the cost of adding an assumption (see Assumption 1.1.1 below) that may be regarded as the natural generalization to polytopic grids of the classical shape-regularity assumption [60]. Here, we adopt the setting of [58, 60]. In particular, in Section 1.1, we introduce the notation related to the discretization of domains using polytopic elements and we state the regularity assumptions on the meshes. In Section 1.2 we define the DG discrete spaces and introduce standard jump and average operators. Finally, in Section 1.3, starting from the mesh assumption of Section 1.1, we state trace inverse inequalities and approximation results for general polytopic elements that are sensitive to the type of face degeneracy described above. We also remark that the capability of the method of handling faces with arbitrarily small measure is intimately related to the correct choice of the discontinuity-penalization function, which will be introduced in the next chapters.

We will employ the following notation. For an open, bounded domain $D \subset \mathbb{R}^d$, $d = 2, 3$, we denote by $H^s(D)$ the standard Sobolev space of order s, for a real number $s \geq 0$. For $s = 0$, we write $L^2(D)$ in place of $H^0(D)$. The usual norm on $H^s(D)$ is denoted by $||\cdot||_{H^s(D)}$ and the usual seminorm by $|\cdot|_{H^s(D)}$. We also introduce the standard space $H_{\mathrm{div}}(D) = \{\mathbf{v} : D \to \mathbb{R}^d : ||\mathbf{v}||_{L^2(D)} + ||\nabla \cdot \mathbf{v}||_{L^2(D)} < \infty\}$. Given a decomposition of the domain into elements $\mathcal{T}_h$, we will denote by $H^s(\mathcal{T}_h)$ the standard *broken* Sobolev space, equipped with the broken norm $||\cdot||_{s,\mathcal{T}_h}$. Furthermore, we will denote by $\mathbb{P}_k(D)$ the space of polynomials of *total* degree less than or equal to $k \geq 1$ on D. The symbol $\lesssim$ (and $\gtrsim$) will signify that the inequalities hold up to multiplicative constants that are independent of the discretization parameters, but might depend on the physical parameters. If both $\lesssim$ and $\gtrsim$ hold, we will write $\approx$.

1.1 Grid assumptions

First, following [61, 59, 6], we introduce the notation related to the discretization of the domains by means of polytopic meshes. We consider classes of meshes $\mathcal{T}_h$ made of disjoint open *polygonal/polyhedral* elements E. For each element $E \in \mathcal{T}_h$, we denote by $|E|$ its measure, by h_E its diameter and we set $h = \max_{E \in \mathcal{T}_h} h_E$. With the aim of handling hanging nodes, we introduce the concept of mesh *interface*, defined as the intersection of the $(d-1)$-dimensional facets of two neighbouring elements. We need now to distinguish between the case when $d = 3$ and $d = 2$:

- when $d = 3$, each interface consists of a general polygon, which we assume may be decomposed into a set of co-planar triangles. We assume that a sub-triangulation of each interface is provided and we denote the set of all these triangles by $\mathcal{F}_h$. We then use the terminology *face* to refer to one of the triangular elements in $\mathcal{F}_h$;

- when $d = 2$, each interface simply consists of a line segment, so that the concepts of face and interface are in this case coincident. We still denote by $\mathcal{F}_h$ the set of all faces.

Note that $\mathcal{F}_h$ is always defined as a set of $(d-1)$-dimensional simplices (triangles or line segments).

In order to introduce the DG formulation, it is useful to further subdivide the set $\mathcal{F}_h$ into

$$\mathcal{F}_h = \mathcal{F}_h^I \cup \mathcal{F}_h^B$$

where $\mathcal{F}_h^I$ is the set of interior faces and $\mathcal{F}_h^B$ is the set of faces lying on the boundary of the domain $\partial\Omega$. Moreover, if $\partial\Omega$ is split into the Dirichlet boundary $\partial\Omega_D$ and the Neumann boundary $\partial\Omega_N$, we will further decompose the set $\mathcal{F}_h^B = \mathcal{F}_h^D \cup \mathcal{F}_h^N$, where $\mathcal{F}_h^D$ and $\mathcal{F}_h^N$ are the boundary faces contained in $\partial\Omega_D$ and $\partial\Omega_N$, respectively. Implicit in this definition is the assumption that the mesh $\mathcal{T}_h$ is conforming to the partition of $\partial\Omega$. Finally, given an element $E \in \mathcal{T}_h$, for any face $F \subset \partial E$, with $F \in \mathcal{F}_h$, we define $\mathbf{n}_F$ as the unit normal vector on F that points outward of E.

Next, we outline the key assumptions that the polytopic mesh $\mathcal{T}_h$ needs to satisfy in order to derive suitable inverse inequalities and approximation results.

Definition 1.1.1. A mesh $\mathcal{T}_h$ is said to be *polytopic-regular* if, for any $E \in \mathcal{T}_h$, there exists a set of n_E non-overlapping (not necessarily shape-regular) d-dimensional simplices $\{S_E^i\}_{i=1}^{n_E}$ contained in E, such that $\bar{F} = \partial\bar{E} \cap \bar{S}_E^i$, for any face $F \subseteq \partial E$, and

$$h_E \lesssim \frac{d|S_E^i|}{|F|}, \qquad i = 1, \dots, n_E, \tag{1.1}$$

with the hidden constant independent of the discretization parameters, the number of faces of the element n_E, and the face measure.

We remark that the union of simplices S_E^i does *not* have to cover, in general, the whole element E, that is $\cup_{i=1}^{n_E} \bar{S}_E^i \subseteq \bar{E}$, see Figure 1.1 for an example. In the following, for simplicity and clarity we shall write S_E^F instead of S_E^i. We also underline that this definition does not give any restriction on the number of faces per element, nor on their measure. In particular, it allows the size of a face $|F|$ be arbitrarily small compared to the diameter of the element h_E, provided that the height of the corresponding simplex S_E^F is comparable to h_E. Figure 1.1 shows two examples of elements belonging to a polytopic-regular mesh, while Figure 1.2 shows an element which does not satisfy the definition. We refer to [60] for more details.

Assumption 1.1.1. *We assume that the mesh $\mathcal{T}_h$ is* polytopic-regular.

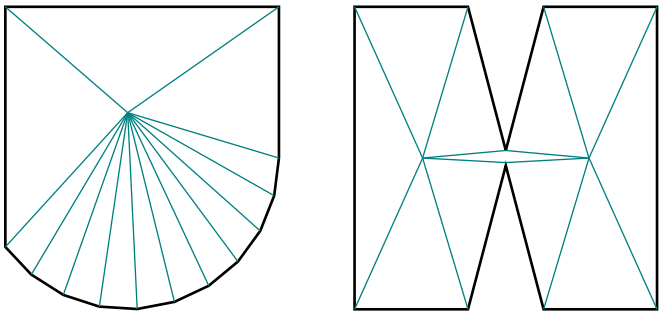

Figure 1.1: Two examples of polytopic-regular elements as in Definition 1.1.1. Here, all the triangles S_E^F (coloured in teal) have height of size comparable to the diameter h_E. Note also that the element on the right is not covered by the union of the simplices.

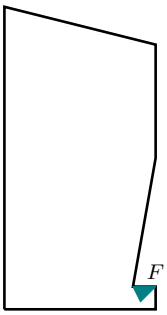

Figure 1.2: Example of an element that violates polytopic-regularity: the shape of the polygon does not allow for the definition of a triangle S_E^F with base F whose height is comparable to the diameter h_E.

This assumption will allow us to state the inverse trace estimate in Lemma 1.3.2 below.

The next definition and assumption are instrumental for the validity of the approximation results contained in Lemma 1.3.3 below.

Definition 1.1.2. [61, 59, 6, 58, 60] A *covering* $\mathcal{T}_\# = \{T_E\}$ related to the polytopic mesh $\mathcal{T}_h$ is a set of shape-regular d-dimensional simplices T_E, such that for each $E \in \mathcal{T}_h$, there exists a $T_E \in \mathcal{T}_\#$ such that $E \subset T_E$.

Assumption 1.1.2. *[61, 59, 6, 58, 60] There exists a covering $\mathcal{T}_\#$ of $\mathcal{T}_h$ (see Definition 1.1.2) and a positive constant O_Ω, independent of the mesh parameters, such that*

$$\max_{E\in\mathcal{T}_h} card\{E' \in \mathcal{T}_h : \ E' \cap T_E \neq \emptyset, T_E \in \mathcal{T}_\# \ \ s.t. \ E \subset T_E\} \leq O_\Omega,$$

and $h_{T_E} \lesssim h_E$ for each pair $E \in \mathcal{T}_h$ and $T_E \in \mathcal{T}_\#$, with $E \subset T_E$.

Note that the mesh-regularity is assumed for the covering $\mathcal{T}_\#$, and *not* for the mesh $\mathcal{T}_h$. Assumption 1.1.2 implies that when the computational mesh $\mathcal{T}_h$ is refined, the amount of overlap present in the covering $\mathcal{T}_\#$ remains bounded.

1.2 DG discrete spaces

Given a polytopic mesh $\mathcal{T}_h$, partition of the domain Ω, the corresponding scalar and vector-valued discontinuous finite element spaces are defined as

$$Q_h^{DG} = \{q_h \in L^2(\Omega) : \ q_h|_E \in \mathbb{P}_{k_E}(E) \ \forall E \in \mathcal{T}_h\}, \qquad k_E \geq 1 \, \forall E \in \mathcal{T}_h,$$
$$\mathbf{W}_h^{DG} = \{\mathbf{v} \in [L^2(\Omega)]^d : \ \mathbf{v}|_E \in [\mathbb{P}_{k_E}(E)]^d \ \forall E \in \mathcal{T}_h\}, \qquad k_E \geq 1 \, \forall E \in \mathcal{T}_h.$$

Remark 1. From the implementation point of view, an essential feature of polyDG methods is that the local elemental polynomial spaces can be defined in the physical space, without the need to introduce a mapping to a reference element, as typically done for classical FEMs. This allows DG methods to naturally deal with general polytopic elements and with polynomial degrees varying from one element to the other. A possible approach for the definition of the basis functions was first proposed in [61]. It is based on the definition of the polynomial spaces over suitably defined bounding boxes of each polytopic element. More precisely, given an element $E \in \mathcal{T}_h$, we can define (for example) its Cartesian bounding box B_E, such that the sides of B_E are aligned with the Cartesian axes and $\bar{E} \subseteq \bar{B}_E$. On the Cartesian bounding box B_E, we can then define a standard polynomial space, employing, for example, tensor-product Legendre polynomials. Finally, the polynomial basis over the general polytopic element may be defined by simply restricting the support of the basis functions to E. We refer to [60] for further details. We also mention that another key aspect related to the implementation of DG methods is the design of efficient numerical integration schemes over polytopic elements. This is still an open and active area of research and we refer in particular to the recent work [20].

In order to efficiently deal with discontinuous functions, we now introduce the concepts of average and jump across a face, which play a central role in the design and analysis of all DG methods [27]. Let $F \in \mathcal{F}_h^I$ be an interior face shared by the elements E_1 and E_2. We define $\mathbf{n}_1$ and $\mathbf{n}_2$ to be the unit normal vectors on F pointing exterior to E_1 and E_2, respectively. Then, for a (regular enough) scalar-valued function q and a (regular enough) vector-valued function $\mathbf{v}$, we define the standard *jump* $[\![\cdot]\!]$and *average* $\{\cdot\}$ operators across

F as

$$\begin{aligned} \{q\} &= \frac{1}{2}(q_1 + q_2) \qquad & [\![q]\!] &= q_1\mathbf{n}_1 + q_2\mathbf{n}_2, \\ \{\mathbf{v}\} &= \frac{1}{2}(\mathbf{v}_1 + \mathbf{v}_2) \qquad & [\![\mathbf{v}]\!] &= \mathbf{v}_1 \cdot \mathbf{n}_1 + \mathbf{v}_2 \cdot \mathbf{n}_2, \end{aligned} \tag{1.2}$$

where the subscript $i = 1, 2$ denotes the trace on F of the functions restricted to E_i. Note that the jump of a scalar-valued function is a vector parallel to the normal, while the jump of a vector-valued function is a scalar quantity. Note also that these definitions do not depend on assigning an ordering to the elements E_i.

For future use, we remark that on every $F \in \mathcal{F}_h^I$ we can use the definition of jump and average to write

$$[\![q\mathbf{v}]\!] = [\![\mathbf{v}]\!]\{q\} + \{\mathbf{v}\} \cdot [\![q]\!]. \tag{1.3}$$

Moreover, if, for a boundary face $F \in \mathcal{F}_h^B$, we extend the definitions of jump and average as

$$[\![q]\!] = q\mathbf{n}_F, \qquad \{\mathbf{v}\} = \mathbf{v}, \tag{1.4}$$

identity (1.3) implies the following well-known formula [26]:

$$\sum_{E \in \mathcal{T}_h} \int_{\partial E} q\mathbf{v} \cdot \mathbf{n}_E = \int_{\mathcal{F}_h^I \cup \mathcal{F}_h^B} \{\mathbf{v}\} \cdot [\![q]\!] + \int_{\mathcal{F}_h^I} [\![\mathbf{v}]\!]\{q\}, \tag{1.5}$$

where we have used the compact notation $\int_{\mathcal{F}_h} = \sum_{F \in \mathcal{F}_h} \int_F$.

1.3 Inverse estimates and polynomial approximation on polytopic meshes

Trace inverse estimates and *hp*-interpolation bounds are the tools at the base of stability and error analysis. In particular, Lemma 1.6 is required to establish the stability of the DGFEM approximation, while the approximation Lemma 1.3.3 is instrumental for the convergence analysis.

1.3.1 Trace inverse estimates

Trace inverse estimates bound the norm of a polynomial on an element's face/edge by the norm on the element itself. First, we recall a classical *hp*-version inverse estimate

valid for generic simplices [118].

Lemma 1.3.1. *Let $S \subset \mathbb{R}^d$ be a simplex, and let $q \in \mathbb{P}_k(S)$. Then, for each $F \subset \partial S$ we have*

$$||q||^2_{L^2(F)} \leq \frac{(k+1)(k+d)}{d} \frac{|F|}{|S|} ||q||^2_{L^2(S)}.$$

The inverse estimate for polytopic elements is then obtained under the polytopic-regular assumption 1.1.1 as in [58], Lemma 4.1, and [19, 60]. The proof is reported here for completeness.

Lemma 1.3.2. *Let E be a polygon/polyhedron satisfying Assumption 1.1.1 and let $q \in \mathbb{P}_{k_E}(E)$. Then, we have*

$$||q||^2_{L^2(\partial E)} \lesssim \frac{k_E^2}{h_E} ||q||^2_{L^2(E)}, \tag{1.6}$$

where the hidden constant depends on the dimension d, but it is independent of the discretization parameters and of the number of faces of the element.

Proof. The proof follows immediately if we apply Lemma 1.3.1 to each simplex $S_E^F \subset E$ and from Assumption 1.1.1, together with (1.1). More in detail, we have

$$\begin{aligned} ||q||^2_{L^2(\partial E)} &= \sum_{F \subset \partial E} ||q||^2_{L^2(F)} \lesssim k_E^2 \sum_{F \subset \partial E} \frac{|F|}{|S_E^F|} ||q||^2_{L^2(S_E^F)} \lesssim \frac{k_E^2}{h_E} ||q||^2_{L^2(\bigcup_{F \subset \partial E} S_E^F)} \\ &\leq \frac{k_E^2}{h_E} ||q||^2_{L^2(E)}. \end{aligned}$$

□

Note that the estimate bounds the L^2-norm of the polynomial on the whole boundary of E, not just on one of its edges/faces. This will be of fundamental importance in the analysis for dealing with elements with an arbitrary number of faces.

1.3.2 Approximation results

The tool at the base of the error analysis are *hp*-interpolation estimates. In [61, 59, 6] standard results on simplices are extended to polytopic elements, considering appropriate coverings and submeshes made of d-dimensional simplices (where standard results can be applied) and using appropriate extension operators. In [58] these results are

further extended in order to be successfully applied also in the case when the number of edges/faces is unbounded. Here, we summarize the results contained in [61, 59, 6, 58, 60]. We also mention that other *hp*-interpolation results that do not require the introduction of a covering for the polytopic mesh (valid in the $d = 2$ setting and for non-degenerate faces) were proposed in [41, 42].

Let $\mathscr{E} : H^s(\Omega) \to H^s(\mathbb{R}^d)$, $s \geq 0$, be the classical continuous extension operator introduced in [113], such that $\mathscr{E}(q)|_\Omega = v$ and $||\mathscr{E}q||_{H^s(\mathbb{R}^d)} \lesssim ||\mathscr{E}q||_{H^s(\Omega)}$. Based on the existence of a suitable covering of the polytopic mesh (see Definition 1.1.2)), we can state the following approximation result:

Lemma 1.3.3. [61, 59, 6, 58] *Let $E \in \mathcal{T}_h$ and $T_E \in \mathcal{T}_\#$ denote the corresponding simplex such that $E \subset T_E$ (see Definition 1.1.2). Suppose that $q \in H^{r_E}(E)$ is such that $\mathscr{E}q|_{T_E} \in H^{r_E}(T_E)$, for some $r_E \geq 0$. Then, if $\mathcal{T}_h$ satisfies Assumption 1.1.2, given an integer $k_E \geq 0$, there exists a polynomial $\widetilde{\Pi}_E^{k_E} q \in \mathbb{P}_{k_E}(E)$ such that the following bound holds*

$$||q - \widetilde{\Pi}_E^{k_E} q||_{H^m(E)} \lesssim \frac{h_E^{s_E - m}}{k_E^{r_E - m}} ||\mathscr{E}q||_{H^{r_E}(T_E)}, \qquad 0 \leq m \leq r_E. \tag{1.7}$$

Moreover, if $r_E \geq 1 + d/2$,

$$||q - \widetilde{\Pi}_E^{k_E} q||_{L^2(\partial E)} \lesssim \frac{h_E^{s_E - 1/2}}{k_E^{r_E - 1/2}} ||\mathscr{E}q||_{H^{r_E}(T_E)}. \tag{1.8}$$

Here, $s_E = \min(k_E + 1, r_E)$ and the hidden constants depend on the shape-regularity of T_E, but are independent of q, h_E, k_E and the number of faces per element.

Proof. See [61] for a detailed proof of (1.7) and [58] for the proof of (1.8). □

Note that the fact that estimate (1.8) holds on the whole boundary ∂E is fundamental for treating the case when the number of faces/edges is not uniformly bounded.

Remark 2. (Global approximant). If $q \in L^2(\Omega)$ and Lemma 1.3.3 holds for all $E \in \mathcal{T}_h$, then we can define a global approximation $\widetilde{\Pi} q \in Q_h^{DG}$, which satisfies bounds (1.7) and (1.8) on each $E \in \mathcal{T}_h$. Moreover, in case of uniform mesh-size and polynomial order, i.e. if $h_E \approx h$ and $k_E \approx k$ for all $E \in \mathcal{T}_h$, and $q \in H^r(\Omega)$, with $r \geq k + 1$, the following global bound holds:

$$||q - \widetilde{\Pi} q||_{H^m(\mathcal{T}_h)} \lesssim \frac{h^{k+1-m}}{k^{r-m}} ||q||_{H^r(\Omega)}, \qquad 0 \leq m \leq r.$$

2 | Pressure-Pressure formulation and its polyDG discretization

In this chapter, we present a numerical approximation of Darcy's flow through a porous medium that is cut by one single non-immersed fracture, represented by a $(d-1)$-dimensional interface between two d-dimensional subdomains, $d = 2, 3$. We consider the *primal* formulation of Darcy's law for modelling the flow both in the bulk and along the fracture with suitable (physically consistent) conditions coupling the two problems. We propose a discretization that combines a DG approximation for the problem in the bulk, with a *conforming* finite element approximation in the fracture. For the DG approximation in the bulk we employ the Symmetric Interior Penalty discontinuous Galerkin (SIPDG) method [119, 26], generalized to the polytopic setting that we have introduced in Chapter 1 taking as a reference [61, 59, 6, 58, 19, 60]. We remark that the use of standard conforming finite elements for approximating the flow in the fracture is made only in order to keep the analysis of the method as clear as possible, so that we can put better focus on the polyDG-discretization of the problem in the bulk and on the coupling of the two problems. The chapter is structured as follows. In Section 2.1 we introduce the governing equations for the coupled problem. The problem is then written in a weak form in Section 2.2, where we also prove its well-posedness. In Section 2.3 we introduce the DG discretization on polytopic grids of the coupled problem. The main results in the analysis of the method are included in Section 2.4, where we state (and prove) Theorem 2.4.3 about well-posedness and Theorem 2.4.5 containing an a priori error estimate in a suitable (mesh-dependent) norm. Section 2.5 is devoted to the presentation of a series of two-dimensional numerical experiments assessing both the validity of the theoretical error estimates and the capability of the method of handling more complicated cases, including networks of partially immersed fractures.

The results of this chapter are original, and have been published in [12].

2.1 Model problem

In the following we present the governing equations for our model, which is the model for single-phase flow in fractured porous media presented in [101]. The key idea of the model is to treat fractures as $(d-1)$-dimensional interfaces between d-dimensional porous matrices, $d = 2, 3$, justified in case of fractures with very small width. This model has been first introduced in [2, 1] under the assumption of large permeability in the fracture. In [101] it has been generalised to handle fractures with low permeability. The extension to the case of two-phase flows has been addressed in [91] and [97], while a totally immersed fracture has been considered in [3]. This model is valid both for fractures with low permeability (i.e., acting as barriers for the flow) and for very permeable fractures. For simplicity, we assume that there is only a single fracture in the porous medium and that the fracture cuts the domain exactly into two disjoint connected subregions (see Figure 2.1). More precisely, Let $\Omega \subset \mathbb{R}^d$, $d = 2, 3$, be an open, bounded, convex polygonal/polyhedral domain representing the porous matrix. We suppose that the fracture is a $(d-1)$-dimensional $\mathcal{C}^\infty$ manifold with no curvature $\Gamma \subset \mathbb{R}^{d-1}$, $d = 2, 3$, whose measure satisfies $|\Gamma| = \mathcal{O}(1)$, and assume that Γ separates Ω into two connected subdomains, which are disjoint, i.e., $\Omega \setminus \Gamma = \Omega_1 \cup \Omega_2$ with $\Omega_1 \cap \Omega_2 = \emptyset$. For $i = 1, 2$, we denote by $\partial\Omega_i$ the part of boundary of Ω_i shared with the boundary of Ω, i.e., $\partial\Omega_i = \partial\Omega_i \cap \partial\Omega$. Moreover, if we decompose the boundary of Ω into two disjoint subsets $\partial\Omega_D$ and $\partial\Omega_N$, *i.e.*, $\partial\Omega = \partial\Omega_D \cup \partial\Omega_N$, with $\partial\Omega_D \cap \partial\Omega_N = \emptyset$, we can define $\partial\Omega_{D,i} = \partial\Omega_D \cap \partial\Omega_i$ and $\partial\Omega_{N,i} = \partial\Omega_N \cap \partial\Omega_i$, for $i = 1, 2$. Finally, we denote by $\mathbf{n}_\Gamma$ the normal unit vector on Γ with a fixed orientation from Ω_1 to Ω_2, so that we have $\mathbf{n}_\Gamma = \mathbf{n}_1 = -\mathbf{n}_2$.

If we assume that the fractures are filled by a porous medium with different porosity and permeability than the surroundings, Darcy's law can be used both for modelling the flow in the porous matrix and for the $(d-1)$-dimensional flow problem along the fracture. The flow of an incompressible fluid through a fractured d-dimensional porous medium, $d = 2, 3$, can then be described by the following three ingredients:

1. the governing equations for the flow in the porous medium;

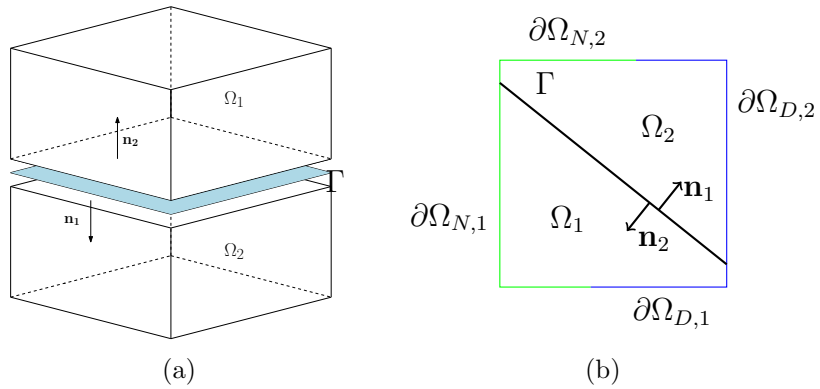

Figure 2.1: The subdomains Ω_1 and Ω_2 separated by the fracture Γ considered as an interface, for $d = 3$ (left) and $d = 2$ (right).

2. the governing equations for the flow in the fractures;

3. a set of physically consistent conditions which couple the problems in the bulk and fracture along their interface.

2.1.1 Governing equations

According to the above discussion, we suppose that the flow in the bulk is governed by Darcy's law. Let $\boldsymbol{\nu} = \boldsymbol{\nu}(x) \in \mathbb{R}^{d\times d}$ be the bulk permeability tensor, which satisfies the following regularity assumptions:

(i) $\boldsymbol{\nu}$ is a symmetric, positive definite tensor whose entries are bounded, piecewise continuous real-valued functions;

(ii) $\boldsymbol{\nu}$ is uniformly bounded from below and above, i.e.,

$$\mathbf{x}^T\mathbf{x} \lesssim \mathbf{x}^T\boldsymbol{\nu}\mathbf{x} \lesssim \mathbf{x}^T\mathbf{x}, \forall \mathbf{x} \in \mathbb{R}^d.$$

Given a function $f \in L^2(\Omega)$ representing a source term and $g \in H^{1/2}(\partial\Omega)$, the motion of an incompressible fluid in each domain Ω_i, $i = 1, 2$, with pressure p_i is described by:

$$-\nabla \cdot (\boldsymbol{\nu}_i \nabla p_i) = f_i \qquad \text{in } \Omega_i, \quad i = 1, 2, \tag{2.1a}$$

$$p_i = g_i \qquad \text{on } \partial\Omega_{D,i}, \quad i = 1, 2, \tag{2.1b}$$

$$\boldsymbol{\nu}_i \nabla p_i \cdot \mathbf{n} = 0 \qquad \text{on } \partial\Omega_{D,i}, \quad i = 1, 2. \tag{2.1c}$$

Here, we have denoted by $\boldsymbol{\nu}_i$ and f_i, the restrictions of $\boldsymbol{\nu}$ and f to Ω_i, $i = 1, 2$, respectively, and by g_i the restriction of g to $\Omega_{D,i}$, $i = 1, 2$ and $\mathbf{n}$ is the unit normal vector pointing outward of Ω. For simplicity, in the following we will impose Dirichlet boundary conditions on the whole $\partial\Omega$, i.e. we will take $\partial\Omega_N = \emptyset$.

The second ingredient for the model is represented by the governing equations for the fracture flow. In our model the fracture is treated as a $(d-1)$-dimensional manifold immersed in a d-dimensional object. If we assume that the fracture is filled by a porous medium with different porosity and permeability than the surroundings, Darcy's law can be used also for modelling the flow along the fracture [37]. The reduced model is then obtained through a process of averaging across the fracture: in the beginning the fracture is treated as a d-dimensional subdomain of Ω, that separates it into two disjoint subdomains. Then Darcy's equations are written on the fracture in the normal and tangential components and the tangential component is integrated along the thickness $\ell_\Gamma > 0$ of the fracture domain, which is typically some orders of magnitude smaller than the size of the domain. We refer to [101] for a rigorous derivation of the reduced mathematical model.
The fracture flow is then characterized by the fracture permeability tensor $\boldsymbol{\nu}_\Gamma$, which is assumed to satisfy the same regularity assumptions as those satisfied by the bulk permeability $\boldsymbol{\nu}$ and to have a block-diagonal structure of the form

$$\boldsymbol{\nu}_\Gamma = \begin{bmatrix} \nu_\Gamma^n & 0 \\ 0 & \boldsymbol{\nu}_\Gamma^\tau \end{bmatrix}, \tag{2.2}$$

when written in its normal and tangential components. Here, $\boldsymbol{\nu}_\Gamma^\tau \in \mathbb{R}^{(d-1)\times(d-1)}$ is a positive definite, uniformly bounded tensor (it reduces to a positive number for $d = 2$) representing the tangential component of the permeability of the fracture.

Setting $\partial\Gamma = \Gamma \cap \partial\Omega$, and denoting by p_Γ the fracture pressure, the governing equations for the fracture flow read

$$-\nabla_\tau \cdot (\boldsymbol{\nu}_\Gamma^\tau \ell_\Gamma \nabla_\tau p_\Gamma) = \ell_\Gamma f_\Gamma + [\![-\boldsymbol{\nu}\nabla p]\!] \qquad \text{in } \Gamma, \tag{2.3a}$$

$$p_\Gamma = g_\Gamma \qquad \text{on } \partial\Gamma, \tag{2.3b}$$

where $f_\Gamma \in L^2(\Gamma)$, $g_\Gamma \in H^{1/2}(\partial\Gamma)$ and ∇_τ and $\nabla_\tau\cdot$ denote the tangential gradient

and divergence operators, respectively. Equation (2.3a) represents Darcy's law in the direction tangential to the fracture and a source term $[\![-\boldsymbol{\nu}\nabla p]\!]$ is introduced to take into account the contribution of the bulk flow to the fracture flow [101]. For the sake of simplicity, we impose Dirichlet boundary conditions at the boundary $\partial\Gamma$ of the fracture Γ.

Finally, following [101], we provide the interface conditions to couple problems (2.1a)-(2.1b)-(2.1c) and (2.3a)-(2.3b). Let ξ be a positive real number, $\xi \neq \frac{1}{2}$, that will be chosen later on. The coupling conditions are given by

$$\xi(-\boldsymbol{\nu}_1\nabla p_1 \cdot \mathbf{n}_\Gamma) + (1-\xi)(-\boldsymbol{\nu}_2\nabla p_2 \cdot \mathbf{n}_\Gamma) = \frac{1}{\eta_\Gamma}(p_1 - p_\Gamma), \tag{2.4}$$

$$(1-\xi)(-\boldsymbol{\nu}_1\nabla p_1 \cdot \mathbf{n}_\Gamma) + \xi(-\boldsymbol{\nu}_2\nabla p_2 \cdot \mathbf{n}_\Gamma) = \frac{1}{\eta_\Gamma}(p_\Gamma - p_2), \tag{2.5}$$

where $\eta_\Gamma = \frac{\ell_\Gamma}{\nu_\Gamma^n}$, $\ell_\Gamma > 0$ and ν_Γ^n being the fracture width and the normal component of the fracture permeability tensor, see (2.2). These equations are obtained through a process of averaging the flux across the fracture in the normal direction, together with a suitable condition on the behaviour of the pressure through the fracture (a different value of the parameter ξ should represent a different condition imposed on the pressure's behaviour). The introduction of the parameter ξ thus yields a family of models, see [101] for more details.

Next, we observe that the interface conditions (2.4) and (2.5) can be rewritten, after summing and subtracting the equations, using classical jump and average operators (1.2) as

$$-\{\boldsymbol{\nu}\nabla p\} \cdot \mathbf{n}_\Gamma = \beta_\Gamma(p_1 - p_2) \qquad \text{on } \Gamma, \tag{2.6a}$$

$$-[\![\boldsymbol{\nu}\nabla p]\!] = \alpha_\Gamma(\{p\} - p_\Gamma) \qquad \text{on } \Gamma, \tag{2.6b}$$

where

$$\beta_\Gamma = \frac{1}{2\eta_\Gamma}, \qquad \alpha_\Gamma = \frac{2}{\eta_\Gamma(2\xi - 1)}. \tag{2.7}$$

Condition (2.6a) implies that the jump in the bulk pressure across the fracture induces a net flux, while condition (2.6b) entails that the difference between the average bulk pressure across the fracture and the fracture pressure p_Γ induces a net bulk-fracture flow. We also remark that the reformulation of the coupling conditions using jump and average

operators will be convenient for employing DG methods in the discretization.

In conclusion, the coupled model problem reads:

$$\begin{aligned}
-\nabla \cdot (\boldsymbol{\nu}_i \nabla p_i) &= f_i && \text{in } \Omega_i, \quad i = 1,2, \\
p_i &= g_i && \text{on } \partial\Omega_i, \quad i = 1,2, \\
-\nabla_\tau \cdot (\boldsymbol{\nu}_\Gamma^\tau \ell_\Gamma \nabla_\tau p_\Gamma) &= \ell_\Gamma f_\Gamma + [\![-\boldsymbol{\nu}\nabla p]\!] && \text{in } \Gamma, \\
p_\Gamma &= g_\Gamma && \text{on } \partial\Gamma, \\
-\{\boldsymbol{\nu}\nabla p\} \cdot \mathbf{n}_\Gamma &= \beta_\Gamma (p_1 - p_2) && \text{on } \Gamma, \\
-[\![\boldsymbol{\nu}\nabla p]\!] &= \alpha_\Gamma (\{p\} - p_\Gamma) && \text{on } \Gamma.
\end{aligned} \tag{2.8}$$

This system can be seen as a domain decomposition problem, with non-standard boundary conditions between the subdomains. We remark that problem (2.8) depends actually on two physical, fracture-dependent coefficients: the product $\boldsymbol{\nu}_\Gamma^\tau \ell_\Gamma$ and the ratio $\frac{\nu_\Gamma^n}{\ell_\Gamma}$, which appears in the coefficient η_Γ. The first coefficient is related to the jump in the normal component of the velocity (discontinuity of the Darcy velocity across the fracture), whereas the second one is related to the pressure jump (discontinuity of the pressure across the fracture).

2.2 Weak formulation and its well-posedness

In this section we present a weak formulation of our model problem (2.8) where the coupling conditions (2.6a)-(2.6b) are imposed in a weak sense, and prove its well-posedness. In order to combine the problem in the bulk and in the fracture, we define a bilinear form which is the sum of three different terms, each representing a specific part of the problem, namely the bulk flow, the fracture flow and the coupling conditions. Similarly, we build a linear operator summing the contributions from the bulk and the fracture. The well-posedness of the resulting weak problem is proved in Theorem 2.2.1.
For the sake of simplicity we will assume that *homogeneous* Dirichlet boundary conditions are imposed for both the bulk and fracture problems, i.e., $g_i = 0$, $i = 1, 2$, and $g_\Gamma = 0$. The extension to the general non-homogeneous case is straightforward. We introduce the

following spaces

$$Q^b = \{q = (q_1, q_2) \in Q_1^b \times Q_2^b\}, \qquad Q^\Gamma = H_0^1(\Gamma) \cap H^s(\Gamma),$$

where we define, for $i = 1, 2$ and $s \geq 1$, $Q_i^b = H^s(\Omega_i) \cap H^1_{0,\partial\Omega_i}(\Omega_i)$, with $H^1_{0,\partial\Omega_i}(\Omega_i) = \{q \in H^1(\Omega_i) \,\text{s.t.}\, q|_{\partial\Omega_i} = 0\}$.

Next we introduce the bilinear forms $\mathcal{A}_b : Q^b \times Q^b \to \mathbb{R}$, $\mathcal{A}_\Gamma : Q^\Gamma \times Q^\Gamma \to \mathbb{R}$ and $\mathcal{C} : (Q^b \times Q^\Gamma) \times (Q^b \times Q^\Gamma) \to \mathbb{R}$ defined as

$$\mathcal{A}_b(p, q) = \sum_{i=1}^{2} \int_{\Omega_i} \boldsymbol{\nu}_i \nabla p_i \cdot \nabla q_i, \qquad \mathcal{A}_\Gamma(p_\Gamma, q_\Gamma) = \int_\Gamma \boldsymbol{\nu}_\Gamma^\tau \ell_\Gamma \nabla_\tau p_\Gamma \cdot \nabla_\tau q_\Gamma,$$

$$\mathcal{C}((p, p_\Gamma), (q, q_\Gamma)) = \int_\Gamma \beta_\Gamma [\![p]\!] \cdot [\![q]\!] + \int_\Gamma \alpha_\Gamma (\{p\} - p_\Gamma)(\{q\} - q_\Gamma),$$

where α_Γ and β_Γ are defined as in (2.7). Clearly, the bilinear forms $\mathcal{A}_b(\cdot, \cdot)$ and $\mathcal{A}_\Gamma(\cdot, \cdot)$ take into account the problems in the bulk and in the fracture, respectively, while $\mathcal{C}(\cdot, \cdot)$ takes into account the coupling conditions at the interface (2.6). We also introduce the linear functional $\mathcal{L}_b : Q^b \to \mathbb{R}$ defined as $\mathcal{L}_b(q) = \sum_{i=1}^2 \int_{\Omega_i} f q_i$, and the linear functional $\mathcal{L}_\Gamma : Q^\Gamma \to \mathbb{R}$ defined as $\mathcal{L}_\Gamma(q_\Gamma) = \int_\Gamma \ell_\Gamma f_\Gamma q_\Gamma$, that represent the source terms in the bulk and fracture, respectively.
With the above notation, the weak formulation of our model problem reads as follows: Find $(p, p_\Gamma) \in Q^b \times Q^\Gamma$ such that, for all $(q, q_\Gamma) \in Q^b \times Q^\Gamma$,

$$\mathcal{A}\left((p, p_\Gamma), (q, q_\Gamma)\right) = \mathcal{L}(q, q_\Gamma), \tag{2.9}$$

where $\mathcal{A} : (Q^b \times Q^\Gamma) \times (Q^b \times Q^\Gamma) \to \mathbb{R}$ is defined as the sum of the bilinear forms just introduced:

$$\mathcal{A}\left((p, p_\Gamma), (q, q_\Gamma)\right) = \mathcal{A}_b(p, q) + \mathcal{A}_\Gamma(p_\Gamma, q_\Gamma) + \mathcal{C}((p, p_\Gamma), (q, q_\Gamma)), \tag{2.10}$$

and the linear operator $\mathcal{L} : Q^b \times Q^\Gamma \to \mathbb{R}$ is defined as

$$\mathcal{L}(q, q_\Gamma) = \mathcal{L}_b(q) + \mathcal{L}_\Gamma(q_\Gamma).$$

Next, we show that formulation (2.9) is well-posed. To this aim we introduce the following norm on $Q^b \times Q^\Gamma$:

$$||(q, q_\Gamma)||^2 = \sum_{i=1}^{2} ||\boldsymbol{\nu}_i^{1/2} \nabla q_i||^2_{L^2(\Omega_i)} + ||(\boldsymbol{\nu}_\Gamma^\tau \ell_\Gamma)^{1/2} \nabla_\tau q_\Gamma||^2_{L^2(\Gamma)} + ||\beta_\Gamma^{1/2} [\![q]\!]||^2_{L^2(\Gamma)} + ||\alpha_\Gamma^{1/2} (\{q\} - q_\Gamma)||^2_{L^2(\Gamma)}. \quad (2.11)$$

This is clearly a norm if $\alpha_\Gamma \geq 0$. Since $\alpha_\Gamma = \frac{2}{\eta_\Gamma(2\xi-1)}$, see (2.7), from now on, we will assume that $\xi > 1/2$. We remark that the same condition on the parameter ξ has been found also in [101] and [15].

Theorem 2.2.1. *Let $\xi > 1/2$. Then, problem (2.9) is well-posed.*

Proof. We show that $\mathcal{A}(\cdot, \cdot)$ is continuous and coercive on $Q^b \times Q^\Gamma$ equipped with the norm (2.11), as well as $\mathcal{L}(\cdot)$ is continuous on $Q^b \times Q^\Gamma$ with respect to the same norm. Then, existence and uniqueness of the solution, as well as linear dependence on the data, follow directly from Lax-Milgram's lemma. Coercivity is straightforward, as we clearly have that $\mathcal{A}((q, q_\Gamma), (q, q_\Gamma)) = ||(q, q_\Gamma)||^2$ for any $(q, q_\Gamma) \in Q^b \times Q^\Gamma$. On the other hand, continuity is a direct consequence of Cauchy-Schwarz inequality, while continuity of $\mathcal{L}(\cdot)$ on $Q^b \times Q^\Gamma$ is guaranteed by the regularity of the forcing term f. □

2.3 Numerical discretization

In this section we present a numerical discretization of our problem which combines a Discontinuous Galerkin approximation on general polytopic elements for the problem in the bulk, with a conforming finite element approximation in the fracture (see Remark 4 below). DG methods result to be very convenient for handling the discontinuity of the bulk pressure across the fracture, as well as the coupling of the bulk-fracture problems, which has been formulated using jump and average operators. As a result, we can employ the tools offered by DG methods to prove the well-posedness of our discrete method (see Proposition 2.4.3, below). In particular, we will adopt the techniques developed in [61, 59, 6, 58] (that we have summarized in Chapter 1), where an *hp*-version interior penalty discontinuous Galerkin method for the numerical solution of elliptic problems on polytopic meshes has been proposed and analysed.

For the discretization of the bulk problem, we consider a family of meshes $\mathcal{T}_h$ made of general polytopic elements, which are aligned with the fracture Γ, so that any element $E \in \mathcal{T}_h$ cannot be cut by Γ. Note that, since Ω_1 and Ω_2 are disjoint, each element E belongs exactly to one of the two subdomains.

Clearly, each mesh $\mathcal{T}_h$ induces a subdivision of the fracture Γ into faces, that we will denote by Γ_h. It follows that, if we denote as in Chapter 1 by $\mathcal{F}_h$ the set of all the faces of the mesh $\mathcal{T}_h$, we can decompose

$$\mathcal{F}_h = \mathcal{F}_h^I \cup \mathcal{F}_h^B \cup \Gamma_h,$$

where $\mathcal{F}_h^I$ is the set of interior faces not belonging to the fracture (see also Remark 5) and $\mathcal{F}_h^B$ is the set of boundary faces (since we are imposing Dirichlet boundary conditions on the whole $\partial\Omega$ we have $\mathcal{F}_h^B = \mathcal{F}_h^D$).

With the aim of building a DG-conforming finite element approximation, we choose to set the discrete problem in the finite-dimensional spaces

$$\begin{aligned} Q_h^b &= \{q_h \in L^2(\Omega) : \ q_h|_E \in \mathbb{P}_{k_E}(E) \ \forall E \in \mathcal{T}_h\}, && k_E \geq 1, \forall E \in \mathcal{T}_h \\ Q_h^\Gamma &= \{q_{\Gamma,h} \in \mathcal{C}^0(\Gamma) : \ q_{\Gamma,h}|_F \in \mathbb{P}_k(F) \ \forall F \in \Gamma_h\} && k \geq 1. \end{aligned}$$

Note that to each element $E \in \mathcal{T}_h$ is associated the polynomial degree k_E. We also remark that the polynomial degrees in the bulk and fracture discrete spaces just defined are chosen independently.
Next, we introduce the bilinear forms $\mathcal{A}_b^{DG} : Q_h^b \times Q_h^b \to \mathbb{R}$ and $\mathcal{C}^{DG} : (Q_h^b \times Q_h^\Gamma) \times (Q_b^h \times Q_h^\Gamma) \to \mathbb{R}$, defined as follows

$$\begin{aligned} \mathcal{A}_b^{DG}(p_h, q_h) = &\sum_{E \in \mathcal{T}_h} \int_E \boldsymbol{\nu} \nabla p_h \cdot \nabla q_h - \sum_{F \in \mathcal{F}_h \setminus \Gamma_h} \int_F \{\boldsymbol{\nu} \nabla p_h\} \cdot [\![q_h]\!] \\ &- \sum_{F \in \mathcal{F}_h \setminus \Gamma_h} \int_F \{\boldsymbol{\nu} \nabla q_h\} \cdot [\![p_h]\!] + \sum_{F \in \mathcal{F}_h \setminus \Gamma_h} \int_F \sigma_F [\![p_h]\!] \cdot [\![q_h]\!], \end{aligned}$$

$$\mathcal{C}^{DG}((p_h, p_{\Gamma,h}), (q_h, q_{\Gamma,h})) = \sum_{F \in \Gamma_h} \int_F \beta_\Gamma [\![p_h]\!] \cdot [\![q_h]\!] + \sum_{F \in \Gamma_h} \int_F \alpha_\Gamma (\{p_h\} - p_{\Gamma,h})(\{q_h\} - q_{\Gamma,h}).$$

The non-negative function $\sigma \in L^\infty(\mathcal{F}_h \setminus \Gamma_h)$ is the *discontinuity penalization parameter*

($\sigma_F = \sigma|_F$, for $F \in \mathcal{F}_h \setminus \Gamma_h$). The precise definition of σ will be presented in Definition 2.4.1 below. Finally we define the linear functional $\mathcal{L}_b^{DG} : Q_h^b \to \mathbb{R}$ as

$$\mathcal{L}_b^{DG}(q_h) = \sum_{E \in \mathcal{T}_h} \int_E f q_h.$$

Remark 3. Since we are imposing homogeneous boundary conditions, $\mathcal{L}_b^{DG}$ has the same structure of the linear functional $\mathcal{L}_b$ previously defined. In general, for $g \neq 0$, $\mathcal{L}_b^{DG}$ contains some additional terms:

$$\mathcal{L}_b^{DG}(q_h) = \sum_{E \in \mathcal{T}_h} \int_E f q_h + \sum_{F \in \mathcal{F}_h^D} \int_F (-\boldsymbol{\nu} \nabla q_h \cdot \mathbf{n}_F + \sigma_F q_h) g.$$

The DG discretization of problem (2.9) reads as follows: Find $(p_h, p_{\Gamma,h}) \in Q_h^b \times Q_h^\Gamma$ such that

$$\mathcal{A}_h \left((p_h, p_{\Gamma,h}), (q_h, q_{\Gamma,h}) \right) = \mathcal{L}_h(q_h, q_{\Gamma,h}) \quad \forall (q_h, q_{\Gamma,h}) \in Q_h^b \times Q_h^\Gamma, \tag{2.12}$$

where $\mathcal{A}_h : (V_h^b \times Q_h^\Gamma) \times (Q_h^b \times Q_h^\Gamma) \to \mathbb{R}$ is defined as

$$\mathcal{A}_h \left((p_h, p_{\Gamma,h}), (q_h, q_{\Gamma,h}) \right) = \mathcal{A}_b^{DG}(p_h, q_h) + \mathcal{A}_\Gamma(p_{\Gamma,h}, q_{\Gamma,h}) + \mathcal{C}^{DG}((p_h, p_{\Gamma,h}), (q_h, q_{\Gamma,h})),$$

and $\mathcal{L}_h : Q_h^b \times Q_h^\Gamma \to \mathbb{R}$ is defined as

$$\mathcal{L}_h(q_h, q_{\Gamma,h}) = \mathcal{L}_b^{DG}(q_h) + \mathcal{L}_\Gamma(q_{\Gamma,h}).$$

Note that the discrete bilinear form $\mathcal{A}_h$ has the same structure as the bilinear form $\mathcal{A}$ previously defined in (2.10), being the sum of three different components, each representing a specific part of the problem.

Remark 4. The choice of employing a conforming finite element approximation for the flow in the fracture has been made only in order to keep the analysis of the numerical method as clear as possible and to put the focus on the discretization of the bulk problem and on the imposition of the coupling conditions, cf. Section 2.4. The analysis of the numerical method with a DG discretization for both the bulk and fracture problems will be addressed in Chapter 3, see also Remark 5 below.

We now want to consider the stability and the error analysis of formulation (2.12).

2.4 Theoretical analysis

For simplicity, we suppose that the bulk permeability tensor $\boldsymbol{\nu}$ is piecewise *constant* on mesh elements, i.e., $\boldsymbol{\nu}|_E \in [\mathbb{P}_0(E)]^{d\times d}$ for all $E \in \mathcal{T}_h$, and that the fracture permeability tensor is constant on the whole domain, i.e. $\boldsymbol{\nu}_\Gamma \in [\mathbb{P}^0(\Gamma)]^{(d-1)\times(d-1)}$. In the following, we will employ the notation $\bar{\boldsymbol{\nu}}_E = |\sqrt{\boldsymbol{\nu}|_E}|_2^2$, where $|\cdot|_2$ denotes the l_2-norm.

In order to show the stability and the error analysis of formulation (2.12), we will employ the technical results for polytopic discretizations summarized in Chapter 1. In particular, we will assume that the bulk meshes $\mathcal{T}_h$ satisfy the polytopic-regularity Assumption 1.1.1 and the covering Assumption 1.1.2.

Remark 5. The induced subdivision of the fracture Γ_h consists of the faces of the elements of $\mathcal{T}_h$ that share part of their boundary with the fracture, so that, according to the definition of $\mathcal{F}_h$ given in Section 1.1, Γ_h is made up of line segments when $d = 2$ and of triangles when $d = 3$. Since we are employing a conforming finite element approximation for the flow in the fracture, we need to assume that, when $d = 3$, these triangles are shape-regular and that they do not present hanging nodes. However, we remark that the use of DG methods for the fracture problem as well would make this assumption unnecessary, thus allowing for the use of very general meshes, see Chapter 3, Section 3.3.

To complete the definition of our method, we need to specify the form of the discontinuity penalization parameter σ. Taking as a reference [61, 59, 6, 58], we give the following

Definition 2.4.1. The discontinuity-penalization parameter $\sigma : \mathcal{F}_h \setminus \Gamma_h \to \mathbb{R}^+$ is defined facewise by

$$\sigma(\mathbf{x}) = \sigma_0 \begin{cases} \max_{E\in\{E^+,E^-\}} \frac{\bar{\boldsymbol{\nu}}_E k_E^2}{h_E}, & \text{if } \mathbf{x} \in F \in \mathcal{F}_h^I,\ \bar{F} = \partial\bar{E}^+ \cap \partial\bar{E}^- \\ \frac{\bar{\boldsymbol{\nu}}_E k_E^2}{h_E}, & \text{if } \mathbf{x} \in F \in \mathcal{F}_h^B,\ \bar{F} = \partial\bar{E} \cap \partial\bar{\Omega}, \end{cases} \tag{2.13}$$

with $\sigma_0 > 0$ independent of k_E, $|E|$ and $|F|$.

Following [61, 59, 6, 58], we base our analysis on the introduction of an appropriate *inconsistent* formulation for the problem in the bulk. This choice is determined by the necessity of avoiding to make further (unnatural) regularity requirements for the exact solution, cf. Assumption 2.4.4 below. Indeed, those would be in need if we wanted

to obtain optimal *hp*-approximation estimates for the $H^1(\mathcal{F}_h)$-seminorm on polytopic meshes, as those enunciated in Chapter 1, Lemma 1.3.3. To this end we define the following extension of the forms $\mathcal{A}_b^{DG}$ and $\mathcal{L}_b^{DG}$:

$$\begin{aligned}\tilde{\mathcal{A}}_b^{DG}(p,q) = &\sum_{E\in\mathcal{T}_h}\int_E \nu\nabla p\cdot\nabla q - \sum_{F\in\mathcal{F}_h\setminus\Gamma_h}\int_F \{\boldsymbol{\nu}\Pi_2(\nabla p)\}\cdot[\![q]\!]\\ &- \sum_{F\in\mathcal{F}_h\setminus\Gamma_h}\int_F \{\boldsymbol{\nu}\Pi_2(\nabla q)\}\cdot[\![p]\!] + \sum_{F\in\mathcal{F}_h\setminus\Gamma_h}\sigma_F\int_F [\![p]\!]\cdot[\![q]\!],\\ \tilde{\mathcal{L}}_b^{DG}(q) = &\sum_{E\in\mathcal{T}_h}\int_E fq + \left[\sum_{F\in\mathcal{F}_h^B}\int_F(-\boldsymbol{\nu}\Pi_2(\nabla q)\cdot\mathbf{n}_F + \sigma_F q)g\right],\end{aligned}$$

where the integral between square brackets vanishes if we consider homogeneous boundary conditions. Here, $\Pi_2 : [L^2(\Omega)]^d \to [Q_h^b]^d$ denotes the orthogonal L^2 - projection onto the bulk finite element space $[Q_h^b]^d$. It follows that these forms are well defined on the space

$$Q^b(h) = Q_h^b + Q^b,$$

since the terms $\{\boldsymbol{\nu}\Pi_2(\nabla q)\}$ and $\{\boldsymbol{\nu}\Pi_2(\nabla p)\}$ are traces of elementwise polynomial functions. Moreover, it is clear that

$$\tilde{\mathcal{A}}_b^{DG}(p_h,q_h) = \mathcal{A}_b^{DG}(p_h,q_h) \quad \text{for all } q_h, p_h \in Q_h^b$$

and

$$\tilde{\mathcal{L}}_b^{DG}(q_h) = \mathcal{L}_b^{DG}(q_h) \quad \text{for all } q_h \in Q_h^b.$$

Thereby, $\tilde{\mathcal{A}}_b^{DG}(\cdot,\cdot)$ and $\tilde{\mathcal{L}}_b^{DG}(\cdot)$ are extensions of $\mathcal{A}_b^{DG}(\cdot,\cdot)$ and $\mathcal{L}_b^{DG}(\cdot)$ to $Q^b(h)\times Q^b(h)$ and $Q^b(h)$, respectively. Hence, we may rewrite our discrete problem (2.12) in the following *equivalent* form:
Find $(p_h, p_{\Gamma,h}) \in Q_h^b \times Q_h^\Gamma$ such that

$$\tilde{\mathcal{A}}_h\left((p_h,p_{\Gamma,h}),(q_h,q_{\Gamma,h})\right) = \tilde{\mathcal{L}}_h(q_h,q_{\Gamma,h}) \quad \forall (q_h,q_{\Gamma,h}) \in Q_h^b \times Q_h^\Gamma, \tag{2.14}$$

where $\tilde{\mathcal{A}}_h$ is obtained from $\mathcal{A}_h$ by replacing the bilinear form $\mathcal{A}_b^{DG}(\cdot,\cdot)$ with its inconsistent version $\tilde{\mathcal{A}}_b^{DG}(\cdot,\cdot)$, and $\tilde{\mathcal{L}}_h$ is obtained by replacing the linear operator $\mathcal{L}_b^{DG}(\cdot)$ with $\tilde{\mathcal{L}}_b^{DG}(\cdot)$. We remark that formulation (2.14) is no longer consistent due to the discrete nature of

the L^2-projection operator Π_2.

Next, we equip the space $Q^b(h)$ 2.4 with the following norm

$$|||(q, q_{\Gamma,h})|||^2 = ||q||^2_{DG} + ||q_{\Gamma,h}||^2_{\Gamma} + ||(q, q_{\Gamma,h})||^2_{\mathcal{C}},$$

where

$$\begin{aligned}
||q||^2_{DG} &= \sum_{E\in\mathcal{T}_h} ||\boldsymbol{\nu}^{1/2}\nabla q||^2_{L^2(E)} + \sum_{F\in\mathcal{F}_h\setminus\Gamma_h} ||\sigma_F^{1/2}[\![q]\!]||^2_{L^2(F)},\\
||q_{\Gamma,h}||^2_{\Gamma} &= \sum_{F\in\Gamma_h} ||(\boldsymbol{\nu}^{\tau}_{\Gamma}\ell_{\Gamma})^{1/2}\nabla_{\tau} q_{\Gamma,h}||^2_{L^2(F)},\\
||(q, q_{\Gamma,h})||^2_{\mathcal{C}} &= \sum_{F\in\Gamma_h} ||\beta_{\Gamma}^{1/2}[\![q]\!]||^2_{L^2(F)} + \sum_{F\in\Gamma_h} ||\alpha_{\Gamma}^{1/2}(\{q\} - q_{\Gamma,h})||^2_{L^2(F)}.
\end{aligned}$$

It is easy to show that $||\cdot||_{DG}$ is a norm if $\sigma_F > 0$ for all $F \in \mathcal{F}_h \setminus \Gamma_h$ and that $|||\cdot|||$ is a norm if $\alpha_\Gamma \geq 0$ (that is $\xi > 1/2$). Note that $|||\cdot|||$ is also well defined on the extended space $Q^b(h) \times Q^\Gamma(h)$.

2.4.1 Stability analysis

We can now proceed with the stability analysis of our method. We remark that well-posedness of the discrete problem (2.12) is guaranteed if we show that, more in general, problem (2.14) *extended* to the space $Q^b(h) \times Q^\Gamma_h$ is well-posed. The choice of proving this more general property is made for future use in the error analysis.

Taking as a reference [61, 59, 6, 58], we state and prove the following result. Note that, for the proof, the polytopic-regularity Assumption 1.1.1 will play a fundamental role as well as the choice of the discontinuity-penalization parameter σ, see Definition 2.4.1. Before proving that formulation (2.12) is well-posed, we state (and prove) some auxiliary results, see Lemma 2.4.1 and 2.4.2 below.

Lemma 2.4.1. *Let $\sigma : \mathcal{F}_h \setminus \Gamma_h \to \mathbb{R}^+$ be defined as in* (2.13)*. Then, if Assumption 1.1.1 holds, the bilinear form $\tilde{\mathcal{A}}^{DG}_b(\cdot,\cdot)$ is continuous on $Q^b(h) \times Q^b(h)$ and, provided that σ_0 is*

sufficiently large, it is also coercive on $Q^b(h) \times Q^b(h)$, i.e.,

$$\tilde{\mathcal{A}}_b^{DG}(p,q) \lesssim ||q||_{DG}||p||_{DG}, \qquad \tilde{\mathcal{A}}_b^{DG}(q,q) \gtrsim ||q||_{DG}^2,$$

for any $q, p \in Q^b(h)$.

Proof. For the proof we follow [61] and [58]. We start with coercivity. For any $q \in Q^b(h)$,

$$\begin{aligned}\tilde{\mathcal{A}}_b^{DG}(q,q) &= ||q||_{DG}^2 - 2\sum_{F\in\mathcal{F}_h\setminus\Gamma_h}\int_F \{\boldsymbol{\nu}\Pi_2(\nabla q)\}\cdot[\![q]\!] \\ &= I + II.\end{aligned}$$

In order to bound term II, we employ Cauchy-Schwarz's, triangular and Young's inequalities to obtain

$$\begin{aligned}\int_{\mathcal{F}_h\setminus\Gamma_h}\{\boldsymbol{\nu}\Pi_2(\nabla q)\}\cdot[\![q]\!] &\lesssim ||\sigma_F^{-1/2}\boldsymbol{\nu}(\Pi_2(\nabla q^+)+\Pi_2(\nabla q^-))||_{0,\mathcal{F}_h\setminus\Gamma_h}\,||\sigma_F^{1/2}[\![q]\!]||_{0,\mathcal{F}_h\setminus\Gamma_h} \\ &\lesssim \varepsilon\sum_{F\in\mathcal{F}_h\setminus\Gamma_h}\Big(\bar{\boldsymbol{\nu}}_{E^+\sigma_F}||\Pi_2(\nabla q^+)||_{L^2(F)}^2 \\ &\qquad + \bar{\boldsymbol{\nu}}_{E^-\sigma_F}||\Pi_2(\nabla q^-)||_{L^2(F)}^2\Big) + \frac{1}{4\varepsilon}||\sigma_F^{1/2}[\![q]\!]||_{L^2(F)}^2,\end{aligned}$$

with $\varepsilon > 0$. Employing the inverse inequality of Lemma 1.3.1 over the simplices S_E^F and the definition of the interior penalty parameter σ (2.13), we have

$$\begin{aligned}\sum_{F\in\mathcal{F}_h\setminus\Gamma_h}\int_F\{\boldsymbol{\nu}\Pi_2(\nabla q)\}\cdot[\![q]\!] &\lesssim \frac{\varepsilon}{\sigma_0}\sum_{E\in\mathcal{T}_h}\sum_{F\in\partial E}\frac{h_E|F|}{d|S_E^F|}||\Pi_2(\nabla q)||_{L^2(S_E^F)}^2 \\ &\quad + \frac{1}{4\varepsilon}\sum_{F\in\mathcal{F}_h\setminus\Gamma_h}||\sigma_F^{1/2}[\![q]\!]||_{L^2(F)}^2 \\ &\lesssim \frac{\varepsilon}{\sigma_0}\sum_{E\in\mathcal{T}_h}||\boldsymbol{\nu}^{1/2}\nabla q||_{L^2(E)}^2 + \frac{1}{4\varepsilon}\sum_{F\in\mathcal{F}_h\setminus\Gamma_h}||\sigma_F^{1/2}[\![q]\!]||_{L^2(F)}^2,\end{aligned}$$

where we have used Assumption 1.1.1 and bound (1.1), together with the L^2-stability of the projector Π_2 and the boundedness of tensor $\boldsymbol{\nu}$. In conclusion, using the polytopic-regularity Assumption 1.1.1, we proved that

$$\tilde{\mathcal{A}}_b^{DG}(q,q) \gtrsim ||q||_{DG}^2 \quad \text{for all } \; q \in Q^b(h),$$

for an appropriate choice of the constant ε and for σ_0 large enough. The proof of continuity can be obtained employing analogous arguments. □

Lemma 2.4.2. *The bilinear form $\mathcal{A}_\Gamma(\cdot,\cdot)$ is coercive and continuous on $Q_h^\Gamma \times Q_h^\Gamma$ with respect to the norm $||\cdot||_\Gamma$.*

Proof. Since $\mathcal{A}_\Gamma(q_{\Gamma,h}, q_{\Gamma,h}) = ||q_{\Gamma,h}||_\Gamma^2$ for any $q_{\Gamma,h} \in Q_h^\Gamma$, $\mathcal{A}_\Gamma(\cdot,\cdot)$ is clearly coercive. Continuity follows directly from Cauchy-Schwarz's inequality. □

Employing Lemma 2.4.1 and Lemma 2.4.2, we can easily prove the well-posedness of the discrete problem (2.12). We can then state the following stability result.

Theorem 2.4.3. *Let σ be defined as is* (2.13)*. Then, if σ_0 is chosen sufficiently large, problem* (2.12) *is well-posed.*

Proof. We have that, for any $(q, q_{\Gamma,h}) \in Q^b(h) \times Q_h^\Gamma$, it holds $\mathcal{C}^{DG}((q_h, q_{\Gamma,h}), (q, q_{\Gamma,h})) = ||(q, q_{\Gamma,h})||_{\mathcal{C}}^2$. Moreover from Lemma 2.4.1 and Lemma 2.4.2 we know that $\tilde{\mathcal{A}}_b^{DG}(q,q) \gtrsim ||q||_{DG}^2$ and $\mathcal{A}_\Gamma(q_{\Gamma,h}, q_{\Gamma,h}) = ||q_{\Gamma,h}||_\Gamma^2$, respectively. Therefore

$$\tilde{\mathcal{A}}_h\left((q, q_{\Gamma,h}), (q, q_{\Gamma,h})\right) \gtrsim |||(q, q_{\Gamma,h})|||^2 \quad \forall (q, q_{\Gamma,h}) \in Q^b(h) \times Q_h^\Gamma.$$

Next we prove continuity. Let $(q, q_{\Gamma,h})$, $(w, w_h^\Gamma) \in Q^b(h) \times Q_h^\Gamma$. Then, from Lemma 2.4.1 and Lemma 2.4.2

$$\begin{aligned}
\tilde{\mathcal{A}}_b^{DG}(q,w) &\lesssim ||q||_{DG}||w||_{DG} \lesssim |||(q, q_{\Gamma,h})||| \cdot |||(w, w_h^\Gamma)|||, \\
\mathcal{A}_\Gamma(q_{\Gamma,h}, w_h^\Gamma) &\lesssim ||q_{\Gamma,h}||_\Gamma ||w_h^\Gamma||_\Gamma \lesssim |||(q_h, q_{\Gamma,h})||| \cdot |||(w_h, w_h^\Gamma)|||.
\end{aligned}$$

Finally, from Cauchy-Schwarz inequality, we get

$$\begin{aligned}
\mathcal{C}^{DG}((q, q_{\Gamma,h}), (w, w_h^\Gamma)) &\leq \sum_{F \in \Gamma_h} ||\beta_\Gamma^{1/2} [\![q]\!]||_{L^2(F)}^2 ||\beta_\Gamma^{1/2} [\![w]\!]||_{L^2(F)}^2 \\
&\quad + \sum_{F \in \Gamma_h} ||\alpha_\Gamma^{1/2}(\{q\} - q_{\Gamma,h})||_{L^2(F)}^2 ||\alpha_\Gamma^{1/2}(\{w\} - w_h^\Gamma)||_{L^2(F)}^2 \\
&\leq |||(q, q_{\Gamma,h})||| \cdot |||(w, w_h^\Gamma)|||.
\end{aligned}$$

In conclusion we have proved that

$$\tilde{\mathcal{A}}_h\left((q, q_{\Gamma,h}), (w, w_h^\Gamma)\right) \lesssim |||(q, q_{\Gamma,h})||| \cdot |||(w, w_h^\Gamma)|||.$$

The continuity of $\tilde{\mathcal{L}}_h(\cdot)$ on $Q^b(h) \times Q_h^\Gamma$ can be easily proved using Cauchy-Schwarz inequality, thanks to the regularity assumptions on the forcing terms f and f_Γ.

□

2.4.2 Error analysis

In this section we prove that the discrete solution $(p_h, p_{\Gamma,h})$ to problem (2.12) (or, equivalently, to problem (2.14)) converges to the exact solution (p, p_Γ) to problem (2.9). and provide an *a priori* error estimate.

For $i = 1, 2$, we denote by $\mathscr{E}_i$ the classical continuous extension operator, cf. [113] (see also Chapter 1, Section 1.3.2), $\mathscr{E}_i : H^s(\Omega_i) \to H^s(\mathbb{R}^d)$, for $s \in \mathbb{N}_0$, and make the following regularity assumptions for the exact solution (p, p_Γ):

Assumption 2.4.4. *We assume that the exact solution $((p_1, p_2), p_\Gamma)$ is such that:*

A1. *for every $E \in \mathcal{T}_h$, if $E \subset \Omega_i$, it holds $\mathscr{E}_i p_i|_{T_E} \in H^{r_E}(T_E)$, with $r_E \geq 1 + d/2$ and $T_E \in \mathcal{T}_\#$ with $E \subset T_E$. Moreover, we assume that the normal components of the exact fluxes $\boldsymbol{\nu}\nabla p$ are continuous across internal mesh interfaces, that is $[\![\boldsymbol{\nu}\nabla p]\!] = 0$ on $\mathcal{F}_h^I$;*

A2. $p_\Gamma \in H^r(\Gamma)$, *with* $r \geq 1$.

We can then state the following error estimate.

Theorem 2.4.5. *Let $\mathcal{T}_\# = \{T_E\}$ denote the covering related to $\mathcal{T}_h$ consisting of shape-regular simplexes as in Definition 1.1.2, satisfying Assumption 1.1.2. Let (p, p_Γ) be the solution of problem (2.9) and $(p_h, p_{\Gamma,h}) \in Q_h^b \times Q_h^\Gamma$ be its approximation obtained with the method (2.12) with the penalization parameter given by (2.13) and σ_0 sufficiently large. Moreover, suppose that the exact solution (p, p_Γ) satisfies the regularity Assumption 2.4.4.*

Then, the following error bound holds:

$$|||(p,p_\Gamma)-(p_h,p_{\Gamma,h})|||^2 \lesssim \sum_{E\in\mathcal{T}_h}\frac{h_E^{2(s_E-1)}}{k_E^{2(r_E-1)}}G_E^b(h_E,k_E,\bar{\boldsymbol{\nu}}_E)||\mathscr{E}p||^2_{H^{r_E}(T_E)} + \sum_{F\in\Gamma_h}\frac{h_F^{2k}}{k^{2(r-1)}}|p_\Gamma|^2_{H^r(F)}, \tag{2.15}$$

where the $\mathscr{E}p$ is to be interpreted as $\mathscr{E}_1p_1$ when $E\subset\Omega_1$ and as $\mathscr{E}_2p_2$ when $E\subset\Omega_2$. Moreover, $s_E=\min(k_E+1,r_E)$ and

$$G_E^b(h_E,k_E,\bar{\boldsymbol{\nu}}_E)=\bar{\boldsymbol{\nu}}_E+h_Ek_E^{-1}\max_{F\subset\partial E\setminus\Gamma}\sigma_F+(\alpha_\Gamma+\beta_\Gamma)h_Ek_E^{-1} + \bar{\boldsymbol{\nu}}_Eh_E^{-1}k_E\max_{F\subset\partial E\setminus\Gamma}\sigma_F^{-1}+\bar{\boldsymbol{\nu}}_Eh_E^{-1}k_E^2\max_{F\subset\partial E\setminus\Gamma}\sigma_F^{-1}.$$

Remark 6. (Uniform orders and mesh size) In case of uniform mesh-size and polynomial order, i.e. if $h_E\approx h$ and $k_E\approx k\geq 1$ for all $E\in\mathcal{T}_h$, and $h_F\approx h$ for all $F\in\Gamma_h$, if the exact solutions in the bulk and in the fracture satisfy $p\in H^r(\Omega)$ and $p_\Gamma\in H^r(\Gamma)$, with $r\geq k+1$, then the error estimate (2.15)reduces to

$$|||(p,p_\Gamma)-(p_h,p_h^\Gamma)|||\lesssim\frac{h^k}{k^{r-3/2}}||p||_{H^r(\Omega)}+\frac{h^{k_\Gamma}}{k_\Gamma^{r-1}}||p_\Gamma||_{H^r(\Gamma)}.$$

We point out that Galerkin's orthogonality does not hold true, due to the inconsistency of the bilinear form $\tilde{\mathcal{A}}_h$. Thereby, the error bound will be derived starting from Strang's second lemma. From Proposition 2.4.3 and Strang's second lemma we directly obtain the following abstract error bound on the error.

Lemma 2.4.6. *Assuming that the hypotheses of Proposition 2.4.3 are satisfied, it holds*

$$|||(p,p_\Gamma)-(p_h,p_{\Gamma,h})|||\lesssim\inf_{(q_h,q_{\Gamma,h})\in Q_h^b\times Q_h^\Gamma}|||(p,p_\Gamma)-(q_h,q_{\Gamma,h})||| + \sup_{(w_h,w_h^\Gamma)\in Q_h^b\times Q_h^\Gamma}\frac{|\mathcal{R}_h((p,p_\Gamma),(w_h,w_h^\Gamma))|}{|||(w_h,w_h^\Gamma)|||},$$

where the residual $\mathcal{R}_h$ is defined as

$$\mathcal{R}_h((p,p_\Gamma),(w_h,w_h^\Gamma))=\tilde{\mathcal{A}}_h((p,p_\Gamma),(w_h,w_h^\Gamma))-\mathcal{L}_h(w_h,w_h^\Gamma).$$

We can now proceed with the proof of Theorem 2.4.5.

Proof of Theorem 2.4.5. From Lemma 2.4.6 we know that the error satisfies the following bound

$$|||(p,p_\Gamma)-(p_h,p_{\Gamma,h})||| \lesssim \underbrace{\inf_{(q_h,q_{\Gamma,h})\in Q_h^b\times Q_h^\Gamma} |||(p,p_\Gamma)-(q_h,q_{\Gamma,h})|||}_{I} + \underbrace{\sup_{(w_h,w_h^\Gamma)\in Q_h^b\times Q_h^\Gamma} \frac{|\mathcal{R}_h((p,p_\Gamma),(w_h,w_h^\Gamma))|}{|||(w_h,w_h^\Gamma)|||}}_{II}. \quad (2.16)$$

We bound the two terms on the right-hand side of (2.16) separately. We can rewrite term I as

$$I = \underbrace{\inf_{q_h\in Q_h^b} ||p-q_h||_{DG}^2}_{(a)} + \underbrace{\inf_{q_{\Gamma,h}\in Q_h^\Gamma} ||p_\Gamma-q_{\Gamma,h}||_\Gamma^2}_{(b)} + \underbrace{\inf_{(q_h,q_{\Gamma,h})\in Q_h^b\times Q_h^\Gamma} ||(p-q_h,p_\Gamma-q_{\Gamma,h})||_{\mathcal{C}}^2}_{(c)}.$$

Again we consider each of the three terms separately. To bound term (a), we exploit the two approximation results stated in Lemma 1.3.3; we obtain that

$$\begin{aligned}
(a) &\le ||p-\widetilde{\Pi}p||_{DG}^2 = \sum_{E\in\mathcal{T}_h} ||\boldsymbol{\nu}^{1/2}\nabla(p-\widetilde{\Pi}p)||_{L^2(E)}^2 + \sum_{F\in\mathcal{F}_h\setminus\Gamma_h} \sigma_F||[\![p-\widetilde{\Pi}p]\!]||_{L^2(F)}^2 \\
&\lesssim \sum_{E\in\mathcal{T}_h}\left[\bar{\boldsymbol{\nu}}_E|p-\widetilde{\Pi}p|_{H^1(E)}^2 + (\max_{F\subset\partial E\setminus\Gamma}\sigma_F)||p-\widetilde{\Pi}p||_{L^2(\partial E\setminus\Gamma)}^2\right] \\
&\lesssim \sum_{E\in\mathcal{T}_h}\left[\frac{h_E^{2(s_E-1)}}{k_E^{2(r_E-1)}}\bar{\boldsymbol{\nu}}_E||\mathscr{E}p||_{H^{r_E}(T_E)}^2 + \frac{h_E^{2(s_E-1/2)}}{k_E^{2(r_E-1/2)}}(\max_{F\subset\partial E\setminus\Gamma}\sigma_F)||\mathscr{E}p||_{H^{r_E}(T_E)}^2\right] \\
&= \sum_{E\in\mathcal{T}_h}\frac{h_E^{2(s_E-1)}}{k_E^{2(r_E-1)}}||\mathscr{E}p||_{H^{r_E}(T_E)}^2\left(\bar{\boldsymbol{\nu}}_E + \frac{h_E}{k_E}(\max_{F\subset\partial E\setminus\Gamma}\sigma_F)\right).
\end{aligned}$$

Using classical interpolation estimates [30] we can bound term (b) as follows:

$$(b) \le ||p_\Gamma - p_\Gamma^I||_\Gamma^2 \lesssim \sum_{F\in\Gamma_h}\frac{h_F^{2k}}{k^{2(r-1)}}|p_\Gamma|_{H^r(F)}^2.$$

Finally, for term (c), we have

$$(c) \leq ||(p-\widetilde{\Pi}p, p_\Gamma - p_\Gamma^I)||_{\mathcal{C}}^2 \lesssim \beta_\Gamma \sum_{F\in\Gamma_h} |||[\![p-\widetilde{\Pi}p]\!]||_{L^2(F)}^2 + \alpha_\Gamma \sum_{F\in\Gamma_h} ||\{p-\widetilde{\Pi}p\}||_{L^2(F)}^2 + \alpha_\Gamma \sum_{F\in\Gamma_h} ||p_\Gamma - p_\Gamma^I||_{L^2(F)}^2.$$

Exploiting the approximation result (1.8), we obtain

$$\begin{aligned}\beta_\Gamma \sum_{F\in\Gamma_h} |||[\![p-\widetilde{\Pi}p]\!]||_{L^2(F)}^2 &\leq \beta_\Gamma \sum_{\substack{E\in\mathcal{T}_h \\ \partial E\cap\Gamma\neq\emptyset}} ||p-\widetilde{\Pi}p||_{L^2(\partial E)}^2 \lesssim \beta_\Gamma \sum_{\substack{E\in\mathcal{T}_h \\ \partial E\cap\Gamma\neq\emptyset}} \frac{h_E^{2(s_E-\frac{1}{2})}}{k_E^{2(r_E-\frac{1}{2})}} ||\mathscr{E}p||_{H^{r_E}(T_E)}^2 \\ &= \beta_\Gamma \sum_{\substack{E\in\mathcal{T}_h \\ \partial E\cap\Gamma\neq\emptyset}} \frac{h_E^{2(s_E-1)}}{k_E^{2(r_E-1)}} ||\mathscr{E}p||_{H^{r_E}(T_E)}^2 \frac{h_E}{k_E}.\end{aligned}$$

Similarly, we have

$$\alpha_\Gamma \sum_{F\in\Gamma_h} ||\{p-\widetilde{\Pi}p\}||_{L^2(F)}^2 \lesssim \alpha_\Gamma \sum_{\substack{E\in\mathcal{T}_h \\ \partial E\cap\Gamma\neq\emptyset}} \frac{h_E^{2(s_E-1)}}{k_E^{2(r_E-1)}} \frac{h_E}{k_E} ||\mathscr{E}p||_{H^{r_E}(T_E)}^2.$$

Finally, using again classical interpolation estimates, we deduce that

$$\alpha_\Gamma \sum_{F\in\Gamma_h} ||p_\Gamma - p_\Gamma^I||_{L^2(F)}^2 \lesssim \alpha_\Gamma \sum_{F\in\Gamma_h} \frac{h_F^{2k}}{k^{2(r-1)}} |p_\Gamma|_{H^r(F)}^2.$$

In conclusion, combining all the previous estimates, we can bound the term I on the right-hand side of (2.16) as follows:

$$\begin{aligned}I \lesssim & \sum_{F\in\Gamma_h} h_F^{2k} |p_\Gamma|_{H^{k+1}(F)}^2 \\ & + \sum_{E\in\mathcal{T}_h} \frac{h_E^{2(s_E-1)}}{k_E^{2(r_E-1)}} ||\mathscr{E}p||_{H^{r_E}(T_E)}^2 \left[\bar{\boldsymbol{\nu}}_E + h_E k_E^{-1} (\max_{F\subset\partial E\setminus\Gamma} \sigma_F) + (\alpha_\Gamma + \beta_\Gamma) h_E k_E^{-1} \right]. \quad (2.17)\end{aligned}$$

Next, we derive a bound on the term II on the right-hand side of (2.16). First, we note that, integrating by parts elementwise and using that the couple (p, p_Γ) satisfies (2.9) as

well as the regularity assumption 2.4.4, we can rewrite the residual $\mathcal{R}_h$ as

$$\mathcal{R}_h((p,p_\Gamma),(w_h,w_h^\Gamma)) = \sum_{F\in\mathcal{F}_h\backslash\Gamma_h}\int_F \{\boldsymbol{\nu}(\nabla p - \Pi_2(\nabla p))\}\cdot[\![w_h]\!].$$

Employing Cauchy-Schwarz inequality and the definition of the norm $|||\cdot|||$, we then obtain

$$II \leq \left(\sum_{F\in\mathcal{F}_h\backslash\Gamma_h}\sigma_F^{-1}\int_F |\{\boldsymbol{\nu}(\nabla p - \Pi_2(\nabla p))\}|^2\right)^{1/2}.$$

If we still denote by $\widetilde{\Pi}$ the vector-valued generalization of the projection operator $\widetilde{\Pi}$ defined in Lemma 1.3.3, we observe that

$$\begin{aligned}\sum_{F\in\mathcal{F}_h\backslash\Gamma_h}\sigma_F^{-1}\int_F |\{\boldsymbol{\nu}(\nabla p - \Pi_2(\nabla p))\}|^2 \lesssim & \sum_{F\in\mathcal{F}_h\backslash\Gamma_h}\sigma_F^{-1}\int_F |\{\boldsymbol{\nu}(\nabla p - \widetilde{\Pi}(\nabla p))\}|^2 \\ & + \sum_{F\in\mathcal{F}_h\backslash\Gamma_h}\sigma_F^{-1}\int_F |\{\boldsymbol{\nu}\Pi_2(\nabla p - \widetilde{\Pi}(\nabla p))\}|^2 \\ & \equiv (1)+(2).\end{aligned}$$

To bound term (1), we proceed as above, employing the approximation result stated in Lemma 1.3.3. We obtain

$$(1) \lesssim \sum_{E\in\mathcal{T}_h}\frac{h_E^{2(s_E-1)}}{k_E^{2(r_E-1)}}\Big(\bar{\boldsymbol{\nu}}_E(\max_{F\subset\partial E\backslash\Gamma}\sigma_F^{-1})\frac{h_E^{-1}}{k_E^{-1}}\Big)||\mathscr{E}p||^2_{H^{r_E}(T_E)}.$$

Exploiting, in order, the boundedness of the permeability tensor $\boldsymbol{\nu}$, the inverse inequality (1.6), the L^2-stability of the projector Π_2 and the approximation results stated in Lemma 1.3.3, we can bound term (2) as follows:

$$\begin{aligned}(2) &\lesssim \sum_{E\in\mathcal{T}_h}(\max_{F\subset\partial E\backslash\Gamma}\sigma_F^{-1})\bar{\boldsymbol{\nu}}_E||\Pi_2(\widetilde{\Pi}(\nabla p)-\nabla p)||^2_{L^2(\partial E\backslash\Gamma)} \\ &\lesssim \sum_{E\in\mathcal{T}_h}(\max_{F\subset\partial E\backslash\Gamma}\sigma_F^{-1})\bar{\boldsymbol{\nu}}_E\frac{k_E^2}{h_E}||\widetilde{\Pi}(\nabla p)-\nabla p||^2_{L^2(E)} \\ &\lesssim \sum_{E\in\mathcal{T}_h}\frac{h_E^{2(s_E-1)}}{k_E^{2(r_E-1)}}||\mathscr{E}p||^2_{H^{r_E}(T_E)}\left(\bar{\boldsymbol{\nu}}_E\frac{k_E^2}{h_E}(\max_{F\subset\partial E\backslash\Gamma}\sigma_F^{-1})\right).\end{aligned}$$

Hence, term II on the right-hand side of (2.16) may be bounded as:

$$II \lesssim \sum_{E\in\mathcal{T}_h} \frac{h_E^{2(s_E-1)}}{k_E^{2(r_E-1)}} ||\mathscr{E}p||^2_{H^{r_E}(T_E)} \Bigg[\bar{\boldsymbol{\nu}}_E (\max_{F\subset\partial E\setminus\Gamma} \sigma_F^{-1}) h_E^{-1} k_E + \bar{\boldsymbol{\nu}}_E (\max_{F\subset\partial E\setminus\Gamma} \sigma_F^{-1}) h_E^{-1} k_E^2 \Bigg]. \quad (2.18)$$

Finally, substituting (2.17) and (2.18) into (2.16), leads to the thesis. □

2.5 Numerical results

In this section we present some two-dimensional numerical experiments to confirm the validity of the *a priori* error estimates that we have derived for our method. The test cases have been chosen intentionally with increasing complexity: we start with some academic numerical tests that aim at validating the convergence properties of the method, and we end the section with a physical experiment that investigates the effect of large and low permeability in the fracture to the bulk flow.
The numerical results have been obtained in MATLAB®. Throughout this section we set the fracture thickness (appearing in the coupling conditions (2.6a)-(2.6b)) equal to $\ell_\Gamma = 0.001 = \eta_\Gamma$ and $\boldsymbol{\nu}_\Gamma^\tau = 1$. For the generation of polygonal meshes conforming to the fractures we have suitably modified the MATLAB® code `PolyMesher` developed by G.H. Paulino and collaborators [117].

2.5.1 Example 1

In this first test case we take $\Omega = (0,1)^2$, and choose as exact solutions in the bulk and in the fracture $\Gamma = \{(x,y) \in \Omega : \ x + y = 1\}$ as

$$p = \begin{cases} e^{x+y} & \text{in } \Omega_1, \\ e^{x+y} + \frac{4\eta_\Gamma}{\sqrt{2}} e & \text{in } \Omega_2, \end{cases} \qquad p_\Gamma = e + \frac{2\eta_\Gamma}{\sqrt{2}} e.$$

It is easy to prove that p and p_Γ satisfy the coupling conditions (2.6a)-(2.6b) with $\xi = 1$ and $\boldsymbol{\nu} = \mathbf{I}$. Finally we need to adjust the source terms for the bulk accordingly as $f = -2e^{x+y}$ in Ω_1 and Ω_2. Note that in this case $f_\Gamma = 0$ since the solution is constant and $[\![\boldsymbol{\nu}\nabla p]\!] = 0$. In Figure 2.2 we report three successive levels of refinement of the polygonal

mesh conforming to the fracture employed in this set of experiments. .

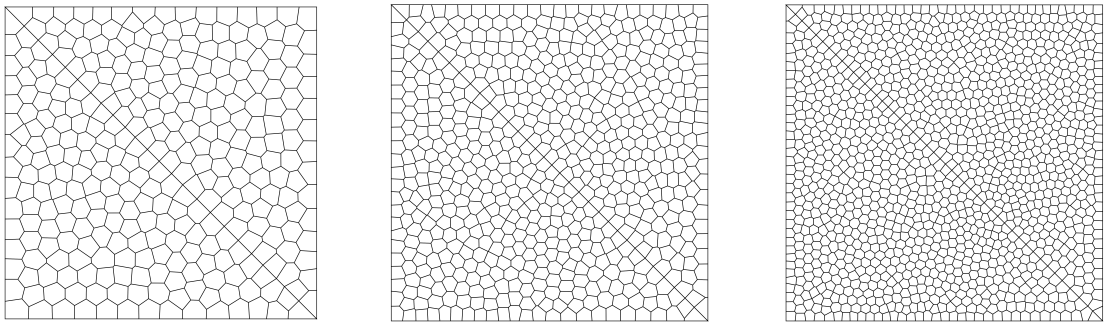

(a) (b) (c)

Figure 2.2: Example 1: Three refinements of the polygonal mesh grid conforming to the fracture.

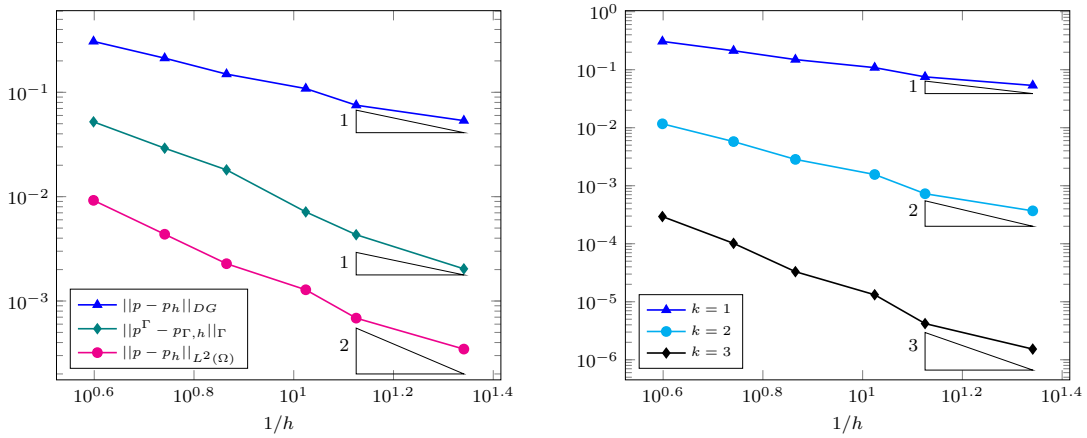

(a) Bulk and fracture $k = 1$ (b) Bulk $k = 1, 2, 3$

Figure 2.3: Example 1: Computed errors in the bulk and in the fracture as a function of the inverse of the mesh size (loglog scale) with polynomial degree $k = 1$ on the left, and computed errors $||p - p_h||_{DG}$ in the bulk for polynomial degrees $k = 1, 2, 3$ on the right.

In Figure 2.3(a) we plot the computed errors $||p - p_h||_{DG}$ and $||p_\Gamma - p_{\Gamma,h}||_\Gamma$ as a function of inverse of the mesh size (loglog scale). Here we have taken the polynomial degree $k_E = 1$ $\forall E \in \mathcal{T}_h$ and $k = 1$ for the fracture finite dimensional space. In both cases the numerical results are in agreement with the theoretical estimates, i.e., the error goes to zero at a rate $\mathcal{O}(h)$. In the same plot we also report the behaviour of the error $||p - p_h||_{L^2(\Omega)}$. One order of convergence is clearly gained. Finally, in Figure 2.3(b) we report the computed errors in the bulk $||p - p_h||_{DG}$ as a function of $1/h$ for $k_E = k = 1, 2, 3$. The theoretical convergence rates are clearly achieved.

2.5.2 Example 2

In the second test case we take $\Omega = (0,1)^2$, and choose as exact solutions in the bulk and in the fracture $\Gamma = \{(x,y) \in \Omega : \ x + y = 1\}$ as

$$p = \begin{cases} e^{x+y} & \text{in } \Omega_1, \\ \frac{e^{x+y}}{2} + (\frac{1}{2} + \frac{3\eta_\Gamma}{\sqrt{2}})e & \text{in } \Omega_2, \end{cases} \qquad p_\Gamma = e(1 + \sqrt{2}\eta_\Gamma).$$

It is easy to prove that p and p_Γ satisfy the coupling conditions (2.6a)-(2.6b) with $\xi = 1$ and $\boldsymbol{\nu} = \mathbf{I}$. Finally we need to adjust the source terms for the bulk and fracture problems accordingly: We choose $\xi = 1$ and take $\boldsymbol{\nu} = \mathbf{I}$. In this case we set the source term as

$$f = \begin{cases} -2e^{x+y} & \text{in } \Omega_1, \\ -e^{x+y} & \text{in } \Omega_2 \end{cases} \qquad f_\Gamma = \frac{e}{\sqrt{2}\ell_\Gamma}.$$

Notice that on the fracture the source term satisfies $\ell_\Gamma f_\Gamma = -\nabla_\tau \cdot (\boldsymbol{\nu}_\Gamma^\tau \ell_\Gamma \nabla_\tau p_\Gamma) + [\![\boldsymbol{\nu}\nabla p]\!]$, and, since p_Γ is constant, it holds $f_\Gamma = [\![\boldsymbol{\nu}\nabla p]\!]$.

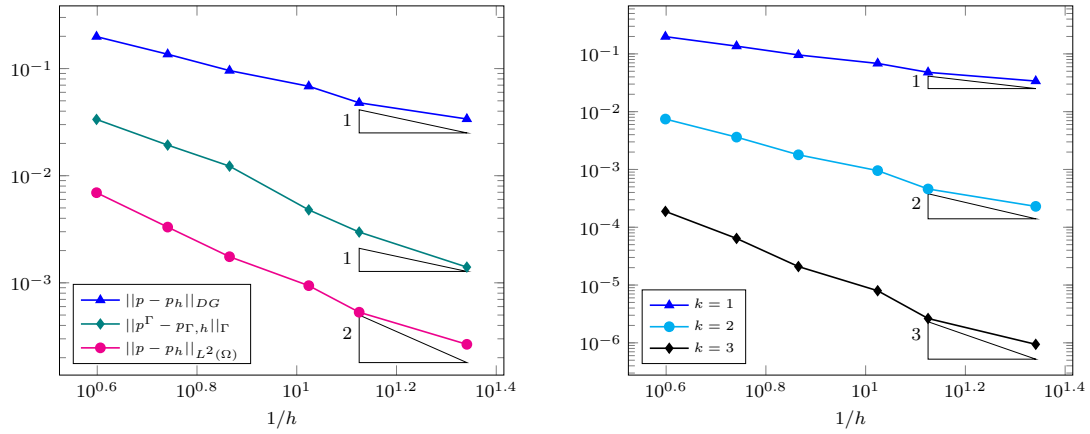

(a) Bulk and fracture $k = 1$ (b) Bulk $k = 1, 2, 3$

Figure 2.4: Example 2: (a) Computed errors in the bulk and in the fracture as a function of the inverse of the mesh size (loglog scale) with polynomial degree $k = 1$. (b) Computed errors $||p - p_h||_{DG}$ in the bulk for polynomial degrees $k = 1, 2, 3$.

Figure 2.4(a) shows the computed errors $||p - p_h||_{DG}$ for the bulk problem and the corresponding computed errors $||p_\Gamma - p_{\Gamma,h}||_\Gamma$ in the fracture. The results have been obtained taking the polynomial degree $k = 1$ for both the bulk and fracture problems. As predicted from our theoretical error bounds, a convergence of order 1 is clearly observed

for both $||p - p_h||_{DG}$ and $||p_\Gamma - p_{\Gamma,h}||_\Gamma$. Moreover from Figure 2.4(a) one can clearly see that also in this test case one order of convergence is gained if we compute the error $||p - p_h||_{L^2(\Omega)}$. In Figure 2.4(b) we plot the computed errors in the bulk $||p - p_h||_{DG}$ for polynomial degrees $k_E = k = 1, 2, 3$. The observed convergence rate is of $\mathcal{O}(h^k)$.

2.5.3 Example 3

In this third example we consider the circular fracture $\Gamma = \{(x, y) \in \Omega : \ x^2 + y^2 = R\}$, with $R = 0.7$ included in the domain $\Omega = (0, 1)^2$. We choose the exact solutions in the bulk and in the fracture as follows

$$p = \begin{cases} \frac{x^2+y^2}{R^2} & \text{in } \Omega_1, \\ \frac{x^2+y^2}{2R^2} + \frac{3}{R}\eta_\Gamma + \frac{1}{2} & \text{in } \Omega_2, \end{cases} \qquad p_\Gamma = 1 + \frac{7}{4}\frac{\eta_\Gamma}{R},$$

so that they satisfy the coupling conditions (2.6a)-(2.6b) with $\xi = \frac{3}{4}$ and $\boldsymbol{\nu} = \mathbf{I}$. The source term is chosen as

$$f = \begin{cases} -\frac{4}{R^2} & \text{in } \Omega_1, \\ -\frac{2}{R^2} & \text{in } \Omega_2 \end{cases} \qquad \ell_\Gamma f_\Gamma = \frac{1}{R}.$$

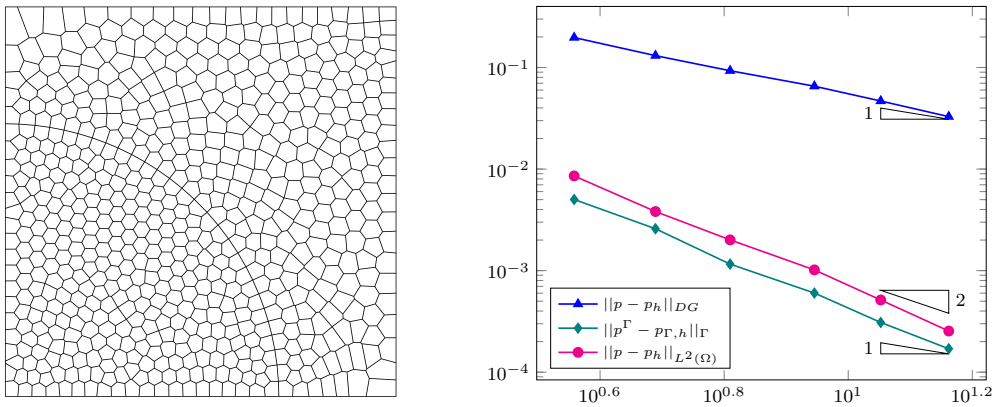

(a) Mesh grid (b) Errors

Figure 2.5: Example 3: (a) Example of the polygonal mesh grid with circular fracture. (b) Computed errors as a function of inverse of the mesh size (loglog scale) with polynomial degree $k = 1$.

Figure 2.5(a) shows an example of mesh grid employed in this set of experiments. One can see that here the fracture is approximated by a polygonal line.

In Figure 2.5(b) we report the computed errors $||p - p_h||_{DG}$ and $||p^\Gamma - p_{\Gamma,h}||_\Gamma$ as a function of $1/h$ for $k_E = k = 1$ (we disregard the variational crime coming from the polygonal approximation of the circular fracture). The numerical experiments validate the theoretical estimates, as a linear decay of the error is clearly observed.

2.5.4 Example 4

We consider the domain $\Omega = (0,1)^2$ and the fracture $\Gamma = \{(x,y) \in \Omega : \quad x = 0.5\}$. Following [65], we choose the exact solutions in the bulk and in the fracture as follows

$$p = \begin{cases} \sin(4x)\cos(\pi y) & \text{if } x < 0.5, \\ \cos(4x)\cos(\pi y) & \text{if } x > 0.5, \end{cases} \qquad p_\Gamma = \frac{3}{4}[\cos(2) + \sin(2)]\cos(\pi y),$$

so that they satisfy the coupling conditions (2.6a)-(2.6b) with $\xi = \frac{3}{4}$ and $\boldsymbol{\nu} = \mathbf{I}$. We also choose the fracture thickness to be equal to $\ell_\Gamma = 0.25$ and the tangential and normal components of the permeability tensor in the fracture to be $\boldsymbol{\nu}_\Gamma^\tau = 1$ and $\nu_\Gamma^n = 1$, respectively. We impose Dirichlet boundary conditions on the whole $\partial\Omega$ and also on $\partial\Gamma$. Finally the source terms are chosen accordingly as

$$f = \begin{cases} \sin(4x)\cos(\pi y)(16 + \pi^2) & \text{if } x < 0.5, \\ \cos(4x)\cos(\pi y)(16 + \pi^2) & \text{if } x > 0.5, \end{cases} \quad f_\Gamma = \cos(\pi y)[\cos(2) + \sin(2)](4 + \frac{3}{16}\pi^2).$$

The exact solution in the bulk is shown in Figure 2.6(a). In Figure 2.6(b) we show the computed errors in the bulk and in the fracture for polynomial degree equal to 1 for both the bulk and fracture problems. In Figure 2.7(a) we report the errors $||p - p_h||_{DG}$ obtained with polynomial degrees $k_E = 1, 2, 3$ in the bulk and $k = 1$ in the fracture. We observe that for $k_E = 3$ the convergence rate is suboptimal. This is due to the fact that the polynomial degree in the fracture is not accurate enough. In fact, if we assume to know the exact solution p_Γ in the fracture and we solve the problem in the bulk, we recover the expected rates, as shown in Figure 2.7(b). This behaviour did not appear in the previous test cases, where the solution in the fracture was chosen to be constant.

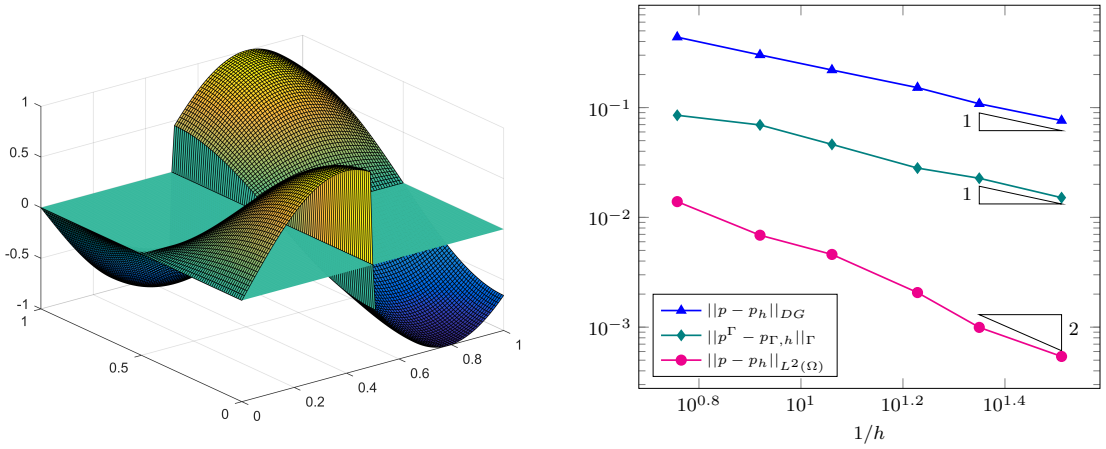

(a) Exact solution (b) Errors

Figure 2.6: Example 4: Exact solution in the bulk with the plane $x = y = 0$ (left) and Computed errors as a function of inverse of the mesh size (loglog scale) with polynomial degree $k = 1$ (right).

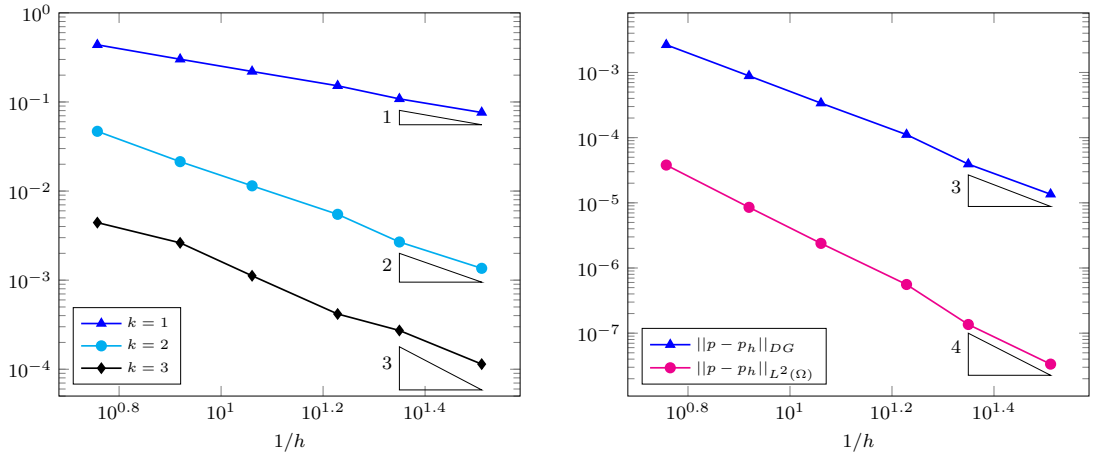

(a) (b)

Figure 2.7: Example 4: (a) Computed errors $||p - p_h||_{DG}$ in the bulk as a function of the inverse of the mesh size (loglog scale) for polynomial degrees $k = 1, 2, 3$. (b) Computed errors in the bulk with polynomial degree $k = 3$ and known fracture pressure.

2.5.5 Quarter five-spot problem

The quarter five-spot problem is often used to validate numerical schemes for the approximation of Darcy's flow, see for example [65, 92]. A five-spot is a standard technique used in petroleum engineering for oil recovery, where four injection wells are located at the corner of a square and one production well is located in its center. Fluid (typically water, steam or gas) is injected simultaneously through the four injection wells causing

the displacement of the oil toward the production well in the center. Since the problem is symmetric, we can consider only a quarter of this injection pattern, represented by the domain $\Omega = (0,1)^2$. The single injection well will be then located in $(0,0)$ and the production well in $(1,1)$. Their presence is included in the model via the source term

$$f(x) = 10.1\Big[\tan(200(0.2 - \sqrt{x^2+y^2})) - \tanh(200(0.2 - \sqrt{(x-1)^2+(y-1)^2}))\Big].$$

Moreover, we enforce *homogeneous* Neumann and Dirichlet boundary conditions, respectively, on $\partial\Omega_N = \{x = 0 \text{ or } y = 0\}$ and $\partial\Omega_D = \{x = 1 \text{ or } y = 1\}$. We also assume that the domain is cut by the fracture of equation $\Gamma = \{(x,y) \in \Omega : \ x + y = 1\}$ with thickness $\ell_\Gamma = 0.005$, and we let $f_\Gamma = 0$. Finally, we impose homogeneous Dirichlet boundary conditions on $\partial\Gamma$. The domain configuration is reported in Figure 2.8(a) for clarity. We aim, in particular, at investigating the effect of large and small permeability in the fracture to the overall flow. We perform two numerical experiments:

1. **Permeable** fracture: we choose $\nu_\Gamma^n = 1$ and $\boldsymbol{\nu}_\Gamma^\tau = 100$.
2. **Impermeable** fracture: we choose $\nu_\Gamma^n = 10^{-2}$ and $\boldsymbol{\nu}_\Gamma^\tau = 1$.

In both cases we let the bulk permeability tensor $\boldsymbol{\nu} = \mathbf{I}$ and we solve the problem choosing a polygonal mesh with $h = 7.5 \cdot 10^{-2}$ and the polynomial degree $k_E = 2$ in the bulk and $k = 1$ in the fracture.
The bulk pressures obtained are shown in Figure 2.9. As expected, in both cases the bulk pressure has a peak in correspondence of injection well and it decreases going toward the production well. In the permeable case, the decrease is continuous, while in the impermeable case we can observe a clear jump of the pressure across the fracture. This behaviour is better captured in Figure 2.8(b), where we have plotted the trend of the pressure along the line $x = y$ in both cases. Our qualitative results are in agreement with those obtained in [65].

2.5.6 Immersed fractures

We now investigate the capability of our discretization method to deal with *immersed* fractures. We take as a reference [3], where the model developed in [101] has been extended to fully immersed fractures. In particular, our set of equations (2.8) needs to be supplemented with a condition on the boundary $\partial\Gamma$ immersed in the porous medium.

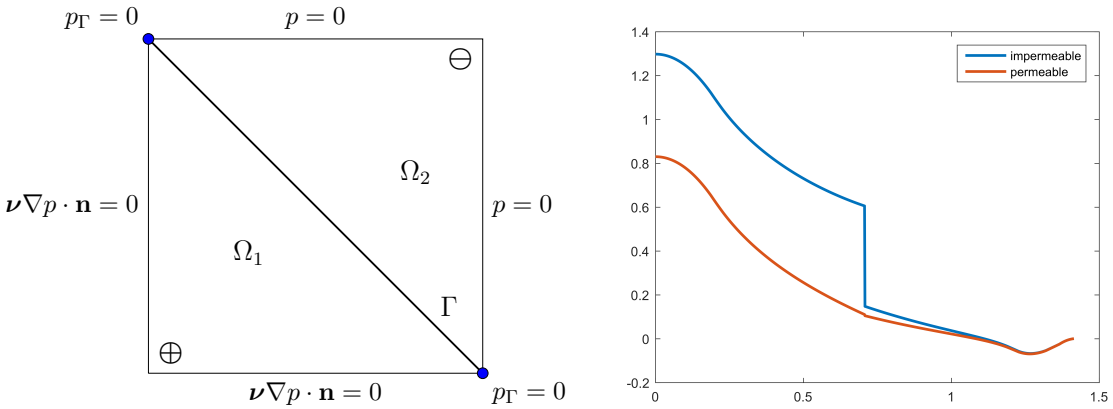

(a) (b)

Figure 2.8: Quarter five-spot: The subdomains Ω_1 and Ω_2 separated by the fracture Γ and boundary conditions (left) and pressure in the bulk along the line $x = y$ (right).

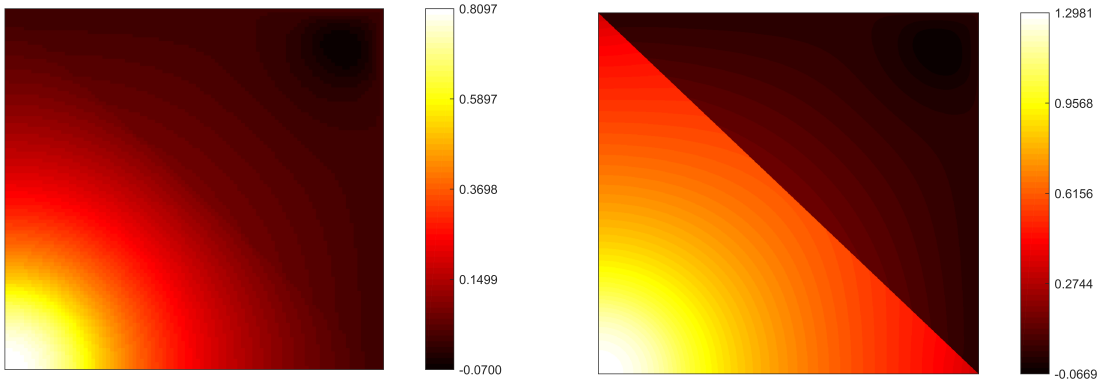

(a) Permeable fracture (b) Impermeable fracture

Figure 2.9: Quarter five-spot: Pressure in the bulk for the quarter-five spot problem with permeable (left) and impermeable (right) fracture.

Following [3], we will we assume that the mass transfer across the immersed tip can be neglected, imposing the Neumann boundary condition $\boldsymbol{\nu}_\Gamma^T \nabla_\tau p_\Gamma \cdot \boldsymbol{\tau} = 0$ on $\partial\Gamma$. On the fracture tip intersecting the bulk boundary, i.e., $\partial\Gamma \cap \partial\Omega$, we impose boundary conditions coincident with those imposed on $\partial\Omega$.

We perform two sets of numerical experiments, that were already proposed in [3]. The aim is that of investigating the flow depending on the physical properties of the fractures (permeable, impermeable), first in the case of a single fracture, and then in the more complex situation of a network of partially immersed fractures. Our results are in perfect agreement with those obtained in [3], thus showing that our method can be easily extended

to the treatment of more complex and realistic situations.
For all the experiments we take as computational domain $\Omega = (0,1)^2$ and we assume that the bulk permeability tensor is isotropic, i.e., $\boldsymbol{\nu} = \mathrm{Id}$. Moreover we take the forcing terms $f = f_\Gamma = 0$, so that the flow is only generated by boundary conditions. Finally, we choose the parameter $\xi = 0.55$. Our results have been obtained with cartesian grids with approximately the same number of elements as those employed in [3]. Note that the grids are aligned with the fractures so that the immersed tips coincide with one of the mesh vertices.

Single partially immersed fracture

In the first experiment we study the case when the porous medium is cut by the fracture $\Gamma = \{(x,y) \in (0,1)^2 : x = 0.5, y \geq 0.5\}$ that is partially immersed in the domain and has constant aperture $\ell_\Gamma = 0.001$. We consider two different configurations where we vary the boundary conditions and the permeability of the fracture:

1. **Permeable** fracture: we choose $\nu_\Gamma^n = 100$ and $\boldsymbol{\nu}_\Gamma^\tau = 10^6$ and impose Dirichlet boundary condition on the whole $\partial\Omega$ as described in Figure 2.10(a).

2. **Impermeable** fracture: we choose $\nu_\Gamma^n = \boldsymbol{\nu}_\Gamma^\tau = 10^{-7}$ and impose mixed boundary conditions on $\partial\Omega$ as in Figure 2.10(b) .

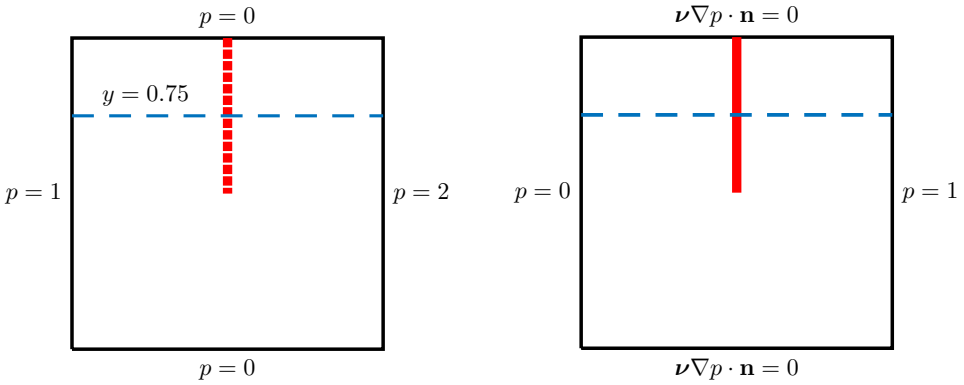

(a) Permeable fracture (b) Impermeable fracture

Figure 2.10: Single immersed fracture: Configurations and boundary conditions for the permeable test case (left) with $\boldsymbol{\nu}_\Gamma^\tau = 10^6$, $\nu_\Gamma^n = 10^2$, and the impermeable test case (right) with $\boldsymbol{\nu}_\Gamma^\tau = \nu_\Gamma^n = 10^{-7}$.

The results obtained with a mesh of 16128 elements are shown in Figure 2.11. In both cases, on the left part of the figure, we show the pressure field in the bulk (where the

intensity of the color increases with the increasing of the pressure) together with the streamlines of the Darcy's velocity. In the middle, we report the behaviour of the bulk pressure along the line $y = 0.75$. Finally, on the right we plot the pressure field in the fracture. As expected, in the impermeable case we can observe a clear jump of the bulk pressure across the fracture, that it is not present in the permeable case. The results presented in Figure 2.11 are in agreement with those of [3].

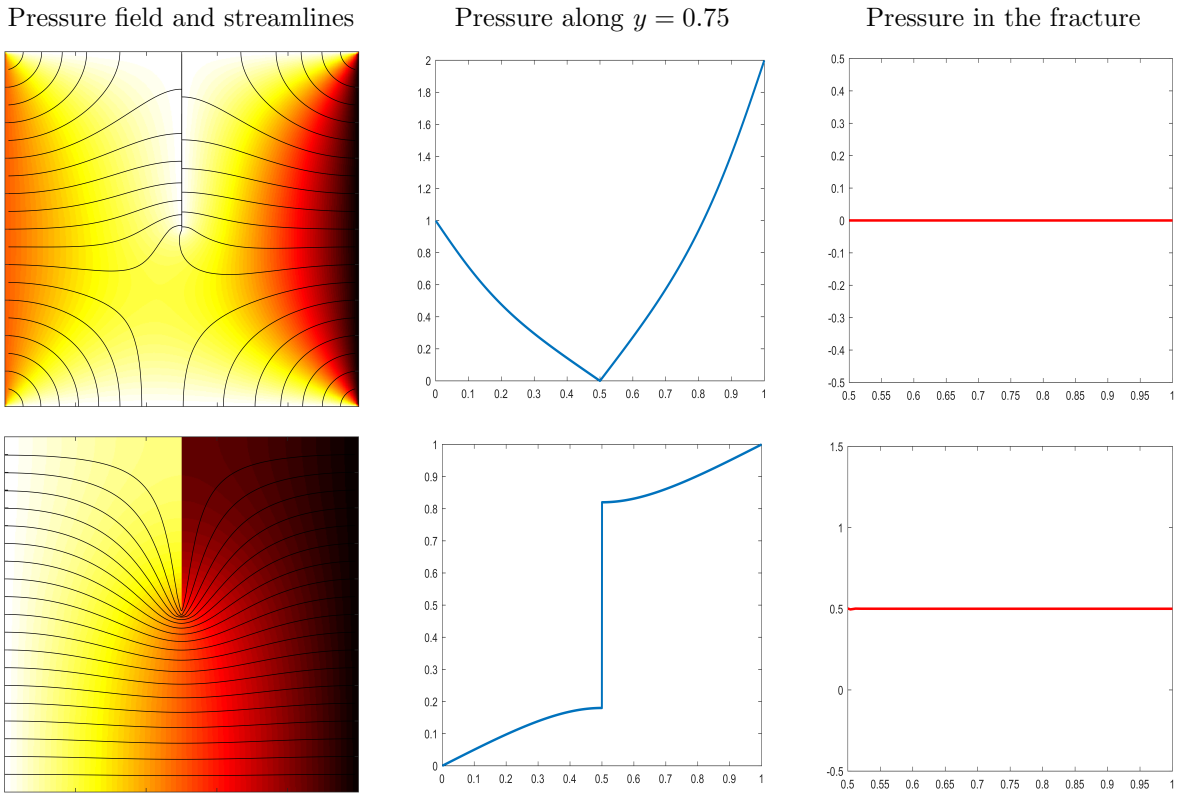

Figure 2.11: Single immersed fracture: permeable case (top) and impermeable case (bottom).

Network of partially immersed fractures

In the second experiment we consider a network of four partially immersed fractures of aperture $\ell_\Gamma = 0.01$, namely $\Gamma_1 = \{(x, y) \in (0, 1)^2 : x \geq 0.3, y = 0.2\}$, $\Gamma_2 = \{(x, y) \in (0, 1)^2 : x \leq 0.7, y = 0.4\}$, $\Gamma_3 = \{(x, y) \in (0, 1)^2 : x \geq 0.3, y = 0.6\}$, $\Gamma_4 = \{(x, y) \in (0, 1)^2 : x \leq 0.7, y = 0.8\}$. The fractures Γ_2 and Γ_4 are impermeable ($\boldsymbol{\nu}_\Gamma^\tau = \nu_\Gamma^n = 10^{-2}$), while Γ_1 and Γ_3 are partially permeable ($\nu_\Gamma^n = 10^{-2}$, $\boldsymbol{\nu}_\Gamma^\tau \in \{100, 1\}$). We consider two different configurations, varying the value of the permeability $\boldsymbol{\nu}_\Gamma^\tau$ on the

partially permeable fractures Γ_1 and Γ_3 and the boundary conditions as illustrated in Figure 2.12(a).

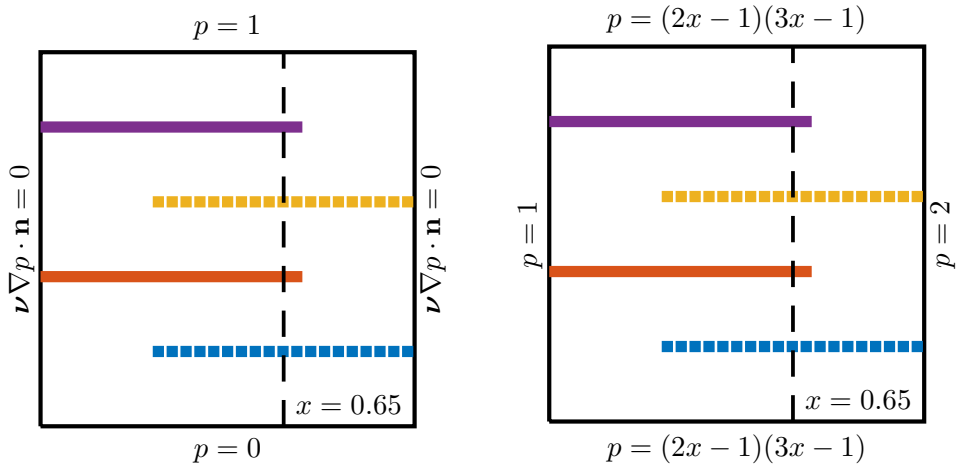

(a) Configuration 1: $\boldsymbol{\nu}_\Gamma^\tau = 100$ on Γ_1, Γ_3 (b) Configuration 2: $\boldsymbol{\nu}_\Gamma^\tau = 1$ on Γ_1, Γ_3

Figure 2.12: Network of immersed fractures: Configurations and boundary condition for the two test cases.

In Figure 2.13 we show the results obtained for the two test cases with a mesh of 26051 elements. In particular, we report the pressure field in the bulk with the streamlines of the velocity (left), the value of the bulk pressure along the line $x = 0.65$ (middle) and the pressure field inside the four fractures (right). Again, we can see a perfect agreement between our results and those obtained in [3].

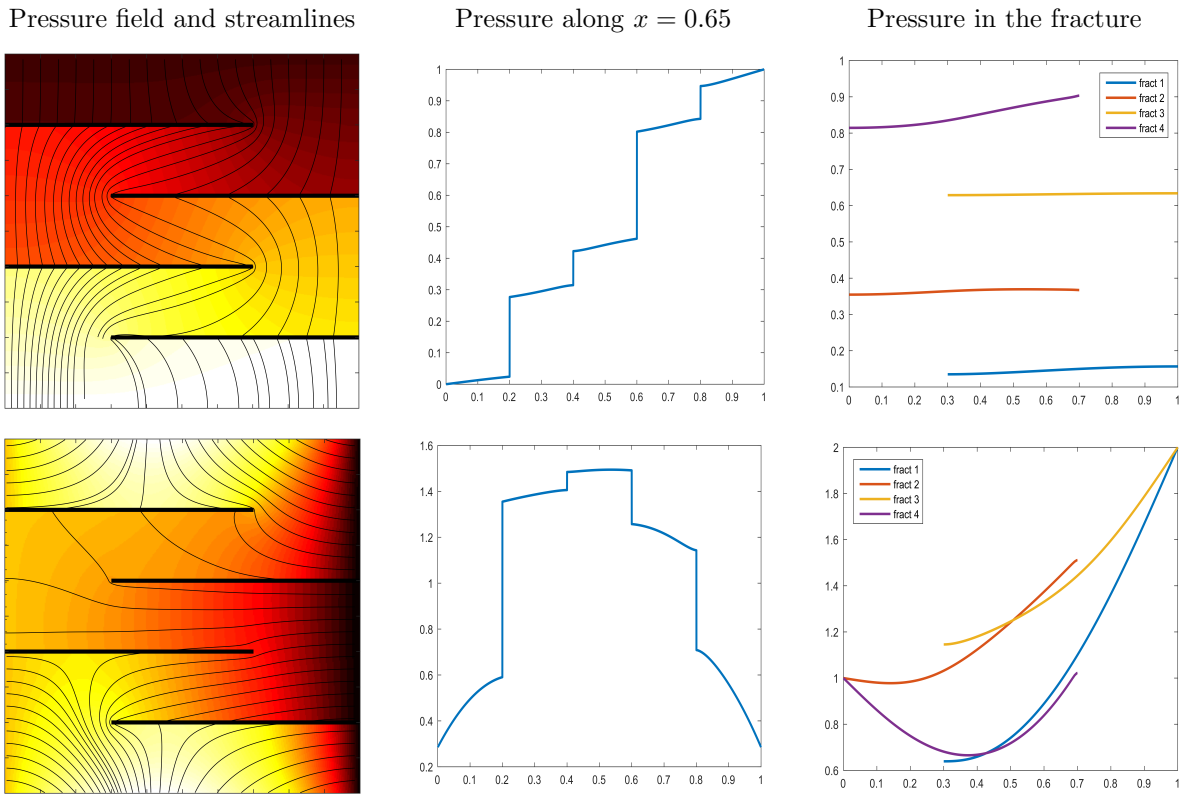

Figure 2.13: Network of immersed fractures: first configuration (top) and second configuration (bottom).

3 | Unified analysis of polyDG approximation of flows in fractured porous media

The aim of this chapter is to extend the results presented in Chapter 2, where the mathematical model and its discretization based on PolyDG methods were in a primal setting (with pressure as only unknown) for both the bulk and fracture problems. Indeed, when dealing with the approximation of Darcy's flow, one may also resort to a mixed approach, where the flow is described through an additional unknown representing the (averaged) velocity of the fluid. This variable, often referred to as Darcy's velocity, is of primary interest in many engineering applications [105, 53], so that the mixed setting is often preferred to the primal one, which may only return velocity after post-processing the computed pressure, thus entailing loss of accuracy. On the other hand, the primal approach is easier to solve, featuring a smaller number of degrees of freedom. For this reason, our aim is to design a unified setting where, according to the desired approximation properties of the model, one may resort to either a primal or mixed approximation for the problem in the bulk, as well as to a primal or mixed approximation for the problem in the fracture. In particular, for the primal discretizations we employ the Symmetric Interior Penalty discontinuous Galerkin method [119, 26], whereas for the mixed discretizations we employ the local DG (LDG) method of [72], both in their generalization to polytopic grids [61, 59, 6, 58, 60]. Our main reference for the design of such setting is the work by Arnold, Brezzi et al. [27], where a *unified* analysis of all DG methods present in the literature is performed. This framework is based on the flux-formulation, where the so-called numerical fluxes are introduced on elemental interfaces as approximations of the exact solution. Different choices of the numerical fluxes affect the stability and the

accuracy of the DG method and provide conservation properties of desired quantities such as, for example, mass, momentum, and energy [60]. In the particular context of flow in fractured porous media, we also show that the coupling conditions between bulk and fracture problems may be imposed through a suitable definition of the numerical fluxes on the fracture faces. Such an abstract setting allows to analyse theoretically at the same time all the possible combinations of primal-primal, mixed-primal, primal-mixed and mixed-mixed formulations for the bulk and fracture problems, respectively.
The chapter is organized as follows. In Section 3.1 we introduce the model problem; its weak formulation is discussed in Section 3.2. The discretization based on employing PolyDG methods is presented, in the unified setting of [27], in Section 3.3. In Section 3.4, we address the problem of stability and prove that all formulations, namely primal-primal (PP), mixed-primal (MP), primal-mixed (PM) and mixed-mixed (MM) are well-posed. The corresponding error analysis is presented in Section 3.5. Several numerical tests, focusing, for the sake of brevity, on the mixed-primal (MP) case, are presented in Section 3.6 to confirm the theoretical bounds. Moreover, we assess the capability of the method of handling more complicated geometries, presenting some test cases featuring networks of partially immersed fractures.

The results presented in this chapter are original and are contained in [14].

3.1 Model problem

We recall that we are adopting the mathematical model of [101], which we have introduced in Section 2.1. We consider again the case where a porous medium is cut by a single, non immersed fracture. However, in this chapter, we deal with the governing equations in their mixed form. This means that, for both the problem in the bulk and in the fracture, we will introduce an auxiliary vector-valued variable, called Darcy's velocity. This quantity is of primary interest in many engineering applications, such as oil recovery and groundwater pollution modelling. Indeed, in these cases, in order to be effective, the simulation of the phenomenon requires very accurate approximation of the velocities of the involved fluids.
As in the previous chapter, the porous matrix is represented by the open, bounded, convex and polygonal/polyhedral domain $\Omega \subset \mathbb{R}^d$, $d = 2, 3$ and the fracture is described

by the $(d-1)$-dimensional $\mathcal{C}^\infty$ manifold (with no curvature) $\Gamma \subset \mathbb{R}^{d-1}$, $d = 2, 3$. Since we are assuming that Γ is not immersed, it separates Ω into the two connected disjoint subdomains Ω_1 and Ω_2.

We now introduce the governing equations in mixed form. In the bulk, in each domain Ω_i, $i = 1, 2$, the motion of an incompressible fluid with pressure p_i and velocity $\mathbf{u}_i$ may be described by:

$$\begin{cases} \mathbf{u}_i = \boldsymbol{\nu}_i \nabla p_i & \text{in } \Omega_i, \\ -\nabla \cdot \mathbf{u}_i = f_i & \text{in } \Omega_i, \\ p_i = g_{D,i} & \text{on } \partial\Omega_{D,i}, \\ \mathbf{u}_i \cdot \mathbf{n}_i = 0 & \text{on } \partial\Omega_{N,i}, \end{cases} \tag{3.1}$$

where we have adopted the same notation as in the previous Chapter, so that $f \in L^2(\Omega)$ represents a source term, $g_D \in H^{1/2}(\partial\Omega_D)$ is the Dirichlet boundary datum and $\boldsymbol{\nu} = \boldsymbol{\nu}(x) \in \mathbb{R}^{d\times d}$ is the bulk permeability tensor, which we still assume to be symmetric, positive definite, uniformly bounded from below and above and with entries that are bounded, piecewise continuous real-valued functions.

On the manifold Γ representing the fracture, we formulate a reduced version of Darcy's law in the tangential direction and assume that the fracture permeability tensor $\boldsymbol{\nu}_\Gamma$, has a block-diagonal structure when written in its normal and tangential components and that $\boldsymbol{\nu}_\Gamma^\tau \in \mathbb{R}^{(d-1)\times(d-1)}$ is positive definite, uniformly bounded. Moreover, $\boldsymbol{\nu}_\Gamma$ satisfies the same regularity assumptions as those satisfied by the bulk permeability $\boldsymbol{\nu}$. Denoting by p_Γ and $\mathbf{u}_\Gamma$ the fracture pressure and velocity, the governing equations for the fracture flow are

$$\begin{cases} \mathbf{u}_\Gamma = \boldsymbol{\nu}_\Gamma^\tau \ell_\Gamma \nabla_\tau p_\Gamma & \text{in } \Gamma, \\ -\nabla_\tau \cdot \mathbf{u}_\Gamma = \ell_\Gamma f_\Gamma - [\![\mathbf{u}]\!] & \text{in } \Gamma, \\ p_\Gamma = g_\Gamma & \text{on } \partial\Gamma_D, \\ \mathbf{u}_\Gamma \cdot \boldsymbol{\tau} = 0 & \text{on } \partial\Gamma_N, \end{cases} \tag{3.2}$$

where $f_\Gamma \in L^2(\Gamma)$, $g_\Gamma \in H^{1/2}(\partial\Gamma)$, $\boldsymbol{\tau}$ is vector in the tangent plane of Γ normal to $\partial\Gamma$ and ∇_τ and $\nabla_\tau\cdot$ denote the tangential gradient and divergence operators, respectively.

Finally, we close the model providing the interface conditions in mixed form:

$$-\{\mathbf{u}\} \cdot \mathbf{n}_\Gamma = \beta_\Gamma [\![p]\!] \cdot \mathbf{n}_\Gamma \qquad \text{on } \Gamma, \tag{3.3a}$$

$$-[\![\mathbf{u}]\!] = \alpha_\Gamma(\{p\} - p_\Gamma) \qquad \text{on } \Gamma, \tag{3.3b}$$

where we recall that $\beta_\Gamma = \frac{1}{2\eta_\Gamma}$ and $\alpha_\Gamma = \frac{2}{\eta_\Gamma(2\xi-1)}$ with $\eta_\Gamma = \frac{\ell_\Gamma}{\nu_\Gamma^n}$ and that $\mathbf{n}_\Gamma$ denotes the normal unit vector on Γ with a fixed orientation from Ω_1 to Ω_2. We also recall that the conditions depend on the parameter $\xi \neq \frac{1}{2}$ that will be chosen later on.
In conclusion, the coupled bulk-fracture model problem in mixed form is the following:

$$\begin{cases} \mathbf{u}_i = \boldsymbol{\nu}_i \nabla p_i & \text{in } \Omega_i, \\ -\nabla \cdot \mathbf{u}_i = f_i & \text{in } \Omega_i, \\ p_i = g_{D,i} & \text{on } \gamma_{D,i}, \\ \mathbf{u}_i \cdot \mathbf{n}_i = 0 & \text{on } \gamma_{N,i} \\ \mathbf{u}_\Gamma = \boldsymbol{\nu}_\Gamma^\tau \ell_\Gamma \nabla_\tau p_\Gamma & \text{in } \Gamma, \\ -\nabla_\tau \cdot \mathbf{u}_\Gamma = \ell_\Gamma f_\Gamma - [\![\mathbf{u}]\!] & \text{in } \Gamma, \\ p_\Gamma = g_\Gamma & \text{on } \partial\Gamma_D, \\ \mathbf{u}_\Gamma \cdot \boldsymbol{\tau} = 0 & \text{on } \partial\Gamma_N, \\ -\{\mathbf{u}\} \cdot \mathbf{n}_\Gamma = \beta_\Gamma [\![p]\!] \cdot \mathbf{n}_\Gamma & \text{on } \Gamma, \\ -[\![\mathbf{u}]\!] = \alpha_\Gamma(\{p\} - p_\Gamma) & \text{on } \Gamma. \end{cases} \tag{3.4}$$

3.2 Weak formulation

In this section we introduce the weak formulation of our model problem (3.4) and prove its well-posedness. We start with the introduction of the functional setting.

3.2.1 Functional setting

Here, we introduce the functional spaces for our weak formulation. For the bulk pressure and velocity, we introduce the spaces $M^b = L^2(\Omega)$ and $\mathbf{V}^b = \{\mathbf{v} \in H_{\mathrm{div}}(\Omega) : [\![\mathbf{v}]\!]|_\Gamma \in L^2(\Gamma), \{\mathbf{v}\}|_\Gamma \in [L^2(\Gamma)]^d, \mathbf{v} \cdot \mathbf{n}|_{\partial\Omega_N} = 0\}$, and equip the space $\mathbf{V}^b$ with the norm $||\mathbf{v}||^2_{\mathbf{V}^b} = ||\mathbf{v}||^2_{L^2(\Omega)} + ||\nabla \cdot \mathbf{v}||^2_{L^2(\Omega)} + ||[\![\mathbf{v}]\!]||^2_{L^2(\Gamma)} + ||\{\mathbf{v}\}||^2_{L^2(\Gamma)}$. Similarly, for the fracture pressure and velocity we define the spaces $M^\Gamma = L^2(\Gamma)$ and $\mathbf{V}^\Gamma = \{\mathbf{v}_\Gamma \in H_{\mathrm{div},\tau}(\Gamma) : \mathbf{v}_\Gamma \cdot \boldsymbol{\tau}|_{\partial\Gamma} = 0\}$. The norm on $\mathbf{V}^\Gamma$ is given by $||\mathbf{v}_\Gamma||^2_{\mathbf{V}^\Gamma} = ||\mathbf{v}_\Gamma||^2_{L^2(\Gamma)} + ||\nabla_\tau \cdot \mathbf{v}_\Gamma||^2_{L^2(\Gamma)}$. Finally, we define the global spaces for the pressure and the velocity as $M = M^b \times M^\Gamma$ and $\mathbf{W} = \mathbf{V}^b \times \mathbf{V}^\Gamma$, equipped with the canonical norms for product spaces. In order to deal with non-homogeneous boundary conditions, we also introduce the affine spaces $V_g^b = \mathcal{L}_g + \mathbf{V}^b$ and $V_g^\Gamma = \mathcal{L}_{g_\Gamma} + \mathbf{V}^\Gamma$, where $\mathcal{L}_g \in H_{\mathrm{div}}(\Omega)$ and

$\mathcal{L}_{g_\Gamma} \in H_{\mathrm{div},\tau}(\Gamma)$ are liftings of the boundary data g and g_Γ, respectively. We can then define the global space $\mathbf{W}_g = \mathbf{V}_g^b \times \mathbf{V}_g^\Gamma$.

3.2.2 Weak problem

We can now formulate problem (3.4) in weak form as follows: Find $(\mathbf{u}, \mathbf{u}_\Gamma) \in \mathbf{W}_g$ and $(p, p_\Gamma) \in M$ such that

$$\begin{cases} A((\mathbf{u}, \mathbf{u}_\Gamma), (\mathbf{v}, \mathbf{v}_\Gamma)) + B((\mathbf{v}, \mathbf{v}_\Gamma), (p, p_\Gamma)) = F^{\mathbf{u}}(\mathbf{v}, \mathbf{v}_\Gamma) \\ -B((\mathbf{u}, \mathbf{u}_\Gamma), (q, q_\Gamma)) = F^p(q, q_\Gamma) \end{cases} \tag{3.5}$$

where the bilinear form $A(\cdot,\cdot) : \mathbf{W}_g \times \mathbf{W}_g \to \mathbb{R}$ is defined as $A((\mathbf{u}, \mathbf{u}_\Gamma), (\mathbf{v}, \mathbf{v}_\Gamma)) = a(\mathbf{u}, \mathbf{v}) + a_\Gamma(\mathbf{u}_\Gamma, \mathbf{v}_\Gamma)$ with

$$\begin{aligned} a(\mathbf{u}, \mathbf{v}) &= \int_\Omega \boldsymbol{\nu}^{-1}\mathbf{u} \cdot \mathbf{v} + \int_\Gamma \frac{1}{\alpha_\Gamma}[\![\mathbf{u}]\!][\![\mathbf{v}]\!] + \int_\Gamma \frac{1}{\beta_\Gamma}\{\mathbf{u}\} \cdot \{\mathbf{v}\}, \\ a_\Gamma(\mathbf{u}_\Gamma, \mathbf{v}_\Gamma) &= \int_\Gamma (\boldsymbol{\nu}_\Gamma^\tau \ell_\Gamma)^{-1}\mathbf{u}_\Gamma \cdot \mathbf{v}_\Gamma, \end{aligned}$$

and the bilinear form $B(\cdot,\cdot) : \mathbf{W}_g \times M \to \mathbb{R}$ is defined as $B((\mathbf{v}, \mathbf{v}_\Gamma), (q, q_\Gamma)) = b(\mathbf{v}, q) + b_\Gamma(\mathbf{v}_\Gamma, q_\Gamma) + d(\mathbf{v}, q_\Gamma)$, with

$$b(\mathbf{v}, q) = \int_\Omega \nabla \cdot \mathbf{v}\, q, \qquad b_\Gamma(\mathbf{v}_\Gamma, q_\Gamma) = \int_\Gamma \nabla_\tau \cdot \mathbf{v}_\Gamma\, q_\Gamma, \qquad d(\mathbf{v}, q_\Gamma) = -\int_\Gamma [\![\mathbf{v}]\!] q_\Gamma.$$

Finally the linear operators $F^{\mathbf{u}}(\cdot) : \mathbf{W}_g \to \mathbb{R}$ and $F^p(\cdot) : M \to \mathbb{R}$ are defined as

$$F^{\mathbf{u}}(\mathbf{v}, \mathbf{v}_\Gamma) = \int_{\partial\Omega} g\mathbf{v} \cdot \mathbf{n} + \int_{\partial\Gamma} g_\Gamma \mathbf{v}_\Gamma \cdot \boldsymbol{\tau}, \qquad F^p(q, q_\Gamma) = \int_\Omega fq + \int_\Gamma \ell_\Gamma f_\Gamma q_\Gamma.$$

Next, we prove that formulation (3.5) is well-posed. For the sake of simplicity, we will assume that homogeneous Dirichlet boundary conditions are imposed for both the bulk and fracture problems, i.e., $g_{D,i} = 0$, $i = 1; 2$, and $g_\Gamma = 0$ and that the domain and fracture are smooth enough. The extension to the general non-homogeneous case is straightforward. Note that the existence and uniqueness of the problem can be proven only under the condition that the parameter $\xi > 1/2$.

Theorem 3.2.1. *Suppose that $\xi > 1/2$. Then problem* (3.5) *admits a unique solution.*

Proof. For the proof we follow the technique of [101]. First, we define the subspace of $\mathbf{W}$, $\widehat{\mathbf{W}} = \{(\mathbf{v}, \mathbf{v}_\Gamma) \in \mathbf{W} : B((\mathbf{v}, \mathbf{v}_\Gamma), (q, q_\Gamma)) = 0 \ \forall (q, q_\Gamma) \in M\}$. To show existence and uniqueness of the solution of (3.5), we only need to show that $A(\cdot, \cdot)$ is $\widehat{\mathbf{W}}$-elliptic and that $B(\cdot, \cdot)$ satisfies the inf-sup condition, that is

$$\inf_{(\mathbf{v},\mathbf{v}_\Gamma)\in\widehat{\mathbf{W}}} \frac{A((\mathbf{v}, \mathbf{v}_\Gamma), (\mathbf{v}, \mathbf{v}_\Gamma))}{||(\mathbf{v}, \mathbf{v}_\Gamma)||^2_{\mathbf{W}}} \gtrsim 1, \qquad \inf_{(q,q_\Gamma)\in M} \sup_{(\mathbf{v},\mathbf{v}_\Gamma)\in\mathbf{W}} \frac{B((\mathbf{v}, \mathbf{v}_\Gamma), (q, q_\Gamma))}{||(q, q_\Gamma)||_M ||(\mathbf{v}, \mathbf{v}_\Gamma)||_{\mathbf{W}}} \gtrsim 1.$$

First, we prove that $A(\cdot, \cdot)$ is $\widehat{\mathbf{W}}$-elliptic. Since for elements in $(\mathbf{v}, \mathbf{v}_\Gamma) \in \widehat{\mathbf{W}}$ we have $\nabla \cdot \mathbf{v} = 0$ in $L^2(\Omega)$ and $\nabla_\tau \cdot \mathbf{v}_\Gamma = [\![\mathbf{v}]\!]|_\Gamma$ in $L^2(\Gamma)$, the norm $||(\mathbf{v}, \mathbf{v}_\Gamma)||_{\mathbf{W}}$ is equivalent to $||\mathbf{v}||^2_{L^2(\Omega)} + ||\mathbf{v}_\Gamma||^2_{L^2(\Gamma)} + ||[\![v]\!]||^2_{L^2(\Gamma)} + ||\{\mathbf{v}\}||^2_{L^2(\Gamma)}$. Owing to the regularity properties of the permeability tensors $\boldsymbol{\nu}$ and $\boldsymbol{\nu}_\Gamma$, this implies that

$$A((\mathbf{v}, \mathbf{v}_\Gamma), (\mathbf{v}, \mathbf{v}_\Gamma)) \gtrsim ||(\mathbf{v}, \mathbf{v}_\Gamma)||^2_{\mathbf{W}}.$$

Note that the hidden constant also depends on the parameter α_Γ, and that we need to assume $\alpha_\Gamma > 0$, or, equivalently, $\xi > 1/2$, for the inequality to hold true.

To show that B satisfies the inf-sup condition, given $(q, q_\Gamma) \in M$, we construct, exploiting the adjoint problem, $(\mathbf{v}, \mathbf{v}_\Gamma) \in \mathbf{W}$ such that $B((\mathbf{v}, \mathbf{v}_\Gamma), (q, q_\Gamma)) = ||(q, q_\Gamma)||^2_M$ and $||(\mathbf{v}, \mathbf{v}_\Gamma)||_{\mathbf{W}} \lesssim ||(q, q_\Gamma)||_M$. Given $(q, q_\Gamma) \in M$, let (ϕ, ϕ_Γ) be the solution of

$$\begin{cases} -\Delta\phi = q, & \text{on } \Omega \\ \phi = 0, & \text{on } \partial\Omega \end{cases} \qquad \text{and} \qquad \begin{cases} -\Delta_\tau\phi_\Gamma = q_\Gamma, & \text{on } \Gamma \\ \phi_\Gamma = 0, & \text{on } \partial\Gamma. \end{cases}$$

If we set $\mathbf{v} = (\mathbf{v}_1, \mathbf{v}_2)$ with $\mathbf{v}_i = -\nabla\phi|_{\Omega_i}$, $i = 1, 2$, and $\mathbf{v}_\Gamma = -\nabla_\tau\phi_\Gamma$, we obtain $\nabla \cdot \mathbf{v} = q$, $\nabla_\tau \cdot \mathbf{v}_\Gamma = q_\Gamma$ and $[\![\mathbf{v}]\!]|_\Gamma = 0$, since $\mathbf{v} \in H^1(\Omega)$. This implies that $(\mathbf{v}, \mathbf{v}_\Gamma) \in \mathbf{W}$ and $B((\mathbf{v}, \mathbf{v}_\Gamma), (q, q_\Gamma)) = ||q||^2_{L^2(\Omega)} + ||q_\Gamma||^2_{L^2(\Gamma)} = ||(q, q_\Gamma)||^2_M$. Finally, from elliptic regularity, we have

$$\begin{aligned} ||(\mathbf{v}, \mathbf{v}_\Gamma)||^2_{\mathbf{W}} &= ||\nabla\phi||^2_{L^2(\Omega)} + ||\nabla_\tau\phi_\Gamma||^2_{L^2(\Gamma)} + ||q||^2_{L^2(\Omega)} + ||q_\Gamma||^2_{L^2(\Gamma)} + ||\{\nabla\phi\}||^2_{L^2(\Gamma)} \\ &\lesssim ||q||^2_{L^2(\Omega)} + ||q_\Gamma||^2_{L^2(\Gamma)}, \end{aligned}$$

and this concludes the proof.

□

3.3 Numerical dicretization based on PolyDG methods

In this section we present a family of discrete formulations for the coupled bulk-fracture problem (3.5), which are based on Discontinuous Galerkin methods on polytopic grids. In particular, since we can choose to discretize the problem in the bulk and the one in the fracture either in their mixed or in their primal form, we derive four formulations that embrace all the possible combinations of primal-primal, mixed-primal, primal-mixed and mixed-mixed discretizations. The mixed discretizations will be based on the Local Discontinuous Galerkin method (LDG) [72, 64, 109], while the primal discretizations on the Symmetric Interior Penalty method (SIPDG) [26, 119], all supporting polytopic grids [61, 59, 6, 58, 60]. The derivation of our discrete formulations will be carried out following the same strategy as in [27], so that it will be based on the introduction of the *numerical fluxes*, which approximate the trace of the solutions on the boundary of each mesh element. In particular, the imposition of the coupling conditions (3.3a)-(3.3b) will be achieved through a proper definition of the numerical fluxes on the faces belonging to the fracture.

We consider meshes $\mathcal{T}_h$ that are aligned with the fracture Γ and we denote, as in Chapter 1, by $\mathcal{F}_h$ the set of all the faces of the mesh $\mathcal{T}_h$, that we can decompose in $\mathcal{F}_h = \mathcal{F}_h^I \cup \mathcal{F}_h^B \cup \Gamma_h$, where $\mathcal{F}_h^I$ is the set of interior faces not belonging to the fracture, $\mathcal{F}_h^B$ is the set of faces lying on the boundary of the domain $\partial\Omega$ (which can be further decomposed into $\mathcal{F}_h^B = \mathcal{F}_h^D \cup \mathcal{F}_h^N$) and Γ_h is the set of fracture faces. In particular, as already observed in Remark 5, the induced subdivision of the fracture Γ_h consists of the faces of the elements of $\mathcal{T}_h$ that share part of their boundary with the fracture, so that, according to the definition of $\mathcal{F}_h$ given in Section 1.1, Γ_h is made up of line segments when $d = 2$ and of triangles when $d = 3$. In the latter case, the triangles are not necessarily shape-regular and they may present hanging nodes, due to the fact that the sub-triangulations of each elemental interface is chosen independently from the others. For this reason, we here extend the concept of *interface* introduced in Section 1.1 also to the $(d-2)$-dimensional facets of elements in Γ_h, defined again as intersection of boundaries of two neighbouring elements. When $d = 2$, the interfaces reduce to points (see Figure 3.1), while when $d = 3$ they consists of line segments. Moreover, since we aim at employing DG methods also for the discretization of the problem in the fracture, we denote by $\mathcal{E}_{\Gamma,h}$

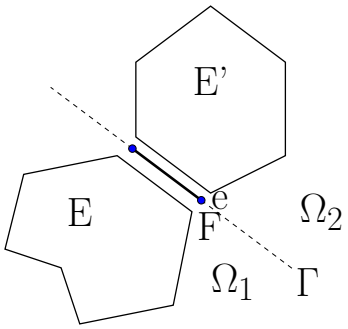

Figure 3.1: Example of two neighbouring elements of a polygonal bulk mesh aligned with the fracture and of the induced subdivision.

the set of all the interfaces (that we will also call edges) of the elements in Γ_h, and we write, accordingly to the previous notation, $\mathcal{E}_{\Gamma,h} = \mathcal{E}^I_{\Gamma,h} \cup \mathcal{E}^B_{\Gamma,h}$, with $\mathcal{E}^B_{\Gamma,h} = \mathcal{E}^D_{\Gamma,h} \cup \mathcal{E}^N_{\Gamma,h}$.
For the forthcoming stability and the error analyses, we will make use once again of the technical results for polytopic discretizations summarized in Chapter 1. In particular, we will assume that both the bulk meshes $\mathcal{T}_h$ and the fracture meshes Γ_h satisfy the polytopic-regularity Assumption 1.1.1 and the covering Assumption 1.1.2.
We have now all the ingredients to introduce the discrete formulation of model problem (3.5).

3.3.1 Discrete formulation

For simplicity in the forthcoming analysis, we will suppose that the permeability tensors $\boldsymbol{\nu}$ and $\boldsymbol{\nu}_\Gamma$ are piecewise *constant* on mesh elements, i.e., $\boldsymbol{\nu}|_E \in [\mathbb{P}_0(E)]^{d\times d}$ for all $E \in \mathcal{T}_h$, and $\boldsymbol{\nu}_\Gamma|_F \in [\mathbb{P}_0(F)]^{(d-1)\times(d-1)}$ for all $F \in \Gamma_h$. First, we introduce the finite-dimensional spaces where we will set our discrete problem. We set

$$
\begin{aligned}
Q_h^b &= \{q \in L^2(\Omega) : \ q|_E \in \mathbb{P}_{k_E}(E) \ \forall E \in \mathcal{T}_h\} \\
\mathbf{W}_h^b &= \{\mathbf{v} \in [L^2(\Omega)]^d : \ \mathbf{v}|_E \in [\mathbb{P}_{k_E}(E)]^d \ \forall E \in \mathcal{T}_h\} \\
Q_h^\Gamma &= \{q_\Gamma \in L^2(\Gamma) : \ q_\Gamma|_F \in \mathbb{P}_{k_F}(F) \ \forall F \in \Gamma_h\} \\
\mathbf{W}_h^\Gamma &= \{\mathbf{v}_\Gamma \in [L^2(\Gamma)]^{d-1} : \ \mathbf{v}_\Gamma|_F \in [\mathbb{P}_{k_F}(F)]^{d-1} \ \forall F \in \Gamma_h\}.
\end{aligned}
$$

Note that, to each element $E \in \mathcal{T}_h$ is associated the polynomial degree $k_E \geq 1$, as well as to each face $F \in \Gamma_h$ is associated the degree $k_F \geq 1$. We remark that the polynomial degrees in the bulk and fracture discrete spaces just defined are chosen *independently* of each other. Note also that here, unlike in Chapter 2, test functions are not characterised

by the subscript h, for easier reading.

We first focus on the problem in the bulk. Multiplying the first and second equations in (3.1) by test functions $\mathbf{v} \in \mathbf{W}_h^b$ and $q \in Q_h^b$, respectively, and integrating by parts over an element $E \in \mathcal{T}_h$, we obtain

$$\int_E \boldsymbol{\nu}^{-1}\mathbf{u}\cdot\mathbf{v} = -\int_E p\nabla\cdot\mathbf{v} + \int_{\partial E} p\mathbf{v}\cdot\mathbf{n}_E,$$
$$\int_E \mathbf{u}\cdot\nabla q = \int_{\partial E} q\,\mathbf{u}\cdot\mathbf{n}_E + \int_E fq.$$

In the spirit of [27], we start the derivation of our DG discretization from these equations. Adding over the elements $E \in \mathcal{T}_h$, the general discrete formulation for the problem in the bulk will then be: Find $p_h \in Q_h^b$ and $\mathbf{u}_h \in \mathbf{W}_h^b$, such that for all $E \in \mathcal{T}_h$ we have

$$\sum_{E\in\mathcal{T}_h}\int_E \boldsymbol{\nu}^{-1}\mathbf{u}_h\cdot\mathbf{v} = -\sum_{E\in\mathcal{T}_h}\int_E p_h\,\nabla\cdot\mathbf{v} + \sum_{E\in\mathcal{T}_h}\int_{\partial E}\widehat{p}_E\mathbf{v}\cdot\mathbf{n}_E$$
$$\sum_{E\in\mathcal{T}_h}\int_E \mathbf{u}_h\cdot\nabla q = \sum_{E\in\mathcal{T}_h}\int_{\partial E} q\,\widehat{\mathbf{u}}_E\cdot\mathbf{n}_E + \sum_{E\in\mathcal{T}_h}\int_E fq,$$

where the *numerical fluxes* $\widehat{p}_E$ and $\widehat{\mathbf{u}}_E$ are approximations to the exact solutions $\mathbf{u}$ and p, respectively, on the boundary of E. The definition of the numerical fluxes in terms of p_h, $\mathbf{u}_h$, of the boundary data and of the coupling conditions (3.3a)-(3.3b) will determine the method. Using identity (1.5), we get

$$\int_{\mathcal{T}_h}\boldsymbol{\nu}^{-1}\mathbf{u}_h\cdot\mathbf{v} = -\int_{\mathcal{T}_h} p_h\nabla\cdot\mathbf{v} + \int_{\mathcal{F}_h^I\cup\Gamma_h}\{\widehat{p}\}[\![\mathbf{v}]\!] + \int_{\mathcal{F}_h^I\cup\mathcal{F}_h^B\cup\Gamma_h}[\![\widehat{p}]\!]\cdot\{\mathbf{v}\}, \tag{3.6}$$
$$\int_{\mathcal{T}_h}\mathbf{u}_h\cdot\nabla q - \int_{\mathcal{F}_h^I\cup\mathcal{F}_h^B\cup\Gamma_h}\{\widehat{\mathbf{u}}\}\cdot[\![q]\!] - \int_{\mathcal{F}_h^I\cup\Gamma_h}[\![\widehat{\mathbf{u}}]\!]\{q\} = \int_{\mathcal{T}_h} fq, \tag{3.7}$$

where we have introduced $\hat{p} = (\hat{p}_E)_{E\in\mathcal{T}_h}$ and $\hat{\mathbf{u}} = (\hat{\mathbf{u}}_E)_{E\in\mathcal{T}_h}$. The numerical fluxes $\hat{p}$ and $\hat{\mathbf{u}}$ must be interpreted as linear functionals taking values in the spaces $\Pi_{E\in\mathcal{T}_h}L^2(\partial E)$ and $[\Pi_{E\in\mathcal{T}_h}L^2(\partial E)]^d$, respectively. In particular, this means that they are, in general, double-valued on $\mathcal{F}_h^I\cup\Gamma_h$ and single-valued on $\mathcal{F}_h^B$. We also observe for future use that, after integrating by parts and using again identity (1.5), equation (3.6) may also be rewritten as

$$\int_{\mathcal{T}_h}\boldsymbol{\nu}^{-1}\mathbf{u}_h\cdot\mathbf{v} = \int_{\mathcal{T}_h}\nabla p_h\cdot\mathbf{v} + \int_{\mathcal{F}_h^I\cup\Gamma_h}\{\widehat{p}-p_h\}[\![\mathbf{v}]\!] + \int_{\mathcal{F}_h^I\cup\mathcal{F}_h^B\cup\Gamma_h}[\![\widehat{p}-p_h]\!]\cdot\{\mathbf{v}\}. \tag{3.8}$$

We now reason analogously for the fracture. Multiplying the first and second equations in (3.2) by test functions $\mathbf{v}_\Gamma$ and q_Γ, respectively, integrating by parts over an element $F \in \Gamma_h$ and summing over all the elements in Γ_h we obtain the following problem: Find $p_{\Gamma,h} \in Q_h^\Gamma$ and $\mathbf{u}_{\Gamma,h} \in \mathbf{W}_h^\Gamma$ such that for all $F \in \Gamma_h$ we have

$$\sum_{F\in\Gamma_h}\int_F (\boldsymbol{\nu}_\Gamma^\tau \ell_\Gamma)^{-1}\mathbf{u}_{\Gamma,h}\cdot\mathbf{v}_\Gamma = -\sum_{F\in\Gamma_h}\int_F p_{\Gamma,h}\nabla\cdot\mathbf{v}_\Gamma + \sum_{F\in\Gamma_h}\int_{\partial F}\widehat{p}_{\Gamma,F}\mathbf{v}\cdot\mathbf{n}_F,$$
$$\sum_{F\in\Gamma_h}\int_F \mathbf{u}_{\Gamma,h}\cdot\nabla q_\Gamma - \sum_{F\in\Gamma_h}\int_{\partial F} q_\Gamma\widehat{\mathbf{u}}_{\Gamma,F}\cdot\mathbf{n}_F = \sum_{F\in\Gamma_h}\int_F \ell_\Gamma f_\Gamma q_\Gamma - \sum_{F\in\Gamma_h}\int_F [\![\widehat{\mathbf{u}}]\!] q_\Gamma.$$

Here, we have introduced the numerical fluxes $\widehat{p}_{\Gamma,F}$ and $\widehat{\mathbf{u}}_{\Gamma,F}$. Again, the idea is that they represent approximations on the boundary of the fracture face F of the exact solutions p_Γ and $\mathbf{u}_\Gamma$, respectively. Note also that here $\widehat{\mathbf{u}}$ is the numerical flux approximating the bulk velocity on Γ_h. Using identity (1.5), we get

$$\int_{\Gamma_h}(\boldsymbol{\nu}_\Gamma^\tau\ell_\Gamma)^{-1}\mathbf{u}_{\Gamma,h}\cdot\mathbf{v}_\Gamma = -\sum_{F\in\Gamma_h}\int_F p_{\Gamma,h}\nabla\cdot\mathbf{v}_\Gamma + \int_{\mathcal{E}^I_{\Gamma,h}}\{\widehat{p}_\Gamma\}[\![\mathbf{v}_\Gamma]\!] + \int_{\mathcal{E}_{\Gamma,h}}\{\mathbf{v}_\Gamma\}\cdot[\![\widehat{p}_\Gamma]\!] \tag{3.9}$$
$$\int_{\Gamma_h}\mathbf{u}_{\Gamma,h}\cdot\nabla q_\Gamma - \int_{\mathcal{E}^I_{\Gamma,h}}\{q_\Gamma\}[\![\widehat{\mathbf{u}}_\Gamma]\!] - \int_{\mathcal{E}_{\Gamma,h}}\{\widehat{\mathbf{u}}_\Gamma\}\cdot[\![q_\Gamma]\!] = \int_{\Gamma_h}\ell_\Gamma f_\Gamma q_\Gamma - \int_{\Gamma_h}[\![\widehat{\mathbf{u}}]\!] q_\Gamma \tag{3.10}$$

We point out that, in all previous equations, the gradient and divergence operators are actually *tangent* operators. Here, we have dropped the subscript τ in order to simplify the notation.
In the following, we explore all possible combinations of primal-primal, mixed-primal, primal mixed and mixed-mixed formulations for the bulk and fracture, respectively.

Primal-Primal formulation

In order to obtain the primal-primal formulation, we need to eliminate the velocities $\mathbf{u}_h$ and $\mathbf{u}_{\Gamma,h}$ from equations (3.6)-(3.7) and (3.9)-(3.10). To do so, we need to express $\mathbf{u}_h$ solely in terms of p_h (and $p_{\Gamma,h}$), and $\mathbf{u}_{\Gamma,h}$ solely in terms of $p_{\Gamma,h}$. As in [27] this will be achieved via the definition of proper *lifting operators*.

We start by focusing on the problem in the bulk. In order to complete the specification of the DG method that we want to use for the approximation, we need to give an expression to the numerical fluxes. We choose the classic *symmetric interior penalty*

method (SIPDG). Moreover, coupling conditions (3.3a)-(3.3b) are imposed through a suitable definition of the numerical fluxes on the fracture faces. Since we want a primal formulation, the definition of $\hat{p}$ and $\hat{\mathbf{u}}$ will not contain $\mathbf{u}_h$. The numerical fluxes are defined as follows:

$$\hat{p} = \hat{p}(p_h) = \begin{cases} \{p_h\} & \text{on } \mathcal{F}_h^I \\ g_D & \text{on } \mathcal{F}_h^D \\ p_h & \text{on } \mathcal{F}_h^N \\ p_h & \text{on } \Gamma_h \end{cases}$$

$$\hat{\mathbf{u}} = \hat{\mathbf{u}}(p_h, p_{\Gamma,h}) = \begin{cases} \{\boldsymbol{\nu}\nabla p_h\} - \sigma_F[\![p_h]\!] & \text{on } \mathcal{F}_h^I \\ \boldsymbol{\nu}\nabla p_h - \sigma_F(p_h - g_D)\mathbf{n}_F & \text{on } \mathcal{F}_h^D \\ 0 & \text{on } \mathcal{F}_h^N \\ -[\alpha_\Gamma(\{p_h\} - p_{\Gamma,h})\frac{\mathbf{n}_F}{2} + \beta_\Gamma[\![p_h]\!]] & \text{on } \Gamma_h \end{cases} \tag{3.11}$$

Here, we have introduced the discontinuity penalization parameter σ. In particular, σ is a non-negative bounded function, i.e., $\sigma \in L^\infty(\mathcal{F}_h^I \cup \mathcal{F}_h^D)$ and its precise definition will be given in Definition 3.4.1 below. Moreover, we have used the notation $\sigma_F = \sigma|_F$, for $F \in \mathcal{F}_h^I \cup \mathcal{F}_h^D$. We remark that, with this choice, the numerical flux $\hat{p}$ is doubled valued on Γ_h and single valued on $\mathcal{F}_h^I \cup \mathcal{F}_h^B$.
Using the definition of the numerical fluxes, it follows that

$$\begin{aligned}
&\{\hat{p} - p_h\} = 0, && [\![\hat{\mathbf{u}}]\!] = 0 && \text{on } \mathcal{F}_h^I, \\
&\{\hat{p} - p_h\} = 0, && [\![\hat{\mathbf{u}}]\!] = -\alpha_\Gamma(\{p_h\} - p_{\Gamma,h}) && \text{on } \Gamma_h, \\
&[\![\hat{p} - p_h]\!] = -[\![p_h]\!], && \{\hat{\mathbf{u}}\} = \{\boldsymbol{\nu}\nabla p_h\} - \sigma_F[\![p_h]\!] && \text{on } \mathcal{F}_h^I, \\
&[\![\hat{p} - p_h]\!] = (g_D - p_h)\mathbf{n}_F, && \{\hat{\mathbf{u}}\} = \boldsymbol{\nu}\nabla p_h - \sigma_F(p_h - g_D)\mathbf{n}_F && \text{on } \mathcal{F}_h^D, \\
&[\![\hat{p} - p_h]\!] = 0, && \{\hat{\mathbf{u}}\} = 0 && \text{on } \mathcal{F}_h^N, \\
&[\![\hat{p} - p_h]\!] = 0, && \{\hat{\mathbf{u}}\} = -\beta_\Gamma[\![p_h]\!] && \text{on } \Gamma_h,
\end{aligned}$$

so we rewrite (3.8) as

$$\int_{\mathcal{T}_h} \boldsymbol{\nu}^{-1}\mathbf{u}_h \cdot \mathbf{v} = \int_{\mathcal{T}_h} \nabla p_h \cdot \mathbf{v} - \int_{\mathcal{F}_h^I \cup \mathcal{F}_h^D} [\![p_h]\!] \cdot \{\mathbf{v}\} + \int_{\mathcal{F}_h^D} g_D \mathbf{v} \cdot \mathbf{n}. \tag{3.12}$$

At this point, we proceed with the elimination of the auxiliary variable $\mathbf{u}_h$ from our equations. To this aim, we introduce the *lifting operator* $\mathscr{L}_b^{SIP} : [L^1(\mathcal{F}_h^I \cup \mathcal{F}_h^D)]^d \to \mathbf{W}_h^b$ defined by

$$\int_{\mathcal{T}_h} \mathscr{L}_b^{SIP}(\boldsymbol{\xi}) \cdot \mathbf{v} = -\int_{\mathcal{F}_h^I \cup \mathcal{F}_h^D} \{\mathbf{v}\} \cdot \boldsymbol{\xi} \quad \forall \mathbf{v} \in \mathbf{W}_h^b. \tag{3.13}$$

Similarly, we define the lifting $\mathcal{G}_b(g_D) \in \mathbf{W}_h^b$ of the Dirichlet boundary datum g_D as

$$\int_{\mathcal{T}_h} \mathcal{G}_b \cdot \mathbf{v} = \int_{\mathcal{F}_h^D} g_D \mathbf{v} \cdot \mathbf{n} \quad \forall \mathbf{v} \in \mathbf{W}_h^b. \tag{3.14}$$

Thanks to the introduction of the lifting operators, equation (3.12) may be rewritten as

$$\int_{\mathcal{T}_h} \Big(\mathbf{u}_h - \boldsymbol{\nu}[\nabla p_h + \mathscr{L}_b^{SIP}([\![p_h]\!]) + \mathcal{G}_b] \Big) \cdot \mathbf{v} = 0.$$

Since $\nabla Q_h^b \subseteq \mathbf{W}_h^b$, we can write

$$\mathbf{u}_h = \boldsymbol{\nu}[\nabla p_h + \mathscr{L}_b^{SIP}([\![p_h]\!]) + \mathcal{G}_b], \tag{3.15}$$

where $\nabla p_h + \mathscr{L}_b^{SIP}([\![p_h]\!]) + \mathcal{G}_b$ can be seen as a discrete approximation of the gradient ∇p.

We can then rewrite equation (3.7) as

$$\int_{\mathcal{T}_h} \boldsymbol{\nu}[\nabla p_h + \mathscr{L}_b^{SIP}([\![p_h]\!]) + \mathcal{G}_b] \cdot \nabla q - \int_{\mathcal{F}_h^I \cup \mathcal{F}_h^B \cup \Gamma_h} \{\widehat{\mathbf{u}}\} \cdot [\![q]\!] - \int_{\mathcal{F}_h^I \cup \Gamma_h} [\![\widehat{\mathbf{u}}]\!]\{q\} = \int_{\mathcal{T}_h} fq.$$

Using the definition of the discrete gradient (3.15), of the lifting operators (3.13) and (3.14) and of the numerical flux $\hat{\mathbf{u}}$ (3.11), we have

$$\begin{aligned} \int_{\mathcal{T}_h} \boldsymbol{\nu} \nabla p_h \cdot \nabla q + \int_{\mathcal{T}_h} \boldsymbol{\nu} \mathscr{L}_b^{SIP}([\![p_h]\!]) \cdot \nabla q + \int_{\mathcal{T}_h} \boldsymbol{\nu} \mathscr{L}_b^{SIP}([\![q]\!]) \cdot \nabla p_h + \int_{\mathcal{F}_h^I \cup \mathcal{F}_h^D} \sigma_F [\![p_h]\!] \cdot [\![q]\!] \\ + \int_{\Gamma_h} \beta_\Gamma [\![p_h]\!] \cdot [\![q]\!] + \int_{\Gamma_h} \alpha_\Gamma (\{p_h\} - p_{\Gamma,h})\{q\} \\ = \int_{\mathcal{T}_h} fq + \int_{\mathcal{F}_h^D} g_D \sigma_F q - \int_{\mathcal{T}_h} \boldsymbol{\nu} \mathcal{G}_b \cdot \nabla q. \end{aligned} \tag{3.16}$$

Now we move our attention to the problem in the fracture. We define the numerical fluxes

$\hat{p}_\Gamma$ and $\hat{\mathbf{u}}_\Gamma$ in order to obtain a symmetric interior penalty approximation as follows:

$$\hat{p}_\Gamma = \hat{p}_\Gamma(p_{\Gamma,h}) = \begin{cases} \{p_{\Gamma,h}\} & \text{on } \mathcal{E}^I_{\Gamma,h} \\ g_\Gamma & \text{on } \mathcal{E}^D_{\Gamma,h} \\ p_{\Gamma,h} & \text{on } \mathcal{E}^N_{\Gamma,h}, \end{cases}$$

$$\hat{\mathbf{u}}_\Gamma = \hat{\mathbf{u}}_\Gamma(p_{\Gamma,h}) = \begin{cases} \{\boldsymbol{\nu}^\tau_\Gamma \ell_\Gamma \nabla p_{\Gamma,h}\} - \sigma_e [\![p_{\Gamma,h}]\!] & \text{on } \mathcal{E}^I_{\Gamma,h} \\ \boldsymbol{\nu}^\tau_\Gamma \ell_\Gamma \nabla p_{\Gamma,h} - \sigma_e (p_{\Gamma,h} - g_\Gamma)\mathbf{n}_e & \text{on } \mathcal{E}^D_{\Gamma,h} \\ 0 & \text{on } \mathcal{E}^N_{\Gamma,h}. \end{cases} \tag{3.17}$$

Again, we have introduced the discontinuity penalization parameter $\sigma_\Gamma \in L^\infty(\mathcal{E}^I_{\Gamma,h} \cup \mathcal{E}^D_{\Gamma,h})$ and we set $\sigma_e = \sigma_\Gamma|_e$ for $e \in \mathcal{E}^I_{\Gamma,h} \cup \mathcal{E}^D_{\Gamma,h}$. Its precise definition will be given in Definition 3.4.2 below. Next, as before, we introduce the lifting operator $\mathscr{L}^{SIP}_\Gamma : [L^1(\mathcal{E}^I_{\Gamma,h} \cup \mathcal{E}^D_{\Gamma,h})]^{d-1} \to \mathbf{W}^\Gamma_h$ and the lifting of the boundary datum $\mathcal{G}_\Gamma(g_{\Gamma,D}) \in \mathbf{W}^\Gamma_h$ defined by

$$\int_{\Gamma_h} \mathscr{L}^{SIP}_\Gamma(\boldsymbol{\xi}_\Gamma) \cdot \mathbf{v}_\Gamma = -\int_{\mathcal{E}^I_{\Gamma,h} \cup \mathcal{E}^D_{\Gamma,h}} \boldsymbol{\xi}_\Gamma \cdot \{\mathbf{v}_\Gamma\} \qquad \forall \mathbf{v}_\Gamma \in \mathbf{W}^\Gamma_h, \tag{3.18}$$

$$\int_{\Gamma_h} \mathcal{G}_\Gamma \cdot \mathbf{v}_\Gamma = \int_{\mathcal{E}^D_{\Gamma,h}} g_{\Gamma,D} \mathbf{v}_\Gamma \cdot \mathbf{n}_\tau \qquad \forall \mathbf{v}_\Gamma \in \mathbf{W}^\Gamma_h. \tag{3.19}$$

Integrating by parts and using (1.5), we can rewrite equation (3.9) as

$$\int_{\Gamma_h} \Big(\mathbf{u}_{\Gamma,h} - \boldsymbol{\nu}^\tau_\Gamma \ell_\Gamma [\nabla p_{\Gamma,h} + \mathscr{L}^{SIP}_\Gamma([\![p_{\Gamma,h}]\!]) + \mathcal{G}_\Gamma] \Big) \cdot \mathbf{v}_\Gamma = 0.$$

Again, since $\nabla Q^\Gamma_h \subseteq \mathbf{W}^\Gamma_h$ elementwise, we can write

$$\mathbf{u}_{\Gamma,h} = \boldsymbol{\nu}^\tau_\Gamma \ell_\Gamma [\nabla p_{\Gamma,h} + \mathscr{L}^{SIP}_\Gamma([\![p_{\Gamma,h}]\!]) + \mathcal{G}_\Gamma].$$

Plugging this last identity and the definition of the numerical fluxes $\widehat{\mathbf{u}}$ (see (3.11)) and

$\hat{\mathbf{u}}_\Gamma$ (see (3.17)) into equation (3.10), we obtain

$$\int_{\Gamma_h} \boldsymbol{\nu}_\Gamma^\tau \ell_\Gamma \nabla p_{\Gamma,h} \cdot \nabla q_\Gamma + \int_{\Gamma_h} \boldsymbol{\nu}_\Gamma^\tau \ell_\Gamma \mathscr{L}_\Gamma^{SIP}([\![p_{\Gamma,h}]\!]) \cdot \nabla q_\Gamma + \int_{\Gamma_h} \boldsymbol{\nu}_\Gamma^\tau \ell_\Gamma \mathscr{L}_\Gamma^{SIP}([\![q_\Gamma]\!]) \cdot \nabla p_{\Gamma,h} + \int_{\mathcal{E}_{\Gamma,h}^I \cup \mathcal{E}_{\Gamma,h}^D} \sigma_e [\![p_{\Gamma,h}]\!] \cdot [\![q_\Gamma]\!] + \int_{\Gamma_h} \alpha_\Gamma p_{\Gamma,h} q_\Gamma - \int_{\Gamma_h} \alpha_\Gamma \{p_h\} q_\Gamma = \int_{\Gamma_h} \ell_\Gamma f_\Gamma q_\Gamma + \int_{\mathcal{E}_{\Gamma,h}^D} g_\Gamma \sigma_e q_\Gamma - \int_{\Gamma_h} \boldsymbol{\nu}_\Gamma^\tau \ell_\Gamma \mathcal{G}_\Gamma \cdot \nabla q_\Gamma. \quad (3.20)$$

In conclusion, summing equations (3.16) and (3.20) we obtain the following discrete formulation: Find $(p_h, p_h^\Gamma) \in Q_h^b \times Q_h^\Gamma$ such that

$$\mathcal{A}_h^{PP}\left((p_h, p_h^\Gamma), (q, q_\Gamma)\right) = \mathcal{L}_h^{PP}(q, q_\Gamma) \quad \forall (q, q_\Gamma) \in Q_h^b \times Q_h^\Gamma, \quad (3.21)$$

where PP stands for *primal-primal* and where $\mathcal{L}_h : Q_h^b \times Q_h^\Gamma \to \mathbb{R}$ is defined as $\mathcal{L}_h^{PP}(q, q_\Gamma) = \mathcal{L}_b^P(q) + \mathcal{L}_\Gamma^P(q_\Gamma)$ and $\mathcal{A}_h^{PP} : (Q_h^b \times Q_h^\Gamma) \times (Q_h^b \times Q_h^\Gamma) \to \mathbb{R}$ is defined as

$$\mathcal{A}_h^{PP}\left((p_h, p_h^\Gamma), (q, q_\Gamma)\right) = \mathcal{A}_b^P(p_h, q) + \mathcal{A}_\Gamma^P(p_{\Gamma,h}, q_\Gamma) + \mathcal{C}((p_h, p_{\Gamma,h}), (q, q_\Gamma)),$$

with

$$\mathcal{A}_b^P(p_h, q) = \int_{\mathcal{T}_h} \boldsymbol{\nu} \nabla p_h \cdot \nabla q + \int_{\mathcal{T}_h} \boldsymbol{\nu} \mathscr{L}_b^{SIP}([\![p_h]\!]) \cdot \nabla q + \int_{\mathcal{T}_h} \boldsymbol{\nu} \mathscr{L}_b^{SIP}([\![q]\!]) \cdot \nabla p_h + \int_{\mathcal{F}_h^I \cup \mathcal{F}_h^D} \sigma_F [\![p_h]\!] \cdot [\![q]\!], \quad (3.22)$$

$$\mathcal{A}_\Gamma^P(p_{\Gamma,h}, q_\Gamma) = \int_{\Gamma_h} \boldsymbol{\nu}_\Gamma^\tau \ell_\Gamma \nabla p_{\Gamma,h} \cdot \nabla q_\Gamma + \int_{\Gamma_h} \boldsymbol{\nu}_\Gamma^\tau \ell_\Gamma \mathscr{L}_\Gamma^P([\![p_{\Gamma,h}]\!]) \cdot \nabla q_\Gamma + \int_{\Gamma_h} \boldsymbol{\nu}_\Gamma^\tau \ell_\Gamma \mathscr{L}_\Gamma^{SIP}([\![q_\Gamma]\!]) \cdot \nabla p_{\Gamma,h} + \int_{\mathcal{E}_{\Gamma,h}^I \cup \mathcal{E}_{\Gamma,h}^D} \sigma_e [\![p_{\Gamma,h}]\!] \cdot [\![q_\Gamma]\!], \quad (3.23)$$

$$\mathcal{C}((p_h, p_{\Gamma,h}), (q, q_\Gamma)) = \int_{\Gamma_h} \beta_\Gamma [\![p_h]\!] \cdot [\![q]\!] + \int_{\Gamma_h} \alpha_\Gamma (\{p_h\} - p_{\Gamma,h})(\{q\} - q_{\Gamma,h}), \quad (3.24)$$

and

$$\mathcal{L}_b^P(q) = \int_{\mathcal{T}_h} fq + \int_{\mathcal{F}_h^D} g_D \sigma_F q - \int_{\mathcal{T}_h} \boldsymbol{\nu} \mathcal{G}_b \cdot \nabla q, \quad (3.25)$$

$$\mathcal{L}_\Gamma^P(q_\Gamma) = \int_{\Gamma_h} \ell_\Gamma f_\Gamma q_\Gamma + \int_{\mathcal{E}_{\Gamma,h}^D} g_\Gamma \sigma_e q_\Gamma - \int_{\Gamma_h} \boldsymbol{\nu}_\Gamma^\tau \ell_\Gamma \mathcal{G}_\Gamma \cdot \nabla q_\Gamma. \quad (3.26)$$

We remark that we have recovered the formulation already obtained in Chapter 2 (in its not strongly consistent version), the only difference being that the bilinear form for the problem in the fracture is in the shape of SIPDG method, instead of classical conforming finite elements.

Mixed-Primal formulation

In this section, we discretize the problem in the bulk in its mixed form. To this aim, we use the local discontinuous Galerkin (LDG) method [72, 64, 108, 109]. The LDG method is a particular DG method that can be included in the class of mixed finite element methods. However, the variable $\mathbf{u}_h$ can be *locally* solved in terms of p_h and then eliminated from the equations, giving rise to a primal formulation with p_h as only unknown.

In what follows, we first derive the formulation of our method in a mixed setting. After that, we recast it in a primal setting, in order to perform the analysis in the framework of [27, 108]. However, we remark that the mixed formulation is the one that will actually be implemented for the numerical experiments of Section 3.6. As far as the problem in the fracture is concerned, we work again in a primal setting, using the SIPDG method for the discretization.

In the bulk, we define the numerical fluxes as

$$\hat{p} = \hat{p}(p_h) = \begin{cases} \{p_h\} + \mathbf{b} \cdot [\![p_h]\!] & \text{on } \mathcal{F}_h^I \\ g_D & \text{on } \mathcal{F}_h^D \\ p_h & \text{on } \mathcal{F}_h^N \\ p_h & \text{on } \Gamma_h \end{cases}$$

$$\hat{\mathbf{u}} = \hat{\mathbf{u}}(\mathbf{u}_h, p_h, p_{\Gamma,h}) = \begin{cases} \{\mathbf{u}_h\} - \mathbf{b}[\![\mathbf{u}_h]\!] - \sigma_F[\![p_h]\!] & \text{on } \mathcal{F}_h^I \\ \mathbf{u}_h - \sigma_F(p_h\mathbf{n}_F - g_D\mathbf{n}_F) & \text{on } \mathcal{F}_h^D \\ 0 & \text{on } \mathcal{F}_h^N \\ -[\alpha_\Gamma(\{p_h\} - p_{\Gamma,h})\frac{\mathbf{n}_F}{2} + \beta_\Gamma[\![p_h]\!]] & \text{on } \Gamma_h \end{cases}$$

Here, $\mathbf{b} \in [L^\infty(\mathcal{F}_h^I)]^d$ is a (possibly null) vector-valued function which is constant on each

face. It is chosen such that

$$||\mathbf{b}||_{\infty,\mathcal{F}_h^I} \leq B, \tag{3.27}$$

with $B \geq 0$ independent if the discretization parameters. Moreover, σ is the penalization parameter introduced in (3.11) , whose precise definition will be given in (3.45) below. Note that the numerical flux $\hat{p}$ does *not* depend on $\mathbf{u}_h$. This will allow for an element-by-element elimination of the variable $\mathbf{u}_h$, generating a primal formulation of the problem. We also point out that the definition of the numerical fluxes on the fracture faces is the same as in the primal SIPDG setting.

With this definition of the numerical fluxes, and after integration by parts as in (3.8), equation (3.6) becomes

$$\int_{\mathcal{T}_h} \boldsymbol{\nu}^{-1}\mathbf{u}_h \cdot \mathbf{v} - \int_{\mathcal{T}_h} \nabla p_h \cdot \mathbf{v} + \int_{\mathcal{F}_h^I} [\![p_h]\!] \cdot (\{\mathbf{v}\} - \mathbf{b}[\![\mathbf{v}]\!]) + \int_{\mathcal{F}_h^D} p_h \mathbf{v} \cdot \mathbf{n}_F = \int_{\mathcal{F}_h^D} g_D \mathbf{v} \cdot \mathbf{n}_F, \tag{3.28}$$

while equation (3.7) turns into

$$\begin{aligned}\int_{\mathcal{T}_h} \mathbf{u}_h \cdot \nabla q - \int_{\mathcal{F}_h^I} (\{\mathbf{u}_h\} - \mathbf{b}[\![\mathbf{u}_h]\!]) \cdot [\![q]\!] + \int_{\mathcal{F}_h^I \cup \mathcal{F}_h^D} \sigma_F [\![p_h]\!] \cdot [\![q]\!] - \int_{\mathcal{F}_h^D} q\mathbf{u}_h \cdot \mathbf{n}_F \\ + \int_{\Gamma_h} \beta_\Gamma [\![p_h]\!] \cdot [\![q]\!] + \int_{\Gamma_h} \alpha_\Gamma (\{p_h\} - p_{\Gamma,h})\{q\} = \int_{\mathcal{T}_h} fq + \int_{\mathcal{F}_h^D} \sigma_F g_D q.\end{aligned} \tag{3.29}$$

If we discretize the problem in the fracture with the SIPDG method, we obtain the following discrete mixed problem: Find $\left((p_h, \mathbf{u}_h), p_h^\Gamma\right) \in Q_h^b \times \mathbf{W}_h^b \times Q_h^\Gamma$ such that

$$\begin{aligned} \mathcal{M}_b(\mathbf{u}_h, \mathbf{v}) + \mathcal{B}_b(p_h, \mathbf{v}) &= F_b(\mathbf{v}) && \forall \mathbf{v} \in \mathbf{W}_h^b, \\ -\mathcal{B}_b(q, \mathbf{u}_h) + \mathcal{S}_b(p_h, q) + \mathcal{C}_1(p_h, q, p_{\Gamma,h}) &= G_b(q) && \forall q \in Q_h^b, \\ \mathcal{A}_\Gamma^P(p_{\Gamma,h}, q_\Gamma) + \mathcal{C}_2(p_h, p_{\Gamma,h}, q_\Gamma) &= \mathcal{L}_\Gamma^P(q_\Gamma) && \forall q_\Gamma \in Q_h^\Gamma, \end{aligned} \tag{3.30}$$

where

$$\begin{aligned}
\mathcal{M}_b(\mathbf{u}_h, \mathbf{v}) &= \int_{\mathcal{T}_h} \boldsymbol{\nu}^{-1}\mathbf{u}_h \cdot \mathbf{v}, \\
\mathcal{B}_b(p_h, \mathbf{v}) &= -\int_{\mathcal{T}_h} \nabla p_h \cdot \mathbf{v} + \int_{\mathcal{F}_h^I} [\![p_h]\!] \cdot (\{\mathbf{v}\} - \mathbf{b}[\![\mathbf{v}]\!]) + \int_{\mathcal{F}_h^D} p_h \mathbf{v} \cdot \mathbf{n}_F, \\
\mathcal{S}_b(p_h, q) &= \int_{\mathcal{F}_h^I \cup \mathcal{F}_h^D} \sigma_F [\![p_h]\!] \cdot [\![q]\!], \\
\mathcal{C}_1(p_h, q, p_{\Gamma,h}) &= \int_{\Gamma_h} \beta_\Gamma [\![p_h]\!] \cdot [\![q]\!] + \int_{\Gamma_h} \alpha_\Gamma (\{p_h\} - p_{\Gamma,h})\{q\}, \\
\mathcal{C}_2(p_h, p_{\Gamma,h}, q_\Gamma) &= \int_{\Gamma_h} \alpha_\Gamma (p_{\Gamma,h} - \{p_h\}) q_\Gamma, \\
F_b(\mathbf{v}) &= \int_{\mathcal{F}_h^D} g_D \mathbf{v} \cdot \mathbf{n}_F, \\
G_b(q) &= \int_{\mathcal{T}_h} fq + \int_{\mathcal{F}_h^D} \sigma_F g_D q,
\end{aligned}$$

and $\mathcal{A}_\Gamma^P(\cdot,\cdot)$ and $\mathcal{L}_\Gamma^P(\cdot)$ are defined as in (3.23) and (3.26), respectively. Also note that we have $\mathcal{C}((p_h, p_{\Gamma,h}), (q, q_\Gamma)) = \mathcal{C}_1(p_h, q, p_{\Gamma,h}) + \mathcal{C}_2(p_h, p_{\Gamma,h}, q_\Gamma)$.

We now focus on rewriting the problem in the bulk in a primal form, taking advantage of the local solvability of LDG method. We proceed as in the SIPDG case and introduce an appropriate *lifting operator*, $\mathscr{L}_b^{LDG} : [L^1(\mathcal{F}_h^I \cup \mathcal{F}_h^D)]^d \to \mathbf{W}_h^b$, defined by

$$\int_{\mathcal{T}_h} \mathscr{L}_b^{LDG}(\boldsymbol{\xi}) \cdot \mathbf{v} = -\int_{\mathcal{F}_h^I} (\{\mathbf{v}\} - \mathbf{b}[\![\mathbf{v}]\!]) \cdot \boldsymbol{\xi} - \int_{\mathcal{F}_h^D} \boldsymbol{\xi} \cdot \mathbf{v} \quad \forall\, \mathbf{v} \in \mathbf{W}_h^b \tag{3.31}$$

From equation (3.28) we obtain

$$\mathbf{u}_h = \boldsymbol{\nu}(\nabla p_h + \mathscr{L}_b^{LDG}([\![p_h]\!]) + \mathcal{G}_b), \tag{3.32}$$

where $\mathcal{G}_b$ is the lifting of the Dirichlet boundary datum defined in (3.14). Equation (3.29)

now becomes

$$\int_{\mathcal{T}_h} \boldsymbol{\nu}\nabla p_h \cdot \nabla q + \int_{\mathcal{T}_h} \boldsymbol{\nu}\mathscr{L}_b^{LDG}([\![p_h]\!]) \cdot \nabla q_h + \int_{\mathcal{T}_h} \boldsymbol{\nu}\mathcal{G}_b \cdot \nabla q$$
$$- \int_{\mathcal{F}_h^I} (\{\mathbf{u}_h\} + \mathbf{b}[\![\mathbf{u}_h]\!]) \cdot [\![q]\!] - \int_{\mathcal{F}_h^D} q\mathbf{u}_h \cdot \mathbf{n}_F + \int_{\mathcal{F}_h^I \cup \mathcal{F}_h^D} \sigma_F [\![p_h]\!] \cdot [\![q]\!]$$
$$+ \int_{\Gamma_h} \beta_\Gamma [\![p_h]\!] \cdot [\![q]\!] + \int_{\Gamma_h} \alpha_\Gamma (\{p_h\} - p_{\Gamma,h})\{q\} = \int_{\mathcal{T}_h} fq + \int_{\mathcal{F}_h^D} \sigma_F q g_D.$$

Using again the definition of the lifting $\mathscr{L}_b^{LDG}$ and the identity (3.32), we obtain

$$\int_{\mathcal{T}_h} \boldsymbol{\nu}(\nabla p_h + \mathscr{L}_b^{LDG}([\![p_h]\!])) \cdot (\nabla q + \mathscr{L}_b^{LDG}([\![q]\!])) + \int_{\mathcal{F}_h^I \cup \mathcal{F}_h^D} \sigma_F [\![p_h]\!] \cdot [\![q]\!]$$
$$+ \int_{\Gamma_h} \beta_\Gamma [\![p_h]\!] \cdot [\![q]\!] + \int_{\Gamma_h} \alpha_\Gamma (\{p_h\} - p_\Gamma)\{q\}$$
$$= \int_{\mathcal{T}_h} fq + \int_{\mathcal{F}_h^D} \sigma_F q g_D - \int_{\mathcal{T}_h} \boldsymbol{\nu}\mathcal{G}_b \cdot (\nabla q + \mathscr{L}_b^{LDG}([\![q]\!])). \quad (3.33)$$

Summing equations (3.33) and (3.20) we obtain the following discrete formulation: Find $(p_h, p_h^\Gamma) \in Q_h^b \times Q_h^\Gamma$ such that

$$\mathcal{A}_h^{MP}\left((p_h, p_h^\Gamma), (q, q_\Gamma)\right) = \mathcal{L}_h^{MP}(q, q_\Gamma) \quad \forall (q, q_\Gamma) \in Q_h^b \times Q_h^\Gamma, \quad (3.34)$$

where MP stands for *mixed-primal* and where $\mathcal{A}_h^{MP} : (Q_h^b \times Q_h^\Gamma) \times (Q_h^b \times Q_h^\Gamma) \to \mathbb{R}$ is defined as

$$\mathcal{A}_h^{MP}\left((p_h, p_h^\Gamma), (q, q_\Gamma)\right) = \mathcal{A}_b^M(p_h, q) + \mathcal{A}_\Gamma^P(p_{\Gamma,h}, q_\Gamma) + \mathcal{C}((p_h, p_{\Gamma,h}), (q, q_\Gamma)),$$

and $\mathcal{L}_h^{MP} : Q_h^b \times Q_h^\Gamma \to \mathbb{R}$ is defined as

$$\mathcal{L}_h^{MP}(q, q_\Gamma) = \mathcal{L}_b^M(q) + \mathcal{L}_\Gamma^P(q_\Gamma)$$

with

$$\mathcal{A}_b^M(p_h,q)=\int_{\mathcal{T}_h}\boldsymbol{\nu}(\nabla p_h+\mathscr{L}_b^{LDG}([\![p_h]\!]))\cdot(\nabla q+\mathscr{L}_b^{LDG}([\![q]\!]))+\int_{\mathcal{F}_h^I\cup\mathcal{F}_h^D}\sigma_F[\![p_h]\!]\cdot[\![q]\!]$$
$$+\int_{\Gamma_h}\beta_\Gamma[\![p_h]\!]\cdot[\![q]\!]+\int_{\Gamma_h}\alpha_\Gamma(\{p_h\}-p_\Gamma)\{q\},\tag{3.35}$$
$$\mathcal{L}_b^M(q)=\int_{\mathcal{T}_h}fq+\int_{\mathcal{F}_h^D}\sigma_F q g_D-\int_{\mathcal{T}_h}\boldsymbol{\nu}\mathcal{G}_b\cdot(\nabla q+\mathscr{L}_b^{LDG}([\![q]\!])).$$

Note that the mixed formulation (3.30) is equivalent to the primal formulation (3.34) together with the definition of the lifting operator (3.31) and equation (3.32).

Primal-Mixed formulation

We now want to approximate the problem in the fracture in mixed form, employing the LDG method and the problem in the bulk using the SIPDG method. We define the numerical fluxes as follows

$$\hat{p}_\Gamma=\hat{p}_\Gamma(p_{\Gamma,h})=\begin{cases}\{p_{\Gamma,h}\}+\mathbf{b}_\Gamma\cdot[\![p_{\Gamma,h}]\!] & \text{on }\mathcal{E}_{\Gamma,h}^I\\ g_\Gamma & \text{on }\mathcal{E}_{\Gamma,h}^D\\ p_{\Gamma,h} & \text{on }\mathcal{E}_{\Gamma,h}^N\end{cases}$$
$$\hat{\mathbf{u}}_\Gamma=\hat{\mathbf{u}}_\Gamma(\mathbf{u}_{\Gamma,h},p_{\Gamma,h})=\begin{cases}\{\mathbf{u}_{\Gamma,h}\}-\mathbf{b}_\Gamma[\![\mathbf{u}_{\Gamma,h}]\!]-\sigma_e[\![p_{\Gamma,h}]\!] & \text{on }\mathcal{E}_{\Gamma,h}^I\\ \mathbf{u}_{\Gamma,h}-\sigma_e(p_{\Gamma,h}\mathbf{n}_e-g_\Gamma\mathbf{n}_e) & \text{on }\mathcal{E}_{\Gamma,h}^D\\ 0 & \text{on }\mathcal{E}_{\Gamma,h}^N\end{cases}$$

Here, $\mathbf{b}_\Gamma\in[L^\infty(\mathcal{E}_{\Gamma,h}^I)]^{d-1}$ is a vector-valued function that is constant on each edge and it is chosen such that $||\mathbf{b}_\Gamma||_{\infty,\mathcal{E}_{\Gamma,h}^I}\leq B_\Gamma$, with $B_\Gamma\leq 0$ independent of the discretization parameters. Equations (3.9) and (3.10) now become

$$\int_{\Gamma_h}(\boldsymbol{\nu}_\Gamma^\tau\ell_\Gamma)^{-1}\mathbf{u}_{\Gamma,h}\cdot\mathbf{v}_\Gamma-\int_{\Gamma_h}\mathbf{v}_\Gamma\cdot\nabla p_{\Gamma,h}+\int_{\mathcal{E}_{\Gamma,h}^I}[\![p_{\Gamma,h}]\!]\cdot(\{\mathbf{v}_\Gamma\}-\mathbf{b}_\Gamma[\![\mathbf{v}_\Gamma]\!])$$
$$+\int_{\mathcal{E}_{\Gamma,h}^D}p_{\Gamma,h}\mathbf{v}_\Gamma\cdot\mathbf{n}_e=\int_{\mathcal{E}_{\Gamma,h}^D}g_\Gamma\mathbf{v}_\Gamma\cdot\mathbf{n}_e\tag{3.36}$$

$$\int_{\Gamma_h} \mathbf{u}_{\Gamma,h}\cdot\nabla q_\Gamma - \int_{\mathcal{E}^I_{\Gamma,h}} [\![q_\Gamma]\!]\cdot(\{\mathbf{u}_{\Gamma,h}\} - \mathbf{b}_\Gamma[\![\mathbf{u}_{\Gamma,h}]\!]) + \int_{\mathcal{E}_{\Gamma,h}} \sigma_e[\![p_{\Gamma,h}]\!]\cdot[\![q_\Gamma]\!]$$
$$- \int_{\mathcal{E}^D_{\Gamma,h}} q_\Gamma \mathbf{u}_{\Gamma,h}\cdot\mathbf{n}_e = \int_{\Gamma_h} \ell_\Gamma f_\Gamma q_\Gamma + \int_{\Gamma_h} \alpha_\Gamma(\{p_h - p_{\Gamma,h}\})q_\Gamma + \int_{\mathcal{E}_{\Gamma,h}} \sigma_e g_\Gamma q_\Gamma, \quad (3.37)$$

where we have also used the definition of the numerical flux $\widehat{\mathbf{u}}$ on Γ_h (see (3.11)) to rewrite $-[\![\widehat{\mathbf{u}}]\!] = \alpha_\Gamma(\{p_h\} - p_{\Gamma,h})$. For the bulk we proceed as in the primal-primal setting using for the discretization the SIPDG method. We then obtain the following primal-mixed problem: Find $\Big(p_h, (p_h^\Gamma, \mathbf{u}_{\Gamma,h})\Big) \in Q_h^b \times Q_h^\Gamma \times \mathbf{W}_h^\Gamma$ such that

$$\begin{aligned}
\mathcal{A}_b^P(p_h, q) + \mathcal{C}_1((p_h, q), p_{\Gamma,h}) &= \mathcal{L}_b^P(q) \quad && \forall q \in Q_h^b \\
\mathcal{M}_\Gamma(\mathbf{u}_{\Gamma,h}, \mathbf{v}_\Gamma) + \mathcal{B}_\Gamma(p_{\Gamma,h}, \mathbf{v}_\Gamma) &= F_\Gamma(\mathbf{v}_\Gamma) \quad && \forall \mathbf{v}_\Gamma \in \mathbf{W}_h^\Gamma, \\
-\mathcal{B}_\Gamma(q_\Gamma, \mathbf{u}_{\Gamma,h}) + \mathcal{S}_\Gamma(p_{\Gamma,h}, q_\Gamma) + \mathcal{C}_2(p_h, (p_{\Gamma,h}, q_\Gamma)) &= G_\Gamma(q_\Gamma) \quad && \forall q_\Gamma \in Q_h^\Gamma,
\end{aligned} \quad (3.38)$$

where

$$\begin{aligned}
\mathcal{M}_\Gamma(\mathbf{u}_{\Gamma,h}, \mathbf{v}_\Gamma) &= \int_{\Gamma_h} (\boldsymbol{\nu}_\Gamma^\tau \ell_\Gamma)^{-1} \mathbf{u}_{\Gamma,h}\cdot\mathbf{v}_\Gamma, \\
\mathcal{B}_\Gamma(p_{\Gamma,h}, \mathbf{v}_\Gamma) &= -\int_{\Gamma_h} \mathbf{v}_\Gamma\cdot\nabla p_{\Gamma,h} + \int_{\mathcal{E}^I_{\Gamma,h}} [\![p_{\Gamma,h}]\!]\cdot(\{\mathbf{v}_\Gamma\} - \mathbf{b}_\Gamma[\![\mathbf{v}_\Gamma]\!]) + \int_{\mathcal{E}^D_{\Gamma,h}} p_{\Gamma,h}\mathbf{v}_\Gamma\cdot\mathbf{n}_e, \\
\mathcal{S}_b(p_{\Gamma,h}, q_\Gamma) &= \int_{\mathcal{E}_{\Gamma,h}} \sigma_e[\![p_{\Gamma,h}]\!]\cdot[\![q_\Gamma]\!], \\
F_\Gamma(\mathbf{v}_\Gamma) &= \int_{\mathcal{E}^D_{\Gamma,h}} g_\Gamma \mathbf{v}_\Gamma\cdot\mathbf{n}_e, \\
G_\Gamma(q_\Gamma) &= \int_{\Gamma_h} \ell_\Gamma f_\Gamma q_\Gamma + \int_{\mathcal{E}_{\Gamma,h}} \sigma_e g_\Gamma q_\Gamma,
\end{aligned}$$

and $\mathcal{A}_b^P(p_h, q)$ and $\mathcal{L}_b^P(q)$ are defined as in (3.22) and (3.25), respectively.

Aiming at rewriting the problem in the fracture in primal form, we introduce the lifting operator, $\mathscr{L}_\Gamma^{LDG} : [L^1(\mathcal{E}_h^I \cup \mathcal{E}_h^D)]^d \to \mathbf{W}_h^\Gamma$, defined by

$$\int_{\Gamma_h} \mathscr{L}_\Gamma^{LDG}(\boldsymbol{\xi}_\Gamma)\cdot\mathbf{v}_\Gamma = -\int_{\mathcal{E}^I_{\Gamma,h}} (\{\mathbf{v}_\Gamma\} - \mathbf{b}_\Gamma[\![\mathbf{v}_\Gamma]\!])\cdot\boldsymbol{\xi}_\Gamma - \int_{\mathcal{E}^D_{\Gamma,h}} \boldsymbol{\xi}_\Gamma\cdot\mathbf{v}_\Gamma \quad \forall\, \mathbf{v}_\Gamma \in \mathbf{W}_h^\Gamma \quad (3.39)$$

From equation (3.36) we obtain

$$\mathbf{u}_{\Gamma,h} = \boldsymbol{\nu}_\Gamma^\tau \ell_\Gamma [\nabla p_{\Gamma,h} + \mathscr{L}_\Gamma^{LDG}([\![p_{\Gamma,h}]\!]) + \mathcal{G}_\Gamma] \tag{3.40}$$

where $\mathcal{G}_\Gamma$ is the lifting of the Dirichlet boundary datum defined in (3.19). Equation (3.37) now becomes

$$\int_{\Gamma_h} \boldsymbol{\nu}_\Gamma^\tau \ell_\Gamma (\nabla p_{\Gamma,h} + \mathscr{L}_\Gamma^{LDG}([\![p_{\Gamma,h}]\!])) \cdot (\nabla q_\Gamma + \mathscr{L}_\Gamma^{LDG}([\![q_\Gamma]\!])) + \int_{\mathcal{E}^I_{\Gamma,h} \cup \mathcal{E}^D_{\Gamma,h}} \sigma_e [\![p_{\Gamma,h}]\!] \cdot [\![q_\Gamma]\!]$$
$$+ \int_{\Gamma_h} \alpha_\Gamma (p_{\Gamma,h}) - \{p_h\}) = \int_{\Gamma_h} \ell_\Gamma f_\Gamma q_\Gamma + \int_{\mathcal{E}^D_{\Gamma,h}} \sigma_e q_\Gamma g_\Gamma - \int_{\Gamma_h} \boldsymbol{\nu}_\Gamma^\tau \ell_\Gamma \mathcal{G}_\Gamma \cdot (\nabla q_\Gamma + \mathscr{L}_\Gamma^{LDG}([\![q_\Gamma]\!])).$$

We obtain the following primal formulation: Find $(p_h, p_h^\Gamma) \in Q_h^b \times Q_h^\Gamma$ such that

$$\mathcal{A}_h^{PM}\left((p_h, p_h^\Gamma), (q, q_\Gamma)\right) = \mathcal{L}_h^{PM}(q, q_\Gamma) \quad \forall (q, q_\Gamma) \in Q_h^b \times Q_h^\Gamma, \tag{3.41}$$

where PM stands for *primal-mixed* and where $\mathcal{A}_h^{PM} : (Q_h^b \times Q_h^\Gamma) \times (Q_h^b \times Q_h^\Gamma) \to \mathbb{R}$ is defined as

$$\mathcal{A}_h^{PM}\left((p_h, p_h^\Gamma), (q, q_\Gamma)\right) = \mathcal{A}_b^P(p_h, q) + \mathcal{A}_\Gamma^M(p_{\Gamma,h}, q_\Gamma) + \mathcal{C}((p_h, p_{\Gamma,h}), (q, q_\Gamma)),$$

and $\mathcal{L}_h^{PM} : Q_h^b \times Q_h^\Gamma \to \mathbb{R}$ is defined as

$$\mathcal{L}_h^{PM}(q, q_\Gamma) = \mathcal{L}_b^P(q) + \mathcal{L}_\Gamma^M(q_\Gamma)$$

with

$$\begin{aligned} \mathcal{A}_\Gamma^M(p_{\Gamma,h}, q_\Gamma) = \int_{\Gamma_h} \boldsymbol{\nu}_\Gamma^\tau \ell_\Gamma (\nabla p_{\Gamma,h} + \mathscr{L}_\Gamma^{LDG}([\![p_{\Gamma,h}]\!])) \cdot (\nabla q_\Gamma + \mathscr{L}_\Gamma^{LDG}([\![q_\Gamma]\!])) \\ + \int_{\mathcal{E}^I_{\Gamma,h} \cup \mathcal{E}^D_{\Gamma,h}} \sigma_e [\![p_{\Gamma,h}]\!] \cdot [\![q_\Gamma]\!], \end{aligned} \tag{3.42}$$
$$\mathcal{L}_\Gamma^M(q_\Gamma) = \int_{\Gamma_h} \ell_\Gamma f_\Gamma q_\Gamma + \int_{\mathcal{E}^D_{\Gamma,h}} \sigma_e q_\Gamma g_\Gamma - \int_{\Gamma_h} \boldsymbol{\nu}_\Gamma^\tau \ell_\Gamma \mathcal{G}_\Gamma \cdot (\nabla q_\Gamma + \mathscr{L}_\Gamma^{LDG}([\![q_\Gamma]\!])).$$

Mixed-Mixed formulation

Finally, if we approximate both the problem in the bulk and in the fracture with the LDG method, we obtain the following formulation: Find $(p_h, p_{\Gamma,h}) \in Q_h^b \times Q_h^\Gamma$ and $(\mathbf{u}_h, \mathbf{u}_{\Gamma,h}) \in \mathbf{W}_h^b \times \mathbf{W}_h^\Gamma$ such that

$$\begin{aligned}
\mathcal{M}_b(\mathbf{u}_h, \mathbf{v}) + \mathcal{B}_b(p_h, \mathbf{v}) &= F_b(\mathbf{v}) \quad && \forall \mathbf{v} \in \mathbf{W}_h^b, \\
-\mathcal{B}_b(q, \mathbf{u}_h) + \mathcal{S}_b(p_h, q) + \mathcal{C}_1(p_h, q, p_{\Gamma,h}) &= G_b(q) \quad && \forall q \in Q_h^b, \\
\mathcal{M}_\Gamma(\mathbf{u}_{\Gamma,h}, \mathbf{v}_\Gamma) + \mathcal{B}_\Gamma(p_{\Gamma,h}, \mathbf{v}_\Gamma) &= F_\Gamma(\mathbf{v}_\Gamma) \quad && \forall \mathbf{v}_\Gamma \in \mathbf{W}_h^\Gamma, \\
-\mathcal{B}_\Gamma(q_\Gamma, \mathbf{u}_{\Gamma,h}) + \mathcal{S}_\Gamma(p_{\Gamma,h}, q_\Gamma) + \mathcal{C}_2(p_h, (p_{\Gamma,h}, q_\Gamma)) &= G_\Gamma(q_\Gamma) \quad && \forall q_\Gamma \in Q_h^\Gamma,
\end{aligned} \tag{3.43}$$

This formulation, together with the definition of the lifting operators (3.31) and (3.39) and of the discrete gradients (3.32) and (3.40) is equivalent to the following: Find $(p_h, p_{\Gamma,h}) \in Q_h^b \times Q_h^\Gamma$ such that

$$\mathcal{A}_h^{MM}\left((p_h, p_h^\Gamma), (q, q_\Gamma)\right) = \mathcal{L}_h^{MM}(q, q_\Gamma) \quad \forall (q, q_\Gamma) \in Q_h^b \times Q_h^\Gamma, \tag{3.44}$$

where MM stands for *mixed-mixed* and where $\mathcal{A}_h^{MM} : (Q_h^b \times Q_h^\Gamma) \times (Q_h^b \times Q_h^\Gamma) \to \mathbb{R}$ is defined as

$$\mathcal{A}_h^{MM}\left((p_h, p_h^\Gamma), (q, q_\Gamma)\right) = \mathcal{A}_b^M(p_h, q) + \mathcal{A}_\Gamma^M(p_{\Gamma,h}, q_\Gamma) + \mathcal{C}((p_h, p_{\Gamma,h}), (q, q_\Gamma)),$$

and $\mathcal{L}_h^{MM} : Q_h^b \times Q_h^\Gamma \to \mathbb{R}$ is defined as

$$\mathcal{L}_h^{MM}(q, q_\Gamma) = \mathcal{L}_b^M(q) + \mathcal{L}_\Gamma^M(q_\Gamma).$$

Next, we perform a unified analysis of all of the derived DG discretizations for the fully-coupled bulk-fracture problem. We remark that the analysis will be performed considering the mixed LDG discretizations recast in their primal form, following [108]. For clarity, in Table 3.1 we summarize the bilinear forms for all the four approaches.

Method	Primal bilinear form
Primal-Primal (PP)	$\mathcal{A}_b^P(p,q) + \mathcal{A}_\Gamma^P(p_\Gamma, q_\Gamma) + \mathcal{C}((p,q),(p_\Gamma,q_\Gamma))$
Mixed-Primal (MP)	$\mathcal{A}_b^M(p,q) + \mathcal{A}_\Gamma^P(p_\Gamma, q_\Gamma) + \mathcal{C}((p,q),(p_\Gamma,q_\Gamma))$
Primal-Mixed (PM)	$\mathcal{A}_b^P(p,q) + \mathcal{A}_\Gamma^M(p_\Gamma, q_\Gamma) + \mathcal{C}((p,q),(p_\Gamma,q_\Gamma))$
Mixed-Mixed (MM)	$\mathcal{A}_b^M(p,q) + \mathcal{A}_\Gamma^M(p_\Gamma, q_\Gamma) + \mathcal{C}((p,q),(p_\Gamma,q_\Gamma))$

Table 3.1: Primal forms for the DG discretizations of the bulk-fracture problems.

The bulk, fracture and interface bilinear forms are defined in:

$\mathcal{A}_b^P(p,q)$: (3.22) $\mathcal{A}_\Gamma^P(p_\Gamma,q_\Gamma)$: (3.23) $\mathcal{C}((p,q),(p_\Gamma,q_\Gamma))$: (3.24)
$\mathcal{A}_b^M(p,q)$: (3.35) $\mathcal{A}_\Gamma^M(p_\Gamma,q_\Gamma)$: (3.42)

3.4 Well-posedness of the discrete formulations

In this section, we address the problem of stability. We prove that the primal-primal (PP) (3.21), mixed-primal (MP) (3.34), primal-mixed (PM) (3.41) and mixed-mixed (MM)(3.44) formulations are well-posed. We remark that all these formulations are *not* strongly consistent, due to the presence of the lifting operators. This implies that the analysis will be based on Strang's second Lemma, [114].

We recall that, for simplicity in the analysis, we are assuming the permeability tensors $\boldsymbol{\nu}$ and $\boldsymbol{\nu}_\Gamma^\tau$ to be piecewise constant and that we employ the following notation $\bar{\boldsymbol{\nu}}_E = |\sqrt{\boldsymbol{\nu}|_E}|_2^2$ and $\bar{\boldsymbol{\nu}}_F^\tau = |\sqrt{\boldsymbol{\nu}_\Gamma^\tau|_F}|_2^2$, where $|\cdot|_2$ denotes the l_2-norm.

To consider the boundedness and stability of our primal bilinear forms, we introduce the spaces $Q^b(h) = Q_h^b + \tilde{Q}^b$ and $Q^\Gamma(h) = Q_h^\Gamma + \tilde{Q}^\Gamma$ where $\tilde{Q}^b = \{q = (q_1, q_2) \in H^1(\Omega_1) \times H^1(\Omega_2)\} \cap H^2(\mathcal{T}_h)$ and $\tilde{Q}^\Gamma = H^1(\Gamma) \cap H^2(\Gamma_h)$. We remark that all the bilinear forms $\mathcal{A}_h^{**}(\cdot,\cdot)$ are also well-defined on the extended space $Q^b(h) \times Q^\Gamma(h)$.
Further, we introduce the following *energy* norm on the discrete space $Q_h^b \times Q_h^\Gamma$

$$|||(q, q_\Gamma)|||^2 = ||q||_{b,DG}^2 + ||q_\Gamma||_{\Gamma,DG}^2 + ||(q, q_\Gamma)||_{\mathcal{C}}^2$$

where

$$
\begin{aligned}
||q||^2_{b,DG} &= ||\boldsymbol{\nu}^{1/2}\nabla q||^2_{0,\mathcal{T}_h} + ||\sigma_F^{1/2}[\![q]\!]||^2_{0,\mathcal{F}_h^I\cup\mathcal{F}_h^D} \\
||q_\Gamma||^2_{\Gamma,DG} &= ||(\boldsymbol{\nu}_{\boldsymbol{\Gamma}}^{\boldsymbol{\tau}}\ell_\Gamma)^{1/2}\nabla q_\Gamma||^2_{0,\Gamma_h} + ||\sigma_e^{1/2}[\![q_\Gamma]\!]||^2_{0,\mathcal{E}^I_{\Gamma,h}\cup\mathcal{E}^D_{\Gamma,h}} \\
||(q,q_\Gamma)||^2_{\mathcal{C}} &= ||\beta_\Gamma^{1/2}[\![q]\!]||^2_{0,\Gamma_h} + ||\alpha_\Gamma^{1/2}(\{q\}-q_\Gamma)||^2_{0,\Gamma_h}
\end{aligned}
$$

Note that $|||\cdot|||$ is also well defined on the extended space $Q^b(h)\times Q^\Gamma(h)$.

Next, we need to give an appropriate definition of the discontinuity penalization parameter, so that we can work in a polytopic framework. Taking as a reference [61, 59, 6, 58, 60] as in Chapter 2, we give the following two definitions for the bulk and fracture penalty functions:

Definition 3.4.1. The discontinuity-penalization parameter $\sigma : \mathcal{F}_h \setminus \Gamma_h \to \mathbb{R}^+$ for the bulk problem is defined facewise as

$$
\sigma(\mathbf{x}) = \sigma_0 \begin{cases} \max_{E\in\{E^+,E^-\}} \frac{\bar{\boldsymbol{\nu}}_E k_E^2}{h_E} & \text{if } \mathbf{x}\subset F\in\mathcal{F}_h^I,\ \bar{F}=\partial\bar{E}^+\cap\partial\bar{E}^-, \\ \frac{\bar{\boldsymbol{\nu}}_E k_E^2}{h_E} & \text{if } \mathbf{x}\subset F\in\mathcal{F}_h^D,\ \bar{F}=\partial\bar{E}\cap\partial\bar{\Omega}, \end{cases} \tag{3.45}
$$

with $\sigma_0 > 0$ independent of k_E, $|E|$ and $|F|$.

Definition 3.4.2. The discontinuity-penalization parameter $\sigma_\Gamma : \mathcal{E}_{\Gamma,h} \to \mathbb{R}^+$ for the fracture problem is defined edgewise as

$$
\sigma_\Gamma(\mathbf{x}) = \sigma_{0,\Gamma} \begin{cases} \max_{F\in\{F^+,F^-\}} \frac{\bar{\boldsymbol{\nu}}_F^\tau k_F^2}{h_F} & \text{if } \mathbf{x}\subset e\in\mathcal{E}^I_{\Gamma,h},\ \bar{e}=\partial\bar{F}^+\cap\partial\bar{F}^-, \\ \frac{\bar{\boldsymbol{\nu}}_F^\tau k_F^2}{h_F}, & \text{if } \mathbf{x}\subset e\in\mathcal{E}^D_{\Gamma,h},\ \bar{e}=\partial\bar{F}\cap\partial\bar{\Gamma}, \end{cases} \tag{3.46}
$$

with $\sigma_{0,\Gamma} > 0$ independent of k_F, $|F|$ and $|e|$.

Next, we will state and prove some estimates that will be instrumental for the proof of the well-posedness of our discrete formulations. We start deriving some bounds on the lifting operators, with arguments similar to those of [108, 109, 18]. Note that all the results hold true on the extended spaces $Q^b(h)$ and $Q^\Gamma(h)$.

Lemma 3.4.1. *Let $\mathscr{L}_b^{SIP}(\cdot)$ be the lifting operator defined in* (3.13)*. Then, for every $q \in Q^b(h)$ it holds*

$$||\boldsymbol{\nu}^{1/2}\mathscr{L}_b^{SIP}([\![q]\!])||_{L^2(\Omega)} \lesssim \frac{1}{\sigma_0^{1/2}}||\sigma_F^{1/2}[\![q]\!]||_{0,\mathcal{F}_h^I\cup\mathcal{F}_h^D}. \tag{3.47}$$

Proof. Denoting by $\boldsymbol{\Pi}_{\mathbf{W}_h^b}$ the L^2-projection onto $\mathbf{W}_h^b$, by definition of the lifting operator $\mathscr{L}_b^{SIP}$ and Cauchy-Schwarz inequality, we have

$$\begin{aligned}
||\boldsymbol{\nu}^{1/2}\mathscr{L}_b^{SIP}([\![q]\!])||_{L^2(\Omega)} &= \sup_{\mathbf{z}\in[L^2(\Omega)]^d} \frac{\int_\Omega \boldsymbol{\nu}^{1/2}\mathscr{L}_b^{SIP}([\![q]\!])\cdot\mathbf{z}}{||\mathbf{z}||_{L^2(\Omega)}} \\
&= \sup_{\mathbf{z}\in[L^2(\Omega)]^d} \frac{\int_\Omega \mathscr{L}_b^{SIP}([\![q]\!])\cdot\boldsymbol{\Pi}_{\mathbf{W}_h^b}(\boldsymbol{\nu}^{1/2}\mathbf{z})}{||\mathbf{z}||_{L^2(\Omega)}} \\
&= -\sup_{\mathbf{z}\in[L^2(\Omega)]^d} \frac{\int_{\mathcal{F}_h^I\cup\mathcal{F}_h^D}\sigma_F^{1/2}[\![q]\!]\cdot\sigma_F^{-1/2}\{\boldsymbol{\Pi}_{\mathbf{W}_h^b}(\boldsymbol{\nu}^{1/2}\mathbf{z})\}}{||\mathbf{z}||_{L^2(\Omega)}} \\
&\leq \sup_{\mathbf{z}\in[L^2(\Omega)]^d} \frac{||\sigma_F^{1/2}[\![q]\!]||_{0,\mathcal{F}_h^I\cup\mathcal{F}_h^D}||\sigma_F^{-1/2}\{\boldsymbol{\Pi}_{\mathbf{W}_h^b}(\boldsymbol{\nu}^{1/2}\mathbf{z})\}||_{0,\mathcal{F}_h^I\cup\mathcal{F}_h^D}}{||\mathbf{z}||_{L^2(\Omega)}}.
\end{aligned}$$

Using the triangular inequality, the definition of the penalization coefficient σ_F (3.45), the inverse inequality (1.6), the assumptions on the permeability tensor $\boldsymbol{\nu}$ and the continuity property of the L^2-projector we have

$$\begin{aligned}
||\sigma_F^{-1/2}\{\boldsymbol{\Pi}_{\mathbf{W}_h^b}(\boldsymbol{\nu}^{1/2}\mathbf{z})\}||^2_{0,\mathcal{F}_h^I\cup\mathcal{F}_h^D} &\lesssim \sum_{E\in\mathcal{T}_h}\frac{1}{\sigma_0}\frac{h_E}{\bar{\boldsymbol{\nu}}_E k_E^2}||\boldsymbol{\Pi}_{\mathbf{W}_h^b}(\boldsymbol{\nu}^{1/2}\mathbf{z})||^2_{L^2(\partial E)} \\
&\lesssim \sum_{E\in\mathcal{T}_h}\frac{1}{\bar{\boldsymbol{\nu}}_E}\frac{1}{\sigma_0}||\boldsymbol{\Pi}_{\mathbf{W}_h^b}(\boldsymbol{\nu}^{1/2}\mathbf{z})||^2_{L^2(E)} \lesssim \frac{1}{\sigma_0}\sum_{E\in\mathcal{T}_h}||z||^2_{L^2(E)} = \frac{1}{\sigma_0}||z||^2_{L^2(\Omega)}.
\end{aligned} \tag{3.48}$$

This proves the desired estimate.

□

Lemma 3.4.2. *Let $\mathscr{L}_\Gamma^{SIP}(\cdot)$ be the lifting operator defined in* (3.18)*. Then, for every $q_\Gamma \in Q^\Gamma(h)$ it holds*

$$||(\boldsymbol{\nu}_\Gamma^\tau\ell_\Gamma)^{1/2}\mathscr{L}_\Gamma^{SIP}([\![q_\Gamma]\!])||_{L^2(\Gamma)} \lesssim \frac{1}{\sigma_{0,\Gamma}^{1/2}}||\sigma_e^{1/2}[\![q_\Gamma]\!]||_{0,\mathcal{E}_{\Gamma,h}^I\cup\mathcal{E}_{\Gamma,h}^D}.$$

Proof. Same arguments as in in the proof of Lemma 3.4.1. □

Lemma 3.4.3. *Let $\mathscr{L}_b^{LDG}(\cdot)$ be the lifting operator defined in* (3.31)*. Then, for every $q \in Q^b(h)$ it holds*

$$||\boldsymbol{\nu}^{1/2}\mathscr{L}_b^{LDG}([\![q]\!])||_{L^2(\Omega)} \lesssim \frac{1+B}{\sigma_0^{1/2}}||\sigma_F^{1/2}[\![q]\!]||_{0,\mathcal{F}_h^I\cup\mathcal{F}_h^D}. \tag{3.49}$$

Proof. We proceed as in the proof of Lemma 3.4.1. By definition of the lifting operator $\mathscr{L}_b^{LDG}$ and Cauchy-Schwarz inequality, we have

$$\begin{aligned}
||\boldsymbol{\nu}^{1/2}\mathscr{L}_b^{LDG}([\![q]\!])||_{L^2(\Omega)} &= \sup_{\mathbf{z}\in[L^2(\Omega)]^d}\frac{\int_\Omega \boldsymbol{\nu}^{1/2}\mathscr{L}_b^{LDG}([\![q]\!])\cdot\mathbf{z}}{||\mathbf{z}||_{L^2(\Omega)}}\\
&= \sup_{\mathbf{z}\in[L^2(\Omega)]^d}\frac{\int_\Omega \mathscr{L}_b^{LDG}([\![q]\!])\cdot\boldsymbol{\Pi}_{\mathbf{W}_h^b}(\boldsymbol{\nu}^{1/2}\mathbf{z})}{||\mathbf{z}||_{L^2(\Omega)}}\\
&\le \sup_{\mathbf{z}\in[L^2(\Omega)]^d}\frac{\left|-\int_{\mathcal{F}_h^I}\sigma_F^{1/2}[\![q]\!]\cdot\sigma_F^{-1/2}(\{\boldsymbol{\Pi}_{\mathbf{W}_h^b}(\boldsymbol{\nu}^{1/2}\mathbf{z})\}-\mathbf{b}[\![\boldsymbol{\Pi}_{\mathbf{W}_h^b}(\boldsymbol{\nu}^{1/2}\mathbf{z})]\!])\right|}{||\mathbf{z}||_{L^2(\Omega)}}\\
&\quad+\sup_{\mathbf{z}\in[L^2(\Omega)]^d}\frac{\left|-\int_{\mathcal{F}_h^D}\sigma_F^{1/2}[\![q]\!]\cdot\sigma_F^{-1/2}\boldsymbol{\Pi}_{\mathbf{W}_h^b}(\boldsymbol{\nu}^{1/2}\mathbf{z})\right|}{||\mathbf{z}||_{L^2(\Omega)}}\\
&\le \sup_{\mathbf{z}\in[L^2(\Omega)]^d}\frac{||\sigma_F^{1/2}[\![q]\!]||_{0,\mathcal{F}_h^I\cup\mathcal{F}_h^D}||\sigma_F^{-1/2}\{\boldsymbol{\Pi}_{\mathbf{W}_h^b}(\boldsymbol{\nu}^{1/2}\mathbf{z})\}||_{0,\mathcal{F}_h^I\cup\mathcal{F}_h^D}}{||\mathbf{z}||_{L^2(\Omega)}}\\
&\quad+\sup_{\mathbf{z}\in[L^2(\Omega)]^d}\frac{||\sigma_F^{1/2}[\![q]\!]||_{0,\mathcal{F}_h^I}||\sigma_F^{-1/2}\mathbf{b}[\![\boldsymbol{\Pi}_{\mathbf{W}_h^b}(\boldsymbol{\nu}^{1/2}\mathbf{z})]\!]||_{0,\mathcal{F}_h^I}}{||\mathbf{z}||_{L^2(\Omega)}}\\
&= (a)+(b)
\end{aligned}$$

From (3.48) we know that $(a)\lesssim\frac{1}{\sigma_0^{1/2}}||\sigma_F^{1/2}[\![q]\!]||_{0,\mathcal{F}_h^I\cup\mathcal{F}_h^D}$, while using similar arguments and bound (3.27) on $\mathbf{b}$, we can prove that

$$||\sigma_F^{-1/2}\mathbf{b}[\![\boldsymbol{\Pi}_{\mathbf{W}_h^b}(\boldsymbol{\nu}^{1/2}\mathbf{z})]\!]||^2_{0,\mathcal{F}_h^I}\lesssim\frac{B^2}{\sigma_0}||\mathbf{z}||^2_{L^2(\Omega)},$$

so that $(b)\lesssim\frac{B}{\sigma_0^{1/2}}||\sigma_F^{1/2}[\![q]\!]||_{0,\mathcal{F}_h^I\cup\mathcal{F}_h^D}$. This concludes the proof. □

Lemma 3.4.4. *Let $\mathscr{L}_\Gamma^{LDG}(\cdot)$ be the lifting operator defined in* (3.39)*. Then, For every*

$q_\Gamma \in Q^\Gamma(h)$ *it holds*

$$||(\boldsymbol{\nu}_\Gamma^\tau \ell_\Gamma)^{1/2} \mathscr{L}_\Gamma^{LDG}([\![q_\Gamma]\!])||_{L^2(\Gamma)} \lesssim \frac{1+B_\Gamma}{\sigma_{0,\Gamma}^{1/2}} ||\sigma_e^{1/2}[\![q_\Gamma]\!]||_{0,\mathcal{E}_{\Gamma,h}^I \cup \mathcal{E}_{\Gamma,h}^D}.$$

Proof. Same arguments as in in the proof of Lemma 3.4.3. □

Using these results, we can now prove that the bilinear forms for the bulk problem $\mathcal{A}_b^P(\cdot,\cdot)$ and $\mathcal{A}_b^M(\cdot,\cdot)$ are continuous on $Q^b(h)$ and coercive on Q_h^b, as well as the fracture bilinear forms $\mathcal{A}_\Gamma^P(\cdot,\cdot)$ and $\mathcal{A}_\Gamma^M(\cdot,\cdot)$ are continuous on $Q^\Gamma(h)$ and coercive on Q_h^Γ.

Lemma 3.4.5. *$\mathcal{A}_b^P(\cdot,\cdot)$ is coercive on $Q_h^b \times Q_h^b$ and continuous on $Q^b(h) \times Q^b(h)$, that is*

$$\begin{aligned} &\mathcal{A}_b^P(q,q) \gtrsim ||q||_{b,DG}^2 && \forall q \in Q_h^b, \\ &\mathcal{A}_b^P(p,q) \lesssim ||p||_{b,DG}\, ||q||_{b,DG} && \forall p,q \in Q^b(h), \end{aligned}$$

provided that σ_0 is chosen big enough.

Proof. We start with coercivity. Taking $p = q \in Q_h^b$, we have

$$\mathcal{A}_b^P(q,q) = \sum_{E\in\mathcal{T}_h} \left[||\boldsymbol{\nu}^{1/2}\nabla q||_{L^2(E)}^2 + 2\int_E \boldsymbol{\nu}\mathscr{L}_b^{SIP}([\![q]\!])\cdot\nabla q \right] + \sum_{F\in\mathcal{F}_h^I\cup\mathcal{F}_h^D} ||\sigma_F^{1/2}[\![q]\!]||_{L^2(F)}^2$$

From Young inequality we have

$$\begin{aligned} 2\int_E \boldsymbol{\nu}\mathscr{L}_b^{SIP}([\![q]\!])\cdot\nabla q &\geq -2||\boldsymbol{\nu}^{1/2}\mathscr{L}_b^{SIP}([\![q]\!])||_{L^2(E)}||\boldsymbol{\nu}^{1/2}\nabla q||_{L^2(E)} \\ &\geq -\varepsilon||\boldsymbol{\nu}^{1/2}\mathscr{L}_b^{SIP}([\![q]\!])||_{L^2(E)}^2 - \frac{1}{\varepsilon}||\boldsymbol{\nu}^{1/2}\nabla q||_{L^2(E)}^2, \end{aligned}$$

so that, using the bound on the lifting (3.47), we obtain

$$\begin{aligned}\mathcal{A}_b^P(q,q) &\geq \sum_{E\in\mathcal{T}_h}\left[(1-\varepsilon)\|\boldsymbol{\nu}^{1/2}\nabla q\|_{L^2(E)}^2 - \frac{1}{\varepsilon}\|\boldsymbol{\nu}^{1/2}\mathscr{L}_b^{SIP}([\![q]\!])\|_{L^2(E)}^2\right] \\ &\quad + \sum_{F\in\mathcal{F}_h^I\cup\mathcal{F}_h^D} ||\sigma_F^{1/2}[\![q]\!]||_{L^2(F)}^2 \\ &\gtrsim (1-\varepsilon)\sum_{E\in\mathcal{T}_h}\|\boldsymbol{\nu}^{1/2}\nabla q\|_{L^2(E)}^2 + \left(1-\frac{1}{\sigma_0\varepsilon}\right)\sum_{F\in\mathcal{F}_h^I\cup\mathcal{F}_h^D} ||\sigma_F^{1/2}[\![q]\!]||_{L^2(F)}^2 \\ &\gtrsim ||q||_{b,DG}^2,\end{aligned}$$

for σ_0 big enough.

Continuity directly follows from Cauchy Schwarz inequality and the bound on the lifting (3.47). □

Lemma 3.4.6. *$\mathcal{A}_\Gamma^P(\cdot,\cdot)$ is coercive on $Q_h^\Gamma \times Q_h^\Gamma$ and continuous on $Q^\Gamma(h)\times Q^\Gamma(h)$, that is*

$$\begin{aligned}\mathcal{A}_\Gamma^P(q_\Gamma,q_\Gamma) &\gtrsim ||q_\Gamma||_{\Gamma,DG}^2 && \forall q_\Gamma\in Q_h^\Gamma,\\ \mathcal{A}_\Gamma^P(p_\Gamma,q_\Gamma) &\lesssim ||p_\Gamma||_{\Gamma,DG}\,||q_\Gamma||_{\Gamma,DG} && \forall p_\Gamma,q_\Gamma\in Q^\Gamma(h),\end{aligned}$$

provided that $\sigma_{0,\Gamma}$ is chosen big enough.

Proof. Analogous to the proof of Lemma 3.4.5. □

Lemma 3.4.7. *$\mathcal{A}_b^M(\cdot,\cdot)$ is coercive on $Q_h^b\times Q_h^b$ and continuous on $Q^b(h)\times Q^b(h)$, that is*

$$\begin{aligned}\mathcal{A}_b^M(q,q) &\gtrsim ||q||_{b,DG}^2 && \forall q\in Q_h^b,\\ \mathcal{A}_b^M(p,q) &\lesssim ||p||_{b,DG}\,||q||_{b,DG} && \forall p,q\in Q^b(h).\end{aligned}$$

Proof. We start with coercivity. From Young's inequality and the bound on the lifting

(3.49) we have, for every $0 < \varepsilon < 1$,

$$\begin{aligned}
\mathcal{A}_b^M(q,q) = \sum_{E\in\mathcal{T}_h} \Bigg[& ||\boldsymbol{\nu}^{1/2}\nabla q||^2_{L^2(E)} + ||\boldsymbol{\nu}^{1/2}\mathscr{L}_b^{LDG}([\![q]\!])||^2_{L^2(E)} \\
& + 2\int_E \boldsymbol{\nu}\mathscr{L}_b^{LDG}([\![q]\!])\cdot\nabla q \Bigg] + \sum_{F\in\mathcal{F}_h^I\cup\mathcal{F}_h^D} ||\sigma_F^{1/2}[\![q]\!]||^2_{L^2(F)} \\
\geq \sum_{E\in\mathcal{T}_h} & \left[(1-\varepsilon)\|\boldsymbol{\nu}^{1/2}\nabla q\|^2_{L^2(E)} + \left(1-\frac{1}{\varepsilon}\right)||\boldsymbol{\nu}^{1/2}\mathscr{L}_b^{LDG}([\![q]\!])||^2_{L^2(E)} \right] \\
& + \sum_{F\in\mathcal{F}_h^I\cup\mathcal{F}_h^D} ||\sigma_F^{1/2}[\![q]\!]||^2_{L^2(F)} \\
\gtrsim (1-\varepsilon) & \sum_{E\in\mathcal{T}_h} \|\boldsymbol{\nu}^{1/2}\nabla q\|^2_{L^2(E)} + (1+C) \sum_{F\in\mathcal{F}_h^I\cup\mathcal{F}_h^D} ||\sigma_F^{1/2}[\![q]\!]||^2_{L^2(F)}
\end{aligned}$$

with $C = \frac{(1+B)}{\sigma_0\varepsilon}(1-\frac{1}{\varepsilon})$, so that $\mathcal{A}_b^M(\cdot,\cdot)$ is coercive for every choice of the parameters $\sigma_0 > 0$ and $B > 0$ [1]. Continuity is again a direct consequence of Cauchy Schwarz's inequality and the bound on the lifting (3.49). □

Lemma 3.4.8. *$\mathcal{A}_\Gamma^M(\cdot,\cdot)$ is coercive on $Q_h^\Gamma \times Q_h^\Gamma$ and continuous on $Q^\Gamma(h)\times Q^\Gamma(h)$, that is*

$$\begin{aligned}
\mathcal{A}_\Gamma^M(q_\Gamma, q_\Gamma) &\gtrsim ||q_\Gamma||^2_{\Gamma,DG} && \forall q_\Gamma \in Q_h^\Gamma, \\
\mathcal{A}_\Gamma^M(p_\Gamma, q_\Gamma) &\lesssim ||p_\Gamma||_{\Gamma,DG}\,||q_\Gamma||_{\Gamma,DG} && \forall p_\Gamma, q_\Gamma \in Q^\Gamma(h).
\end{aligned}$$

Proof. Analogous to the proof of Lemma 3.4.7. □

Employing Lemmas 3.4.5, 3.4.7, 3.4.6 and 3.4.8, we can easily prove the well-posedness of all of our discrete problems, as stated in the following stability result.

Proposition 3.4.9. *Let the penalization parameters σ for the problem in the bulk and in the fracture be defined as in* (3.45) *and* (3.46)*, respectively. Then, the fully-coupled discrete problems PP* (3.21)*, MP* (3.34)*, PM* (3.41) *and MM* (3.44) *are well-posed provided that σ_0 and $\sigma_{0,\Gamma}$ are chosen big enough for the primal formulations.*

[1] More in detail: we need $1 + C > 0$, with $0 < \varepsilon < 1$. We obtain $1 + (1-\frac{1}{\varepsilon})\frac{(1+B)^2}{\sigma_0} > 0$, that is $\varepsilon > \frac{1}{1+\frac{\sigma_0}{(1+B)^2}} = \tilde{C}$, being $0 < \tilde{C} < 1$ for every possible choice of $\sigma_0 > 0$ and $B > 0$.

Proof. In order to use Lax-Milgram Lemma, we prove that the bilinear forms $\mathcal{A}_h^{PP}(\cdot,\cdot)$, $\mathcal{A}_h^{MP}(\cdot,\cdot)$, $\mathcal{A}_h^{PM}(\cdot,\cdot)$ and $\mathcal{A}_h^{MM}(\cdot,\cdot)$ are continuous on $Q^b(h)\times Q^\Gamma(h)$ and coercive on $Q_h^b\times Q_h^\Gamma$. We have, from Cauchy-Schwarz inequality

$$\begin{aligned}
\mathcal{C}((q,q_\Gamma),(q,q_\Gamma)) &= ||(q,q_\Gamma)||_{\mathcal{C}}^2\\
\mathcal{C}((q,q_\Gamma),(w,w_\Gamma)) &\le \sum_{F\in\Gamma_h} ||\beta_\Gamma^{1/2}[\![q]\!]||_{L^2(F)}^2||\beta_\Gamma^{1/2}[\![w]\!]||_{L^2(F)}^2\\
&\quad+\sum_{F\in\Gamma_h} ||\alpha_\Gamma^{1/2}(\{q\}-q_\Gamma)||_{L^2(F)}^2||\alpha_\Gamma^{1/2}(\{w\}-w_\Gamma)||_{L^2(F)}^2\\
&\le |||(q,q_\Gamma)|||\cdot|||(w,w_\Gamma)|||,
\end{aligned}$$

so that coercivity and continuity are a direct consequence of the definition of the norm $|||\cdot|||$ and of Lemmas 3.4.5, 3.4.7, 3.4.6 and 3.4.8. The continuity of the linear operators $\mathcal{L}_h^{PP}(\cdot)$, $\mathcal{L}_h^{MP}(\cdot)$, $\mathcal{L}_h^{PM}(\cdot)$ and $\mathcal{L}_h^{MM}(\cdot)$ on $Q^b(h)\times Q^\Gamma(h)$ can be easily proved by using Cauchy-Schwarz's inequality, thanks to the regularity assumptions on the forcing terms f and f_Γ and on the boundary data g_D and g_Γ. □

3.5 Error analysis

In this section we derive error estimates for our discrete problems.

For each subdomain Ω_i, $i=1,2$, we denote by $\mathscr{E}_i$ the classical continuous extension operator (cf. [113], see also Chapter 2) $\mathscr{E}_i : H^s(\Omega_i)\to H^s(\mathbb{R}^d)$, for $s\in\mathbb{N}_0$. Similarly, we denote by $\mathscr{E}_\Gamma$ the continuous extension operator $\mathscr{E}_\Gamma : H^s(\Gamma)\to H^s(\mathbb{R}^{d-1})$, for $s\in\mathbb{N}_0$. We then make the following regularity assumptions for the exact solution (p,p_Γ) of problem (3.5):

Assumption 3.5.1. *Let $\mathcal{T}_\# = \{T_E\}$ and $\mathcal{F}_\# = \{T_F\}$ denote the associated coverings of Ω and Γ, respectively, of Definition 1.1.2. We assume that the exact solution (p,p_Γ) is such that:*

A1. for every $E\in\mathcal{T}_h$, if $E\subset\Omega_i$, it holds $\mathscr{E}_i p_i|_{T_E}\in H^{r_E}(T_E)$, with $r_E\ge 1+d/2$ and $T_E\in\mathcal{T}_\#$ with $E\subset T_E$;

A2. for every $F\in\Gamma_h$, it holds $\mathscr{E}_\Gamma p_\Gamma|_{T_F}\in H^{r_F}(T_F)$, with $r_F\ge 1+(d-1)/2$ and $T_F\in\mathcal{F}_\#$ with $F\subset T_F$.

Assumption 3.5.2. *We assume that the normal components of the exact fluxes* $\boldsymbol{\nu}\nabla p$ *and* $\ell_\Gamma \boldsymbol{\nu}_\Gamma^\tau \nabla p_\Gamma$ *are continuous across mesh interfaces, that is* $[\![\boldsymbol{\nu}\nabla p]\!] = 0$ *on* $\mathcal{F}_h^I$ *and* $[\![\ell_\Gamma \boldsymbol{\nu}_\Gamma^\tau \nabla p_\Gamma]\!] = 0$ *on* $\mathcal{E}_{\Gamma,h}^I$.

From Proposition 3.4.9 and Strang's second Lemma the following abstract error bound directly follows.

Lemma 3.5.3. *Assuming that the hypotheses of Proposition 3.4.9 are satisfied, for all the discrete problems PP* (3.21)*, MP* (3.34)*, MM* (3.44) *and PM* (3.44) *the following abstract error bound holds*

$$|||(p,p_\Gamma)-(p_h,p_{\Gamma,h})||| \lesssim \inf_{(q,q_\Gamma)\in Q_h^b\times Q_h^\Gamma} |||(p,p_\Gamma)-(q,q_\Gamma)|||+\sup_{(w,w_\Gamma)\in Q_h^b\times Q_h^\Gamma}\frac{|\mathcal{R}_h^{**}((p,p_\Gamma),(w,w_\Gamma))|}{|||(w,w_\Gamma)|||},$$

where the residual $\mathcal{R}_h^{**}$ *is defined as*

$$\mathcal{R}_h^{**}((p,p_\Gamma),(w,w_\Gamma)) = \mathcal{A}_h^{**}((p,p_\Gamma),(w,w_\Gamma)) - \mathcal{L}_h^{**}(w,w_\Gamma),$$

with $** \in \{PP, MP, MM, PM\}$.

Note that, irrespective of the numerical method chosen for the discretization (PP, MP, PM or MM), the residual can always be split into two contributions, one deriving from the approximation of the problem in the bulk and one deriving from the approximation of the problem in the fracture, i.e.,

$$\mathcal{R}_h^{**}((p,p_\Gamma),(w,w_\Gamma)) = \mathcal{R}_b^{*}(p,w) + \mathcal{R}_\Gamma^{*}(p_\Gamma,w_\Gamma) \tag{3.50}$$

It follows that, to derive a bound for the global residual, we can bound each of the two contributions separately. With this in mind, we state and prove the next two lemmas.

Lemma 3.5.4. *Let* (p,p_Γ) *be the exact solution of problem* (3.5) *satisfying the regularity Assumptions 3.5.2 and 3.5.1. Then, for every* $w \in Q^b(h)$ *and* $w_\Gamma \in Q^\Gamma(h)$*, it holds*

$$|\mathcal{R}_b^P(p,w)|^2 \lesssim \sum_{E\in\mathcal{T}_h}\frac{h_E^{2(s_E-1)}}{k_E^{2(r_E-1)}}||\mathscr{E}p||^2_{H^{r_E}(T_E)}\left[\bar{\boldsymbol{\nu}}_E^2 \max_{F\subset\partial E\setminus\Gamma}\sigma_F^{-1}\left(\frac{k_E}{h_E}+\frac{k_E^2}{h_E}\right)\right]\cdot ||w||^2_{b,DG}, \tag{3.51}$$

$$|\mathcal{R}_\Gamma^P(p_\Gamma,w_\Gamma)|^2 \lesssim \sum_{F\in\Gamma_h}\frac{h_F^{2(s_F-1)}}{k_F^{2(r_F-1)}}||\mathscr{E}p_\Gamma||^2_{H^{r_F}(T_F)}\left[(\bar{\boldsymbol{\nu}}_F^\tau\ell_\Gamma)^2 \max_{e\subseteq\partial F}\sigma_e^{-1}\left(\frac{k_F}{h_F}+\frac{k_F^2}{h_F}\right)\right]\cdot ||w_\Gamma||^2_{\Gamma,DG}. \tag{3.52}$$

Proof. First, we prove (3.51). Let $\mathbf{\Pi}_{\mathbf{W}_h^b}$ be the L^2-orthogonal projector onto $\mathbf{W}_h^b$, then, integrating by parts elementwise, using the fact that p satisfies (3.1) and recalling that, from Assumption 3.5.2, $[\![\boldsymbol{\nu}\nabla p]\!]$ vanishes on $\mathcal{F}_h^I$, we obtain the following expression for the residual $\mathcal{R}_b^P$:

$$\mathcal{R}_b^P(p,w) = \sum_{F\in\mathcal{F}_h^I\cup\mathcal{F}_h^D}\int_F \{\boldsymbol{\nu}(\nabla p - \mathbf{\Pi}_{\mathbf{W}_h^b}(\nabla p))\}\cdot[\![w]\!], \qquad \forall w\in Q^b(h).$$

Employing the Cauchy-Schwarz's inequality and the definition of the norm $|||\cdot|||$, we then obtain

$$|\mathcal{R}_b^P(p,w)|^2 \lesssim \left(\sum_{F\in\mathcal{F}_h^I\cup\mathcal{F}_h^D}\sigma_F^{-1}\int_F|\{\boldsymbol{\nu}(\nabla p - \mathbf{\Pi}_{\mathbf{W}_h^b}(\nabla p))\}|^2\right)\cdot||w||_{b,DG}^2, \qquad \forall w\in Q^b(h).$$

If we still denote by $\widetilde{\Pi}$ the vector-valued generalization of the projection operator $\widetilde{\Pi}$ defined in Lemma 1.3.3, we observe that

$$\begin{aligned}\sum_{F\in\mathcal{F}_h^I\cup\mathcal{F}_h^D}\sigma_F^{-1}\int_F|\{\boldsymbol{\nu}(\nabla p - \mathbf{\Pi}_{\mathbf{W}_h^b}(\nabla p))\}|^2 \leq &\sum_{F\in\mathcal{F}_h^I\cup\mathcal{F}_h^D}\sigma_F^{-1}\int_F|\{\boldsymbol{\nu}(\nabla p - \widetilde{\Pi}(\nabla p))\}|^2\\ &+\sum_{F\in\mathcal{F}_h^I\cup\mathcal{F}_h^D}\sigma_F^{-1}\int_F|\{\boldsymbol{\nu}\mathbf{\Pi}_{\mathbf{W}_h^b}(\nabla p - \widetilde{\Pi}(\nabla p))\}|^2\\ &\equiv (1)+(2).\end{aligned}$$

To bound the term (1), we employ the approximation result stated in Lemma 1.3.3. We obtain

$$(1)\lesssim\sum_{E\in\mathcal{T}_h}\frac{h_E^{2(s_E-1)}}{k_E^{2(r_E-1)}}\Big(\bar{\boldsymbol{\nu}}_E^2\max_{F\subset\partial E\setminus\Gamma}\sigma_F^{-1}\frac{h_E^{-1}}{k_E^{-1}}\Big)||\mathscr{E}p||_{H^{r_E}(T_E)}^2.$$

Exploiting, the boundedness of the permeability tensor $\boldsymbol{\nu}$, the inverse inequality (1.6), the L^2-stability of the projector $\mathbf{\Pi}_{\mathbf{W}_h^b}$ and the approximation results stated in Lemma 1.3.3,

we can bound term (2) as follows:

$$\begin{aligned}(2) &\lesssim \sum_{E\in\mathcal{T}_h}\max_{F\subset\partial E\setminus\Gamma}\sigma_F^{-1}\bar{\boldsymbol{\nu}}_E^2||\boldsymbol{\Pi}_{\mathbf{W}_h^b}(\widetilde{\Pi}(\nabla p)-\nabla p)||^2_{L^2(\partial E\setminus\Gamma)}\\ &\lesssim \sum_{E\in\mathcal{T}_h}\max_{F\subset\partial E\setminus\Gamma}\sigma_F^{-1}\bar{\boldsymbol{\nu}}_E^2\frac{k_E^2}{h_E}||\widetilde{\Pi}(\nabla p)-\nabla p||^2_{L^2(E)}\\ &\lesssim \sum_{E\in\mathcal{T}_h}\frac{h_E^{2(s_E-1)}}{k_E^{2(r_E-1)}}||\mathscr{E}p||^2_{H^{r_E}(T_E)}\left(\bar{\boldsymbol{\nu}}_E^2\frac{k_E^2}{h_E}\max_{F\subset\partial E\setminus\Gamma}\sigma_F^{-1}\right),\end{aligned}$$

which concludes the proof of (3.51).
Proceeding as above we obtain the following expression for the residual $\mathcal{R}_\Gamma^P$:

$$\mathcal{R}_\Gamma^P(p_\Gamma,w_\Gamma)=\sum_{e\in\mathcal{E}_{\Gamma,h}^I\cup\mathcal{E}_{\Gamma,h}^D}\int_e\{\boldsymbol{\nu}_{\boldsymbol{\Gamma}}^{\boldsymbol{\tau}}\ell_\Gamma(\nabla p_\Gamma-\boldsymbol{\Pi}_{\mathbf{W}_h^\Gamma}(\nabla p_\Gamma))\}\cdot[\![w_\Gamma]\!].$$

Estimate (3.52) can then be proven with analogous arguments. □

Lemma 3.5.5. *Let (p,p_Γ) be the exact solution of problem (3.5) satisfying the regularity Assumptions 3.5.2 and 3.5.1. Then, for every $w\in Q^b(h)$ and $w_\Gamma\in Q^\Gamma(h)$, it holds*

$$\begin{aligned}|\mathcal{R}_b^M(p,w)|^2 &\lesssim \sum_{E\in\mathcal{T}_h}\frac{h_E^{2(s_E-1)}}{k_E^{2(r_E-1)}}||\mathscr{E}p||^2_{H^{r_E}(T_E)}\left[(1+B)\bar{\boldsymbol{\nu}}_E^2\max_{F\subset\partial E\setminus\Gamma}\sigma_F^{-1}(\frac{k_E}{h_E}+\frac{k_E^2}{h_E})\right]\\ &\quad\cdot||w||^2_{b,DG},\end{aligned}\tag{3.53}$$

$$\begin{aligned}|\mathcal{R}_\Gamma^M(p_\Gamma,w_\Gamma)|^2 &\lesssim \sum_{F\in\Gamma_h}\frac{h_F^{2(s_F-1)}}{k_F^{2(r_F-1)}}||\mathscr{E}p_\Gamma||^2_{H^{r_F}(T_F)}\left[(1+B_\Gamma)(\bar{\boldsymbol{\nu}}_F^{\boldsymbol{\tau}}\ell_\Gamma)^2\max_{e\subseteq\partial F}\sigma_e^{-1}(\frac{k_F}{h_F}+\frac{k_F^2}{h_F})\right]\\ &\quad\cdot||w_\Gamma||^2_{\Gamma,DG}.\end{aligned}\tag{3.54}$$

Proof. We focus on the proof of (3.53), estimate (3.54) can be obtained likewise. Recalling that $\boldsymbol{\Pi}_{\mathbf{W}_h^b}$ denotes the L^2-orthogonal projector onto $\mathbf{W}_h^b$, the residual $\mathcal{R}_b^M$ has the following expression:

$$\begin{aligned}\mathcal{R}_b^M(p,w)=&\sum_{F\in\mathcal{F}_h^I\cup\mathcal{F}_h^D}\int_F\left(\{\boldsymbol{\nu}(\nabla p-\boldsymbol{\Pi}_{\mathbf{W}_h^b}(\nabla p))\}-\mathbf{b}[\![\boldsymbol{\nu}(\nabla p-\boldsymbol{\Pi}_{\mathbf{W}_h^b}(\nabla p))]\!]\right)\cdot[\![w]\!]\\ &+\sum_{F\in\mathcal{F}_h^D}\int_F w\boldsymbol{\nu}(\nabla p-\boldsymbol{\Pi}_{\mathbf{W}_h^b}(\nabla p))\cdot\mathbf{n}_F,\end{aligned}$$

where we have used the identity $\mathscr{L}_b^{LDG}([\![p]\!]) = -\mathcal{G}_b$ and the continuity of $\boldsymbol{\nu}\nabla p$ across internal faces (Assumption 3.5.2). From Cauchy-Schwarz and triangular inequalities and the bound on the coefficient $\mathbf{b}$ (3.27), we have

$$|\mathcal{R}_b^M(p,w)|^2 \lesssim \left(\sum_{F\in\mathcal{F}_h^I\cup\mathcal{F}_h^D} \sigma_F^{-1}\left[\int_F |\{\boldsymbol{\nu}(\nabla p - \widetilde{\Pi}(\nabla p))\}|^2 + \int_F |\{\boldsymbol{\nu}\boldsymbol{\Pi}_{\mathbf{W}_h^b}(\nabla p - \widetilde{\Pi}(\nabla p))\}|^2 \right] \right.$$
$$\left. + B \sum_{F\in\mathcal{F}_h^I\cup\mathcal{F}_h^D} \sigma_F^{-1}\left[\int_F |[\![\boldsymbol{\nu}(\nabla p - \widetilde{\Pi}(\nabla p))]\!]|^2 + \int_F |[\![\boldsymbol{\nu}\boldsymbol{\Pi}_{\mathbf{W}_h^b}(\nabla p - \widetilde{\Pi}(\nabla p))]\!]|^2 \right] \right) \cdot ||w||_{b,DG}^2,$$

where we recall that, with a slight abuse of notation, $\widetilde{\Pi}$ still denotes the vector-valued generalization of the projection operator $\widetilde{\Pi}$ defined in Lemma 1.3.3. The thesis now follows from the boundedness of the permeability tensor $\boldsymbol{\nu}$, the inverse inequality (1.6), the L^2-stability of the projector $\boldsymbol{\Pi}_{\mathbf{W}_h^b}$ and the approximation results stated in Lemma 1.3.3.

□

Theorem 3.5.6. *Let $\mathcal{T}_\# = \{T_E\}$ and $\mathcal{F}_\# = \{T_F\}$ denote the associated coverings of Ω and Γ, respectively, consisting of shape-regular simplexes as in Definition 1.1.2, satisfying Assumption 1.1.2. Let (p, p_Γ) be the solution of problem (3.5) and $(p_h, p_{\Gamma,h}) \in Q_h^b \times Q_h^\Gamma$ be its approximation obtained with the method PP, MP, MM or PM, with the penalization parameters given by (3.45) and (3.46) and σ_0 and $\sigma_{0,\Gamma}$ sufficiently large for the primal formulations. Moreover, suppose that the exact solution (p, p_Γ) satisfies the regularity Assumptions 3.5.2 and 3.5.1. Then, the following error bound holds:*

$$|||(p,p_\Gamma) - (p_h,p_{\Gamma,h})|||^2 \lesssim \sum_{E\in\mathcal{T}_h} \frac{h_E^{2(s_E-1)}}{k_E^{2(r_E-1)}} G_E^*(h_E,k_E,\bar{\boldsymbol{\nu}}_E)||\mathscr{E}p||_{H^{rE}(T_E)}^2 \tag{3.55}$$
$$+ \sum_{F\in\Gamma_h} \frac{h_F^{2(s_F-1)}}{k_F^{2(r_F-1)}} G_F^*(h_F,k_F,\bar{\boldsymbol{\nu}}_F^\tau)||\mathscr{E}_\Gamma p_\Gamma||_{H^{rF}(T_F)}^2,$$

where the $\mathscr{E}p$ is to be interpreted as $\mathscr{E}_1 p_1$ when $E \subset \Omega_1$ or as $\mathscr{E}_2 p_2$ when $E \subset \Omega_2$. Here, $s_E = \min(k_E+1, r_E)$ and $s_F = \min(k_F+1, r_F)$, and the constants are defined according

to the chosen approximation method as follows:

$$
\begin{aligned}
G_E^P(h_E, k_E, \bar{\boldsymbol{\nu}}_E) &= \bar{\boldsymbol{\nu}}_E + h_E k_E^{-1} \max_{F\subset\partial E\setminus\Gamma} \sigma_F + (\alpha_\Gamma + \beta_\Gamma) h_E k_E^{-1} \\
&\quad + \bar{\boldsymbol{\nu}}_E^2 h_E^{-1} k_E \max_{F\subset\partial E\setminus\Gamma} \sigma_F^{-1} + \bar{\boldsymbol{\nu}}_E^2 h_E^{-1} k_E^2 \max_{F\subset\partial E\setminus\Gamma} \sigma_F^{-1}, \\
G_F^P(h_F, k_F, \bar{\boldsymbol{\nu}}_F^\tau) &= \bar{\boldsymbol{\nu}}_F^\tau \ell_\Gamma + h_F k_F^{-1} \max_{e\subseteq\partial F} \sigma_e + \alpha_\Gamma h_F^2 k_F^{-2} \\
&\quad + (\bar{\boldsymbol{\nu}}_F^\tau \ell_\Gamma)^2 h_F^{-1} k_F \max_{e\subseteq\partial F} \sigma_e^{-1} + (\bar{\boldsymbol{\nu}}_F^\tau \ell_\Gamma)^2 h_F^{-1} k_F^2 \max_{e\subseteq\partial F} \sigma_e^{-1}, \\
G_E^M(h_E, k_E, \bar{\boldsymbol{\nu}}_E) &= \bar{\boldsymbol{\nu}}_E + h_E k_E^{-1} \max_{F\subset\partial E\setminus\Gamma} \sigma_F + (\alpha_\Gamma + \beta_\Gamma) h_E k_E^{-1} \\
&\quad + (1+B) \bar{\boldsymbol{\nu}}_E^2 h_E^{-1} k_E \max_{F\subset\partial E\setminus\Gamma} \sigma_F^{-1} + (1+B) \bar{\boldsymbol{\nu}}_E^2 h_E^{-1} k_E^2 \max_{F\subset\partial E\setminus\Gamma} \sigma_F^{-1}, \\
G_F^M(h_F, k_F, \bar{\boldsymbol{\nu}}_F^\tau) &= \bar{\boldsymbol{\nu}}_F^\tau \ell_\Gamma + h_F k_F^{-1} \max_{e\subseteq\partial F} \sigma_e + \alpha_\Gamma h_F^2 k_F^{-2} \\
&\quad + (1+B_\Gamma)(\bar{\boldsymbol{\nu}}_F^\tau \ell_\Gamma)^2 h_F^{-1} k_F \max_{e\subseteq\partial F} \sigma_e^{-1} + (1+B_\Gamma)(\bar{\boldsymbol{\nu}}_F^\tau \ell_\Gamma)^2 h_F^{-1} k_F^2 \max_{e\subseteq\partial F} \sigma_e^{-1}.
\end{aligned}
$$

Remark 7. (Uniform orders and mesh size) Let us assume that the mesh is uniform, i.e. $h_E \approx h$ for all $E \in \mathcal{T}_h$ and thus $h_F \approx h$ for all $F \in \Gamma_h$, and that the polynomial order is the same for each element in the bulk and in the fracture, i.e. $k_E = k \geq 1$ for all $E \in \mathcal{T}_h$ and $k_F = k_\Gamma \geq 1$ for all $F \in \Gamma_h$. Then if the exact solutions in the bulk and in the fracture satisfy $p \in H^r(\Omega)$ with $r \geq k+1$ and $p_\Gamma \in H^{r_\Gamma}(\Gamma)$ with $r_\Gamma \geq k_\Gamma + 1$, then the error estimate (3.55) reduces to

$$
|||(p, p_\Gamma) - (p_h, p_h^\Gamma)||| \lesssim \frac{h^k}{k^{r-3/2}} ||p||_{H^r(\Omega)} + \frac{h^{k_\Gamma}}{k_\Gamma^{r_\Gamma - 3/2}} ||p_\Gamma||_{H^{r_\Gamma}(\Gamma)}.
$$

Proof. From Lemma 3.5.3 we know that the error satisfies the following bound

$$
|||(p, p_\Gamma) - (p_h, p_{\Gamma,h})||| \lesssim \underbrace{\inf_{(q,q_\Gamma)\in Q_h^b \times Q_h^\Gamma} |||(p, p_\Gamma) - (q, q_\Gamma)|||}_{I} + \underbrace{\sup_{(w,w_\Gamma)\in Q_h^b \times Q_h^\Gamma} \frac{|\mathcal{R}_h((p, p_\Gamma), (w, w_\Gamma))|}{|||(w, w_\Gamma)|||}}_{II}. \quad (3.56)
$$

We estimate the two terms on the right-hand side of (3.56) separately. We can rewrite

term I as

$$\begin{aligned} I &= \inf_{(q,q_\Gamma)\in Q_h^b\times Q_h^\Gamma}\left(||p-q||^2_{b,DG}+||p_\Gamma-q_\Gamma||^2_{\Gamma,DG}+||(p-q,p_\Gamma-q_\Gamma||^2_{\mathcal{C}}\right)\\ &\leq \underbrace{||p-\widetilde{\Pi}p||^2_{b,DG}}_{(a)}+\underbrace{||p_\Gamma-\widetilde{\Pi}p_\Gamma||^2_{\Gamma,DG}}_{(b)}+\underbrace{||(p-\widetilde{\Pi}p,p_\Gamma-\widetilde{\Pi}p_\Gamma)||^2_{\mathcal{C}}}_{(c)}. \end{aligned}$$

Again we consider each of the three terms separately. To bound term (a), we exploit the two approximation results stated in Lemma 1.3.3 and obtain

$$\begin{aligned} (a) &\leq ||p-\widetilde{\Pi}p||^2_{b,DG}=\sum_{E\in\mathcal{T}_h}||\boldsymbol{\nu}^{1/2}\nabla(p-\widetilde{\Pi}p)||^2_{L^2(E)}+\sum_{F\in\mathcal{F}_h^I\cup\mathcal{F}_h^D}\sigma_F||[\![p-\widetilde{\Pi}p]\!]||^2_{L^2(F)}\\ &\lesssim \sum_{E\in\mathcal{T}_h}\left[\bar{\boldsymbol{\nu}}_E|p-\widetilde{\Pi}p|^2_{H^1(E)}+(\max_{F\subset\partial E\setminus\Gamma}\sigma_F)||p-\widetilde{\Pi}p||^2_{L^2(\partial E\setminus\Gamma)}\right]\\ &\lesssim \sum_{E\in\mathcal{T}_h}\left[\frac{h_E^{2(s_E-1)}}{k_E^{2(r_E-1)}}\bar{\boldsymbol{\nu}}_E||\mathscr{E}p||^2_{H^{r_E}(T_E)}+\sum_{F\subset\partial E\setminus\Gamma}\frac{h_E^{2(s_E-1/2)}}{k_E^{2(r_E-1/2)}}(\max_{F\subset\partial E\setminus\Gamma}\sigma_F)||\mathscr{E}p||^2_{H^{r_E}(T_E)}\right]\\ &= \sum_{E\in\mathcal{T}_h}\frac{h_E^{2(s_E-1)}}{k_E^{2(r_E-1)}}||\mathscr{E}p||^2_{H^{r_E}(T_E)}\left(\bar{\boldsymbol{\nu}}_E+\frac{h_E}{k_E}(\max_{F\subset\partial E\setminus\Gamma}\sigma_F)\right). \end{aligned}$$

Using analogous interpolation estimates on the fracture we can bound term (b) as follows:

$$\begin{aligned} (b) &\leq ||p_\Gamma-\widetilde{\Pi}p_\Gamma||^2_{\Gamma,DG}\lesssim\sum_{F\in\Gamma_h}||\boldsymbol{\nu}_\Gamma^\tau\ell_\Gamma\nabla(p_\Gamma-\widetilde{\Pi}p_\Gamma)||^2_{L^2(F)}+\sum_{e\in\mathcal{E}^I_{\Gamma,h}\cup\mathcal{E}^D_{\Gamma,h}}\sigma_e||[\![p_\Gamma-\widetilde{\Pi}p_\Gamma]\!]||^2_{L^2(e)}\\ &\lesssim\sum_{F\in\Gamma_h}\frac{h_F^{2(s_F-1)}}{k_F^{2(r_F-1)}}||\mathscr{E}p_\Gamma||^2_{H^{r_F}(T_F)}\left(\bar{\boldsymbol{\nu}}_F^\tau\ell_\Gamma+\frac{h_F}{k_F}\max_{e\subseteq\partial F}\sigma_e\right) \end{aligned}$$

Finally, for term (c), we have

$$\begin{aligned} (c)\leq||(p-\widetilde{\Pi}p,p_\Gamma-\widetilde{\Pi}p_\Gamma)||^2_{\mathcal{C}}\leq\beta_\Gamma\sum_{F\in\Gamma_h}||[\![p-\widetilde{\Pi}p]\!]||^2_{L^2(F)}+\alpha_\Gamma\sum_{F\in\Gamma_h}||\{p-\widetilde{\Pi}p\}||^2_{L^2(F)}\\ +\alpha_\Gamma\sum_{F\in\Gamma_h}||p_\Gamma-\widetilde{\Pi}p_\Gamma||^2_{L^2(F)}. \end{aligned}$$

Exploiting the approximation result (1.8), we obtain

$$\beta_\Gamma \sum_{F\in\Gamma_h} ||[\![p-\widetilde{\Pi}p]\!]||^2_{L^2(F)} \leq \beta_\Gamma \sum_{\substack{E\in\mathcal{T}_h \\ \partial E\cap\Gamma\neq\emptyset}} ||p-\widetilde{\Pi}p||^2_{L^2(\partial E)} \lesssim \beta_\Gamma \sum_{\substack{E\in\mathcal{T}_h \\ \partial E\cap\Gamma\neq\emptyset}} \frac{h_E^{2(s_E-\frac{1}{2})}}{k_E^{2(r_E-\frac{1}{2})}} ||\mathscr{E}p||^2_{H^{r_E}(T_E)}$$
$$= \beta_\Gamma \sum_{\substack{E\in\mathcal{T}_h \\ \partial E\cap\Gamma\neq\emptyset}} \frac{h_E^{2(s_E-1)}}{k_E^{2(r_E-1)}} ||\mathscr{E}p||^2_{H^{r_E}(T_E)} \frac{h_E}{k_E}.$$

Similarly, we have

$$\alpha_\Gamma \sum_{F\in\Gamma_h} ||\{p-\widetilde{\Pi}p\}||^2_{L^2(F)} \lesssim \alpha_\Gamma \sum_{\substack{E\in\mathcal{T}_h \\ \partial E\cap\Gamma\neq\emptyset}} \frac{h_E^{2(s_E-1)}}{k_E^{2(r_E-1)}} ||\mathscr{E}p||^2_{H^{r_E}(T_E)} \frac{h_E}{k_E}.$$

Finally, using the interpolation estimates for the fracture, we deduce that

$$\alpha_\Gamma \sum_{F\in\Gamma_h} ||p_\Gamma-\widetilde{\Pi}p_\Gamma||^2_{L^2(F)} \lesssim \alpha_\Gamma \sum_{F\in\Gamma_h} \frac{h_F^{2s_F}}{k^{2r_F}} ||\mathscr{E}p_\Gamma||^2_{H^{r_F}(T_F)}$$
$$= \alpha_\Gamma \sum_{F\in\Gamma_h} \frac{h_F^{2(s_F-1)}}{k_F^{2(r_F-1)}} ||\mathscr{E}p_\Gamma||^2_{H^{r_F}(T_F)} \frac{h_F^2}{k_F^2}.$$

In conclusion, combining all the previous estimates, we can bound the term I on the right-hand side of (3.56) as follows:

$$I \lesssim \sum_{E\in\mathcal{T}_h} \frac{h_E^{2(s_E-1)}}{k_E^{2(r_E-1)}} ||\mathscr{E}p||^2_{H^{r_E}(T_E)} \left[\bar{\boldsymbol{\nu}}_E + \frac{h_E}{k_E} \max_{F\subset\partial E\setminus\Gamma} \sigma_F + (\alpha_\Gamma+\beta_\Gamma)\frac{h_E}{k_E}\right]$$
$$+ \sum_{F\in\Gamma_h} \frac{h_F^{2(s_F-1)}}{k_F^{2(r_F-1)}} ||\mathscr{E}p_\Gamma||^2_{H^{r_F}(T_F)} \left[\bar{\boldsymbol{\nu}}_F^\tau \ell_\Gamma + \frac{h_F}{k_F} \max_{e\subseteq\partial F} \sigma_e + \alpha_\Gamma \frac{h_F^2}{k_F^2}\right]. \quad (3.57)$$

Finally, the desired estimates follow from the combination of (3.57), together with the bound on Term II deriving from what observed in (3.50) and Lemmas 3.5.4 and 3.5.5. □

Finally, from the above result we can derive some error estimates also for the velocities $\mathbf{u}$ and $\mathbf{u}_\Gamma$.

Theorem 3.5.7. *Let all the hypotheses of Theorem 3.5.6 hold. Let* $(\boldsymbol{u}, \boldsymbol{u}_\Gamma) \in \boldsymbol{W}_g$ *and* $(p, p_\Gamma) \in M$ *be the solution of problem* (3.5)*. Then:*

- *if* $\Big((p_h, \boldsymbol{u}_h), p_{\Gamma,h}\Big) \in Q_h^b \times \boldsymbol{W}_h^b \times Q_h^\Gamma$ *is its approximation obtained with the MP method* (3.30)*, it holds*

$$||\boldsymbol{u} - \boldsymbol{u}_h||^2_{0,\mathcal{T}_h} \lesssim \sum_{E\in\mathcal{T}_h} \frac{h_E^{2(s_E-1)}}{k_E^{2(r_E-1)}} G_E^M ||\mathscr{E}p||^2_{H^{r_E}(T_E)} + \sum_{F\in\Gamma_h} \frac{h_F^{2(s_F-1)}}{k_F^{2(r_F-1)}} G_F^P ||\mathscr{E}_\Gamma p_\Gamma||^2_{H^{r_F}(T_F)};$$

- *if* $\Big(p_h, (p_{\Gamma,h}, \boldsymbol{u}_{\Gamma,h})\Big) \in Q_h^b \times Q_h^\Gamma \times \boldsymbol{W}_h^\Gamma$ *is its approximation obtained with the PM method* (3.38)*, it holds*

$$||\boldsymbol{u}_\Gamma - \boldsymbol{u}_{\Gamma,h}||^2_{0,\Gamma_h} \lesssim \sum_{E\in\mathcal{T}_h} \frac{h_E^{2(s_E-1)}}{k_E^{2(r_E-1)}} G_E^P ||\mathscr{E}p||^2_{H^{r_E}(T_E)} + \sum_{F\in\Gamma_h} \frac{h_F^{2(s_F-1)}}{k_F^{2(r_F-1)}} G_F^M ||\mathscr{E}_\Gamma p_\Gamma||^2_{H^{r_F}(T_F)};$$

- *if* $\Big((p_h, \boldsymbol{u}_h), (p_{\Gamma,h}, \boldsymbol{u}_{\Gamma,h})\Big) \in Q_h^b \times \boldsymbol{W}_h^b \times Q_h^\Gamma \times \boldsymbol{W}_h^\Gamma$ *is its approximation obtained with the MM method* (3.43)*, it holds*

$$\begin{aligned} ||\boldsymbol{u} - \boldsymbol{u}_h||^2_{0,\mathcal{T}_h} + ||\boldsymbol{u}_\Gamma - \boldsymbol{u}_{\Gamma,h}||^2_{0,\Gamma_h} \lesssim & \sum_{E\in\mathcal{T}_h} \frac{h_E^{2(s_E-1)}}{k_E^{2(r_E-1)}} G_E^M ||\mathscr{E}p||^2_{H^{r_E}(T_E)} \\ & + \sum_{F\in\Gamma_h} \frac{h_F^{2(s_F-1)}}{k_F^{2(r_F-1)}} G_F^M ||\mathscr{E}_\Gamma p_\Gamma||^2_{H^{r_F}(T_F)}, \end{aligned}$$

where the constants G_E^M*,* G_F^P*,* G_E^P *and* G_F^M *are defined as in Theorem 3.5.6.*

Proof. Let $\Big((p_h, \mathbf{u}_h), p_{\Gamma,h}\Big)$ and $\Big((p_h, p_{\Gamma,h}), (\mathbf{u}_h, \mathbf{u}_{\Gamma,h})\Big)$ be the discrete solutions obtained with the MP method and with the MM method, respectively. Then, using identity (3.32) and the fact that $\mathscr{L}_b^{LDG}([\![p]\!]) = -\mathcal{G}_b$, we can rewrite

$$\begin{aligned} \mathbf{u}_h - \mathbf{u} &= \boldsymbol{\nu}\nabla p_h + \boldsymbol{\nu}\mathscr{L}_b^{LDG}([\![p_h]\!]) + \boldsymbol{\nu}\mathcal{G}_b - \boldsymbol{\nu}\nabla p \\ &= \boldsymbol{\nu}(\nabla p_h - \nabla p) + \boldsymbol{\nu}\mathscr{L}_b^{LDG}([\![p_h - p]\!]). \end{aligned}$$

From the uniform boundedness of $\boldsymbol{\nu}$, the triangular inequality, the bound on the lifting

(3.49) and the definition of the $||\cdot||_{b,DG}$ norm it follows that

$$\begin{aligned}||\mathbf{u}-\mathbf{u}_h||_{0,\mathcal{T}_h} &\lesssim ||\boldsymbol{\nu}^{1/2}\nabla(p_h-p)||_{0,\mathcal{T}_h}+||\boldsymbol{\nu}^{1/2}\mathscr{L}_b^{LDG}([\![p_h-p]\!])||_{0,\mathcal{T}_h}\\ &\lesssim ||p_h-p||_{b,DG}+\frac{1+B}{\sigma_0^{1/2}}||\sigma_F^{1/2}[\![p_h-p]\!]||_{0,\mathcal{F}_h^I\cup\mathcal{F}_h^D}\\ &\lesssim ||p_h-p||_{b,DG}.\end{aligned}$$

In particular, this implies that

$$||\mathbf{u}-\mathbf{u}_h||_{0,\mathcal{T}_h}\lesssim |||(p,p_\Gamma)-(p_h,p_{\Gamma,h})|||,$$

Similarly, one can prove that, if $\Big(p_h,(p_{\Gamma,h},\mathbf{u}_{\Gamma,h})\Big)$ and $\Big((p_h,p_{\Gamma,h}),(\mathbf{u}_h,\mathbf{u}_{\Gamma,h})\Big)$ are the discrete solutions obtained with the PM method and with the MM method, respectively, it holds

$$||\mathbf{u}_\Gamma-\mathbf{u}_{\Gamma,h}||_{0,\Gamma_h}\lesssim |||(p,p_\Gamma)-(p_h,p_{\Gamma,h})|||.$$

The thesis is now a direct consequence of Theorem 3.5.6. □

3.6 Numerical experiments

In this section we present some two-dimensional numerical experiments with the aim of validating the obtained theoretical convergence results. The validity of the error estimates for the primal-primal setting has been already assessed in Chapter 2. Here, we focus on the paradigmatic *mixed-primal* setting. This means that, for the approximation of the problem in the bulk, we will employ the LDG method, while, for the problem in the fracture, we will employ the SIPDG method (both in their generalization to polygonal grids). All the numerical tests have been implemented in MATLAB®. For the generation of polygonal meshes conforming to the fractures we have suitably modified code `PolyMesher` [117].

In particular, we present three sets of numerical experiments. The first set is obtained assuming that an analytical solution is known and aims at verifying the a-priori error estimates obtained in Theorems 3.5.6 and 3.5.7. The second set is derived form physical considerations and aims at testing how different values of the fracture permeability may influence the flow in the bulk. Finally, the last set of experiments aims at showing how the method is capable of handling more complicated geometries, specifically networks of

partially immersed fractures.

3.6.1 Example 1: Analytical solution

For a start, we consider the same test case of Section 2.5.1, that is, we take $\Omega = (0,1)^2$, and choose as exact solutions in the bulk and in the fracture $\Gamma = \{(x,y) \in \Omega : \ x+y=1\}$

$$p = \begin{cases} e^{x+y} & \text{in } \Omega_1, \\ e^{x+y} + \frac{4\eta_\Gamma}{\sqrt{2}} e & \text{in } \Omega_2, \end{cases} \qquad \mathbf{u} = \begin{cases} -e^{x+y} & \text{in } \Omega_1, \\ -e^{x+y} & \text{in } \Omega_2, \end{cases} \qquad p_\Gamma = e + \frac{2\eta_\Gamma}{\sqrt{2}} e,$$

which satisfy the coupling conditions (3.3a)-(3.3b) with $\xi = 1$, $\ell_\Gamma = 0.001$ and $\boldsymbol{\nu} = \boldsymbol{\nu}_\Gamma = \mathbf{I}$. In order to test the h-convergence properties of our method, we split again the error in the two contributions given by the bulk and fracture errors. In particular, aiming at validating the error estimate in Theorem 3.5.6, we compute $||p - p_h||_{1,\mathcal{T}_h}$ (Figure 3.2(a)) and $||p_\Gamma - p_{\Gamma,h}||_{1,\Gamma_h}$ (Figure 3.2(d)), while to validate the results of Theorem 3.5.7, we compute $||\mathbf{u} - \mathbf{u}_h||_{0,\mathcal{T}_h}$ (Figure 3.2(c)). In addition, we test the behaviour of the L^2-norm of the error for the primal variables, i.e., $||p - p_h||_{0,\mathcal{T}_h}$ (Figure 3.2(b)) and $||p_\Gamma - p_{\Gamma,h}||_{0,\Gamma_h}$ (Figure 3.2(e)). All the plots in Figure 3.2 show the computed errors as a function of the inverse of the mesh size (loglog scale), together with the expected convergence rates. Each plot consists of four lines: every line shows the behaviour of the computed error for a different polynomial degree in the bulk (we consider $k = 1,2,3,4$). For the fracture problem we always choose $k_\Gamma = 2$.

In Figures 3.2(a), 3.2(d) and 3.2(c) the theoretical convergence rates are clearly achieved. We observe that, in Figure 3.2(d), the convergence rate for $||p_\Gamma - p_{\Gamma,h}||_{1,\mathcal{T}_h}$ with $k = 1$ is suboptimal. This is due to the fact that the polynomial degree for the problem in the bulk is not accurate enough. Optimal rates are recovered for bulk polynomial degree $k = 2,3,4$. Finally, Figures 3.2(b) and 3.2(e) show that one order of convergence is gained for the L^2-norm for both the bulk and fracture problems.

3.6.2 Example 2: Discontinuous fracture permeability

Next, we reproduce some numerical experiments first presented in [101]. We examine two test cases with bulk domain $\Omega = (0,2) \times (0,1)$ and fracture domain $\Gamma = \{(x,y) \in \mathbb{R}^2 : x = 1, 0 \leq y \leq 1\}$. In the first case, we consider a fracture

with constant permeability, while in the second case we consider a fracture with lower permeability in its middle part, thus presenting a discontinuity. In particular:

(a) **Case 1: constant permeability**: The permeability tensor in the fracture is given by $\boldsymbol{\nu}_\Gamma^n = \boldsymbol{\nu}_\Gamma^\tau = 100$. The bulk permeability $\boldsymbol{\nu}$ is chosen to be constant and isotropic, i.e., $\boldsymbol{\nu} = \mathbf{I}$. We impose Dirichlet boundary conditions on the left and right side of the bulk domain and homogeneous Neumann conditions on the top and bottom sides. On the fracture boundaries we impose Dirichlet boundary conditions.

(b) **Case 2: discontinous permeabilty**: The fracture Γ is subdivided into two areas having different values for the permeability tensor: in the initial and ending part of the fracture $\Gamma_1 = \{(x, y) \in \Gamma,\ 0 \leq y \leq 0.25 \text{ and } 0.75 \leq y \leq 1\}$ the permeability tensor $\boldsymbol{\nu}_{\Gamma_1}$ is defined as $\boldsymbol{\nu}_{\Gamma_1}^n = \boldsymbol{\nu}_{\Gamma_1}^\tau = 1$, while in the middle part $\Gamma_2 = \{(x, y) \in \Gamma, 0.25 \leq y \leq 0.75\}$ the permeability is low and is defined as $\boldsymbol{\nu}_{\Gamma_2}^n = \boldsymbol{\nu}_{\Gamma_2}^\tau = 0.002$. The bulk permeability tensor is chosen again equal to the identity matrix, i.e., $\boldsymbol{\nu} = \mathbf{I}$. In the bulk, we impose the same boundary conditions as in the previous test case, while at the fracture extremities we impose homogeneous Neumann conditions.

The two geometrical configurations are shown in Figures 3.3(a)-3.3(b), together with the boundary conditions. For both test cases we take the fracture thickness $\ell_\Gamma = 0.01$, the model parameter $\xi = 2/3$ and the source terms $f = f_\Gamma = 0$. Moreover, we discretize the problem in the bulk taking as polynomial degree $k = 1$ and the problem in the fracture taking $k_\Gamma = 2$. The obtained results are shown in Figure 3.4. For both cases (constant at the top, discontinuous at the bottom) we report the pressure field and Darcy velocity in the bulk (here the grid is very coarse only for visualization purposes) and the value of the pressure along the fracture. In the first case, since we have taken $\boldsymbol{\nu}_\Gamma^n = \boldsymbol{\nu}_\Gamma^\tau = 100 > 1$, we can observe that the fluid has the tendency to flow along the fracture. In the second case, one can see that the part of the fracture with low (normal) permeability acts as a geological barrier, so that the fluid tends to avoid it and we can observe a jump of the bulk pressure across it. Our results are in agreement with those obtained in [101].

3.6.3 Example 3: Network of partially immersed fractures

With this last set of numerical experiments we investigate the capability of our discretization method to deal with more complicated geometrical configurations, considering a

network of partially *immersed* fractures. Our reference is again [3], where the mathematical model developed in [101] has been extended to fully immersed fractures. In Chapter 2 we showed that our method in a *primal-primal* setting is capable of efficiently handling the configuration. Here, we reproduce the same numerical experiments to demonstrate that this holds true also in a *mixed-primal* setting.

In order to deal with immersed fractures, we need to supplement our model (3.4) with an equation describing the behaviour of the fracture pressure at the immersed tips. Following [3], we impose a homogeneous Neumann condition, thus assuming that the mass transfer across the immersed tips can be neglected, i.e., $\boldsymbol{\nu}_\Gamma^\tau \nabla_\tau p_\Gamma \cdot \boldsymbol{\tau} = 0$. At the extremities of the fractures that are non-immersed, i.e., $\partial\Gamma \cap \partial\Omega$, we impose boundary conditions that are consistent with those imposed on $\partial\Omega$ in that point.

We consider the bulk domain $\Omega = (0,1)^2$ cut by a network made of four partially immersed fractures: $\Gamma_1 = \{(x,y) \in \Omega : x \geq 0.3, y = 0.2\}$, $\Gamma_2 = \{(x,y) \in \Omega : x \leq 0.7, y = 0.4\}$, $\Gamma_3 = \{(x,y) \in \Omega : x \geq 0.3, y = 0.6\}$ and $\Gamma_4 = \{(x,y) \in \Omega : x \leq 0.7, y = 0.8\}$. We perform two numerical experiments. In both of them, the fractures Γ_2 and Γ_4 are impermeable ($\boldsymbol{\nu}_\Gamma^\tau = \nu_\Gamma^n = 10^{-2}$), while Γ_1 and Γ_3 are partially permeable. In the first configuration, we consider for Γ_1 and Γ_3 the permeabilities $\nu_\Gamma^n = 10^{-2}$ and $\boldsymbol{\nu}_\Gamma^\tau = 100$, while in the second, we consider $\nu_\Gamma^n = 10^{-2}$ and $\boldsymbol{\nu}_\Gamma^\tau = 1$. Moreover, we vary the imposed boundary conditions as illustrated in Figure 3.5.

In both the experiments we consider an isotropic bulk permeability tensor i.e., $\boldsymbol{\nu} = \mathbf{I}$ and we assume that all the fractures have aperture $\ell_\Gamma = 0.01$. The flow is only generated by boundary conditions, since we take all the forcing terms $f = f_\Gamma = 0$. Finally, we choose as model parameter $\xi = 0.55$.

To obtain our results, we employed cartesian grids featuring approximately the same number of elements as those employed in [3] and such that the immersed tips of the fractures coincide with one of the mesh vertices. For the approximation of the problem in the bulk and in the fracture we chose the polynomial degrees $k = k_\Gamma = 2$. In Figure 3.6, we show the results obtained for the two test cases with a mesh of 26051 elements. In particular, we report the pressure field in the bulk with the streamlines of the velocity (left), the value of the bulk pressure along the line $x = 0.65$ (middle) and the pressure field inside the four fractures (right). Our results are in perfect agreement with those obtained in [3] and in [12], thus showing that, also in a *mixed-primal* setting, our method is able to efficiently handle this configuration.

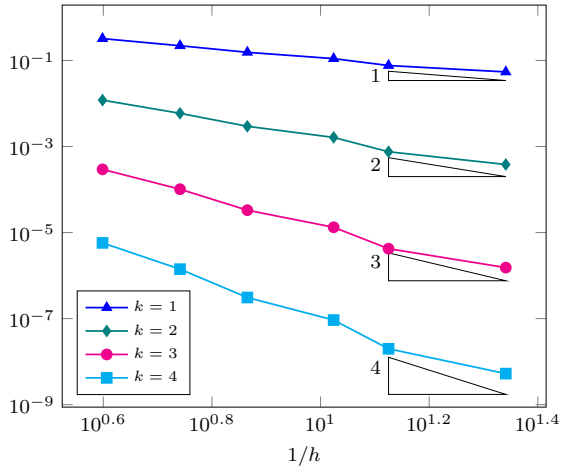

(a) $||p - p_h||_{1,\mathcal{T}_h}$

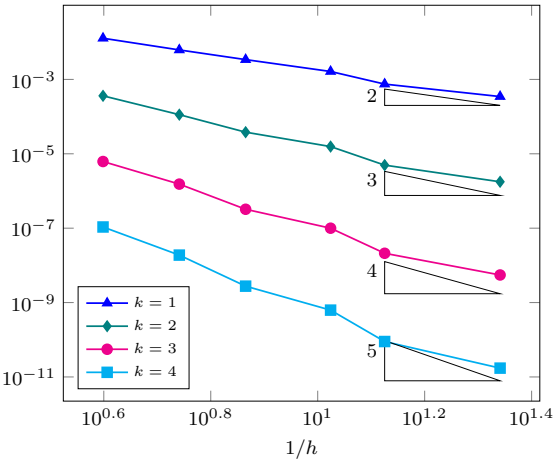

(b) $||p - p_h||_{0,\mathcal{T}_h}$

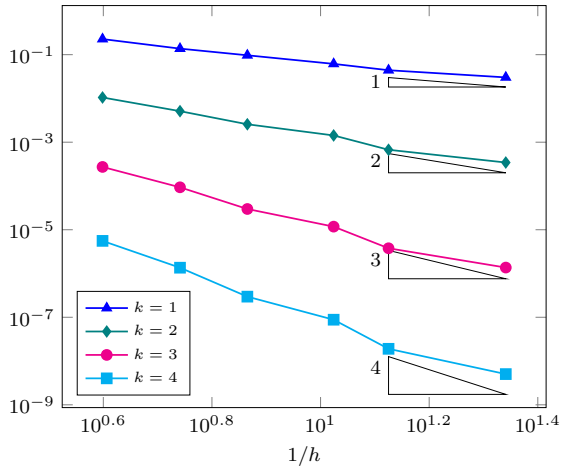

(c) $||\mathbf{u} - \mathbf{u}_h||_{0,\mathcal{T}_h}$

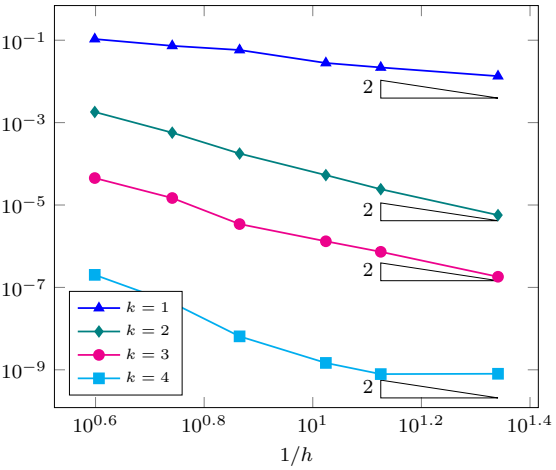

(d) $||p^\Gamma - p_h^\Gamma||_{1,\Gamma_h}$

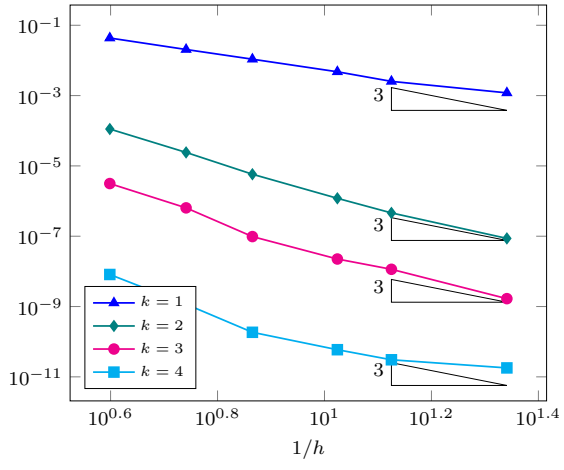

(e) $||p^\Gamma - p_h^\Gamma||_{0,\Gamma_h}$

Figure 3.2: Example 1: Computed errors as a function of $1/h$ (loglog scale) and expected convergence rates for bulk polynomial degree $k = 1, 2, 3, 4$ and fracture polynomial degree $k_\Gamma = 2$.

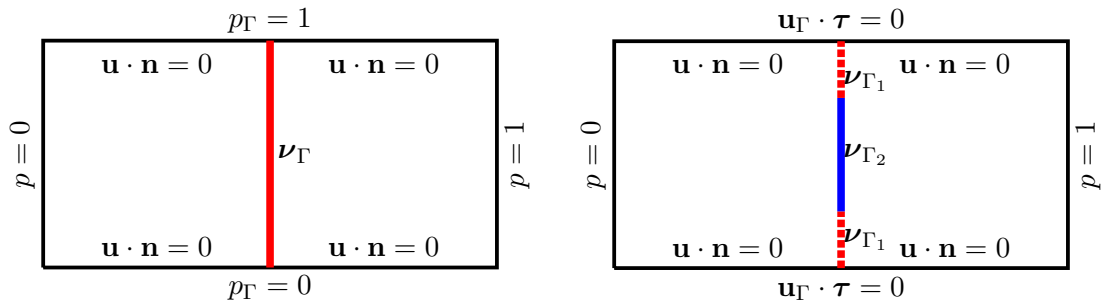

(a) Constant permeability (b) Discontinuous permeability

Figure 3.3: Example 2: Computational domains and boundary conditions for the two test cases. In the second case, on the fracture, the permeable (red, dotted line) and impermeable (blue, solid line) areas are shown.

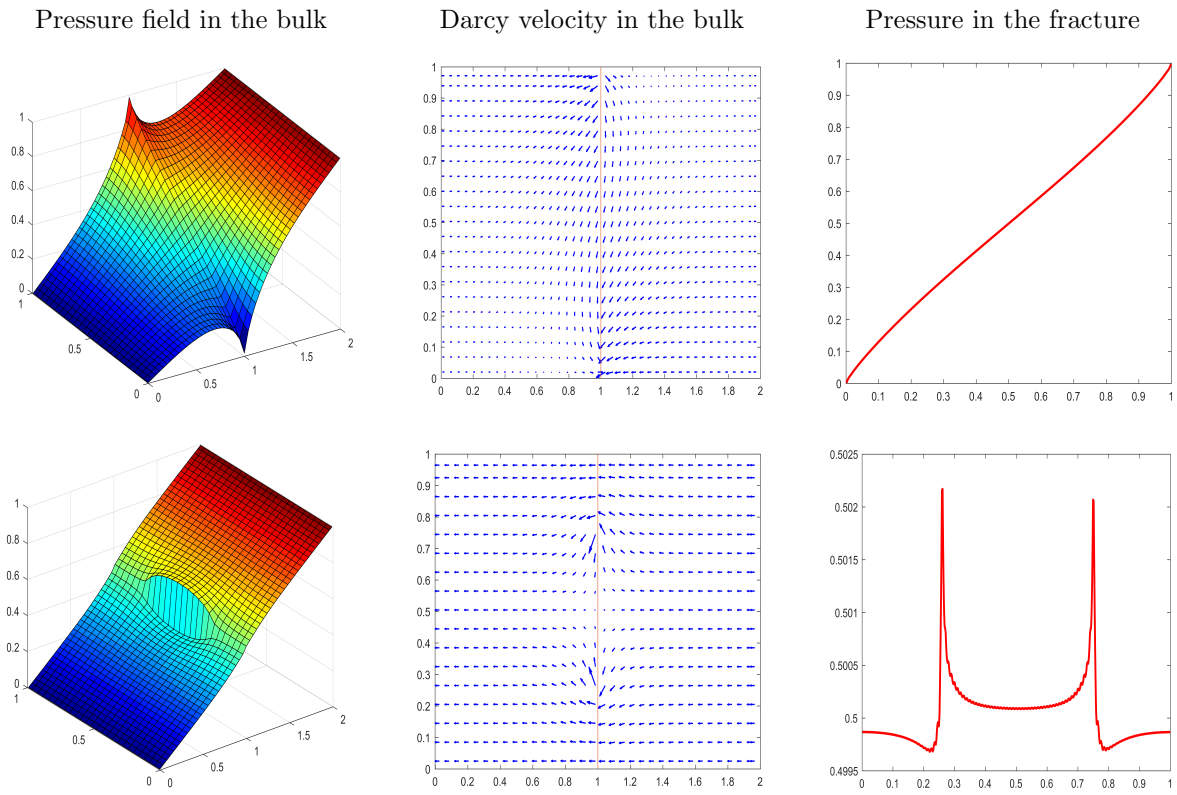

Figure 3.4: Example 2: Bulk pressure field (left), bulk Darcy velocity (middle) and fracture pressure (right) for the constant permeability (top) and discontinuous permeability (bottom) test cases.

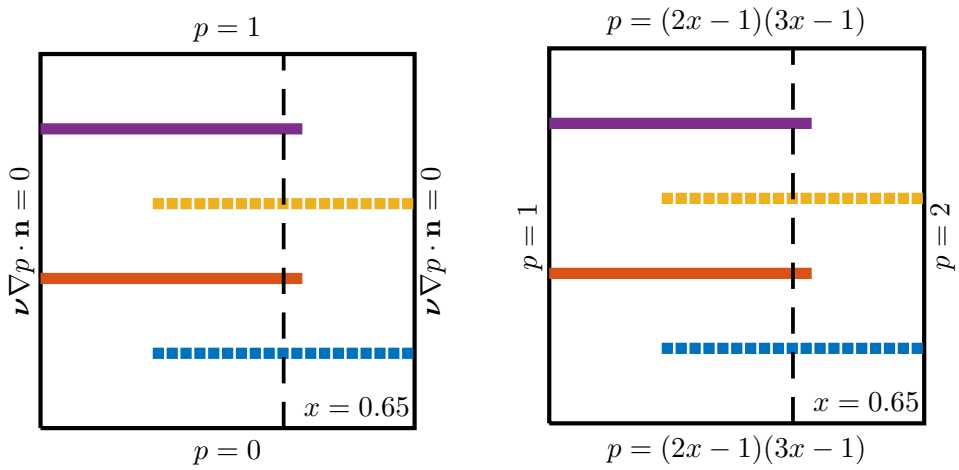

(a) Configuration 1: $\boldsymbol{\nu}_\Gamma^\tau = 100$ on Γ_1, Γ_3 (b) Configuration 2: $\boldsymbol{\nu}_\Gamma^\tau = 1$ on Γ_1, Γ_3

Figure 3.5: Example 3: Configurations and boundary condition for the two test cases.

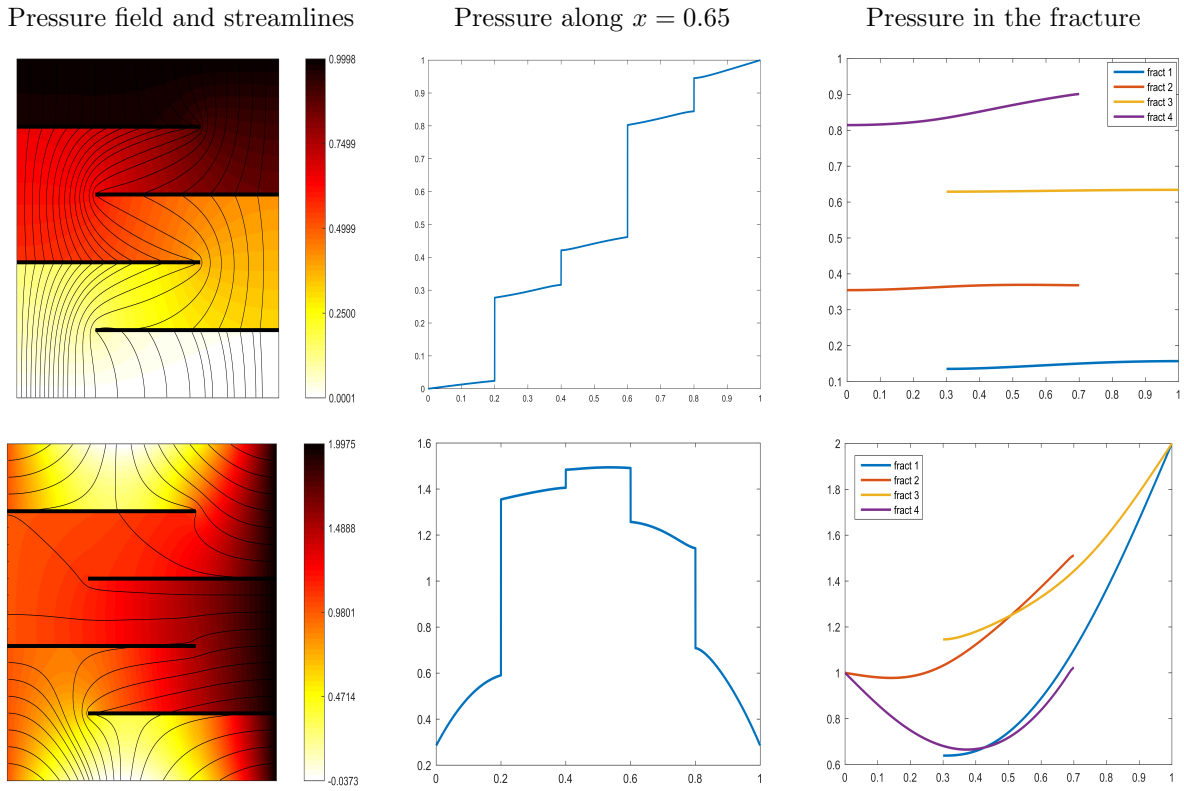

Figure 3.6: Example 3: first configuration (top) and second configuration (bottom).

4 | Networks of intersecting fractures

This chapter aims at extending our formulation to the case of networks of *intersecting* fractures. For simplicity, we consider, as in Chapter 2, the primal-primal setting, so that we can mainly focus on handling the intersections. To this aim, in Section 4.1, we supplement our mathematical model [101] with some suitable physical conditions, prescribing the behaviour of the fluid at the intersections points. Following [87, 51, 45], we impose that:

- pressure between fractures is continuous along the intersections;
- flux is conserved, so that no exchange of fluid between bulk and fracture network takes place along the intersections.

We mention that more general conditions may be imposed. Some examples may be found in [112, 86, 50, 66, 90].
From the DG-discretization point of view, the key instrument for dealing with intersections is the generalization of the concepts of jump and average, see Section 4.3.1 below. Using the newly defined jump and average operators we are able to define a DG approximation for the problem in the bulk combined with a DG approximation for the problem in the fracture network, where the conditions at the intersection are imposed "in the spirit of DG methods ". In particular, this means that continuity is enforced *penalizing the jump* of the pressure (after a suitable definition of the penalization coefficient at the intersection), while balance of fluxes is imposed *naturally*, similarly to how homogeneous Neumann boundary conditions are usually enforced. Both the bulk and fracture discretizations are obtained employing the SIPDG method extended to the polytopic setting.
The rest of the chapter is structured as follows. In Section 4.1, we supplement the

mathematical model introduced in the previous chapters with the conditions prescribing the behaviour of the fluid at the intersections. In Section 4.2, we introduce the weak formulation of the problem and prove its well-posedness. Section 4.3 contains the polyDG discretization of the coupled system based on the new definition of jump and average operators at intersections, which we introduce in Section 4.3.1. Finally, Sections 4.4 and 4.5 enclose the stability and error analysis of the discrete method. We conclude the chapter with Section 4.6, where we present some preliminary numerical experiments with known analytical solution, so that we are able to verify the obtained convergence rates, and one test case featuring a more realistic configuration with a totally immersed network of fractures.

All the results presented in this chapter are original and are contained in [13].

4.1 Mathematical model

We adopt as in the previous chapters the reduced model introduced in [101], but here extended for dealing with networks of intersecting fractures. In particular, we impose some additional conditions in order to describe the behaviour of the fluid at the intersections, taking as a reference [87, 51].

As before, we consider a domain $\Omega \subset \mathbb{R}^d$, with $d = 2, 3$, representing the porous medium. We assume that the fracture network may be approximated by a collection of one co-dimensional planar manifolds $\Gamma \subset \mathbb{R}^{d-1}$. In particular, we consider Γ to be the union of N_Γ fractures γ_k, i.e.

$$\Gamma = \bigcup_{k=1}^{N_\Gamma} \gamma_k,$$

with every γ_k being an open, bounded, connected, planar $(d-1)$-dimensional orientable manifold. Each γ_k is, in fact, the approximation of the actual fracture $\tilde{\gamma}_k$, which we assume may be characterized by

$$\tilde{\gamma}_k = \{\mathbf{x} + d\mathbf{n}_k, \text{ for } \mathbf{x} \in \gamma_k,\ d \in (-\frac{\ell_k(\mathbf{x})}{2}, \frac{\ell_k(\mathbf{x})}{2})\},$$

where $\mathbf{n}_k$ is a unit normal vector to γ_k, whose precise definition is given below, and $\ell_k(\mathbf{x})$ is a $\mathcal{C}^1$ function that describes the fracture aperture. For all $k = 1, \ldots, N_\Gamma$, we assume

there is a constant $\ell_* > 0$ such that $\ell_k > \ell_*$. Finally, we denote by ℓ_Γ the aperture of the whole fracture network, meaning that $\ell_\Gamma|_{\gamma_k} = \ell_k$.
Without loss of generality for the analysis (see Remark 8), we can assume that:

Assumption 4.1.1. *(i) the fracture network is connected;*

(ii) all the fractures intersect in one point if $d = 2$ or line if $d = 3$;

(iii) for each fracture, the intersection point corresponds to one of its endpoints if $d = 2$ or to part of one of its facets if $d = 3$.

We denote by $\mathcal{I}_\cap$ the intersection point/line, i.e.,

$$\mathcal{I}_\cap = \bigcap_{k=1}^{N_\Gamma} \bar{\gamma}_k.$$

We assume that the angle between intersecting fractures is bounded from below, as well as the angles between fractures and $\partial\Omega$, whenever a fracture touches the boundary. This implies, in particular, that the number of fractures joining at the intersection is bounded. We assume that the boundary of the bulk domain may be subdivided into two measurable subsets for the imposition of boundary conditions on the pressure and on the Darcy's velocity, that is $\partial\Omega = \partial\Omega_D \cup \partial\Omega_N$, with $|\partial\Omega_D| > 0$. This induces a subdivision of the boundary of each fracture into four different sets, some of which may be empty: $\partial\gamma_k^D = \partial\gamma_k \cap \partial\Omega_D$, $\partial\gamma_k^N = \partial\gamma_k \cap \partial\Omega_N$, the intersection tips $\partial\gamma_k^\cap = \bigcup_{\substack{j=1 \\ j\neq k}}^{N_\Gamma} (\partial\gamma_k \cap \partial\gamma_j)$ and finally $\partial\gamma_k^F = \partial\gamma_k \setminus (\partial\gamma_k^D \cup \partial\gamma_k^N \cup \partial\gamma_k^\cap)$, which corresponds to the set of immersed tips. We also introduce the corresponding definitions for the network $\partial\Gamma_D = \bigcup_{k=1}^{N_\Gamma} \partial\gamma_k^D$, $\partial\Gamma_N = \bigcup_{k=1}^{N_\Gamma} \partial\gamma_k^N$, $\partial\Gamma_\cap = \bigcup_{k=1}^{N_\Gamma} \partial\gamma_k^\cap$ and $\partial\Gamma_F = \bigcup_{k=1}^{N_\Gamma} \partial\gamma_k^F$. Some of these sets may as well be empty, and also the case of totally immersed network, i.e., $\partial\Gamma_D \cup \partial\Gamma_N = \emptyset$ is admitted. See Figure 4.1(a)-4.1(b) for an explicative example of the notation.
Following the same strategy as in [3, 87, 51], we assume that the fractures can be suitably extended so that the domain Ω is partitioned into a collection of Lipschitz subdomains ω_j, with $j = 1, \ldots, N_\omega$, i.e., $\Omega = \bigcup_{j=1}^{N_\omega} \omega_j$, cf. Figure 4.2. By construction, for each fracture γ_k we have exactly two subdomains, ω_{α^+} and ω_{α^-}, such that $\gamma_k \subset \partial\omega_{\alpha^+} \cap \partial\omega_{\alpha^-}$. This implies that we can identify for each fracture γ_k the normal $\mathbf{n}_k$ defined as $\mathbf{n}_k = \mathbf{n}_{\alpha^+} = -\mathbf{n}_{\alpha^-}$, where $\mathbf{n}_\alpha$ is the unit normal vector pointing outward of the subdomain ω_α. Moreover, we denote by $\mathbf{n}_\Gamma$ the normal to the whole fracture network, meaning that $\mathbf{n}_\Gamma = \mathbf{n}_k$ on γ_k.

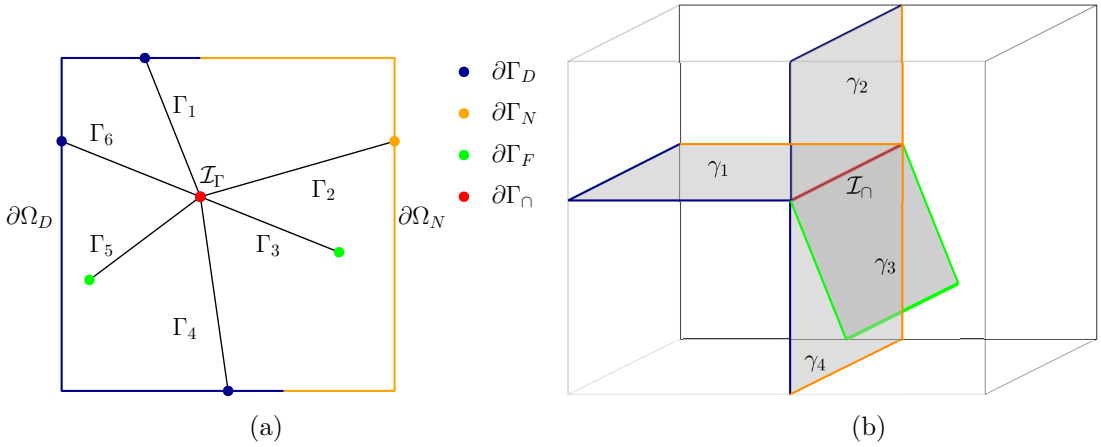

Figure 4.1: Example of fracture network satisfying the geometrical assumptions with subdivision of the boundary into sets for $d = 2$ (left) and $d = 3$ (right), see Assumption 4.1.1.

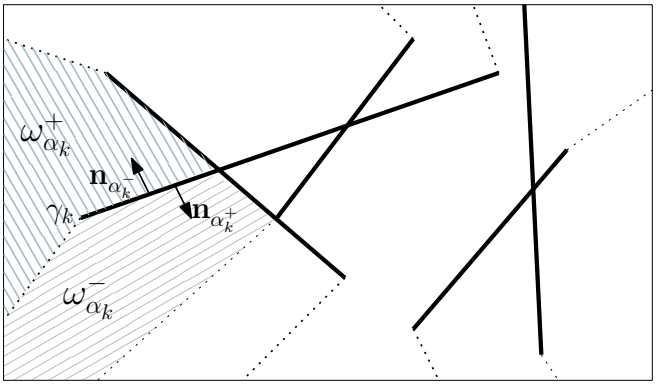

Figure 4.2: Partition of the domain Ω into subdomains ω_j induced by the prolongation of fractures.

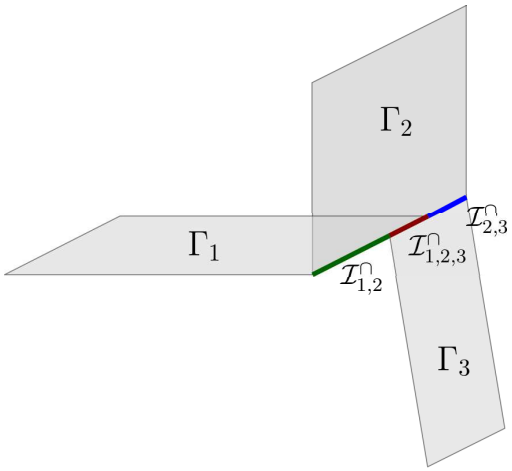

Figure 4.3: Example of multiple intersections for $d = 3$, where an intersection is defined as a segment shared by a fixed subset of fractures. Here, we can define 3 intersections, $\mathcal{I}^\cap_{1,2} = \partial\Gamma_1 \cap \partial\Gamma_2$, $\mathcal{I}^\cap_{1,2,3} = \partial\Gamma_1 \cap \partial\Gamma_2 \cap \partial\Gamma_3$ and $\mathcal{I}^\cap_{2,3} = \partial\Gamma_2 \cap \partial\Gamma_3$

Then, for a regular-enough scalar-valued function q defined on Ω, we can introduce *jump* and *average* across the fracture $\gamma_k \subset \partial\omega_{\alpha_k^+} \cap \partial\omega_{\alpha_k^-}$ in a standard way (see also Section 1.2) as

$$[\![q]\!]_{\gamma_k} = q_{\alpha_k^+}\mathbf{n}_{\alpha_k^+} + q_{\alpha_k^-}\mathbf{n}_{\alpha_k^-}, \qquad \{q\}_{\gamma_k} = \frac{1}{2}(q_{\alpha_k^+} + q_{\alpha_k^-}), \tag{4.1}$$

where $q_{\alpha_k^+}$ and $q_{\alpha_k^-}$ are the restriction to γ_k of the traces of q on $\partial\omega_{\alpha_k^+}$ and $\partial\omega_{\alpha_k^-}$, respectively. We refer to [51] and to [3] for a rigorous definition of the trace operators, also in the case of immersed tips. Similarly, for a regular-enough vector valued function $\mathbf{v}$, we define

$$[\![\mathbf{v}]\!]_{\gamma_k} = \mathbf{v}_{\alpha_k^+} \cdot \mathbf{n}_{\alpha_k^+} + \mathbf{v}_{\alpha_k^-} \cdot \mathbf{n}_{\alpha_k^-}, \qquad \{\mathbf{v}\}_{\gamma_k} = \frac{1}{2}(\mathbf{v}_{\alpha_k^+} + \mathbf{v}_{\alpha_k^-}). \tag{4.2}$$

Moreover, for given functions f_k defined on γ_k, with $k = 1, \dots, N_\Gamma$, we define the function f_Γ on the network Γ, in the sense of product spaces, as $f_\Gamma = \prod_{k=1}^{N_\Gamma} f_k$. We can then define the jump and average of a function q across the fracture network as $[\![q]\!]_\Gamma = \prod_{k=1}^{N_\Gamma} [\![q]\!]_{\gamma_k}$ and $\{q\}_\Gamma = \prod_{k=1}^{N_\Gamma} \{q\}_{\gamma_k}$, respectively.

Remark 8. We remark that the geometric hypotheses on the fracture network were made only for the sake of simplicity and the analysis can be easily extended to more general configurations. More precisely, the case of a network featuring multiple connected components can be treated analogously, as long as the partition of Ω into subdomains ω_α is aligned with all of them. The case of multiple intersections is an easy extension when $d = 2$, and the same holds true when $d = 3$ if we define an intersection as a segment shared by a fixed subset of fractures (see Figure 4.3 for an explicative example). Note that we do not need to impose any condition at the point shared by two intersections, since we are assuming that no flux is present along the intersections.

4.1.1 Governing equations

In what follows, we present the governing equations for our model. In accordance with the previous chapters, we take as a reference the model for single-phase flow derived in [101], where fractures are treated as $(d-1)$-dimensional interfaces between d-dimensional subdomains. In particular, we adopt the extension of the above model to fracture networks developed in [87, 51].

The flow of an incompressible fluid through a fractured d-dimensional porous medium, $d = 2, 3$, may be described by four elements:

1. *Governing equations for the flow in the porous medium*:
   We assume that the flow is governed by Darcy's law. We denote by p the fluid pressure and by $\boldsymbol{\nu}$ the permeability tensor, which we assume to include also the dependency on the viscosity. Given a function $f \in L^2(\Omega)$ representing a source term and a function $g \in H^{-1/2}(\partial\Omega_D)$, the motion of the fluid in the bulk may be then described by the following equations

$$\begin{aligned} -\nabla \cdot (\boldsymbol{\nu} \nabla p) &= f && \text{in } \Omega \setminus \bar{\Gamma}, \\ p &= g_D && \text{on } \partial\Omega_D, \\ \boldsymbol{\nu} \nabla p \cdot \mathbf{n} &= 0 && \text{on } \partial\Omega_N, \end{aligned} \tag{4.3}$$

   where $\mathbf{n}$ is the unit normal vector pointing outward of Ω. We also make some regularity assumptions on the tensor $\boldsymbol{\nu} = \boldsymbol{\nu}(\mathbf{x}) \in \mathbb{R}^{d\times d}$, requiring that it is symmetric, positive definite, uniformly bounded from below and above and with entries that are bounded, piecewise continuous real-valued functions.

2. *Governing equations for the flow in the fracture network*:
   Darcy's law is used also for modelling the flow along the fractures. In order to obtain a reduced model, where fractures are $(d-1)$-dimensional objects immersed in a d-dimensional domain, the same process of integration of the equations across the fracture aperture ℓ_Γ as in [101] is carried on. Reduced variables for the average pressure $p_\Gamma = (p_\Gamma^1, \ldots, p_\Gamma^{N_\Gamma})$ are then defined on each fracture. The flow is also characterized by the permeability tensor $\boldsymbol{\nu}_\Gamma = (\boldsymbol{\nu}_\Gamma^1, \ldots, \boldsymbol{\nu}_\Gamma^{N_\Gamma})$, scaled by viscosity. It is assumed that, on each fracture, $\boldsymbol{\nu}_\Gamma^k$ has a block-diagonal structure of the form

$$\boldsymbol{\nu}_\Gamma^k = \begin{bmatrix} \nu_{\gamma_k}^n & 0 \\ 0 & \boldsymbol{\nu}_{\gamma_k}^\tau \end{bmatrix},$$

   when written in its normal and tangential components, $k = 1, \ldots, N_\Gamma$. Here, $\boldsymbol{\nu}_{\gamma_k}^\tau \in \mathbb{R}^{(d-1)\times(d-1)}$ is a positive definite, uniformly bounded tensor (it reduces to a positive number for $d = 2$) representing the tangential component of the permeability of the fracture γ_k. Given a source term $f_\Gamma = (f_\Gamma^1, \ldots, f_\Gamma^{N_\Gamma}) \in \prod_{k=1}^{N_\Gamma} L^2(\gamma_k)$ and

$g_\Gamma \in H^{1/2}(\partial\Gamma_D)$, the governing equations for the fracture flow read

$$\begin{aligned} -\nabla_\tau \cdot (\boldsymbol{\nu}_\Gamma^\tau \ell_\Gamma \nabla_\tau p_\Gamma) &= \ell_\Gamma f_\Gamma - [\![\boldsymbol{\nu}\nabla p]\!] && \text{in } \Gamma, \\ p_\Gamma &= g_\Gamma && \text{on } \partial\Gamma_D, \\ (\boldsymbol{\nu}_\Gamma^\tau \ell_\Gamma \nabla_\tau p_\Gamma) \cdot \boldsymbol{\tau} &= 0 && \text{on } \partial\Gamma_N, \\ (\boldsymbol{\nu}_\Gamma^\tau \ell_\Gamma \nabla_\tau p_\Gamma) \cdot \boldsymbol{\tau} &= 0 && \text{on } \partial\Gamma_F, \end{aligned} \tag{4.4}$$

Here, $\boldsymbol{\tau} = (\boldsymbol{\tau}_1, \dots, \boldsymbol{\tau}_{N_\Gamma})$ is defined on each fracture γ_k as the vector in its tangent plane normal to $\partial\gamma_k$. Note that, when a certain operator is written on quantities defined on the whole network Γ, it should be interpreted as the product of the corresponding operators on each fracture γ_k.

For the condition on the immersed fracture tips, we have taken as reference [3], where the model developed in [101] has been extended to fully immersed fractures. In particular, we have imposed a homogeneous conditions for the flux, stating that the mass transfer across the immersed tips can be neglected in front of the transversal one.

3. *Coupling conditions between bulk and fractures along their interfaces*:
   The interface conditions to account for the exchange of fluid between the fractures are still described by the following equations:

$$\begin{aligned} -\{\boldsymbol{\nu}\nabla p\} \cdot \mathbf{n}_\Gamma &= \beta_\Gamma [\![p]\!] \cdot \mathbf{n}_\Gamma && \text{on } \Gamma, \\ -[\![\boldsymbol{\nu}\nabla p]\!] &= \alpha_\Gamma (\{p\} - p_\Gamma) && \text{on } \Gamma, \end{aligned} \tag{4.5}$$

   where we recall that

$$\beta_\Gamma = \frac{1}{2\eta_\Gamma}, \qquad \alpha_\Gamma = \frac{2}{\eta_\Gamma(2\xi - 1)}, \qquad \eta_\Gamma = \frac{\ell_\Gamma}{\nu_\Gamma^n}. \tag{4.6}$$

4. *Conditions at the intersection*:
   Finally, following [87], at the fracture intersection $\mathcal{I}_\cap$ we enforce pressure continuity and flux conservation:

$$p_\Gamma^1 = p_\Gamma^2 = \ldots = p_\Gamma^{N_\Gamma} \qquad \text{in } \mathcal{I}_\cap, \tag{4.7a}$$

$$\sum_{k=1}^{N_\Gamma} \boldsymbol{\nu}_{\gamma_k}^\tau \ell_k \nabla_\tau p_\Gamma^k \cdot \boldsymbol{\tau}_k = 0 \qquad \text{in } \mathcal{I}_\cap. \tag{4.7b}$$

We remark that other conditions might be imposed at the intersection. Some examples may be found in [112] or in [86], where the angle between fractures at the intersection is included in the model and jumps of pressure across the intersection are allowed.

4.2 Weak formulation

In this section we introduce the weak formulation of the model problem (4.3)-(4.4)-(4.5)-(4.7) and prove its well-posedness.
For the sake of simplicity we will assume that *homogeneous* Dirichlet boundary conditions are imposed for both the bulk and fracture problems, i.e., $g_D = 0$ and $g_\Gamma = 0$. The extension to the general non-homogeneous case is straightforward.

First, we introduce the functional spaces for our weak formulation. For the bulk and fracture pressure we define

$$\begin{aligned} Q^b &= \{q \in H^1(\Omega \setminus \bar{\Gamma}) : \ q = 0 \text{ on } \partial\Omega_D\}, \\ Q^\Gamma &= \{q_\Gamma = (q_\Gamma^1, \ldots, q_\Gamma^{N^\Gamma}) \in \prod_{k=1}^{N_\Gamma} H^1(\gamma_k) : \ q_\Gamma^k = 0 \ \text{ on } \ \partial\gamma_k^D \ \forall k = 1, \ldots, N_\Gamma \\ &\qquad \text{and } \ q_\Gamma^1 = \cdots = q_\Gamma^{N_\Gamma} \ \text{ on } \mathcal{I}_\cap\}, \end{aligned}$$

where the trace operators are understood. We remark that functions in the fracture space Q^Γ have continuous trace at the intersection. We equip the space $Q^b \times Q^\Gamma$ with the norm

$$||(q, q_\Gamma)||^2 = ||\boldsymbol{\nu}^{1/2} \nabla q||^2_{L^2(\Omega)} + ||(\boldsymbol{\nu}_\Gamma^\tau \ell_\Gamma)^{1/2} \nabla_\tau q_\Gamma||^2_{L^2(\Gamma)} + ||\beta_\Gamma^{1/2} [\![q]\!]||^2_{L^2(\Gamma)} + ||\alpha_\Gamma^{1/2} (\{q\} - q_\Gamma)||^2_{L^2(\Gamma)},$$

assuming from now on that $\alpha_\Gamma > 0$, that is $\xi > \frac{1}{2}$, see (4.6). Moreover, we introduce the bilinear form $\mathcal{A} : (Q^b \times Q^\Gamma) \times (Q^b \times Q^\Gamma) \to \mathbb{R}$ and the linear functional $\mathcal{L} : Q^b \times Q^\Gamma \to \mathbb{R}$,

defined as

$$\begin{aligned}\mathcal{A}\left((p,p_\Gamma),(q,q_\Gamma)\right) &= \int_\Omega \boldsymbol{\nu}\nabla p\cdot\nabla q \quad + \int_\Gamma \boldsymbol{\nu}_\Gamma^\tau \ell_\Gamma \nabla_\tau p_\Gamma\cdot\nabla_\tau q_\Gamma \\ &\quad + \int_\Gamma \beta_\Gamma [\![p]\!]\cdot[\![q]\!] + \int_\Gamma \alpha_\Gamma(\{p\}-p_\Gamma)(\{q\}-q_\Gamma) \\ \mathcal{L}(q,q_\Gamma) &= \int_\Omega fq + \int_\Gamma \ell_\Gamma f_\Gamma q_\Gamma,\end{aligned}$$

respectively. With the above notation, the weak formulation of the model problem (4.3)-(4.4)-(4.5)-(4.7) reads as follows: Find $(p,p_\Gamma)\in Q^b\times Q^\Gamma$ such that, for all $(q,q_\Gamma)\in Q^b\times Q^\Gamma$

$$\mathcal{A}\left((p,p_\Gamma),(q,q_\Gamma)\right) = \mathcal{L}(q,q_\Gamma). \tag{4.8}$$

We can now prove the following well-posedness result.

Theorem 4.2.1. *Let $\xi > 1/2$. Then, problem (4.8) is well-posed.*

Proof. The statement is a direct consequence of Lax-Milgram Lemma. □

We remark that the choice of considering a primal-primal setting for both the bulk and fracture problems is made here only for the sake of simplicity. We refer to [87] for the analysis of the mixed-mixed formulation in the case of a *totally immersed* network of fractures.
Next, we focus on the numerical discretization of the problem based on polyDG methods.

4.3 DG discretization

In this section we present a numerical discretization for the coupled bulk-network problem that is based on DG methods on polytopic grids. In particular, we discretize both the bulk and fracture network problems in primal form, employing the Simmetric Iterior Penalty DG method [26, 119]. The key idea to obtain a DG discretization will be the generalization of the concepts of jump and average at the intersection point/line, so that we will be able to impose the conditions at the intersection (4.7) in the spirit of DG methods. In particular, pressure continuity will be enforced penalizing the jump at the intersection, while balance of fluxes will be imposed "naturally".

We start with the introduction of the notation related to the polytopic discretization of the domains specific for this problem. In the bulk we consider a family of meshes $\mathcal{T}_h$ made of disjoint open *polygonal/polyhedral* elements, which are aligned both with the fracture network Γ and with the decomposition of Ω into subdomains ω_α, $\alpha = 1, \dots, N_\omega$. In particular, any element $E \in \mathcal{T}_h$ cannot be cut by Γ, and, since the subdomains ω_α are disjoint, each element E belongs exactly to one these subdomains.
Each mesh $\mathcal{T}_h$ induces a subdivision of each fracture in the network γ_k into faces, which we will denote by $\gamma_{k,h}$, for $k = 1, \dots, N_\Gamma$. The collection of all the fracture faces is denoted by Γ_h, i.e. $\Gamma_h = \cup_{k=1}^{N_\Gamma} \gamma_{k,h}$. This implies that the set of all the faces $\mathcal{F}_h$ may be decomposed, as before, into the three subsets $\mathcal{F}_h = \mathcal{F}_h^I \cup \mathcal{F}_h^B \cup \Gamma_h$, with $\mathcal{F}_h^B = \mathcal{F}_h^D \cup \mathcal{F}_h^N$. Moreover, we denote (as in Chapter 3) by $\mathcal{E}_{\Gamma,h}$ the set of all the interfaces (edges) of the elements in Γ_h, and we write, accordingly to the previous notation,

$$\mathcal{E}_{\Gamma,h} = \mathcal{E}_{\Gamma,h}^I \cup \mathcal{E}_{\Gamma,h}^B \cup \mathcal{E}_{\Gamma,h}^F \cup \mathcal{E}_{\Gamma,h}^\cap,$$

where:

- $\mathcal{E}_{\Gamma,h}^I$ is the set of interior edges;
- $\mathcal{E}_{\Gamma,h}^B = \mathcal{E}_{\Gamma,h}^D \cup \mathcal{E}_{\Gamma,h}^N$ is the set of edges belonging to the boundaries of the fracture network $\partial\Gamma_D$ and $\partial\Gamma_N$, respectively;
- $\mathcal{E}_{\Gamma,h}^F$ is the set of edges belonging to the immersed tips of the network;
- $\mathcal{E}_{\Gamma,h}^\cap$ is the set of edges on the intersection of the fractures. Note that, since we are considering a network with one single intersection, when $d = 2$ this set consists only of one single point.

We will also write $\mathcal{E}_{\gamma_k,h}^*$, with $* \in \{I, B, F, \cap\}$, to denote the restriction of each of these sets to the fracture γ_k.

4.3.1 Discrete formulation

For simplicity in the forthcoming analysis, we will suppose that the permeability tensors $\boldsymbol{\nu}$ and $\boldsymbol{\nu}_\Gamma$ are piecewise *constant* on mesh elements, i.e., $\boldsymbol{\nu}|_E \in [\mathbb{P}_0(E)]^{d\times d}$ for all $E \in \mathcal{T}_h$, and $\boldsymbol{\nu}_\Gamma|_F \in [\mathbb{P}_0(F)]^{(d-1)\times(d-1)}$ for all $F \in \Gamma_h$.

First, we introduce the finite-dimensional spaces where we will set our discrete problem. For the problem in the bulk we define the broken polynomial space

$$Q_h^b = \{q \in L^2(\Omega) : \ q|_E \in \mathbb{P}_{k_E}(E) \ \forall E \in \mathcal{T}_h\}, \qquad k_E \geq 1 \, \forall E \in \mathcal{T}_h.$$

Similarly, on each fracture γ_k, for $k = 1, \dots N_\Gamma$, we define the space

$$Q_h^{\gamma_k} = \{q_\Gamma^k \in L^2(\gamma_k) : \ q_\Gamma^k|_F \in \mathbb{P}_{k_F}(F) \ \forall F \in \gamma_{h,k}\} \qquad k_F \geq 1 \, \forall F \in \gamma_{h,k},$$

so that on the fracture network we can introduce the product space

$$Q_h^\Gamma = \prod_{k=1}^{N_\Gamma} Q_h^{\gamma_k}.$$

For future use in the analysis, we also introduce the DG vector-valued spaces

$$\begin{aligned}
\mathbf{W}_h^b &= \{\mathbf{v} \in [L^2(\Omega)]^d : \ \mathbf{v}|_E \in [\mathbb{P}_{k_E}(E)]^d \ \forall E \in \mathcal{T}_h\}, && k_E \geq 1 \, \forall E \in \mathcal{T}_h, \\
\mathbf{W}_h^{\gamma_k} &= \{\mathbf{v}_\Gamma^k \in [L^2(\Gamma)]^{d-1} : \ \mathbf{v}_\Gamma^k|_F \in [\mathbb{P}_{k_F}(F)]^{d-1} \ \forall F \in \gamma_{h,k}\}, && k_F \geq 1 \, \forall F \in \gamma_{h,k}, \\
\mathbf{W}_h^\Gamma &= \prod_{k=1}^{N_\Gamma} \mathbf{W}_h^{\gamma_k}.
\end{aligned}$$

In order to derive a DG discrete formulation of problem (4.8), we make the following regularity assumption.

Assumption 4.3.1. *We assume that the exact solution (p, p_Γ) of problem (4.8) is such that:*

A1. $p \in Q^b \cap H^2(\mathcal{T}_h)$ *and* $p_\Gamma \in Q^\Gamma \cap H^2(\Gamma_h)$*;*

A2. the normal components of the exact fluxes $\boldsymbol{\nu}\nabla p$ and $\ell_\Gamma \boldsymbol{\nu}_\Gamma^\tau \nabla p_\Gamma$ are continuous across mesh interfaces, that is $[\![\boldsymbol{\nu}\nabla p]\!] = 0$ on $\mathcal{F}_h^I$ and $[\![\ell_\Gamma \boldsymbol{\nu}_\Gamma^\tau \nabla p_\Gamma]\!] = 0$ on $\mathcal{E}_{\Gamma,h}^I$.

Moreover, for the forthcoming analysis, we introduce the following extended continuous spaces

$$Q^b(h) = Q_h^b \oplus \Big(Q^b \cap H^2(\mathcal{T}_h)\Big) \tag{4.9}$$

$$Q^\Gamma(h) = Q_h^\Gamma \oplus \Big(Q^\Gamma \cap H^2(\Gamma_h)\Big). \tag{4.10}$$

In order to derive a DG formulation for the problem in the bulk, we proceed as in Chapters 2 and 3. We obtain the following: Find $p_h \in Q_h^b$ such that for every test function $q \in Q_h^b$ it holds

$$\int_{\mathcal{T}_h} \boldsymbol{\nu}\nabla p_h \cdot \nabla q - \int_{\mathcal{F}_h^I \cup \mathcal{F}_h^D} \{\boldsymbol{\nu}\nabla p_h\} \cdot [\![q]\!] - \int_{\mathcal{F}_h^I \cup \mathcal{F}_h^D} \{\boldsymbol{\nu}\nabla q\} \cdot [\![p_h]\!] + \int_{\mathcal{F}_h^I \cup \mathcal{F}_h^D} \sigma_F [\![p_h]\!] \cdot [\![q]\!]$$
$$+ \int_{\Gamma_h} \beta_\Gamma [\![p_h]\!] \cdot [\![q]\!] + \int_{\Gamma_h} \alpha_\Gamma (\{p_h\} - p_\Gamma)\{q\} = \int_{\mathcal{T}_h} fq - \int_{\mathcal{F}_h^D} (\boldsymbol{\nu}\nabla q \cdot \mathbf{n}_F - \sigma_F q) g_D,$$

where we have introduced the discontinuity penalization parameter $\sigma \in L^\infty(\mathcal{F}_h^I \cup \mathcal{F}_h^D)$. Its precise definition will be given in Definition 4.4.1 below.

Next, we derive a DG discrete formulation for the problem in the fracture network. For generality, we will write our formulation referring to the case $d = 3$. However, the expressions are valid also when $d = 2$, provided that, when the domain of integration reduces to a point, the integrals are interpreted as evaluations.

First, we focus on a single fracture γ_k. Given a face $F \in \gamma_{k,h}$, we multiply the first equation in (4.4) for a test function $q_\Gamma^k \in Q_h^{\gamma_k}$ and integrate over F. Summing over all $F \in \gamma_{h,k}$ and integrating by parts, we obtain

$$\int_{\gamma_{h,k}} \boldsymbol{\nu}_{\gamma_k}^\tau \ell_k \nabla_\tau p_\Gamma^k \cdot \nabla_\tau q_\Gamma^k - \sum_{F \in \gamma_{h,k}} \int_{\partial F} q_\Gamma^k \boldsymbol{\nu}_{\gamma_k}^\tau \ell_k \nabla_\tau p_\Gamma^k \cdot \mathbf{n}_F = \int_{\gamma_{h,k}} \ell_k f_\Gamma^k q_\Gamma^k - \int_{\gamma_{h,k}} \alpha_\Gamma (\{p\} - p_\Gamma^k) q_\Gamma^k,$$

where we have used the second coupling condition in (4.5) to rewrite $-[\![\boldsymbol{\nu}\nabla p]\!] = \alpha_\Gamma(\{p\} - p_\Gamma^k)$ in the source term. If we sum over all the fractures γ_k in the network and use identity (1.5) on each fracture γ_k, we get

$$\int_{\Gamma_h} \boldsymbol{\nu}_\Gamma^\tau \ell_\Gamma \nabla_\tau p_\Gamma \cdot \nabla_\tau q_\Gamma - \int_{\mathcal{E}_{\Gamma,h}^I} [\![\boldsymbol{\nu}_\Gamma^\tau \ell_\Gamma \nabla_\tau p_\Gamma]\!] \{q_\Gamma\} - \int_{\mathcal{E}_{\Gamma,h}^I \cup \mathcal{E}_{\Gamma,h}^B} \{\boldsymbol{\nu}_\Gamma^\tau \ell_\Gamma \nabla_\tau p_\Gamma\} \cdot [\![q_\Gamma]\!]$$
$$- \sum_{k=1}^{N_\Gamma} \left[\int_{\mathcal{E}_{\gamma_k,h}^F} q_\Gamma^k \boldsymbol{\nu}_{\gamma_k}^\tau \ell_k \nabla_\tau p_\Gamma^k \cdot \boldsymbol{\tau}_k + \int_{\mathcal{E}_{\gamma_k,h}^\cap} q_\Gamma^k \boldsymbol{\nu}_{\gamma_k}^\tau \ell_k \nabla_\tau p_\Gamma^k \cdot \boldsymbol{\tau}_k \right] = \int_{\Gamma_h} \ell_\Gamma f_\Gamma q_\Gamma - \int_{\Gamma_h} \alpha_\Gamma (\{p\} - p_\Gamma) q_\Gamma,$$

where we recall that $\boldsymbol{\tau}_k$ is the vector tangent to the fracture γ_k, pointing outward of $\partial\gamma_k$, and $[\![\cdot]\!]$ and $\{\cdot\}$ are the standard jump and average operators defined in (4.1), (4.2) and

(1.4). In order to treat the term defined on the intersection

$$\sum_{k=1}^{N_\Gamma} \int_{\mathcal{E}^{\cap}_{\gamma_k,h}} q^k_\Gamma \boldsymbol{\nu}^\tau_{\gamma_k} \ell_k \nabla_\tau p^k_\Gamma \cdot \boldsymbol{\tau}_k, \tag{4.11}$$

we will now extend the definition of jump and average operators to the case when a number of planes intersect along one line ($d = 3$) or when a number of segments intersect in one point ($d = 2$).

Jump and average operators at the intersection

Let $\underline{b} = (b_1, b_2, \dots, b_{N_\Gamma})$ and $\underline{\mathbf{a}} = (\mathbf{a}_1, \mathbf{a}_2, \dots, \mathbf{a}_{N_\Gamma})$ be a scalar and vector-valued functions defined on the network Γ (product space), such that for every $k = 1, \dots, N_\Gamma$ the traces of b_k and $\mathbf{a}_k$ are well defined on the intersection $\mathcal{I}_\cap$. Moreover, for $k = 1, \dots, N_\Gamma$, let $\boldsymbol{\tau}_k$ be the vector tangent to the fracture γ_k, pointing outward of the intersection point/line $\mathcal{I}_\cap$.

Definition 4.3.1. We define *jump* and *average* operators for $\underline{\mathbf{a}}$ and $\underline{b}$ at $\mathcal{I}_\cap$ as

$$\begin{aligned}
\{\underline{b}\}_\cap &= \frac{1}{N_\Gamma}(b_1 + b_2 + \cdots + b_{N_\Gamma}) \\
[\![\underline{b}]\!]_\cap &= \Big(b_i - b_k\Big)_{i,k\in\{1,2,\dots,N_\Gamma\},\, i<k} \\
\{\underline{\mathbf{a}}\}_\cap &= \frac{1}{N_\Gamma}\Big(\mathbf{a}_i \cdot \boldsymbol{\tau}_i - \mathbf{a}_k \cdot \boldsymbol{\tau}_k\Big)_{i,k\in\{1,2,\dots,N_\Gamma\},\, i<k} \\
[\![\underline{\mathbf{a}}]\!]_\cap &= \mathbf{a}_1 \cdot \boldsymbol{\tau}_1 + \mathbf{a}_2 \cdot \boldsymbol{\tau}_2 + \cdots + \mathbf{a}_{N_\Gamma} \cdot \boldsymbol{\tau}_{N_\Gamma},
\end{aligned}$$

where trace operators on $\mathcal{I}_\cap$ are understood.

We remark that $\{\underline{b}\}_\cap$ and $[\![\underline{\mathbf{a}}]\!]_\cap$ are scalar-valued, while $[\![\underline{b}]\!]_\cap$ and $\{\underline{\mathbf{a}}\}_\cap$ are vector-valued, taking values in $\in \mathbb{R}^{\binom{N_\Gamma}{2}}$. In particular, for the definition of $[\![\underline{b}]\!]_\cap$ and $\{\underline{\mathbf{a}}\}_\cap$ we take all the pairs of indices in $\{1, \dots, N_\Gamma\}$ such that the first index is smaller than the second one. This is just one possible way of indicating all the pairs of fractures. Accordingly,

these vectors contain $\binom{N_\Gamma}{2} = \frac{N_\Gamma(N_\Gamma-1)}{2}$ elements. For example, for $N_\Gamma = 4$, we have

$$[\![\underline{b}]\!]_\cap = \begin{pmatrix} b_1 - b_2 \\ b_1 - b_3 \\ b_1 - b_4 \\ b_2 - b_3 \\ b_2 - b_4 \\ b_3 - b_4 \end{pmatrix} \in \mathbb{R}^6,$$

while, for $N_\Gamma = 5$, we have

$$[\![\underline{b}]\!]_\cap = \begin{pmatrix} b_1 - b_2 \\ b_1 - b_3 \\ b_1 - b_4 \\ b_1 - b_5 \\ b_2 - b_3 \\ b_2 - b_4 \\ b_2 - b_5 \\ b_3 - b_4 \\ b_3 - b_5 \\ b_4 - b_5 \end{pmatrix} \in \mathbb{R}^{10}.$$

The vector-valued case is analogous. Note also that, when $N_\Gamma = 2$, these definitions coincide with the definitions of jump and average operators introduced in [75, 9], for the generalization of DG methods to curved surfaces. Indeed we have

$$\{\underline{b}\}_\cap = \frac{1}{2}(b_1 + b_2), \qquad [\![\underline{b}]\!]_\cap = b_1 - b_2,$$
$$\{\underline{a}\}_\cap = \frac{1}{2}(\mathbf{a}_1 \cdot \boldsymbol{\tau}_1 - \mathbf{a}_2 \cdot \boldsymbol{\tau}_2), \qquad [\![\underline{a}]\!]_\cap = \mathbf{a}_1 \cdot \boldsymbol{\tau}_1 + \mathbf{a}_2 \cdot \boldsymbol{\tau}_2.$$

Definition 4.3.1 allows us to find an equivalent version of identity (1.3) on the intersection, according to the following property

Proposition 4.3.2. *The following identity holds*

$$[\![\underline{b}\,\underline{\boldsymbol{a}}]\!]_\cap = [\![\underline{\boldsymbol{a}}]\!]_\cap \{\underline{b}\}_\cap + \{\underline{\boldsymbol{a}}\}_\cap \cdot [\![\underline{b}]\!]_\cap, \tag{4.12}$$

where the vector-valued function $\underline{b\,\boldsymbol{a}}$ is defined as $\underline{b\,\boldsymbol{a}} = (b_1\,\boldsymbol{a}_1, b_2\,\boldsymbol{a}_2, \ldots, b_{N_\Gamma}\boldsymbol{a}_{N_\Gamma})$ and $\cdot$ is

the standard scalar-product in $\mathbb{R}^{\binom{N_\Gamma}{2}}$.

Proof. By definition we have

$$[\![\underline{b}\underline{\mathbf{a}}]\!]_\cap = \sum_{k=1}^{N_\Gamma} b_k \mathbf{a}_k \cdot \boldsymbol{\tau}_k.$$

Moreover, we can write

$$[\![\underline{\mathbf{a}}]\!]_\cap \{\underline{b}\}_\cap = \frac{1}{N_\Gamma}\Big(\sum_{k=1}^{N_\Gamma} b_k\Big)\Big(\sum_{j=1}^{N_\Gamma} \mathbf{a}_j \cdot \boldsymbol{\tau}_j\Big) = \frac{1}{N_\Gamma}\sum_{k=1}^{N_\Gamma}(b_k \mathbf{a}_k \cdot \boldsymbol{\tau}_k) + \frac{1}{N_\Gamma}\sum_{k=1}^{N_\Gamma}(b_k \sum_{\substack{j=1\\ j\neq k}}^{N_\Gamma} \mathbf{a}_j \cdot \boldsymbol{\tau}_j),$$

while we have

$$\begin{aligned}
\{\underline{\mathbf{a}}\}_\cap \cdot [\![\underline{b}]\!]_\cap &= \frac{1}{N_\Gamma}\sum_{k=1}^{N_\Gamma}\sum_{j=k+1}^{N_\Gamma}(b_k - b_j)(\mathbf{a}_k \cdot \boldsymbol{\tau}_k - \mathbf{a}_j \cdot \boldsymbol{\tau}_j) \\
&= \frac{1}{N_\Gamma}\sum_{k=1}^{N_\Gamma}\sum_{\substack{j=1\\ j\neq k}}^{N_\Gamma}(b_k - b_j)\mathbf{a}_k \cdot \boldsymbol{\tau}_k \\
&= \frac{1}{N_\Gamma}\sum_{k=1}^{N_\Gamma}\sum_{\substack{j=1\\ j\neq k}}^{N_\Gamma} b_k \mathbf{a}_k \cdot \boldsymbol{\tau}_k - \frac{1}{N_\Gamma}\sum_{k=1}^{N_\Gamma}\Big(\mathbf{a}_k \cdot \boldsymbol{\tau}_k \sum_{\substack{j=1\\ j\neq k}}^{N_\Gamma} b_j\Big) \\
&= \frac{1}{N_\Gamma}\sum_{k=1}^{N_\Gamma}(N_\Gamma - 1) b_k \mathbf{a}_k \cdot \boldsymbol{\tau}_k - \frac{1}{N_\Gamma}\sum_{k=1}^{N_\Gamma} b_k\Big(\sum_{\substack{j=1\\ j\neq k}}^{N_\Gamma} \mathbf{a}_j \cdot \boldsymbol{\tau}_j\Big).
\end{aligned}$$

This implies

$$[\![\underline{\mathbf{a}}]\!]_\cap \{\underline{b}\}_\cap + \{\underline{\mathbf{a}}\}_\cap \cdot [\![\underline{b}]\!]_\cap = \frac{1}{N_\Gamma}\sum_{k=1}^{N_\Gamma} b_k \mathbf{a}_k \cdot \boldsymbol{\tau}_k + \frac{1}{N_\Gamma}\sum_{k=1}^{N_\Gamma}(N_\Gamma - 1) b_k \mathbf{a}_k \cdot \boldsymbol{\tau}_k = \frac{1}{N_\Gamma}\sum_{k=1}^{N_\Gamma} N_\Gamma b_k \mathbf{a}_k \cdot \boldsymbol{\tau}_k,$$

and the proof is concluded. □

Now we take our focus back to the derivation of a DG discrete formulation for the problem in the fracture network. Using the above definition of jump and average at the

intersection 4.3.1 and identity (4.12), we can rewrite (4.11) as

$$\sum_{k=1}^{N_\Gamma} \int_{\mathcal{E}^\cap_{\gamma_k,h}} q^k_\Gamma \boldsymbol{\nu}^\tau_{\gamma_k} \ell_k \nabla_\tau p^k_\Gamma \cdot \boldsymbol{\tau}_k = \int_{\mathcal{E}^\cap_{\Gamma,h}} [\![q_\Gamma \boldsymbol{\nu}^\tau_\Gamma \ell_\Gamma \nabla_\tau p_\Gamma]\!]_\cap$$
$$= \int_{\mathcal{E}^\cap_{\Gamma,h}} [\![q_\Gamma]\!]_\cap \cdot \{ \boldsymbol{\nu}^\tau_\Gamma \ell_\Gamma \nabla_\tau p_\Gamma \}_\cap + \int_{\mathcal{E}^\cap_{\Gamma,h}} [\![\boldsymbol{\nu}^\tau_\Gamma \ell_\Gamma \nabla_\tau p_\Gamma]\!]_\cap \{ q_\Gamma \}_\cap.$$

The formulation on the fracture network becomes

$$\int_{\Gamma_h} \boldsymbol{\nu}^\tau_\Gamma \ell_\Gamma \nabla_\tau p_\Gamma \cdot \nabla_\tau q_\Gamma - \int_{\mathcal{E}^I_{\Gamma,h}} [\![\boldsymbol{\nu}^\tau_\Gamma \ell_\Gamma \nabla_\tau p_\Gamma]\!] \{ q_\Gamma \} - \int_{\mathcal{E}^I_{\Gamma,h} \cup \mathcal{E}^B_{\Gamma,h}} \{ \boldsymbol{\nu}^\tau_\Gamma \ell_\Gamma \nabla_\tau p_\Gamma \} \cdot [\![q_\Gamma]\!]$$
$$- \int_{\mathcal{E}^F_{\Gamma,h}} q_\Gamma \boldsymbol{\nu}^\tau_\Gamma \ell_\Gamma \nabla_\tau p_\Gamma \cdot \boldsymbol{\tau} - \int_{\mathcal{E}^\cap_{\Gamma,h}} [\![q_\Gamma]\!]_\cap \cdot \{ \boldsymbol{\nu}^\tau_\Gamma \ell_\Gamma \nabla_\tau p_\Gamma \}_\cap - \int_{\mathcal{E}^\cap_{\Gamma,h}} [\![\boldsymbol{\nu}^\tau_\Gamma \ell_\Gamma \nabla_\tau p_\Gamma]\!]_\cap \{ q_\Gamma \}_\cap$$
$$= \int_{\Gamma_h} \ell_\Gamma f_\Gamma q_\Gamma - \int_{\Gamma_h} \alpha_\Gamma (\{p\} - p_\Gamma) q_\Gamma. \quad (4.13)$$

From the fact that $p \in Q^\Gamma$ satisfies problem (4.8) and from the regularity Assumption 4.3.1, it holds:

- $[\![\boldsymbol{\nu}^\tau_\Gamma \ell_\Gamma \nabla_\tau p_\Gamma]\!] = 0$ on $\mathcal{E}^I_{\Gamma,h}$;
- $[\![p_\Gamma]\!] = 0$ on $\mathcal{E}^I_{\Gamma,h}$;
- $\boldsymbol{\nu}^\tau_\Gamma \ell_\Gamma \nabla_\tau p_\Gamma \cdot \boldsymbol{\tau} = 0$ on $\mathcal{E}^F_{\Gamma,h} \cup \mathcal{E}^N_{\Gamma,h}$;
- $[\![p_\Gamma]\!]_\cap = 0$ on $\mathcal{E}^\cap_{\Gamma,h}$;
- $[\![\boldsymbol{\nu}^\tau_\Gamma \ell_\Gamma \nabla_\tau p_\Gamma]\!]_\cap = 0$ on $\mathcal{E}^\cap_{\Gamma,h}$.

It follows that, for any test function $q_\Gamma \in Q^\Gamma_h$, identity (4.13) is equivalent to

$$\int_{\Gamma_h} \boldsymbol{\nu}^\tau_\Gamma \ell_\Gamma \nabla_\tau p_\Gamma \cdot \nabla_\tau q_\Gamma - \int_{\mathcal{E}^I_{\Gamma,h} \cup \mathcal{E}^D_{\Gamma,h}} \{ \boldsymbol{\nu}^\tau_\Gamma \ell_\Gamma \nabla_\tau p_\Gamma \} \cdot [\![q_\Gamma]\!] - \int_{\mathcal{E}^I_{\Gamma,h} \cup \mathcal{E}^D_{\Gamma,h}} \{ \boldsymbol{\nu}^\tau_\Gamma \ell_\Gamma \nabla_\tau q_\Gamma \} \cdot [\![p_\Gamma]\!]$$
$$- \int_{\mathcal{E}^\cap_{\Gamma,h}} \{ \boldsymbol{\nu}^\tau_\Gamma \ell_\Gamma \nabla_\tau p_\Gamma \}_\cap \cdot [\![q_\Gamma]\!]_\cap - \int_{\mathcal{E}^\cap_{\Gamma,h}} \{ \boldsymbol{\nu}^\tau_\Gamma \ell_\Gamma \nabla_\tau q_\Gamma \}_\cap \cdot [\![p_\Gamma]\!]_\cap$$
$$+ \int_{\mathcal{E}^I_{\Gamma,h} \cup \mathcal{E}^D_{\Gamma,h}} \sigma^\Gamma_e [\![p_\Gamma]\!] \cdot [\![q_\Gamma]\!] + \int_{\mathcal{E}^\cap_{\Gamma,h}} \sigma^\cap_e [\![p_\Gamma]\!]_\cap \cdot [\![q_\Gamma]\!]_\cap$$
$$= \int_{\Gamma_h} \ell_\Gamma f_\Gamma q_\Gamma + \int_{\Gamma_h} \alpha_\Gamma (\{p\} - p_\Gamma) q_\Gamma - \int_{\mathcal{E}^D_{\Gamma,h}} (\boldsymbol{\nu}^\tau_\Gamma \ell_\Gamma \nabla_\tau q_\Gamma \cdot \boldsymbol{\tau} - \sigma^\Gamma_e q_\Gamma) g_\Gamma,$$

where $\sigma^\Gamma \in L^\infty(\mathcal{E}^I_{\Gamma,h} \cup \mathcal{E}^D_{\Gamma,h})$ and $\sigma^\cap \in L^\infty(\mathcal{E}^\cap_{\Gamma,h})$ are discontinuity penalization parameters, whose precise definition will be given in Definition 4.4.2 below.

In conclusion, we obtain the following discrete formulation for the coupled bulk-network problem:
Find $(p_h, p_{\Gamma,h}) \in Q^b_h \times Q^\Gamma_h$ such that

$$\mathcal{A}_h\left((p_h, p_{\Gamma,h}), (q, q_\Gamma)\right) = \mathcal{L}_h(q, q_\Gamma) \quad \forall (q, q_\Gamma) \in Q^b_h \times Q^\Gamma_h, \tag{4.14}$$

where the bilinear form $\mathcal{A}_h : (Q^b_h \times Q^\Gamma_h) \times (Q^b_h \times Q^\Gamma_h) \to \mathbb{R}$ is defined as

$$\mathcal{A}_h\left((p_h, p_{\Gamma,h}), (q, q_\Gamma)\right) = \mathcal{A}_b(p_h, q) + \mathcal{A}_\Gamma(p_{\Gamma,h}, q_\Gamma) + \mathcal{C}((p_h, p_{\Gamma,h}), (q, q_\Gamma)),$$

and the linear functional $\mathcal{L}_h : Q^b_h \times Q^\Gamma_h \to \mathbb{R}$ is defined as

$$\mathcal{L}_h(q, q_\Gamma) = \mathcal{L}_b(q) + \mathcal{L}_\Gamma(q_\Gamma),$$

with

$$\begin{aligned}
\mathcal{A}_b(p_h, q) = &\int_{\mathcal{T}_h} \boldsymbol{\nu} \nabla p_h \cdot \nabla q - \int_{\mathcal{F}^I_h \cup \mathcal{F}^D_h} \{\boldsymbol{\nu} \nabla p_h\} \cdot [\![q]\!] \\
&- \int_{\mathcal{F}^I_h \cup \mathcal{F}^D_h} \{\boldsymbol{\nu} \nabla q\} \cdot [\![p_h]\!] + \int_{\mathcal{F}^I_h \cup \mathcal{F}^D_h} \sigma_F [\![p_h]\!] \cdot [\![q]\!]
\end{aligned}$$

$$\begin{aligned}
\mathcal{A}_\Gamma(p_{\Gamma,h}, q_\Gamma) = &\int_{\Gamma_h} \boldsymbol{\nu}^\tau_\Gamma \ell_\Gamma \nabla_\tau p_{\Gamma,h} \cdot \nabla_\tau q_\Gamma \\
&- \int_{\mathcal{E}^I_{\Gamma,h} \cup \mathcal{E}^D_{\Gamma,h}} \{\boldsymbol{\nu}^\tau_\Gamma \ell_\Gamma \nabla_\tau p_{\Gamma,h}\} \cdot [\![q_\Gamma]\!] - \int_{\mathcal{E}^I_{\Gamma,h} \cup \mathcal{E}^D_{\Gamma,h}} \{\boldsymbol{\nu}^\tau_\Gamma \ell_\Gamma \nabla_\tau q_\Gamma\} \cdot [\![p_{\Gamma,h}]\!] \\
&- \int_{\mathcal{E}^\cap_{\Gamma,h}} \{\boldsymbol{\nu}^\tau_\Gamma \ell_\Gamma \nabla_\tau p_{\Gamma,h}\}_\cap \cdot [\![q_\Gamma]\!]_\cap - \int_{\mathcal{E}^\cap_{\Gamma,h}} \{\boldsymbol{\nu}^\tau_\Gamma \ell_\Gamma \nabla_\tau q_\Gamma\}_\cap \cdot [\![p_{\Gamma,h}]\!]_\cap \\
&+ \int_{\mathcal{E}^I_{\Gamma,h} \cup \mathcal{E}^D_{\Gamma,h}} \sigma^\Gamma_e [\![p_{\Gamma,h}]\!] \cdot [\![q_\Gamma]\!] + \int_{\mathcal{E}^\cap_{\Gamma,h}} \sigma^\cap_e [\![p_\Gamma]\!]_\cap \cdot [\![q_\Gamma]\!]_\cap
\end{aligned}$$

$$\mathcal{C}((p_h, p_{\Gamma,h}), (q, q_\Gamma)) = \int_{\Gamma_h} \beta_\Gamma [\![p_h]\!] \cdot [\![q]\!] + \int_{\Gamma_h} \alpha_\Gamma (\{p_h\} - p_{\Gamma,h})(\{q\} - q_\Gamma),$$

and

$$\mathcal{L}_b(q) = \int_{\mathcal{T}_h} fq - \int_{\mathcal{F}_h^D} (\boldsymbol{\nu}\nabla q \cdot \mathbf{n}_F - \sigma_F q) g_D,$$
$$\mathcal{L}_\Gamma(q_\Gamma) = \int_{\Gamma_h} \ell_\Gamma f_\Gamma q_\Gamma - \int_{\mathcal{E}_{\Gamma,h}^D} (\boldsymbol{\nu}_\Gamma^\tau \ell_\Gamma \nabla_\tau q_\Gamma \cdot \boldsymbol{\tau} - \sigma_e^\Gamma q_\Gamma) g_\Gamma.$$

In the following, in order to simplify the notation, we will drop the subscript τ for the tangent operators on the fracture network.

4.4 Well-posedness of the discrete formulation

In this section, we prove that formulation (4.14) is well-posed. As in the previous chapters, we make some regularity assumptions on the meshes, so that we can work in the polytopic framework described in Chapter 1. In particular, we will assume that the bulk mesh $\mathcal{T}_h$ and all the fracture meshes $\gamma_{k,h}$, with $k = 1, \dots N_\Gamma$, satisfy the polytopic-regularity Assumption 1.1.1 and the covering Assumption 1.1.2.
Next, following [61, 59, 6, 58, 60], we define the bulk and fracture penalty functions as:

Definition 4.4.1. The discontinuity-penalization parameter $\sigma : \mathcal{F}_h \cup \mathcal{F}_h^D \to \mathbb{R}^+$ for the bulk problem is defined facewise as

$$\sigma(\mathbf{x}) = \sigma_0 \begin{cases} \max_{E \in \{E^+, E^-\}} \frac{\bar{\boldsymbol{\nu}}_E k_E^2}{h_E} & \text{if } \mathbf{x} \subset F \in \mathcal{F}_h^I,\ \bar{F} = \partial\bar{E}^+ \cap \partial\bar{E}^-, \\ \frac{\bar{\boldsymbol{\nu}}_E k_E^2}{h_E} & \text{if } \mathbf{x} \subset F \in \mathcal{F}_h^D,\ \bar{F} = \partial\bar{E} \cap \partial\bar{\Omega}, \end{cases} \tag{4.15}$$

with $\sigma_0 > 0$ independent of k_E, $|E|$ and $|F|$.

Definition 4.4.2. The discontinuity-penalization parameter $\sigma_\Gamma : \mathcal{E}_{\Gamma,h}^I \cup \mathcal{E}_{\Gamma,h}^D \cup \mathcal{E}_{\Gamma,h}^\cap \to \mathbb{R}^+$ for the fracture problem is defined edgewise as

$$\sigma^\Gamma(\mathbf{x}) = \sigma_0^\Gamma \begin{cases} \max_{F \in \{F^+, F^-\}} \frac{\bar{\boldsymbol{\nu}}_F^\tau k_F^2}{h_F} & \text{if } \mathbf{x} \subset e \in \mathcal{E}_{\Gamma,h}^I,\ \bar{e} = \partial\bar{F}^+ \cap \partial\bar{F}^-, \\ \frac{\bar{\boldsymbol{\nu}}_F^\tau k_F^2}{h_F}, & \text{if } \mathbf{x} \subset e \in \mathcal{E}_{\Gamma,h}^D,\ \bar{e} = \partial\bar{F} \cap \partial\bar{\Gamma}, \\ \max_{F \in \{F^1, \dots, F^{N_\Gamma}\}} \frac{\bar{\boldsymbol{\nu}}_F^\tau k_F^2}{h_F} & \text{if } \mathbf{x} \subset e \in \mathcal{E}_{\Gamma,h}^\cap,\ \bar{e} = \partial\bar{F}^1 \cap \dots \cap \partial\bar{F}^{N_\Gamma}, \end{cases} \tag{4.16}$$

with $\sigma_0^\Gamma > 0$ independent of k_F, $|F|$ and $|e|$.

Note that the definition of the fracture parameter on the intersection edges will play a crucial role in proving the well-posedness of our method. In the following we will write $\sigma^\cap$ to denote $\sigma^\Gamma|_{\mathcal{E}^\cap_{\Gamma,h}}$.

We endow the discrete space $Q_h^b \times Q_h^\Gamma$ with the *energy* norm

$$|||(q, q_\Gamma)|||^2 = ||q||^2_{b,DG} + ||q_\Gamma||^2_{\Gamma,DG} + ||(q, q_\Gamma)||^2_{\mathcal{C}},$$

where

$$\begin{aligned} ||q||^2_{b,DG} &= ||\boldsymbol{\nu}^{1/2}\nabla q||^2_{0,\mathcal{T}_h} + ||\sigma_F^{1/2}[\![q]\!]||^2_{0,\mathcal{F}_h^I\cup\mathcal{F}_h^D}, \\ ||q_\Gamma||^2_{\Gamma,DG} &= ||(\boldsymbol{\nu}_{\boldsymbol{\Gamma}}^{\boldsymbol{\tau}}\ell_\Gamma)^{1/2}\nabla q_\Gamma||^2_{0,\Gamma_h} + ||\sigma_e^{1/2}[\![q_\Gamma]\!]||^2_{0,\mathcal{E}^I_{\Gamma,h}\cup\mathcal{E}^D_{\Gamma,h}\cup\mathcal{E}^\cap_{\Gamma,h}}, \\ ||(q, q_\Gamma)||^2_{\mathcal{C}} &= ||\beta_\Gamma^{1/2}[\![q]\!]||^2_{0,\Gamma_h} + ||\alpha_\Gamma^{1/2}(\{q\} - q_\Gamma)||^2_{0,\Gamma_h}. \end{aligned} \tag{4.17}$$

Remark 9. Since we are assuming that there is a single intersection in the fracture network Γ, we have that $||\cdot||_{b,DG}$ is a norm on the bulk space Q_h^b. In the case of a general fracture network, this holds true only if every connected component of $\Omega \setminus \bar{\Gamma}$ has part of its boundary in $\partial\Omega_D$. Otherwise, $||\cdot||_{b,DG}$ is only a seminorm. Similarly, we have that $||\cdot||_{\Gamma,DG}$ is a norm on the network space Q_h^Γ, provided that the network is non-immersed, that is $\partial\Gamma_D \neq \emptyset$. However, we remark that, thanks to the coupling term $||\cdot||_{\mathcal{C}}$, we have that $|||\cdot|||$ is a norm on $Q_h^b \times Q_h^\Gamma$ for every possible configuration of the fracture network, including the totally immersed case. Moreover, $|||\cdot|||$ is well defined also on the extended space $Q^b(h) \times Q^\Gamma(h)$ introduced in (4.9)-(4.10).

The analysis will be based on the introduction of an appropriate *inconsistent* formulation and, consequently, on Strang's second Lemma, [114]. To this end, we introduce the following *extensions* of the forms $\mathcal{A}_b(\cdot,\cdot)$ and $\mathcal{A}_\Gamma(\cdot,\cdot)$ and $\mathcal{L}_b(\cdot)$ and $\mathcal{L}_\Gamma(\cdot)$ to the space

$Q^b(h) \times Q^\Gamma(h)$:

$$\begin{aligned}
\tilde{\mathcal{A}}_b(p,q) &= \int_{\mathcal{T}_h} \boldsymbol{\nu} \nabla p_h \cdot \nabla q - \int_{\mathcal{F}_h^I \cup \mathcal{F}_h^D} \{\boldsymbol{\nu} \boldsymbol{\Pi}_{\mathbf{W}_h^b}(\nabla p_h)\} \cdot [\![q]\!] \\
&\quad - \int_{\mathcal{F}_h^I \cup \mathcal{F}_h^D} \{\boldsymbol{\nu} \boldsymbol{\Pi}_{\mathbf{W}_h^b}(\nabla q)\} \cdot [\![p]\!] + \int_{\mathcal{F}_h^I \cup \mathcal{F}_h^D} \sigma_F [\![p]\!] \cdot [\![q]\!] \\
\tilde{\mathcal{A}}_\Gamma(p_{\Gamma,h}, q_\Gamma) &= \int_{\Gamma_h} \boldsymbol{\nu}_\Gamma^\tau \ell_\Gamma \nabla p_\Gamma \cdot \nabla q_\Gamma - \int_{\mathcal{E}_{\Gamma,h}^I \cup \mathcal{E}_{\Gamma,h}^D \cup \mathcal{E}_{\Gamma,h}^\cap} \{\boldsymbol{\nu}_\Gamma^\tau \ell_\Gamma \boldsymbol{\Pi}_{\mathbf{W}_h^\Gamma}(\nabla p_\Gamma)\} \cdot [\![q_\Gamma]\!] \\
&\quad - \int_{\mathcal{E}_{\Gamma,h}^I \cup \mathcal{E}_{\Gamma,h}^D \cup \mathcal{E}_{\Gamma,h}^\cap} \{\boldsymbol{\nu}_\Gamma^\tau \ell_\Gamma \boldsymbol{\Pi}_{\mathbf{W}_h^\Gamma}(\nabla q_\Gamma)\} \cdot [\![p_\Gamma]\!] + \int_{\mathcal{E}_{\Gamma,h}^I \cup \mathcal{E}_{\Gamma,h}^D \mathcal{E}_{\Gamma,h}^\cap} \sigma_e^\Gamma [\![p_\Gamma]\!] \cdot [\![q_\Gamma]\!] \\
\tilde{\mathcal{L}}_b(q) &= \int_{\mathcal{T}_h} fq - \int_{\mathcal{F}_h^D} (\boldsymbol{\nu} \boldsymbol{\Pi}_{\mathbf{W}_h^b}(\nabla q) \cdot \mathbf{n}_F - \sigma_F q) g_D, \\
\tilde{\mathcal{L}}_\Gamma(q_\Gamma) &= \int_{\Gamma_h} \ell_\Gamma f_\Gamma q_\Gamma - \int_{\mathcal{E}_{\Gamma,h}^D} (\boldsymbol{\nu}_\Gamma^\tau \ell_\Gamma \boldsymbol{\Pi}_{\mathbf{W}_h^\Gamma}(\nabla q_\Gamma) \cdot \boldsymbol{\tau}_e - \sigma_e^\Gamma q_\Gamma) g_\Gamma.
\end{aligned} \tag{4.18}$$

They were obtained by replacing the trace of the gradient operators ∇ and ∇_τ with the trace of their L^2-projection onto the DG vector-valued spaces $\mathbf{W}_h^b$ and $\mathbf{W}_h^\Gamma$, respectively. It follows that these newly introduced forms are well-defined on $Q^b(h) \times Q^\Gamma(h)$ and that they coincide with the formers on the discrete space $Q_h^b \times Q_h^\Gamma$. This means, in particular, that we can consider for the analysis the following *equivalent* version of the discrete problem (4.14):
Find $(p_h, p_{h,\Gamma}) \in Q_h^b \times Q_h^\Gamma$ such that

$$\tilde{\mathcal{A}}_h\left((p_h, p_h^\Gamma), (q, q_\Gamma)\right) = \tilde{\mathcal{L}}_h(q, q_\Gamma) \quad \forall (q, q_\Gamma) \in Q_h^b \times Q_h^\Gamma, \tag{4.19}$$

where $\tilde{\mathcal{A}}_h$ is obtained from $\mathcal{A}_h$ by replacing the bilinear forms with their extended versions (4.18). Note that formulation (4.19) is no longer consistent due to the discrete nature of the L^2-projection operators.

Next, we prove that problem (4.19) extended to the space $Q^b(h) \times Q^\Gamma(h)$ is well-posed. This, on the one hand, will ensure the well-posedness of discrete problem (4.14) and, on the other hand, will be used in the error analysis. We remark that the results involving the bulk problem, contained in Chapter 2 in the case of one single non-immersed fracture, can be easily extended to the case of a network of fractures. For this reason, in this chapter, our focus will mainly be on the fracture problem.
Following the same strategy as in Lemma 2.4.1 of Chapter 2, one can prove that the bulk

bilinear form $\tilde{\mathcal{A}}_b$ is continuous and coercive:

Lemma 4.4.1. *Let $\sigma : \mathcal{F}_h^I \cup \mathcal{F}_h^D \to \mathbb{R}^+$ be defined as in (4.15). Then, if the polytopic-regularity Assumption 1.1.1 holds for $\mathcal{T}_h$, the bilinear form $\tilde{\mathcal{A}}_b(\cdot,\cdot)$ is continuous on $Q^b(h)\times Q^b(h)$ and, provided that σ_0 is sufficiently large, it is also coercive on $Q^b(h)\times Q^b(h)$, i.e.*

$$\tilde{\mathcal{A}}_b(p,q) \lesssim ||q||_{b,DG}||p||_{b,DG}, \qquad \tilde{\mathcal{A}}_b(q,q) \gtrsim ||q||^2_{b,DG},$$

for any $q, p \in Q^b(h)$.

Proof. We refer to Lemma 2.4.1. □

Next, we prove an analogous result for the problem in fracture network.

Lemma 4.4.2. *Let $\sigma^\Gamma : \mathcal{E}^I_{\Gamma,h} \cup \mathcal{E}^D_{\Gamma,h} \cup \mathcal{E}^\cap_{\Gamma,h} \to \mathbb{R}^+$ be defined as in (4.16). Then, if Assumption 1.1.1 on Γ_h holds, the bilinear form $\tilde{\mathcal{A}}_\Gamma(\cdot,\cdot)$ is continuous on $Q^\Gamma(h)\times Q^\Gamma(h)$ and, provided that σ_0^Γ is sufficiently large, it is also coercive on $Q^\Gamma(h)\times Q^\Gamma(h)$, i.e.,*

$$\tilde{\mathcal{A}}_\Gamma(p_\Gamma,q_\Gamma) \lesssim ||q_\Gamma||_{\Gamma,DG}||p_\Gamma||_{\Gamma,DG}, \qquad \tilde{\mathcal{A}}_\Gamma(q_\Gamma,q_\Gamma) \gtrsim ||q_\Gamma||^2_{\Gamma,DG},$$

for any $q_\Gamma, p_\Gamma \in Q^\Gamma(h)$.

Proof. We start with coercivity. For any $q_\Gamma \in Q^\Gamma(h)$, we have

$$\tilde{\mathcal{A}}_\Gamma(q_\Gamma,q_\Gamma) = ||q_\Gamma||^2_{DG} - 2\int_{\mathcal{E}^I_{\Gamma,h}\cup\mathcal{E}^D_{\Gamma,h}} \{\boldsymbol{\nu}_\Gamma^\tau \ell_\Gamma \boldsymbol{\Pi}_{\mathbf{W}_h^\Gamma}(\nabla q_\Gamma)\}\cdot[\![q_\Gamma]\!] - 2\int_{\mathcal{E}^\cap_{\Gamma,h}} \{\boldsymbol{\nu}_\Gamma^\tau \ell_\Gamma \boldsymbol{\Pi}_{\mathbf{W}_h^\Gamma}(\nabla q_\Gamma)\}_\cap\cdot[\![q_\Gamma]\!]_\cap \tag{4.20}$$

$$= I + II + III$$

In order to bound term II, we proceed as in Lemma 2.4.1. We employ Cauchy-Schwarz's, triangular and Young's inequalities to write:

$$\int_{\mathcal{E}^I_{\Gamma,h}\cup\mathcal{E}^D_{\Gamma,h}} \{\boldsymbol{\nu}_\Gamma^\tau \ell_\Gamma \boldsymbol{\Pi}_{\mathbf{W}_h^\Gamma}(\nabla q_\Gamma)\}\cdot[\![q_\Gamma]\!] \lesssim \sum_{\mathcal{E}^I_{\Gamma,h}\cup\mathcal{E}^D_{\Gamma,h}} \left[\varepsilon\int_e (\sigma_e^\Gamma)^{-1}\{\boldsymbol{\nu}_\Gamma^\tau \ell_\Gamma \boldsymbol{\Pi}_{\mathbf{W}_h^\Gamma}(\nabla q_\Gamma)\}^2 + \frac{1}{4\varepsilon}\int_e \sigma_e^\Gamma [\![q_\Gamma]\!]^2\right].$$

From inverse inequality (1.3.2), the definition of the penalty parameter σ^Γ (4.16), As-

sumption 1.1.1 and the L^2-stability of the projector $\mathbf{\Pi}_{\mathbf{W}_h^\Gamma}$, we obtain

$$\int_{\mathcal{E}^I_{\Gamma,h}\cup\mathcal{E}^D_{\Gamma,h}} \{\boldsymbol{\nu}_\Gamma^\tau \ell_\Gamma \mathbf{\Pi}_{\mathbf{W}_h^\Gamma}(\nabla q_\Gamma)\}\cdot[\![q_\Gamma]\!] \lesssim \frac{\varepsilon}{\sigma_{0,\Gamma}}||(\boldsymbol{\nu}_\Gamma^\tau\ell_\Gamma)^{1/2}\nabla q_\Gamma||^2_{0,\Gamma_h} + \frac{1}{4\varepsilon}||\sigma_e^{1/2}[\![q_\Gamma]\!]||^2_{0,\mathcal{E}^I_{\Gamma,h}\cup\mathcal{E}^D_{\Gamma,h}}. \tag{4.21}$$

We now consider the intersection term III. Multiplying and dividing by $\sigma^\cap$ and applying Cauchy-Schwarz's and Young's inequalities we have

$$\int_{\mathcal{E}^\cap_{\Gamma,h}} \{\boldsymbol{\nu}_\Gamma^\tau \ell_\Gamma \mathbf{\Pi}_{\mathbf{W}_h^\Gamma}(\nabla q_\Gamma)\}_\cap\cdot[\![q_\Gamma]\!]_\cap \lesssim \sum_{e\in\mathcal{E}^\cap_{\Gamma,h}}\left[\varepsilon\int_e(\sigma_e^\cap)^{-1}\{\boldsymbol{\nu}_\Gamma^\tau \ell_\Gamma \mathbf{\Pi}_{\mathbf{W}_h^\Gamma}(\nabla q_\Gamma)\}^2_\cap + \frac{1}{4\varepsilon}\int_e\sigma_e^\cap[\![q_\Gamma]\!]^2_\cap\right]. \tag{4.22}$$

Using the definition of $\{\cdot\}_\cap$ (4.3.1) and triangular inequality, we obtain

$$\begin{aligned}
&\int_e \sigma_\cap^{-1}\{\boldsymbol{\nu}_\Gamma^\tau \ell_\Gamma \mathbf{\Pi}_{\mathbf{W}_h^\Gamma}(\nabla q_\Gamma)\}^2_\cap \\
&\qquad= \frac{1}{N_\Gamma}\sum_{\substack{i,k=1\\ i<k}}^{N_\Gamma}\int_e(\sigma_e^\cap)^{-1}(\boldsymbol{\nu}_{\gamma_i}^\tau\ell_i\mathbf{\Pi}_{\mathbf{W}_h^{\gamma_i}}(\nabla q_\Gamma^i)\cdot\boldsymbol{\tau}_i - \boldsymbol{\nu}_{\gamma_k}^\tau\ell_k\mathbf{\Pi}_{\mathbf{W}_h^{\gamma_k}}(\nabla q_\Gamma^k)\cdot\boldsymbol{\tau}_k)^2 \\
&\qquad\le \frac{2}{N_\Gamma}\sum_{\substack{i,k=1\\ i<k}}^{N_\Gamma}\left[\int_e(\sigma_e^\cap)^{-1}(\boldsymbol{\nu}_{\gamma_i}^\tau\ell_i\mathbf{\Pi}_{\mathbf{W}_h^{\gamma_i}}(\nabla q_\Gamma^i)\cdot)^2 + \int_e(\sigma_e^\cap)^{-1}(\boldsymbol{\nu}_{\gamma_k}^\tau\ell_k\mathbf{\Pi}_{\mathbf{W}_h^{\gamma_k}}(\nabla q_\Gamma^k))^2\right] \\
&\qquad= \frac{2(N_\Gamma-1)}{N_\Gamma}\sum_{k=1}^{N_\Gamma}\int_e(\sigma_e^\cap)^{-1}(\boldsymbol{\nu}_{\gamma_k}^\tau\ell_k\mathbf{\Pi}_{\mathbf{W}_h^{\gamma_k}}(\nabla q_\Gamma^k))^2,
\end{aligned}$$

where the last equality follows from the fact that every term appears in the sum exactly $(N_\Gamma-1)$ times. Since we are assuming that $\ell_\Gamma\boldsymbol{\nu}_\tau^\Gamma$ is constant on each $F\in\Gamma_h$, this implies that

$$\begin{aligned}
(a) &= \sum_{e\in\mathcal{E}^\cap_{\Gamma,h}}\int_e\sigma_\cap^{-1}\{\boldsymbol{\nu}_\Gamma^\tau \ell_\Gamma \mathbf{\Pi}_{\mathbf{W}_h^\Gamma}(\nabla q_\Gamma)\}^2_\cap \\
&\le \varepsilon\frac{2(N_\Gamma-1)}{N_\Gamma}\sum_{k=1}^{N_\Gamma}\sum_{\substack{F\in\gamma_{k,h}\\ \partial F\cap\mathcal{I}_\cap\neq\emptyset}}\int_{\partial F}\sigma_\cap^{-1}(\boldsymbol{\nu}_{\gamma_k}^\tau\ell_k\mathbf{\Pi}_{\mathbf{W}_h^{\gamma_k}}(\nabla q_\Gamma^k))^2 \\
&\le \varepsilon\frac{2(N_\Gamma-1)}{N_\Gamma}\sum_{k=1}^{N_\Gamma}\sum_{\substack{F\in\gamma_{k,h}\\ \partial F\cap\mathcal{I}_\cap\neq\emptyset}}\frac{1}{\sigma_{0,\Gamma}}\left(\frac{\bar{\boldsymbol{\nu}}_F^\tau k_F^2)}{h_F}\right)^{-1}\bar{\boldsymbol{\nu}}_F^\tau||(\boldsymbol{\nu}_\Gamma^\tau\ell_\Gamma)^{1/2}\nabla q_\Gamma^k||^2_{L^2(\partial F)},
\end{aligned}$$

where we have employed the definition of σ^Γ and the fact that for all $e \subseteq \partial F$

$$\sigma_e^\Gamma \geq \sigma_{0,\Gamma} \frac{\bar{\boldsymbol{\nu}}_F^\tau k_F^2}{h_F}.$$

Note that this is also true if $e \subseteq \mathcal{I}_\cap$. Finally, employing inverse inequality (1.3.2) and the stability of the projection operator $\boldsymbol{\Pi}_{\mathbf{W}_h^\Gamma}$ we have

$$(a) \lesssim \frac{\varepsilon}{\sigma_{0,\Gamma}} ||(\boldsymbol{\nu}_\Gamma^\tau \ell_\Gamma)^{1/2} \nabla q_\Gamma||_{0,\Gamma_h}^2. \tag{4.23}$$

From (4.20), employing the derived bounds (4.21), (4.22) and (4.23), we obtain that the bilinear $\tilde{\mathcal{A}}_\Gamma(\cdot,\cdot)$ form is coercive, provided that the parameter $\sigma_{0,\Gamma}$ is chosen large enough. Continuity can be proved with analogous arguments. □

Employing Lemma 4.4.1 and Lemma 4.4.2, we can now prove the well-posedness of the discrete problem (4.14).

Proposition 4.4.3. *Let the penalization parameters σ and σ^Γ for the problem in the bulk and in the fracture network be defined as in* (4.15) *and* (4.16)*, respectively. Then, problem* (4.14) *is well-posed, provided that σ_0 and $\sigma_{0,\Gamma}$ are chosen large enough.*

Proof. In order to use Lax-Milgram Lemma, we prove that the bilinear form $\tilde{\mathcal{A}}_h(\cdot,\cdot)$ is continuous and coercive on $Q^b(h) \times Q^\Gamma(h)$. We have, from Cauchy-Schwarz's inequality, that

$$\begin{aligned}
\mathcal{C}((q,q_\Gamma),(q,q_\Gamma)) &= ||(q,q_\Gamma)||_{\mathcal{C}}^2 \\
\mathcal{C}((q,q_\Gamma),(p,p_\Gamma)) &\leq \sum_{F\in\Gamma_h} ||\beta_\Gamma^{1/2}[\![q]\!]||_{L^2(F)}^2 ||\beta_\Gamma^{1/2}[\![p]\!]||_{L^2(F)}^2 \\
&\quad + \sum_{F\in\Gamma_h} ||\alpha_\Gamma^{1/2}(\{q\}-q_\Gamma)||_{L^2(F)}^2 ||\alpha_\Gamma^{1/2}(\{p\}-p_\Gamma)||_{L^2(F)}^2 \\
&\leq |||(q,q_\Gamma)||| \cdot |||(p,p_\Gamma)|||,
\end{aligned}$$

so that coercivity and continuity are a direct consequence of the definition of the norm $|||\cdot|||$ and of Lemma 4.4.1 and Lemma 4.4.2. The continuity of the linear operator $\tilde{\mathcal{L}}_h(\cdot)$ can be easily proved by using the Cauchy-Schwarz inequality, thanks to the regularity assumptions on the forcing terms f and f_Γ and on the boundary data g_D and g_Γ. □

4.5 Error analysis

In this section, we derive a-priori error estimates for the discrete problem (4.14). To this aim, for each subdomain ω_j, $j = 1, \dots, N_\omega$, we denote by $\mathscr{E}_j$ the classical continuous extension operator (cf. [113], see also Chapters 2 and 3) $\mathscr{E}_j : H^s(\Omega_j) \to H^s(\mathbb{R}^d)$, for $s \in \mathbb{N}_0$. Similarly, we denote by $\mathscr{E}_{\gamma_k}$ the continuous extension operator $\mathscr{E}_{\gamma_k} : H^s(\gamma_k) \to H^s(\mathbb{R}^{d-1})$, for $s \in \mathbb{N}_0$. We then make the following regularity assumptions for the exact solution (p, p_Γ) of problem (4.8):

Assumption 4.5.1. *Let $\mathcal{T}_\# = \{T_E\}$ and $\mathcal{F}_\# = \{T_F\}$ denote the associated coverings of Ω and Γ, respectively, of Definition 1.1.2. We assume that the exact solution (p, p_Γ) is such that:*

A1. for every $E \in \mathcal{T}_h$, if $E \subset \omega_j$ and p_j denotes the restriction of p to ω_j, it holds $\mathscr{E}_j p_j|_{T_E} \in H^{r_E}(T_E)$, with $r_E \geq 1 + d/2$ and $T_E \in \mathcal{T}_\#$ with $E \subset T_E$;

A2. for every $F \in \Gamma_h$, if $F \subset \gamma_k$, it holds $\mathscr{E}_{\gamma_k} p_\Gamma^k|_{T_F} \in H^{r_F}(T_F)$, with $r_F \geq 1 + (d-1)/2$ and $T_F \in \mathcal{F}_\#$ with $F \subset T_F$.

From Proposition 4.4.3 and Strang's second Lemma the following abstract error bound directly follows.

Lemma 4.5.2. *Assuming that the hypotheses of Proposition 4.4.3 are satisfied, it holds*

$$|||(p, p_\Gamma) - (p_h, p_{\Gamma,h})||| \lesssim \inf_{(q,q_\Gamma) \in Q_h^b \times Q_h^\Gamma} |||(p, p_\Gamma) - (q, q_\Gamma)||| + \sup_{(w,w_\Gamma) \in Q_h^b \times Q_h^\Gamma} \frac{|\mathcal{R}_h((p, p_\Gamma), (w, w_\Gamma))|}{|||(w, w_\Gamma)|||},$$

where the residual $\mathcal{R}_h$ is defined as

$$\mathcal{R}_h((p, p_\Gamma), (w, w_\Gamma)) = \tilde{\mathcal{A}}_h((p, p_\Gamma), (w, w_\Gamma)) - \tilde{\mathcal{L}}_h(w, w_\Gamma).$$

It is easy to show that the residual is the sum of two contributions, one involving only the bulk problem and one involving only the network problem:

$$\mathcal{R}_h((p, p_\Gamma), (w, w_\Gamma)) = \mathcal{R}_b(p, w) + \mathcal{R}_\Gamma(p_\Gamma, w_\Gamma) \tag{4.24}$$

It follows that, to derive a bound for the global residual, we can bound each of the two contributions separately. Again, we will focus mainly on the term related to the fracture network.

Lemma 4.5.3. *Let (p, p_Γ) be the exact solution of problem (4.8) satisfying the regularity Assumptions 4.3.1 and 4.5.1. Then, for every $w \in Q^b(h)$ and $w_\Gamma \in Q^\Gamma(h)$, it holds*

$$|\mathcal{R}_b(p,w)|^2 \lesssim \sum_{E\in\mathcal{T}_h} \frac{h_E^{2(s_E-1)}}{k_E^{2(r_E-1)}} ||\mathscr{E}p||^2_{H^{r_E}(T_E)} \left[\bar{\boldsymbol{\nu}}_E^2 \max_{F\subset\partial E\setminus(\Gamma\cup\partial\Omega_D)} \sigma_F^{-1}\left(\frac{k_E}{h_E}+\frac{k_E^2}{h_E}\right)\right] \cdot ||w||^2_{b,DG}, \tag{4.25}$$

$$|\mathcal{R}_\Gamma(p_\Gamma,w_\Gamma)|^2 \lesssim \left(\sum_{F\in\Gamma_h} \frac{h_F^{2(s_F-1)}}{k_F^{2(r_F-1)}} ||\mathscr{E}_\Gamma p_\Gamma||^2_{H^{r_F}(T_F)} \left[(\bar{\boldsymbol{\nu}}_F^\tau)^2 \max_{e\subseteq\partial F\setminus(\mathcal{I}_\cap\cup\partial\Gamma_N\cup\partial\Gamma_F)} \sigma_e^{-1}\left(\frac{k_F}{h_F}+\frac{k_F^2}{h_F}\right)\right] \right.$$

$$\left. + \sum_{k=1}^{N_\Gamma} \sum_{\substack{F\in\gamma_{h,k}\\ \partial F\cap\mathcal{I}_\cap\neq\emptyset}} \frac{h_F^{2(s_F-1)}}{k_F^{2(r_F-1)}} ||\mathscr{E}_{\gamma_k} p_\Gamma^k||^2_{H^{r_F}(T_F)} \left[(\bar{\boldsymbol{\nu}}_F^\tau)^2 \max_{e\subset\partial F\cap\mathcal{I}_\cap} (\sigma_e^\cap)^{-1}\left(\frac{k_F}{h_F}+\frac{k_F^2}{h_F}\right)\right] \right) \cdot ||w_\Gamma||^2_{\Gamma,DG}, \tag{4.26}$$

where, in (4.25), the extension operator $\mathscr{E}$ is to be interpreted as $\mathscr{E}_j$ if $E \subset \Omega_j$. Similarly, in (4.26), $\mathscr{E}_\Gamma$ is to be interpreted as $\mathscr{E}_{\gamma_k}$ if $F \subset \gamma_k$.

Proof. Integrating by parts elementwise and using the fact that (p, p_Γ) satisfies (4.8) and the regularity Assumption 4.3.1, we obtain the following expression for the residuals

$$\mathcal{R}_b(p,w) = \sum_{F\in\mathcal{F}_h^I\cup\mathcal{F}_h^D} \int_F \{\boldsymbol{\nu}(\nabla p - \boldsymbol{\Pi}_{\mathbf{W}_h^b}(\nabla p))\}\cdot[\![w]\!],$$

$$\mathcal{R}_\Gamma(p_\Gamma,w_\Gamma) = \sum_{e\in\mathcal{E}_{\Gamma,h}^I\cup\mathcal{E}_{\Gamma,h}^D\cup\mathcal{E}_{\Gamma,h}^\cap} \int_e \{\boldsymbol{\nu}_\Gamma^\tau \ell_\Gamma(\nabla p_\Gamma - \boldsymbol{\Pi}_{\mathbf{W}_h^\Gamma}(\nabla p_\Gamma))\}\cdot[\![w_\Gamma]\!].$$

For the proof of (4.25), we refer to Lemma 3.5.4 in Chapter 3. Here, we only focus on the proof of (4.26). To this aim, we consider the following two terms separately:

$$(a) = \left| \int_{\mathcal{E}_{\Gamma,h}^I\cup\mathcal{E}_{\Gamma,h}^D} \{\ell_\Gamma \boldsymbol{\nu}_\Gamma^\tau(\nabla p_\Gamma - \boldsymbol{\Pi}_{\mathbf{W}_h^\Gamma}(\nabla p_\Gamma))\}\cdot[\![q_\Gamma]\!] \right|,$$

$$(b) = \left| \int_{\mathcal{E}_{\Gamma,h}^\cap} \{\ell_\Gamma \boldsymbol{\nu}_\Gamma^\tau(\nabla p_\Gamma - \boldsymbol{\Pi}_{\mathbf{W}_h^\Gamma}(\nabla p_\Gamma))\}_\cap \cdot [\![q_\Gamma]\!]_\cap \right|.$$

Employing the Cauchy-Schwarz's inequality and the definition (4.17) of the norm $||\cdot||_{\Gamma,DG}$,

we obtain

$$(a) \lesssim \left(\int_{\mathcal{E}^I_{\Gamma,h} \cup \mathcal{E}^D_{\Gamma,h}} \sigma_\Gamma^{-1} |\{\ell_\Gamma \boldsymbol{\nu}^\tau_\Gamma (\nabla p_\Gamma - \boldsymbol{\Pi}_{\mathbf{W}^\Gamma_h}(\nabla p_\Gamma))\}|^2 \right)^{1/2} \cdot ||q_\Gamma||_{\Gamma,DG}.$$

Let $\widetilde{\Pi}$ denote also the vector-valued generalization of the interpolation operator $\widetilde{\Pi}$ defined in Lemma 1.3.3. Then, using the triangular inequality we can write

$$\begin{aligned}
&\sum_{e \in \mathcal{E}^I_{\Gamma,h} \cup \mathcal{E}^D_{\Gamma,h}} \sigma_e^{-1} \int_e |\{\ell_\Gamma \boldsymbol{\nu}^\tau_\Gamma (\nabla p_\Gamma - \boldsymbol{\Pi}_{\mathbf{W}^\Gamma_h}(\nabla p_\Gamma))\}|^2 \\
&\qquad \lesssim \sum_{e \in \mathcal{E}^I_{\Gamma,h} \cup \mathcal{E}^D_{\Gamma,h}} \sigma_e^{-1} \int_e |\{\ell_\Gamma \boldsymbol{\nu}^\tau_\Gamma (\nabla p_\Gamma - \widetilde{\Pi}(\nabla p_\Gamma))\}|^2 \\
&\qquad + \sum_{e \in \mathcal{E}^I_{\Gamma,h} \cup \mathcal{E}^D_{\Gamma,h}} \sigma_e^{-1} \int_e |\{\ell_\Gamma \boldsymbol{\nu}^\tau_\Gamma \boldsymbol{\Pi}_{\mathbf{W}^\Gamma_h}(\nabla p_\Gamma - \widetilde{\Pi}(\nabla p_\Gamma))\}|^2 \\
&\qquad \equiv (a1) + (a2).
\end{aligned}$$

Term $(a1)$ can be bounded, employing the approximation results of Lemma 1.3.3, as

$$(a1) \lesssim \sum_{F \in \Gamma_h} \frac{h_F^{2(s_F-1)}}{k_F^{2(r_F-1)}} \Big((\bar{\boldsymbol{\nu}}^\tau_F)^2 \max_{e \subset \partial F \setminus (\mathcal{I}_\cap \cup \partial\Gamma_N \cup \partial\Gamma_F)} \sigma_e^{-1} \frac{h_F^{-1}}{k_F^{-1}} \Big) ||\mathscr{E}_\Gamma p_\Gamma||^2_{H^{r_F}(T_F)}.$$

Exploiting, in order: the boundedness of the permeability tensor $\ell_\Gamma \boldsymbol{\nu}^\tau_\Gamma$, inverse inequality (1.6), the L^2-stability of the projector $\boldsymbol{\Pi}_{\mathbf{W}^\Gamma_h}$ and the approximation results of Lemma 1.3.3, we can bound term $(a2)$ as:

$$\begin{aligned}
(a2) &\lesssim \sum_{F \in \Gamma_h} \max_{e \subset \partial F \setminus (\mathcal{I}_\cap \cup \partial\Gamma_N \cup \partial\Gamma_F)} \sigma_e^{-1} (\bar{\boldsymbol{\nu}}^\tau_F)^2 ||\boldsymbol{\Pi}_{\mathbf{W}^\Gamma_h}(\widetilde{\Pi}(\nabla p_\Gamma) - \nabla p_\Gamma)||^2_{L^2(\partial F)} \\
&\lesssim \sum_{F \in \Gamma_h} \max_{e \subset \partial F \setminus (\mathcal{I}_\cap \cup \partial\Gamma_N \cup \partial\Gamma_F)} \sigma_e^{-1} (\bar{\boldsymbol{\nu}}^\tau_F)^2 \frac{k_F^2}{h_F} ||\widetilde{\Pi}(\nabla p_\Gamma) - \nabla p_\Gamma||^2_{L^2(F)} \\
&\lesssim \sum_{F \in \Gamma_h} \frac{h_F^{2(s_F-1)}}{k_F^{2(r_F-1)}} ||\mathscr{E}_\Gamma p_\Gamma||^2_{H^{r_F}(T_F)} \left((\bar{\boldsymbol{\nu}}^\tau_F)^2 \frac{k_F^2}{h_F} \max_{e \subset \partial F \setminus (\mathcal{I}_\cap \cup \partial\Gamma_N \cup \partial\Gamma_F)} \sigma_e^{-1} \right).
\end{aligned}$$

Next, we consider term (b). Employing the Cauchy-Schwarz's inequality and the definition

of the average operator at the intersection $\{\cdot\}_{\cap}$, we obtain

$$(b) \lesssim \left(\sum_{k=1}^{N_\Gamma} \sum_{e \in \mathcal{E}^{\cap}_{\gamma_k,h}} \int_e (\sigma_e^{\cap})^{-1} |\ell_\Gamma \boldsymbol{\nu}_\Gamma^\tau (\nabla p_\Gamma^k - \boldsymbol{\Pi}_{\mathbf{W}_h^{\gamma_k}} (\nabla p_\Gamma))|^2 \right)^{1/2} \cdot ||q_\Gamma||_{\Gamma,DG}.$$

Recalling that $\widetilde{\Pi}$ denotes the vector-valued generalization of the interpolation operator of Lemma 1.3.3, we can write

$$\begin{aligned}
&\sum_{k=1}^{N_\Gamma} \sum_{e \in \mathcal{E}^{\cap}_{\gamma_k,h}} \int_e (\sigma_e^{\cap})^{-1} |\ell_k \boldsymbol{\nu}_{\gamma_k}^\tau (\nabla p_\Gamma^k - \boldsymbol{\Pi}_{\mathbf{W}_h^{\gamma_k}} (\nabla p_\Gamma))|^2 \\
&\lesssim \sum_{k=1}^{N_\Gamma} \sum_{e \in \mathcal{E}^{\cap}_{\gamma_k,h}} \Big(\int_e (\sigma_e^{\cap})^{-1} |\ell_k \boldsymbol{\nu}_{\gamma_k}^\tau (\nabla p_\Gamma^k - \widetilde{\Pi}(\nabla p_\Gamma^k))|^2 + \int_e (\sigma_e^{\cap})^{-1} |\ell_k \boldsymbol{\nu}_{\gamma_k}^\tau \boldsymbol{\Pi}_{\mathbf{W}_h^\Gamma} (\nabla p_\Gamma^k - \widetilde{\Pi}(\nabla p_\Gamma^k))|^2 \Big) \\
&\equiv (b1) + (b2).
\end{aligned}$$

Employing arguments analogous to those for bounding terms $(a1)$ and $(a2)$, we can then write

$$(b1) \lesssim \sum_{k=1}^{N_\Gamma} \sum_{\substack{F \in \gamma_{h,k} \\ \partial F \cap \mathcal{I}_\cap \neq \emptyset}} \frac{h_F^{2(s_F-1)}}{k_F^{2(r_F-1)}} \Big((\bar{\boldsymbol{\nu}}_F^\tau)^2 \max_{e \subset \partial F \cap \mathcal{I}_\cap} (\sigma_e^{\cap})^{-1} \frac{h_F^{-1}}{k_F^{-1}} \Big) ||\mathscr{E}_{\gamma_k} p_\Gamma^k||^2_{H^{r_F}(T_F)},$$

and

$$\begin{aligned}
(b2) &\lesssim \sum_{k=1}^{N_\Gamma} \sum_{\substack{F \in \gamma_{h,k} \\ \partial F \cap \mathcal{I}_\cap \neq \emptyset}} \max_{e \subset \partial F \cap \mathcal{I}_\cap} (\sigma_e^{\cap})^{-1} (\bar{\boldsymbol{\nu}}_F^\tau)^2 ||\boldsymbol{\Pi}_{\mathbf{W}_h^\Gamma} (\widetilde{\Pi}(\nabla p_\Gamma^k) - \nabla p_\Gamma^k)||^2_{L^2(\partial F)} \\
&\lesssim \sum_{k=1}^{N_\Gamma} \sum_{\substack{F \in \gamma_{h,k} \\ \partial F \cap \mathcal{I}_\cap \neq \emptyset}} \max_{e \subset \partial F \cap \mathcal{I}_\cap} (\sigma_e^{\cap})^{-1} (\bar{\boldsymbol{\nu}}_F^\tau)^2 \frac{k_F^2}{h_F} ||\widetilde{\Pi}(\nabla p_\Gamma^k) - \nabla p_\Gamma^k||^2_{L^2(F)} \\
&\lesssim \sum_{k=1}^{N_\Gamma} \sum_{\substack{F \in \gamma_{h,k} \\ \partial F \cap \mathcal{I}_\cap \neq \emptyset}} \frac{h_F^{2(s_F-1)}}{k_F^{2(r_F-1)}} ||\mathscr{E}_{\gamma_k} p_\Gamma^k||^2_{H^{r_F}(T_F)} \Big((\bar{\boldsymbol{\nu}}_F^\tau)^2 \frac{k_F^2}{h_F} \max_{e \subset \partial F \cap \mathcal{I}_\cap} (\sigma_e^{\cap})^{-1} \Big).
\end{aligned}$$

This concludes the proof. □

Theorem 4.5.4. *Let $\mathcal{T}_\# = \{T_E\}$ and $\mathcal{F}_\# = \{T_F\}$ denote the associated coverings of Ω*

and Γ*, respectively, consisting of shape-regular simplexes as in Definition 1.1.2, satisfying Assumption 1.1.2. Let* (p, p_Γ) *be the solution of problem* (4.8) *and* $(p_h, p_{\Gamma,h}) \in Q_h^b \times Q_h^\Gamma$ *be its approximation obtained with the method* (4.14)*, with the penalization parameters given by* (4.15) *and* (4.16) *and* σ_0 *and* $\sigma_{0,\Gamma}$ *sufficiently large. Moreover, suppose that the exact solution* (p, p_Γ) *satisfies the regularity Assumptions 4.3.1 and 4.5.1. Then, the following error bound holds:*

$$\begin{aligned}
|||(p, p_\Gamma) - (p_h, p_{\Gamma,h})|||^2 \lesssim & \sum_{E\in\mathcal{T}_h} \frac{h_E^{2(s_E-1)}}{k_E^{2(r_E-1)}} G_E(h_E, k_E, \bar{\boldsymbol{\nu}}_E) ||\mathscr{E} p||^2_{H^{r_E}(T_E)} \\
& + \sum_{F\in\Gamma_h} \frac{h_F^{2(s_F-1)}}{k_F^{2(r_F-1)}} G_F(h_F, k_F, \bar{\boldsymbol{\nu}}_F^\tau) ||\mathscr{E}_\Gamma p_\Gamma||^2_{H^{r_F}(T_F)} \\
& + \sum_{k=1}^{N_\Gamma} \sum_{\substack{F\in\gamma_{h,k} \\ \partial F\cap\mathcal{I}_\cap\neq\emptyset}} \frac{h_F^{2(s_F-1)}}{k_F^{2(r_F-1)}} G_F^\cap(h_F, k_F, \bar{\boldsymbol{\nu}}_F^\tau) ||\mathscr{E}_{\gamma_k} p_\Gamma^k||^2_{H^{r_F}(T_F)},
\end{aligned}$$

where the $\mathscr{E} p$ *is to be interpreted as* $\mathscr{E}_j p_j$ *when* $E \subset \Omega_j$*,* $j = 1, \dots, N_\omega$*, and* $\mathscr{E}_\Gamma p_\Gamma$ *is to be interpreted as* $\mathscr{E}_{\gamma_k} p_\Gamma^k$ *when* $F \subset \gamma_k$*,* $k = 1, \dots, N_\Gamma$*. Here,* $s_E = \min(k_E + 1, r_E)$ *and* $s_F = \min(k_F + 1, r_F)$ *and for every* $E \in \mathcal{T}_h$ *and* $F \in \Gamma_h$*, the constants* G_E*,* G_F *and* $G_F^\cap$ *are defined as:*

$$\begin{aligned}
G_E(h_E, k_E, \bar{\boldsymbol{\nu}}_E) = & \bar{\boldsymbol{\nu}}_E + h_E k_E^{-1} \max_{F\subset\partial E\setminus\Gamma} \sigma_F + (\alpha_\Gamma + \beta_\Gamma) h_E k_E^{-1} \\
& + \bar{\boldsymbol{\nu}}_E^2 h_E^{-1} k_E \max_{F\subset\partial E\setminus\Gamma} \sigma_F^{-1} + \bar{\boldsymbol{\nu}}_E^2 h_E^{-1} k_E^2 \max_{F\subset\partial E\setminus\Gamma} \sigma_F^{-1}, \\
G_F(h_F, k_F, \bar{\boldsymbol{\nu}}_F^\tau) = & \bar{\boldsymbol{\nu}}_F^\tau + h_F k_F^{-1} \max_{e\subseteq\partial F\setminus(\mathcal{I}_\cap\cup\partial\Gamma_N\cup\partial\Gamma_F)} \sigma_e + \alpha_\Gamma h_F^2 k_F^{-2} \\
& + (\bar{\boldsymbol{\nu}}_F^\tau)^2 h_F^{-1} k_F \max_{e\subseteq\partial F\setminus(\mathcal{I}_\cap\cup\partial\Gamma_N\cup\partial\Gamma_F)} \sigma_e^{-1} \\
& + (\bar{\boldsymbol{\nu}}_F^\tau)^2 h_F^{-1} k_F^2 \max_{e\subseteq\partial F\setminus(\mathcal{I}_\cap\cup\partial\Gamma_N\cup\partial\Gamma_F)} \sigma_e^{-1} \\
G_F^\cap(h_F, k_F, \bar{\boldsymbol{\nu}}_F^\tau) = & h_F k_F^{-1} \max_{e\subseteq\partial F\ \cap\mathcal{I}_\cap} \sigma_e^\cap \\
& + (\bar{\boldsymbol{\nu}}_F^\tau)^2 h_F^{-1} k_F \max_{e\subseteq\partial F\cap\mathcal{I}_\cap} (\sigma_e^\cap)^{-1} + (\bar{\boldsymbol{\nu}}_F^\tau)^2 h_F^{-1} k_F^2 \max_{e\subseteq\partial F\cap\mathcal{I}_\cap} (\sigma_e^\cap)^{-1}.
\end{aligned}$$

Proof. From Lemma 4.5.2 we know that the error satisfies the following bound

$$|||(p,p_\Gamma)-(p_h,p_{\Gamma,h})||| \lesssim \underbrace{\inf_{(q,q_\Gamma)\in Q_h^b\times Q_h^\Gamma} |||(p,p_\Gamma)-(q,q_\Gamma)|||}_{I} + \underbrace{\sup_{(w,w_\Gamma)\in Q_h^b\times Q_h^\Gamma} \frac{|\mathcal{R}_h((p,p_\Gamma),(w,w_\Gamma))|}{|||(w,w_\Gamma)|||}}_{II}. \quad (4.27)$$

We estimate the two terms on the right-hand side of (4.27) separately. We can rewrite term I as

$$\begin{aligned} I &= \inf_{(q,q_\Gamma)\in Q_h^b\times Q_h^\Gamma} \left(||p-q||_{b,DG}^2 + ||p_\Gamma - q_\Gamma||_{\Gamma,DG}^2 + ||(p-q,p_\Gamma-q_\Gamma)||_{\mathcal{C}}^2 \right) \\ &\leq \underbrace{||p-\widetilde{\Pi}p||_{b,DG}^2}_{(a)} + \underbrace{||p_\Gamma-\widetilde{\Pi}p_\Gamma||_{\Gamma,DG}^2}_{(b)} + \underbrace{||(p-\widetilde{\Pi}p,p_\Gamma-\widetilde{\Pi}p_\Gamma)||_{\mathcal{C}}^2}_{(c)}. \end{aligned}$$

We consider each of the three terms separately. To bound term (a), we exploit the two approximation results stated in Lemma 1.3.3; we obtain that

$$\begin{aligned} (a) &\leq ||p-\widetilde{\Pi}p||_{b,DG}^2 = \sum_{E\in\mathcal{T}_h} ||\boldsymbol{\nu}^{1/2}\nabla(p-\widetilde{\Pi}p)||_{L^2(E)}^2 + \sum_{F\in\mathcal{F}_h^I\cup\mathcal{F}_h^D} \sigma_F ||[\![p-\widetilde{\Pi}p]\!]||_{L^2(F)}^2 \\ &\lesssim \sum_{E\in\mathcal{T}_h} \left[\bar{\boldsymbol{\nu}}_E |p-\widetilde{\Pi}p|_{H^1(E)}^2 + (\max_{F\subset\partial E\setminus(\Gamma\cup\partial\Omega_N)} \sigma_F) ||p-\widetilde{\Pi}p||_{L^2(\partial E)}^2 \right] \\ &\lesssim \sum_{E\in\mathcal{T}_h} \left[\frac{h_E^{2(s_E-1)}}{k_E^{2(r_E-1)}} \bar{\boldsymbol{\nu}}_E ||\mathscr{E}p||_{H^{r_E}(T_E)}^2 + \frac{h_E^{2(s_E-1/2)}}{k_E^{2(r_E-1/2)}} (\max_{F\subset\partial E\setminus(\Gamma\cup\partial\Omega_N)} \sigma_F) ||\mathscr{E}p||_{H^{r_E}(T_E)}^2 \right] \\ &= \sum_{E\in\mathcal{T}_h} \frac{h_E^{2(s_E-1)}}{k_E^{2(r_E-1)}} ||\mathscr{E}p||_{H^{r_E}(T_E)}^2 \left(\bar{\boldsymbol{\nu}}_E + \frac{h_E}{k_E} (\max_{F\subset\partial E\setminus(\Gamma\cup\partial\Omega_N)} \sigma_F) \right). \end{aligned}$$

Using analogous interpolation estimates on the fracture we can bound term (b) as follows:

$$
\begin{aligned}
(b) \leq ||p_\Gamma - \widetilde{\Pi} p_\Gamma||^2_{\Gamma,DG} &\lesssim \sum_{F\in\Gamma_h} ||\boldsymbol{\nu}^\tau_\Gamma \ell_\Gamma \nabla(p_\Gamma - \widetilde{\Pi} p_\Gamma)||^2_{L^2(F)} + \sum_{e\in\mathcal{E}^I_{\Gamma,h}\cup\mathcal{E}^D_{\Gamma,h}\cup\mathcal{E}^\cap_{\Gamma,h}} \sigma_e ||[\![p_\Gamma - \widetilde{\Pi} p_\Gamma]\!]||^2_{L^2(e)} \\
&\lesssim \sum_{F\in\Gamma_h} \frac{h_F^{2(s_F-1)}}{k_F^{2(r_F-1)}} ||\mathscr{E}_\Gamma p_\Gamma||^2_{H^{r_F}(T_F)} \left(\bar{\boldsymbol{\nu}}^\tau_F + \frac{h_F}{k_F} \max_{e\subseteq\partial F\setminus(\mathcal{I}_\cap\cup\partial\Gamma_N\cup\partial\Gamma_F)} \sigma_e \right) \\
&\quad + \sum_{k=1}^{N_\Gamma} \sum_{\substack{F\in\gamma_{h,k} \\ \partial F\cap\mathcal{I}_\cap\neq\emptyset}} \frac{h_F^{2(s_F-1)}}{k_F^{2(r_F-1)}} ||\mathscr{E}_{\gamma_k} p^k_\Gamma||^2_{H^{r_F}(T_F)} \Big(\frac{h_F}{k_F} \max_{e\subseteq\partial F\ \cap\mathcal{I}_\cap} \sigma^\cap_e \Big).
\end{aligned}
$$

Finally, for term (c), we have

$$
\begin{aligned}
(c) \leq ||(p - \widetilde{\Pi} p, p_\Gamma - \widetilde{\Pi} p_\Gamma)||^2_{\mathcal{C}} \leq \beta_\Gamma \sum_{F\in\Gamma_h} ||[\![p - \widetilde{\Pi} p]\!]||^2_{L^2(F)} + \alpha_\Gamma \sum_{F\in\Gamma_h} ||\{p - \widetilde{\Pi} p\}||^2_{L^2(F)} \\
+ \alpha_\Gamma \sum_{F\in\Gamma_h} ||p_\Gamma - \widetilde{\Pi} p_\Gamma||^2_{L^2(F)}.
\end{aligned}
$$

Exploiting the interpolation result (1.8), we deduce that

$$
\begin{aligned}
\beta_\Gamma \sum_{F\in\Gamma_h} ||[\![p - \widetilde{\Pi} p]\!]||^2_{L^2(F)} \leq \beta_\Gamma \sum_{\substack{E\in\mathcal{T}_h \\ \partial E\cap\Gamma\neq\emptyset}} ||p - \widetilde{\Pi} p||^2_{L^2(\partial E)} &\lesssim \beta_\Gamma \sum_{\substack{E\in\mathcal{T}_h \\ \partial E\cap\Gamma\neq\emptyset}} \frac{h_E^{2(s_E-\frac{1}{2})}}{k_E^{2(r_E-\frac{1}{2})}} ||\mathscr{E} p||^2_{H^{r_E}(T_E)} \\
&= \beta_\Gamma \sum_{\substack{E\in\mathcal{T}_h \\ \partial E\cap\Gamma\neq\emptyset}} \frac{h_E^{2(s_E-1)}}{k_E^{2(r_E-1)}} ||\mathscr{E} p||^2_{H^{r_E}(T_E)} \frac{h_E}{k_E}.
\end{aligned}
$$

Similarly, we have

$$
\alpha_\Gamma \sum_{F\in\Gamma_h} ||\{p - \widetilde{\Pi} p\}||^2_{L^2(F)} \lesssim \alpha_\Gamma \sum_{\substack{E\in\mathcal{T}_h \\ \partial E\cap\Gamma\neq\emptyset}} \frac{h_E^{2(s_E-1)}}{k_E^{2(r_E-1)}} ||\mathscr{E} p||^2_{H^{r_E}(T_E)} \frac{h_E}{k_E}.
$$

Moreover, using the interpolation estimates for the fracture network, we obtain

$$
\begin{aligned}
\alpha_\Gamma \sum_{F\in\Gamma_h} ||p_\Gamma - \widetilde{\Pi} p_\Gamma||^2_{L^2(F)} &\lesssim \alpha_\Gamma \sum_{F\in\Gamma_h} \frac{h_F^{2s_F}}{k^{2r_F}} ||\mathscr{E} p_\Gamma||^2_{H^{r_F}(T_F)} \\
&= \alpha_\Gamma \sum_{F\in\Gamma_h} \frac{h_F^{2(s_F-1)}}{k_F^{2(r_F-1)}} ||\mathscr{E} p_\Gamma||^2_{H^{r_F}(T_F)} \frac{h_F^2}{k_F^2}.
\end{aligned}
$$

Combining all the previous estimates, we can bound term I on the right-hand side of (4.27) as follows:

$$I \lesssim \frac{h_E^{2(s_E-1)}}{k_E^{2(r_E-1)}} ||\mathscr{E}p||^2_{H^{r_E}(T_E)} \left[\bar{\boldsymbol{\nu}}_E + \frac{h_E}{k_E} \max_{F \subset \partial E \setminus (\Gamma \cup \partial\Omega_N)} \sigma_F + (\alpha_\Gamma + \beta_\Gamma) \frac{h_E}{k_E} \right]$$
$$+ \sum_{F \in \Gamma_h} \frac{h_F^{2(s_F-1)}}{k_F^{2(r_F-1)}} ||\mathscr{E}_\Gamma p_\Gamma||^2_{H^{r_F}(T_F)} \left[\bar{\boldsymbol{\nu}}^\tau_F + \frac{h_F}{k_F} \max_{e \subseteq \partial F \setminus (\mathcal{I}_\cap \cup \partial\Gamma_N \cup \partial\Gamma_F)} \sigma_e + \alpha_\Gamma \frac{h_F^2}{k_F^2} \right]$$
$$+ \sum_{k=1}^{N_\Gamma} \sum_{\substack{F \in \gamma_{h,k} \\ \partial F \cap \mathcal{I}_\cap \neq \emptyset}} \frac{h_F^{2(s_F-1)}}{k_F^{2(r_F-1)}} ||\mathscr{E}_{\gamma_k} p^k_\Gamma||^2_{H^{r_F}(T_F)} \left[\frac{h_F}{k_F} \max_{e \subseteq \partial F \ \cap \mathcal{I}_\cap} \sigma^\cap_e \right]. \quad (4.28)$$

Finally, the desired estimate follows from the combination of (4.28), together with the bound on Term II that derives from what observed in (4.24) and Lemma 4.5.3. □

4.6 Numerical experiments

In this section we present several numerical examples, with increasing complexity, in order to validate the theoretical bounds and assess the practical performance of our method. For the first set of experiments the analytical solution is known, so that we are able to verify the convergence rates obtained in Theorem 4.5.4. We point out that choice of the model coefficients is here made only with the aim of testing the effectiveness of the numerical method and it does not intend to have any physical meaning. On the other hand, the last test case considers a more realistic configuration featuring a totally immersed network of fractures.

We remark that, in all the presented test cases, the pressure continuity condition at the intersection points (4.7a) is satisfied, however in some of them the no flux condition (4.7b) does not hold. To take this into account, we need to modify formulation (4.14), adding on the right hand side the term

$$\int_{\mathcal{E}^\cap_{\Gamma,h}} [\![\boldsymbol{\nu}^\tau_\Gamma \ell_\Gamma \nabla_\tau p_\Gamma]\!]_\cap \{q_\Gamma\}_\cap, \quad (4.29)$$

where the quantity $[\![\boldsymbol{\nu}^\tau_\Gamma \ell_\Gamma \nabla_\tau p_\Gamma]\!]_\cap = \sum_{k=1}^{N_\Gamma} \boldsymbol{\nu}^\tau_{\gamma_k} \ell_k \nabla_\tau p^k_\Gamma \cdot \boldsymbol{\tau}_k$ is given.

For all the experiments we choose a quadratic polynomial degree for both the bulk and

fracture problems, i.e. $k_E = 2\ \forall E \in \mathcal{T}_h$ and $k_F = 2\ \forall F \in \Gamma_h$. Moreover, we always choose the permeability tensor in the bulk $\boldsymbol{\nu} = \mathbf{I}$, so as to focus mainly on the fracture problem. All the numerical tests have been implemented in MATLAB® and employ polygonal grids, which have been generated from Cartesian meshes, employing the hybrid mesh generation technique previously described.

4.6.1 Example 1: vertical fracture

As first test case, we modify a test case presented in Section 2.5.4, splitting the single fracture in 3 parts. In particular, we consider the domain $\Omega = (0,1)^2$ and the fracture network composed of the fractures $\gamma_1 = \{(x,y) \in \Omega : \quad x = 0.5,\ 0 < y < 0.5\}$, $\gamma_2 = \{(x,y) \in \Omega : \quad x = 0.5,\ 0.5 < y < 0.75\}$ and $\gamma_3 = \{(x,y) \in \Omega : \quad x = 0.5,\ 0.75 < y < 1\}$, see Figure 4.4(a). Note that both the tips of the fracture γ_2 are intersection tips.

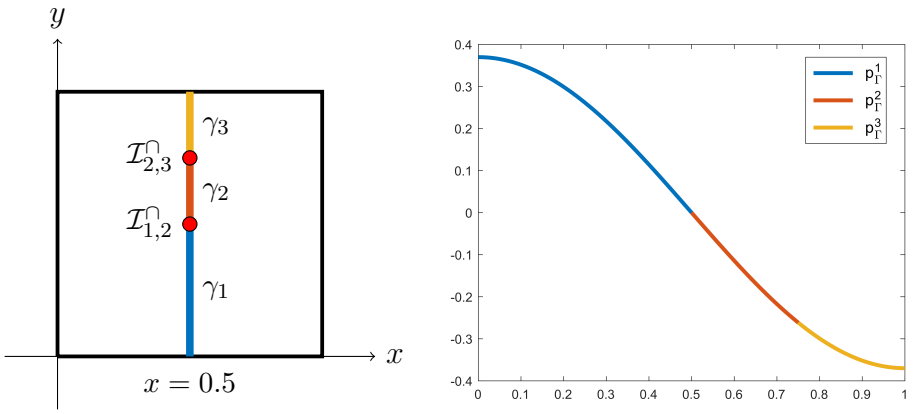

(a) Computational domain (b) Solution in the network

Figure 4.4: Example 1: Computational domain (left) and computed fracture pressures (right).

We choose the exact solutions in the bulk and in the fractures as follows

$$p = \begin{cases} \sin(4x)\cos(\pi y) & \text{if } x < 0.5, \\ \cos(4x)\cos(\pi y) & \text{if } x > 0.5, \end{cases} \qquad p^k_\Gamma = \xi[\cos(2) + \sin(2)]\cos(\pi y),\ k = 1,2,3$$

so that they satisfy the coupling conditions (4.5) with $\boldsymbol{\nu} = \mathbf{I}$, provided that, $\forall k = 1,2,3$, we choose $\beta_{\gamma_k} = 2$, that is $\boldsymbol{\nu}^n_{\gamma_k}/\ell_k = 4$. We impose Dirichlet boundary conditions on the

whole $\partial\Omega$ and also on $\partial\Gamma$. Finally, the source term in the bulk is chosen, accordingly, as

$$f = \begin{cases} \sin(4x)\cos(\pi y)(16+\pi^2) & \text{if } x < 0.5, \\ \cos(4x)\cos(\pi y)(16+\pi^2) & \text{if } x > 0.5, \end{cases}$$

and, given $\forall k = 1, 2, 3$ the values $\boldsymbol{\nu}^{\tau}_{\gamma_k}$ of the tangential components of the permeability tensor in the fracture, the fracture forcing terms are set as

$$f^k_\Gamma = \cos(\pi y)[\cos(2) + \sin(2)](\xi \boldsymbol{\nu}^{\tau}_{\gamma_k}\pi^2 + \frac{4}{\ell_k}).$$

Clearly, pressure continuity at the intersection point (4.7a) is satisfied regardless of the values chosen for the fracture coefficients $\boldsymbol{\nu}^{\tau}_\Gamma$, ν^n_Γ and ℓ_Γ. However, flux conservation (4.7b) does not hold if the values vary from fracture to fracture. For this reason, we need to modify the right hand side of the formulation as in (4.29).
We perform two simulations, varying the values of the fracture coefficients (always satisfying the constraint $\beta_\Gamma = 2$). In particular, we take

- Case (a):

$$\begin{aligned} \boldsymbol{\nu}^{\tau}_\Gamma &= [3\cdot 10^4,\ \ 2\cdot 10^3,\ \ 4\cdot 10^4], \\ \nu^n_\Gamma &= 4 * [10^{-4},\ 10^{-2},\ 10^{-5}], \\ \ell_\Gamma &= [10^{-4},\ 10^{-2},\ 10^{-5}]; \end{aligned} \tag{4.30}$$

- Case (b):

$$\begin{aligned} \boldsymbol{\nu}^{\tau}_\Gamma &= [3\cdot 10^{-4},\ \ 2\cdot 10^{-3},\ \ 4\cdot 10^{-4}], \\ \nu^n_\Gamma &= [10^4,\ 10^2,\ 10^5], \\ \ell_\Gamma &= 0.25 * [10^4,\ 10^2,\ 10^5]; \end{aligned} \tag{4.31}$$

Finally, in all the experiments we set $\xi = 0.75$.

In Figure 4.4(b) we show the numerical solution for the problem in the fracture network for the case (a), where one can clearly see that the continuity condition at the intersection points (4.7a) is satisfied. In Figures 4.5(a)-4.5(b) we report the computed error $||p - p_h||_{b,DG}$ (loglog scale) for the bulk problem as a function of the inverse of the mesh size h and the corresponding computed error $||p_\Gamma - p_{\Gamma,h}||_{\Gamma,DG}$ (loglog scale) in the fracture network. We recall that we are taking the polynomial degree $k = 2$ for

both the bulk and fracture problems. On the left we show the results obtained for test case (a) (with coefficients as in (4.30)), while on the right, we report the results for the case (b) (with coefficient as in (4.31)). As predicted from our theoretical error bounds, a convergence of order 2 is clearly observed for both $||p - p_h||_{b,DG}$ and $||p_\Gamma - p_{\Gamma,h}||_{\Gamma,DG}$. Moreover, the convergence is improved of one order if we consider the errors in the L^2-norms $||p - p_h||_{L^2(\Omega)}$ and $||p_\Gamma - p_{\Gamma,h}||_{L^2(\Gamma)}$.

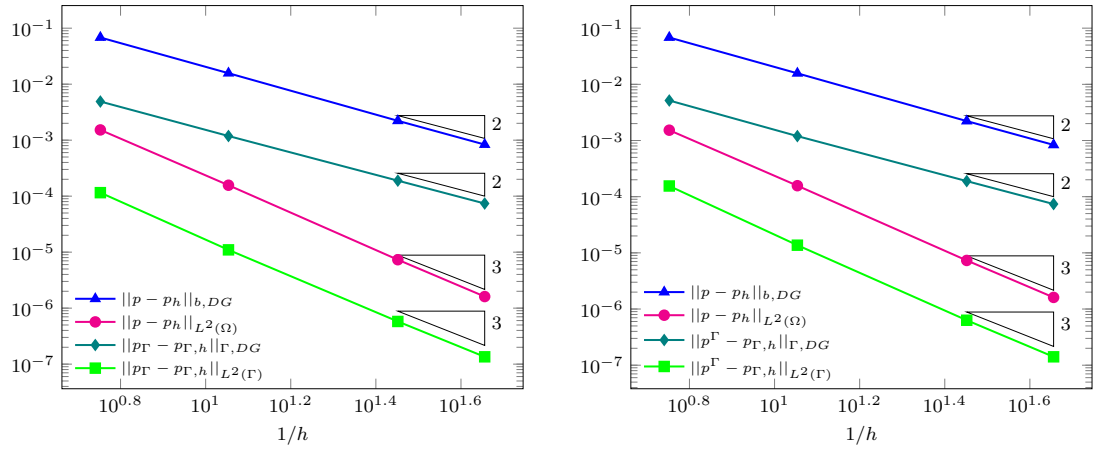

Figure 4.5: Example 1: Computed errors in the bulk and in the fractures as a function of the inverse of the mesh size (loglog scale). Case (a) on the left and case (b) on the right.

4.6.2 Example 2: Y-shaped intersection

In the second test case we take the bulk $\Omega = (-2, 2)^2$ and the fracture network Γ consisting of the fractures $\gamma_1 = \{(x, y) \in \Omega : \quad x = y, \ -2 < y < 0\}$, $\gamma_2 = \{(x, y) \in \Omega : \quad x = y, \ 0 < y < 2\}$ and $\gamma_3 = \{(x, y) \in \Omega : \quad x = 0, \ 0 < y < 2\}$, see Figure 4.6. We choose the exact solution in the whole bulk as $p(x, y) = \cos(xy - x^2)$ and the permeability tensor $\boldsymbol{\nu} = \mathbf{I}$. Note that, even if the bulk solution is continuous across the fractures, the first coupling condition in (4.5) is satisfied because $\nabla p|_\Gamma = \mathbf{0}$. In order for the second coupling condition to hold, we need to choose the solution in the fractures $p_\Gamma^k = p|_{\gamma_k}$ for all $k = 1, 2, 3$, that is $p_\Gamma^k = 1$. Note also that this configuration satisfies the conditions at the intersection (4.7) irrespective of the choice of the model coefficients. Finally, the source terms are chosen accordingly as $f = \cos(xy - x^2)(y^2 + 5x^2 - 4xy) - 2\sin(xy - x^2)$ and $f_\Gamma = \mathbf{0}$. We impose Dirichlet boundary conditions on the whole $\partial\Omega$ and also on $\partial\Gamma$. In the numerical experiments we choose $\xi = 0.55$.

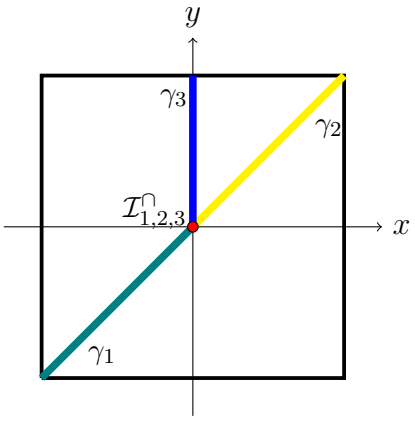

Figure 4.6: Example 2: computational domain.

We perform two simulations, taking the physical parameters in the fracture network as in the previous example, that is for case (a) we choose the coefficients as in (4.30), while for case (b) as in (4.31).

Figures 4.7(a)-4.7(b) show the computed errors (in loglog scale) $||p - p_h||_{b,DG}$ and $||p_\Gamma - p_{\Gamma,h}||_{\Gamma,DG}$ for the bulk and fracture problem, respectively (case (a) on the left and case (b) on the right). Also in this case the theoretical convergence rates are achieved and one order is gained for the L^2-norm.

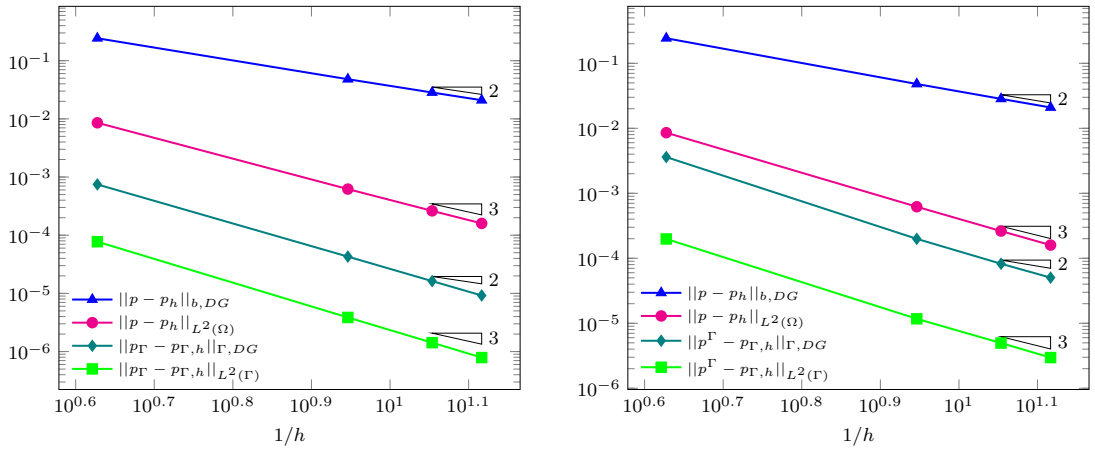

Figure 4.7: Example 2: Computed errors in the bulk and in the fractures as a function of the inverse of the mesh size (loglog scale). Case (a) on the left and case (b) on the right.

4.6.3 Example 3: checkerboard

In the third test case we consider a cross-shaped network of fractures cutting the bulk $\Omega = (-1,1)^2$. The fractures are defined as $\gamma_1 = \{(x,y) \in \Omega : \ y = 0, \ -1 < x < -0.5\}$, $\gamma_2 = \{(x,y) \in \Omega : \ y = 0, \ -0.5 < x < 0\}$, $\gamma_3 = \{(x,y) \in \Omega : \ x = 0, \ -1 < y < 0\}$, $\gamma_4 = \{(x,y) \in \Omega : \ y = 0, \ 0 < x < 1\}$ and $\gamma_5 = \{(x,y) \in \Omega : \ x = 0, \ 0 < x < 1\}$, see Figure 4.8(a). Note that fracture γ_2 presents two intersection tips.

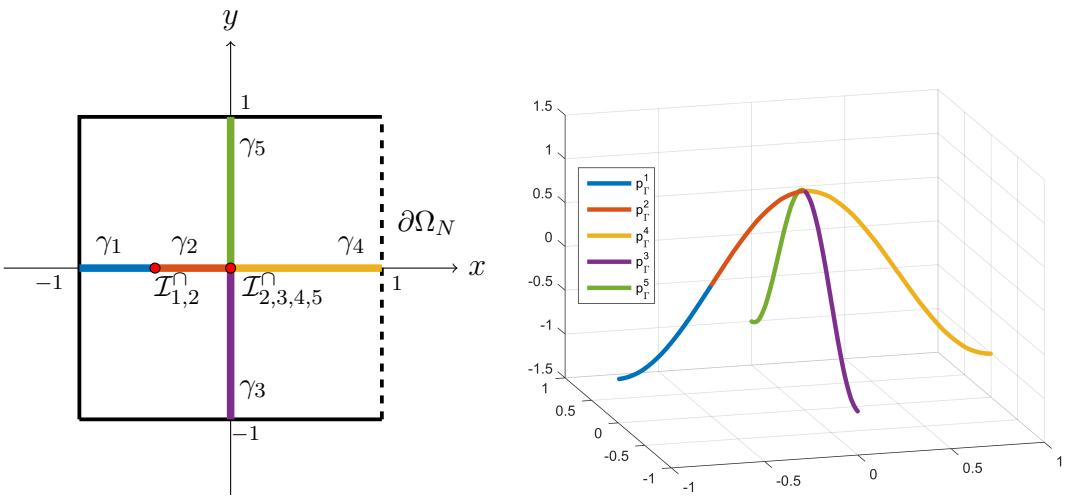

(a) Computational domain (b) Solution in the network

Figure 4.8: Example 3: Computational domain (left) and computed fracture pressures plotted as $3d$-lines (right).

We choose again a solution in the bulk continuous across the fractures $p(x,y) = \cos(\pi x)\cos(\pi y)$ and the permeability tensor $\boldsymbol{\nu} = \mathbf{I}$. In this case, the first coupling condition in (4.5) is satisfied because $\nabla p|_\Gamma \cdot \mathbf{n}_\Gamma = 0$, where $\mathbf{n}_1 = \mathbf{n}_2 = \mathbf{n}_4 = (0,1)^T$ and $\mathbf{n}_3 = \mathbf{n}_5 = (1,0)^T$. The validity of the second coupling condition is satisfied if $p_\Gamma^k = p|_{\Gamma_k}$ for all $k = 1,2,3,4,5$, that is $p_\Gamma^1 = p_\Gamma^2 = p_\Gamma^4 = \cos(\pi x)$ and $p_\Gamma^3 = p_\Gamma^5 = \cos(\pi y)$. In the bulk, we impose Neumann boundary conditions on $\partial\Omega_N = \{(x,y) \in \Omega : \ x = 1\}$ and Dirichlet boundary conditions on the rest of the boundary. Accordingly, at the boundary tips of fractures γ_1, γ_3 and γ_5 we impose Dirichlet conditions, and at the boundary tip of γ_4 we impose Neumann conditions. In the numerical experiments we choose $\xi = 0.55$. Finally, the source term in the bulk is chosen accordingly as $f = 2\pi^2 \cos(\pi x)\cos(\pi y)$ and, given the physical coefficients $\boldsymbol{\nu}_{\Gamma_k}^\tau$ and ℓ_k, for $k = 1,2,3,4,5$, the source term for each fracture is $f_\Gamma^k = \pi^2 \cos(\pi x)\boldsymbol{\nu}_{\gamma_k}^\tau$. Note that, at intersection $\mathcal{I}_{1,2}^\cap$ flux conservation does not hold if the values of the coefficients vary from γ_1 to γ_2, while

at intersection $\mathcal{I}^{\cap}_{2,3,4,5}$ flux conservation is satisfied for every choice, due to the fact that $\nabla p^k_\Gamma|_{\mathcal{I}^{\cap}_{2,3,4,5}} = 0$, for $k = 2, 3, 4, 5$.

We perform two simulations:

- in case (a) we take $\ell_k = \boldsymbol{\nu}^\tau_{\gamma_k} = \nu^n_{\gamma_k} = k \cdot 10^k$, for $k = 1, 2, 3, 4, 5$;
- in case (b) we take $\ell_k = \boldsymbol{\nu}^\tau_{\gamma_k} = \nu^n_{\gamma_k} = k \cdot 10^{-k}$, for $k = 1, 2, 3, 4, 5$.

In Figure 4.8(b) we show the numerical solution for the fracture network problem computed with the coefficients of case (a). The values of the fracture pressures are displayed as lines in the $3d$ space, so that pressure continuity at the intersection points is evident. The plots in Figures 4.9(a)-4.9(b) show the computed errors in loglog scale for the bulk and network problems, together with the expected convergence rates. Test case (a) is on the left and test case (b) is on the right. Once again the results are in agreement with the theoretical estimates.

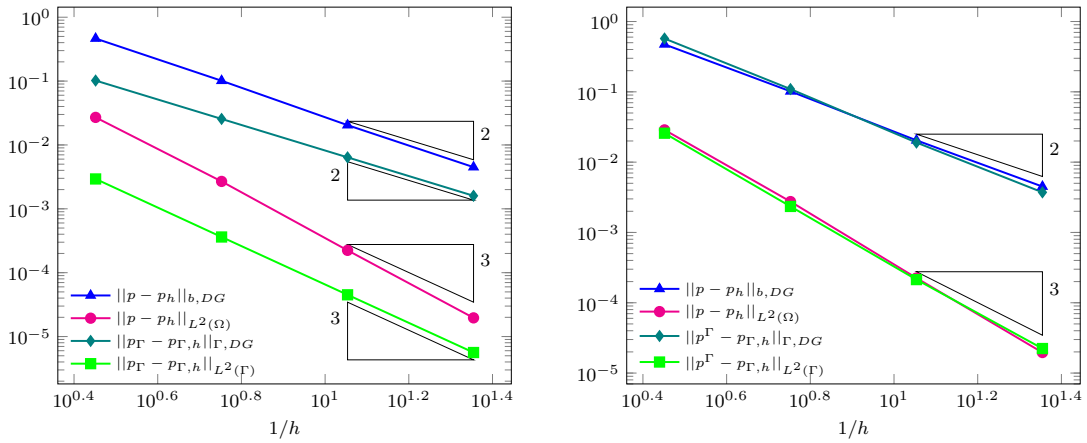

Figure 4.9: Example 3: Computed errors in the bulk and in the fractures as a function of the inverse of the mesh size (loglog scale). Case (a) on the left and case (b) on the right.

4.6.4 Example 4: cross-shaped intersection

We consider the domain $\Omega = (0, 1)^2$ cut by a cross-shaped network made up of the four fractures $\gamma_1 = \{(x, y) \in \Omega : \quad y = 0.5, \ 0 < x < 0.5\}$, $\gamma_2 = \{(x, y) \in \Omega : \ x = 0.5, \ 0 < y < 0.5\}$, $\gamma_3 = \{(x, y) \in \Omega : \ y = 0.5, \ 0.5 < x < 1\}$ and

$\gamma_4 = \{(x, y) \in \Omega : \ x = 0.5, \ 0.5 < y < 1\}$. The bulk domain Ω is then subdivided into the sets

$$\begin{aligned}
\Omega_A &= \{(x, y) \in \Omega : \ 0 < x < 0.5, \ 0 < y < 0.5\}, \\
\Omega_B &= \{(x, y) \in \Omega : \ 0.5 < x < 1, \ 0 < y < 0.5\}, \\
\Omega_C &= \{(x, y) \in \Omega : \ 0.5 < x < 1, \ 0.5 < y < 1\}, \\
\Omega_D &= \{(x, y) \in \Omega : \ 0 < x < 0.5, \ 0.5 < y < 1\},
\end{aligned}$$

as shown in Figure 4.10.

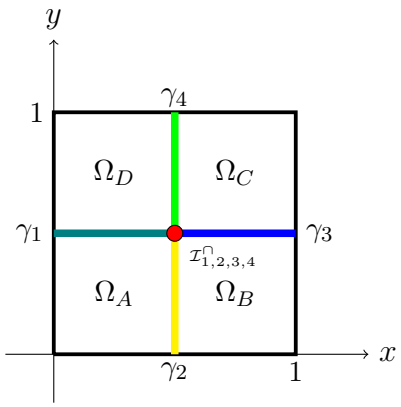

Figure 4.10: Example 4: computational domain.

In order to define the exact solution for the bulk problem, we introduce the functions

$$\begin{aligned}
p_l &= \sin(\frac{\pi}{2}x)\cos(2\pi y), \\
p_r &= \cos(\frac{\pi}{2}x)\cos(2\pi y), \\
p_u &= \cos(\frac{\pi}{2}y)\cos(2\pi x), \\
p_d &= \sin(\frac{\pi}{2}y)\cos(2\pi x),
\end{aligned}$$

where the subscript is related to the position (left, right, up, down). The bulk pressure is

then defined in each subdomain of Ω as

$$p(x,y) = \begin{cases} p_l + p_d & \text{in } \Omega_A, \\ p_r + p_d & \text{in } \Omega_B, \\ p_r + p_u & \text{in } \Omega_C, \\ p_l + p_u & \text{in } \Omega_D. \end{cases}$$

If we choose the permeability tensor $\boldsymbol{\nu} = \mathbf{I}$, the bulk source term will have the following expression $f(x,y) = \frac{17}{4}\pi^2 p(x,y)$. Simple calculations show that $p(x,y)$ satisfies the first coupling condition in (4.5) provided that for $k = 1,2,3,4$, we choose $\beta_{\gamma_k} = \frac{\pi}{4}$, that is $\boldsymbol{\nu}^n_{\gamma_k} = \frac{\pi}{2}\ell_k$. From the second coupling condition we deduce the following expressions for the solutions in the fractures

$$p^1_\Gamma = \xi\sqrt{2}\cos(2\pi x) - \sin(\frac{\pi}{2}x), \qquad p^2_\Gamma = \xi\sqrt{2}\cos(2\pi y) - \sin(\frac{\pi}{2}y),$$
$$p^3_\Gamma = \xi\sqrt{2}\cos(2\pi x) - \cos(\frac{\pi}{2}x), \qquad p^4_\Gamma = \xi\sqrt{2}\cos(2\pi y) - \cos(\frac{\pi}{2}y).$$

Note that, with this choice, pressure continuity at the intersection point (4.7) is ensured by the fact that $\cos(\frac{\pi}{4}) = \sin(\frac{\pi}{4})$. However, flux conservation does not hold, so that we need to modify the right-hand-side of our formulation as in (4.29). Finally the source terms for the fracture problems are chosen accordingly as

$$f^1_\Gamma = \cos(2\pi x)[\frac{\sqrt{2}\pi}{2\ell_1} + 4\pi^2\xi\sqrt{2}\boldsymbol{\nu}^\tau_{\gamma_1}] - \boldsymbol{\nu}^\tau_{\gamma_1}\frac{\pi^2}{4}\sin(\frac{\pi}{2}x),$$
$$f^2_\Gamma = \cos(2\pi y)[\frac{\sqrt{2}\pi}{2\ell_2} + 4\pi^2\xi\sqrt{2}\boldsymbol{\nu}^\tau_{\gamma_2}] - \boldsymbol{\nu}^\tau_{\gamma_2}\frac{\pi^2}{4}\sin(\frac{\pi}{2}y),$$
$$f^3_\Gamma = \cos(2\pi x)[\frac{\sqrt{2}\pi}{2\ell_3} + 4\pi^2\xi\sqrt{2}\boldsymbol{\nu}^\tau_{\gamma_3}] - \boldsymbol{\nu}^\tau_{\gamma_3}\frac{\pi^2}{4}\cos(\frac{\pi}{2}x),$$
$$f^4_\Gamma = \cos(2\pi y)[\frac{\sqrt{2}\pi}{2\ell_4} + 4\pi^2\xi\sqrt{2}\boldsymbol{\nu}^\tau_{\gamma_4}] - \boldsymbol{\nu}^\tau_{\gamma_4}\frac{\pi^2}{4}\cos(\frac{\pi}{2}y).$$

We perform two simulations choosing the values of the physical coefficients as:

- in case (a) we take $\boldsymbol{\nu}^\tau_{\gamma_k} = \nu^n_{\gamma_k} = k \cdot 10^k$ and $\ell_k = \frac{2}{\pi}\nu^n_{\gamma_k}$, for $k = 1,2,3,4$;
- in case (b) we take $\boldsymbol{\nu}^\tau_{\gamma_k} = k \cdot 10^k$, $\ell_k = k \cdot 10^{-k}$ and $\nu^n_{\gamma_k} = \frac{\pi}{2}\ell_k$, for $k = 1,2,3,4$.

In Figure 4.11(a) we show the computed numerical solution for the problem in the bulk,

with the coefficients as in case (a). In Figure 4.11(b) we plot the fracture pressure as lines in the $3d$ space. Pressure continuity at the intersection point is clearly observed.

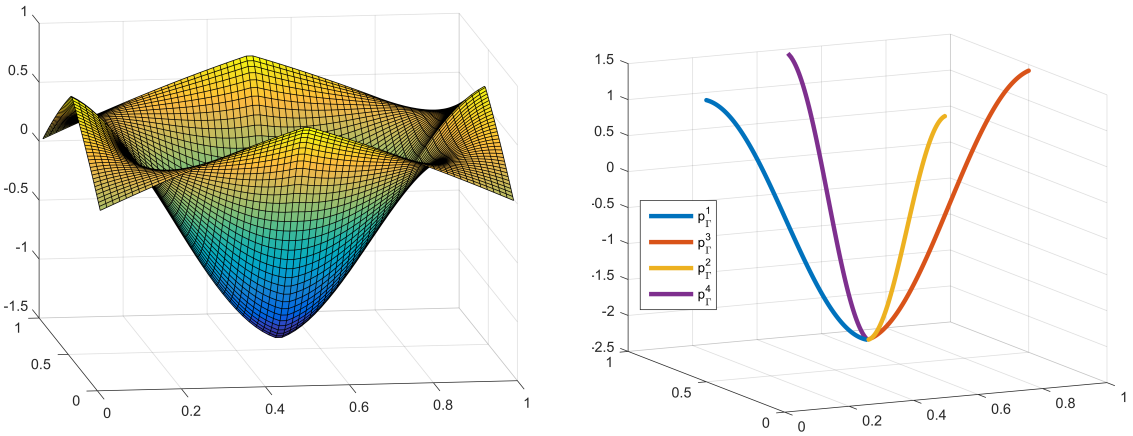

(a) Solution in the bulk

(b) Solution in the fractures

Figure 4.11: Example 4: Computed bulk pressure (left) and computed fracture pressure plotted as $3d$-lines (right).

In Figures 4.5(a)-4.5(b) we report the computed errors $||p - p_h||_{b,DG}$ and $||p_\Gamma - p_{\Gamma,h}||_{\Gamma,DG}$, respectively, in loglog scale for the bulk and fracture problems, as a function of the inverse of the mesh size h. On the left we show the results obtained for test case (a) and on the right for the case (b). Again, a convergence of order 2 is observed for both $||p - p_h||_{b,DG}$ and $||p_\Gamma - p_{\Gamma,h}||_{\Gamma,DG}$, while a convergence of order 3 is observed for the error in the L^2-norm.

4.6.5 Example 6: totally immersed network

The aim of this test case is to investigate the capability of our method to deal with a network of fractures totally immersed in the domain. We reproduce the numerical experiments performed with mimetic finite differences in [15]. We consider the domain $\Omega = (0, 1)^2$ containing 10 intersecting fractures. The geometry of the problem is shown in Figure 4.13(a), where the fractures are highlighted with coloured lines. We remark that for the computations we have employed a mesh made of general polygonal elements, as shown in the zoomed detail reported in Figure 4.13(b).

We impose homogeneous Dirichlet boundary conditions on the whole $\partial\Omega$ and define the

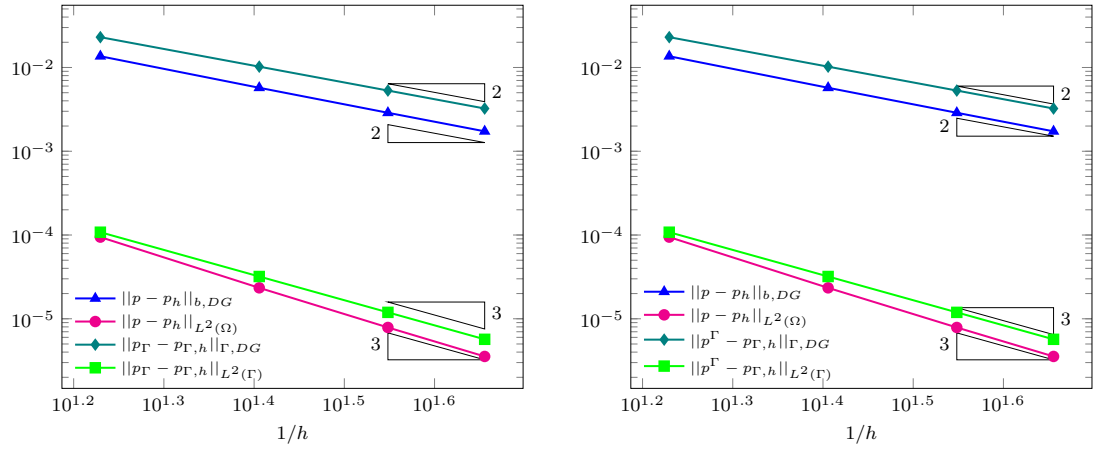

(a) (b)

Figure 4.12: Example 4: Computed errors in the bulk and in the fractures as a function of the inverse of the mesh size (loglog scale). Case (a) on the left and case (b) on the right.

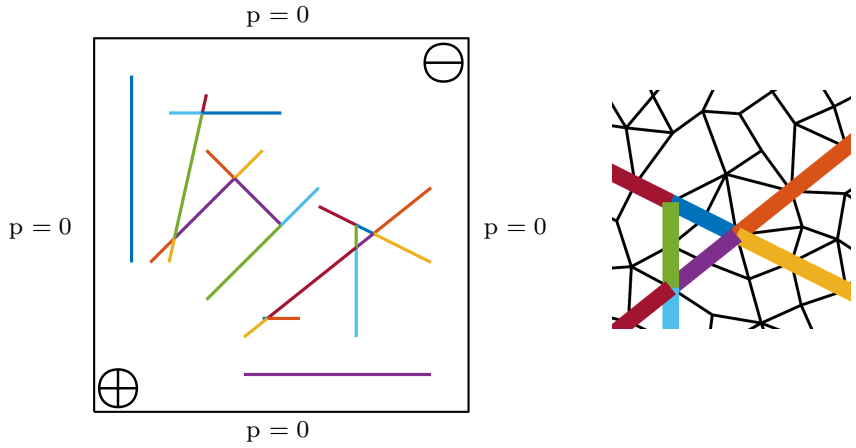

(a) Computational domain (b) Mesh detail

Figure 4.13: Network of intersecting fractures: computational domain (left) and zoomed detail of the polygonal mesh employed for the computations (right).

source term as

$$f(x,y) = \begin{cases} 10 & \text{if } (x-0.1)^2 + (y-0.1)^2 \leq 0.04, \\ -10 & \text{if } (x-0.9)^2 + (y-0.9)^2 \leq 0.04, \end{cases}$$

so that we have a source in the lower left corner of the domain and a sink in its top right corner. The porous medium in the bulk is isotropic and homogeneous, i.e., $\boldsymbol{\nu} = \mathrm{Id}$. The fractures are isotropic, i.e., $\boldsymbol{\nu}_\Gamma^\tau = \nu_\Gamma^n$, with constant thickness $\ell_\Gamma = 0.01$. We consider

three test cases:

1. **No fractures** are present in the porous medium;
2. **Permeable** network: all the fractures have high permeability properties, taking $\boldsymbol{\nu}_\Gamma^\tau = \nu_\Gamma^n = 1000$;
3. **Impermeable** network: all the fractures have blocking properties, taking $\boldsymbol{\nu}_\Gamma^\tau = \nu_\Gamma^n = 0.001$.

In all the test cases, we take $\xi = 0.75$ and $f_\Gamma = \mathbf{0}$. The discrete pressures for the problem in the bulk are reported in Figure 4.14. We observe that, in all the cases, the results are consistent with those obtained in [87] with mimetic finite differences. In the permeable case (see Figure 4.14(b)) the pressure is almost continuous across the fractures, as expected. In agreement with [87], the maximum and minimum values reached by the pressure are slightly lower than those of the non-fractured case, see Figure 4.14(a). In the impermeable case, we observe clear jumps of the bulk pressure across the fractures, see Figure 4.14(c). Once again, our results are in good agreement with those obtained in [87].

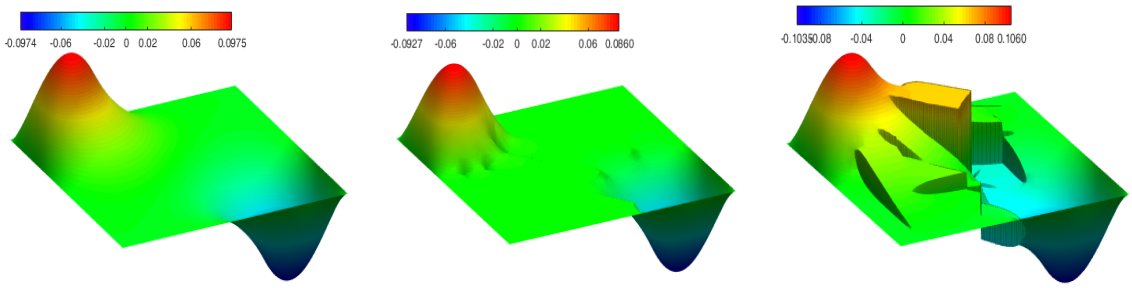

(a) No fractures (b) Permeable (c) Impermeable

Figure 4.14: Network of intersecting fractures: discrete pressure in the bulk for the three test cases, no fractures (left), permeable network $\nu_\Gamma^\tau = \nu_\Gamma^n = 1000$ (middle), impermeable network $\nu_\Gamma^\tau = \nu_\Gamma^n = 0.001$ (right).

5 | Towards Uncertainty Quantification for flow in fractured porous media

This chapter encloses some preliminary results concerning the application of Uncertainty Quantification (UQ) techniques to the problem of approximating the flow in a fractured porous medium. The results are original and contained in [11].

5.1 Introduction to Uncertainty Quantification

Our knowledge of geological and physical aspects of the subsurface is typically incomplete, due to the difficulty in obtaining precise measurements. For this reason, the characterization of fluid dynamics in geological media as well as their geomechanical evolution are classical fields for the application of UQ methodologies [73].

The main goal of Uncertainty Quantification is to devise effective ways to include and treat the uncertainty in a mathematical model. Uncertainty may be contained in the input data in various ways, for example in the model coefficients, forcing terms, boundary conditions and also geometry. In order to obtain a reliable numerical prediction of the phenomenon under investigation, one has to include this lack of knowledge in the model. A common approach is to treat the parameters in the equations as random variables or random fields, so that the model predictions are considered as the outputs of a random input-output map. Such kind of map should be then analyzed with statistical techniques [29]. More precisely, let us consider the general PDE problem: find u such that

$$\mathcal{L}(y(\theta))(u(\theta)) = F(y(\theta)) \in D \subset \mathbb{R}^d \tag{5.1}$$

where $\mathcal{L}$ is a suitable differential operator and some appropriate boundary or initial conditions are imposed. Here, the data of the problem, i.e., the operator $\mathcal{L}$, the forcing term F, the domain D and the initial and boundary conditions may depend on a vector of N random variables $\mathbf{y}(\theta) = (y_1(\theta), \dots, y_N(\theta)) : \Theta \to \mathbb{R}^N$ where $(\Theta, \mathcal{A}, \mathbb{P})$ is a complete probability space (with Θ set of outcomes, $\mathcal{A}$ sigma-algebra of subsets of Θ and $\mathbb{P} : \mathcal{A} \to [0, 1]$ probability measure) and θ denotes an elementary random event. Clearly, in this setting, the solution of the PDE (5.1) is itself a random function, $u = u(\mathbf{y}(\theta), x)$. The main question that UQ wants to address is how to effectively approximate the random function $u(\theta, x)$ or some (random) output Quantities of Interest (QoI) $Q(u)$.

Among the various techniques proposed in the literature for the approximation of the random input-output map, we will take as a reference the stochastic collocation method analysed in the seminal work by Babuška, Nobile and Tempone [29]. Here, a surrogate model of the input-output map is constructed employing standard deterministic techniques in the spatial domain and a tensor product polynomial approximation in the random domain, see Section 5.2 below for a brief introduction to the method.

In the context of fractured porous media, typical quantities that may be affected by uncertainty are the actual position and geometry of the fractures, so that a description of these features is usually only available in the form of probabilistic distributions. Geometric uncertainties are usually challenging to deal with. Indeed, even a small variation in the stochastic parameters may induce an abrupt change in the topological structure of the domain, and this is likely to cause a jump in the values of an associated QoI [63]. For example, the value of a stochastic parameter could determine whether the intersection between two fracture is present or not, thus modifying the network connectivity and possibly the overall direction of the flux. If the considered QoI is non-smooth, applying the standard stochastic collocation approach for its approximation may not be effective. Indeed, the accuracy of polynomial approximations obtained from this kind of methods typically deteriorates in the presence of discontinuous mapping between input parameters and output variables [63, 73].

An innovative methodology to deal with discontinuous dependence between input stochastic parameters and output mapping, is the one proposed in [73] for dealing with sedimentary basins evolution under mechanical and geochemical compaction processes. Here, the authors consider basins composed of multiple layers, each featuring different

physical properties. Since the position of each layer is affected by uncertainty, the state variables describing the material undergo discontinuities in their dependence on the uncertain parameters (different kind of geomaterials may be found at a given depth and time for different realizations of the random parameters). Their innovative methodology relies on a change of coordinate system to align discontinuities within the random parameter space. Starting from the observation that the position of the interface between two materials typically depends smoothly on the stochastic parameters, they create a surrogate model with a two-steps approach: first, a standard sparse-grid approximation for the position of each interface is computed; next this information is used to define a mapping to a reference configuration where discontinuities with respect to depth are aligned; finally, a sparse-grid approximation of the state variables is performed in the new coordinate system, where the method is effective in each homogeneous lithology.

In this chapter, we take inspiration from [73] to address the problem of approximating the flow in a porous medium cut by fractures with uncertain position. We start from the observation that, similarly to [73], the state variables (pressure or Darcy's velocity) may undergo discontinuities in their dependence on the stochastic parameters describing the fracture position. Indeed, fixing, for example, the attention on a given point x^* of the bulk domain, its relative position to the fracture may change and this can cause a jump in the value of the pressure at that point, due to the discontinuous nature of the solution at the bulk-fracture interface. For example, let us consider the simple configuration reported in Figure 5.1. Here, the position of the vertical fracture is determined by the value of the stochastic parameter y. If we now focus on the bulk point x^*, we notice that, according to the different realizations of y, the fracture Γ may be placed either on its left or right. This intuitively implies that the random function describing the pressure in the point x^*, namely $p(\bullet, x^*)$, will undergo a discontinuity with respect to y when the fracture will "walk through"the point x^*. Similarly to the approach of [73], our aim is to align discontinuities. This will be achieved by means of a mapping to a reference domain, where all fractures are aligned, see Figure 5.3 below.

In the rest of the chapter, we will briefly introduce the stochastic collocation method of [29] (Section 5.2) and then illustrate in detail the aligning map technique (Section 5.3). In order to better explain the approach, in Section 5.3.1 we will consider the simple configuration of Figure 5.1, with a single vertical fracture. We will present some

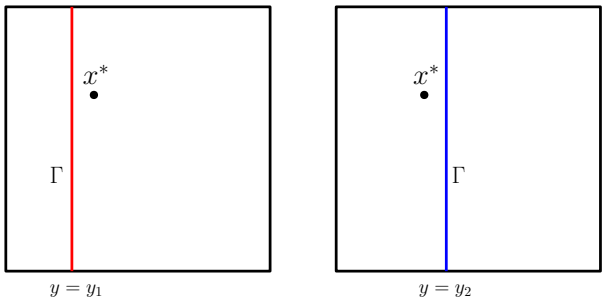

Figure 5.1: Vertical fracture Γ with uncertain position described by the stochastic variable y. According to different realizations of y, Γ may be placed on the left or right of the bulk point x^*.

preliminary convergence numerical results. Extensions of the method and limitations are discussed in Section 5.4.

5.2 The stochastic collocation method

In this section we briefly introduce the stochastic collocation method of [29]. This technique enables to solve numerically the stochastic PDE (5.1), employing standard approximations in space (finite elements, finite volumes, spectral or *hp*-finite elements, etc.) and polynomial approximation in the probability domain. The first step in the approximation process consists in choosing the set of collocation points as the zeros of tensor product orthogonal polynomials with respect to an appropriate probability density (related to the joint probability density of the random variables $\mathbf{y}$). Next, the probabilistic variables $(y_1, \ldots, y_N)$ are evaluated at each collocation point and the solution of the corresponding differential problem (which is now deterministic in the domain D) is computed using the spatial discretization scheme. The final approximation is then recovered by interpolating the semi-discrete approximations in the polynomial space.
In order to illustrate the technique more in detail, let us focus on the following version of problem (5.1): find u such that

$$\begin{cases} \nabla \cdot (a(\mathbf{y}, x)\nabla u(\mathbf{y}, x)) = f(\mathbf{y}, x), & x \in D \\ u(\mathbf{y}, x) = 0, & x \in \partial D, \end{cases} \qquad \forall \mathbf{y} \in \Lambda = \prod_{n=1}^{N} \Lambda_n, \tag{5.2}$$

where $\mathbf{y} = (y_1, \ldots, y_N)$ is a random vector with independent real-valued components and density $\rho(\mathbf{y}) = \prod_{n=1}^{N} \rho_n(y_n)$, the tensor a is such that $0 < a_{\min} \leq a(\mathbf{y}, x) \leq a_{\max}$ for a.e. $x \in D$ and ρ-a.e. $\mathbf{y} \in \Lambda$, and $f(\mathbf{y}, \bullet)$ is square integrable with respect to $\mathbb{P}$ i.e.,

$\int_D E_{\mathbb{P}}[f^2]\, dx < \infty$.

The aim of the collocation method is to look for a numerical approximation of the solution of (5.2) in a finite dimensional space tensor product space $V_{p,h} = \mathcal{P}_p(\Lambda) \otimes H_h(D)$, where $H_h(D) \subset H_0^1(D)$ is, for example, a standard finite element space and $\mathcal{P}_p(\Lambda) \subset L^2_\rho(\Lambda)$ is the span of tensor product polynomials with degree at most $p = (p_1, \ldots, p_N)$. To this end, we first introduce the semi-discrete approximation $u_h : \Lambda \to H_h(D)$, which is obtained, in a finite element fashion, by projecting (5.2) onto the subspace $H_h(D)$, for each $\mathbf{y} \in \Lambda$, i.e.,

$$\int_D a(\mathbf{y}) \nabla u_h(\mathbf{y}, x) \cdot \nabla \varphi_h(x) dx = \int_D f(\mathbf{y}, x) \varphi_h(x) dx \qquad \forall \varphi_h \in H_h(D), \text{ for a.e. } \mathbf{y} \in \Lambda. \tag{5.3}$$

Next, we collocate (5.3) on the zeros of orthogonal polynomials with respect to the densities of the random variables $(y_1, \ldots, y_N)$. More precisely, for each dimension $n = 1, \ldots, N$, we consider the points $\lambda_{n,k_n} \in \Lambda_n$, with $1 \le k_n \le p_n + 1$, which are the $p_n + 1$ roots of the orthogonal polynomial q_{p_n+1} with respect to the density ρ_n, i.e., $\int_{\Lambda_n} q_{p_n+1} v\, \rho_n dy_n = 0$ for all $v \in \mathcal{P}_{p_n}(\Lambda_n)$. We can now consider the tensorized grid of all these roots $\{\boldsymbol{\lambda}_k = (\lambda_{m,k_m})_{m=1}^N, 1 \le k_m \le p_m + 1\}$, where the index k is associated to the vector $(k_1, \ldots, k_N)$ through an appropriate bijection [29]. We denote by M_Λ the cardinality of the tensor grid. After evaluating the semi-discrete approximation u_h at each collocation point $\boldsymbol{\lambda}_k$, with $1 \le k \le M_\Lambda$, we build the fully-discrete solution $u_{p,h} \in \mathcal{P}_p(\Lambda) \otimes H_h(D)$ by interpolating in $\boldsymbol{\lambda}$ the collocated solutions. To this end, we introduce for each $n = 1, 2, \ldots, N$, the Lagrange basis $\{l_{n,j}\}_{j=1}^{p_n+1}$ of the space $\mathcal{P}_{p_n}(\Lambda_n)$, defined such that

$$l_{n,j}(\lambda_{n,m}) = \delta_{jm}, \quad j, m = 1, \ldots, p_n + 1,$$

with δ_{jm} denoting the Kronecker symbol. On the space $\mathcal{P}_p(\Lambda)$ we set, accordingly to the previous notation,

$$l_k(\boldsymbol{\lambda}) = \prod_{n=1}^N l_{n,k_n}(\lambda_n).$$

Therefore, the final approximation of the random solution $u(\mathbf{y}, x)$ is defined as

$$u_{p,h}(\mathbf{y}, x) = \sum_{k=1}^{M_\Lambda} u_h(\boldsymbol{\lambda}_k, x)\, l_k(\mathbf{y}),$$

where $u_h(\boldsymbol{\lambda}_k, x)$ is the semi-discrete solution of problem (5.3) for $\mathbf{y} = \boldsymbol{\lambda}_k$. Note that the stochastic collocation method is equivalent to solve M_Λ deterministic problems.

The convergence of the method has been also addressed in [29]. In particular, an a priori estimate for the total error $u - u_{p,h}$ in the $L^2_\rho(\Gamma) \otimes H^1_0(D)$ norm is presented (see Theorem 4.1), showing that:

- the convergence with respect to p is (sub)exponential (under some regularity assumptions);
- the convergence with respect to h depends on the finite element approximation properties and on the regularity in space of the exact solution u.

Finally, we mention that tensor product spaces suffer from the so-called "curse of dimensionality". Indeed, the dimension of the approximating space M_Λ grows exponentially fast in the number N of random variables, thus leading to a huge computational cost. For this reason, if the number of random variables is even moderately large, one typical approach is to resort to a sparse grid approximation, see [120, 106, 31].

Next, we focus on the applying a suitably modified version of the stochastic collocation technique just introduced to the flow in fractured porous media.

5.3 Uncertain fracture position

We consider a fractured porous medium where the position of the fractures depends on the realization of a random vector $\mathbf{y} \in \Lambda$. We denote by p the variable describing the pressure in the bulk domain Ω according to the coupled model introduced in the previous chapters (see for example Section 2.1). The map p will be itself a random function, that is $p = p(\mathbf{y}, x)$, with $\mathbf{y} \in \Lambda$ and $x \in \Omega$. As previously discussed, the fact that p is discontinuous with respect to the spatial variable x in correspondence of fractures, determines also a discontinuous dependence on the stochastic variables. For this reason, its approximation with the standard stochastic collocation approach introduced in Section 5.2 may not be effective. Similarly to the approach of [73], our aim is to align discontinuities. This will be achieved by means of some mappings to a reference domain, where all fractures are aligned. Let us focus for simplicity on the case where the

porous medium is cut by a single non-immersed fracture. The position of the fracture is determined by the realization of the stochastic vector $\mathbf{y} = \boldsymbol{\lambda} \in \Lambda$, so that we will denote it by $\Gamma_{\boldsymbol{\lambda}}$. In particular, this implies that the value $\boldsymbol{\lambda}$ will determine the subdivision of the domain Ω into the two disjoint subsets $\Omega_1^{\boldsymbol{\lambda}}$ and $\Omega_2^{\boldsymbol{\lambda}}$, i.e., $\Omega = \Omega_1^{\boldsymbol{\lambda}} \cup \Omega_2^{\boldsymbol{\lambda}}$. Next, we introduce the reference domain $\Omega_{ref} \subset \mathbb{R}^d$, $d = 2, 3$, cut by the $(d-1)$-dimensional fracture Γ_{ref}. We assume that $\Omega = \Omega_{ref}$ a.e. with respect to the Lebesgue measure. The fracture Γ_{ref} partitions the domain Ω_{ref} into the disjoint subsets Ω_1^{ref} and Ω_2^{ref}. We can now introduce the family of mappings $\{\Phi_{\boldsymbol{\lambda}}(x)\}_{\boldsymbol{\lambda}\in\Lambda}$ with $\Phi_{\boldsymbol{\lambda}} : \Omega_{ref} \to \Omega$ and the corresponding set of inverse mappings $\{\Phi_{\boldsymbol{\lambda}}^{-1}(x)\}_{\boldsymbol{\lambda}\in\Lambda}$, with $\Phi_{\boldsymbol{\lambda}}^{-1} : \Omega \to \Omega_{ref}$. The single random mapping $\Phi_{\boldsymbol{\lambda}}^{-1}$ maps the domain determined by the realization $\boldsymbol{\lambda} \in \Lambda$ of the random vector $\mathbf{y}$ into the reference configuration such that:

- each bulk subdomain $\Omega_i^{\boldsymbol{\lambda}}$ is mapped into the corresponding subdomain Ω_i^{ref} in the reference configuration, i.e., $\Phi_{\boldsymbol{\lambda}}^{-1}(\Omega_i^{\boldsymbol{\lambda}}) = \Omega_i^{ref}$ for $i = 1, 2$;
- boundaries are preserved;
- the fracture $\Gamma_{\boldsymbol{\lambda}}$ is always mapped into the fracture Γ_{ref}.

See Figure 5.2 below for an explicative example.

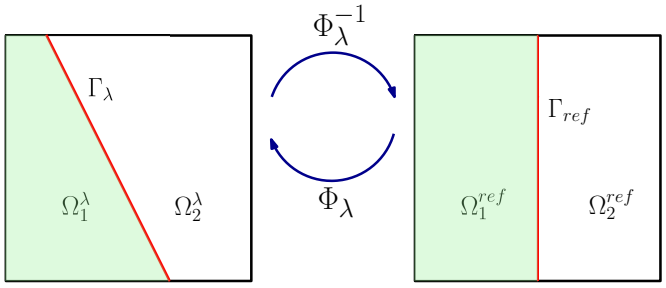

Figure 5.2: Example of mappings $\Phi_{\boldsymbol{\lambda}}$ and $\Phi_{\boldsymbol{\lambda}}^{-1}$ from and to the reference domain Ω_{ref}.

Each mapping $\Phi_{\boldsymbol{\lambda}}$ may be regarded as a change of coordinates, so that instead of considering the random solution mapping $p(\boldsymbol{\lambda}, x)$, we may consider

$$\hat{p}(\boldsymbol{\lambda}, \hat{x}) := p(\boldsymbol{\lambda}, \Phi_{\boldsymbol{\lambda}}(\hat{x})) = p(\boldsymbol{\lambda}, \Phi_{\boldsymbol{\lambda}}(\Phi_{\boldsymbol{\lambda}}^{-1}(x))),$$

with $\hat{x} = \Phi_{\boldsymbol{\lambda}}^{-1}(x)$. Since in the reference domain all fractures are aligned, the map $\hat{p}$ will be continuous with respect to $\boldsymbol{\lambda}$ and we can use standard stochastic collocation techniques for its approximation. It follows that we may construct a semi-discrete approximation of

the exact random pressure at the point $\mathbf{x}^*$ of the bulk domain, for a given realization of the random vector $\mathbf{y} = \boldsymbol{\lambda}^*$ and $\hat{x} = \Phi^{-1}_{\boldsymbol{\lambda}^*}(x)$, as

$$p(\boldsymbol{\lambda}^*, x^*) = \hat{p}(\boldsymbol{\lambda}^*, \hat{x}^*) \approx \sum_{i=1}^{M_\Lambda} \hat{p}(\boldsymbol{\lambda}_i, \hat{x}^*) l_i(\boldsymbol{\lambda}^*) = \sum_{i=1}^{M_\Lambda} p(\boldsymbol{\lambda}_i, \Phi_{\boldsymbol{\lambda}_i}(\Phi^{-1}_{\boldsymbol{\lambda}^*}(x^*))) l_i(\boldsymbol{\lambda}^*),$$

where M_Λ is the number of stochastic interpolation points and $\{l_i\}_{i=1}^{M_\Lambda}$ is the corresponding Lagrange basis. The fully-discretized version of the random map p will then be

$$p(\boldsymbol{\lambda}^*, x^*) \approx p_h^{M_\Lambda}(\boldsymbol{\lambda}^*, x^*) = \sum_{i=1}^{M_\Lambda} p_h(\boldsymbol{\lambda}_i, \Phi_{\boldsymbol{\lambda}_i}(\Phi^{-1}_{\boldsymbol{\lambda}^*}(x^*))) l_i(\boldsymbol{\lambda}^*), \tag{5.4}$$

where $p_h(\boldsymbol{\lambda}_i, \bullet)$ denotes the DG approximation of the bulk pressure collocated in the point $\boldsymbol{\lambda}_i$, i.e., the DG-discrete solution relative to the domain cut by the fracture $\Gamma_{\boldsymbol{\lambda}_i}$. The above may be regarded as an offline-online approach, where we first compute the solutions in all the collocation points (where the position of the fracture is determined by $\boldsymbol{\lambda_i}$) and then use them to reconstruct the solution corresponding to a new configuration (where the position of the fracture is determined by $\boldsymbol{\lambda^*}$). We may then give the following interpretation of the aligning map technique. For reconstructing the value of the pressure in x^* in the new configuration $\Gamma_{\boldsymbol{\lambda}^*}$, we do not employ the value of the pressure at this same point in the configurations $\Gamma_{\boldsymbol{\lambda}_i}$, since it may not be significant. Therefore, for each configuration $\Gamma_{\boldsymbol{\lambda}_i}$, we evaluate the pressure at the image through the aligning map of the point x^*, i.e., $\Phi_{\boldsymbol{\lambda}_i}(\Phi^{-1}_{\boldsymbol{\lambda}^*}(x^*)))$, which has the same relative position with respect to $\Gamma_{\boldsymbol{\lambda_i}}$ as x^* with respect to $\Gamma_{\boldsymbol{\lambda}^*}$. We refer to Figure 5.3 for a visual representation of this composition of mappings.

Remark 10. Due to their discontinuity, DG discrete functions are not uniquely defined at element interfaces. Therefore, in order to be able to evaluate, in formula (5.4), the bulk discrete solution p_h at any point, we will in fact consider its continuous reconstruction $\tilde{p}_h$. The latter may be obtained by post-processing the DG discrete solution with an approach similar to that employed by Karakashian and Pascal in [99] to prove some a-posteriori error estimates for the DG approximation of second-order elliptic PDEs. The setting of [99] considers DG spaces defined on standard conforming simplicial meshes with uniform polynomial order. More precisely, given a simplicial mesh $\mathcal{T}_h$, the polynomial degree k and the corresponding DG discrete space $Q^{DG}_{h,k}$, they associate to the generic function $q_h \in Q^{DG}_{h,k}$ its piecewise polynomial continuous reconstruction $\tilde{q}_h$ belonging to

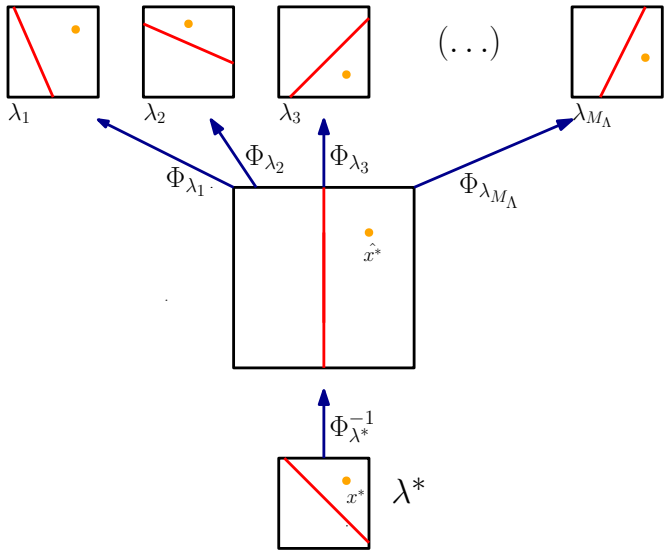

Figure 5.3: Composition of mappings for the approximation of $p(\boldsymbol{\lambda}^*, x^*)$.

the standard finite element space of degree k related to the same mesh $\mathcal{T}_h$. The function $\tilde{q}_h$ is defined with a quite natural argument: at every node of the simplicial mesh $\mathcal{T}_h$ corresponding to a Lagrangian type degree of freedom for polynomial degree k, its value is set to the average of the values of q_h at that node. Moreover, in [99], the reconstruction $\tilde{q}_h$ is proved to have suitable approximation properties with respect to q_h. In order to extend the results to the polytopic setting, we can resort to the following strategy. First, each polytope of the mesh is subdivided into triangles/tetrahedra (for example joining the barycentre of the element with each vertex), so that a simplicial mesh is defined. Then, the continuous reconstruction of the poly-DG function is built with the method of [99], i.e., considering the lagrangian nodes associated to the simplicial mesh and the corresponding average values of the poly-DG function. See Figure 5.4 for an example of simplicial mesh obtained from the polytopic one, joining vertexes with the barycenters, and the corresponding lagrangian nodes for the linear case. In order for the approximation properties proved in [99] to be still valid in the polytopic case, we need to make some shape-regularity assumptions on the simplicial mesh. The extension of these results to more general polytopic meshes has not been explored yet (to the best of our knowledge).

With the aim of better illustrating our approach and testing its effectiveness, we will now present a simple test case.

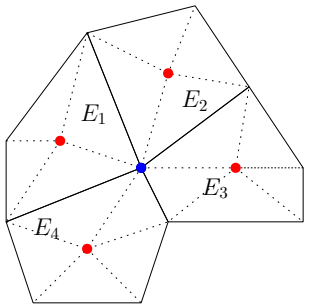

Figure 5.4: Simplicial mesh obtained from a polygonal mesh by joining vertexes with barycenters and lagrangian nodes for the linear case.

5.3.1 Example: vertical fracture

We consider the case where the porous medium is cut by a single, non-immersed vertical fracture, whose position is random and depends on the parameter λ. In particular, we adjust the test case already presented in Section 2.5.4, adding the dependence on the stochastic variable. We take the bulk $\Omega = (0,1)^2$ and the vertical fracture $\Gamma = \Gamma_\lambda = \{(x,y) \in \Omega : \quad x = \lambda\}$, with $\lambda \in \Lambda$. For example, we can assume the distribution of λ to be uniform in $\Lambda = [a,b]$, with $a = 0.1$ and $b = 0.9$. The exact solutions in the bulk and in the fracture are then chosen as follows:

$$p = \begin{cases} \sin(4x)\cos(\pi y) & \text{if } x < \lambda, \\ \cos(4x)\cos(\pi y) & \text{if } x > \lambda, \end{cases} \qquad p_\Gamma = \xi[\cos(4\lambda) + \sin(4\lambda)]\cos(\pi y), \tag{5.5}$$

and the source terms are chosen accordingly as :

$$f = \begin{cases} \sin(4x)\cos(\pi y)(16+\pi^2) & \text{if } x < \lambda, \\ \cos(4x)\cos(\pi y)(16+\pi^2) & \text{if } x > \lambda, \end{cases}$$
$$f_\Gamma = \cos(\pi y)[\cos(4\lambda) + \sin(4\lambda)](\frac{4}{\ell_\Gamma} + \xi\pi^2 \boldsymbol{\nu}_\Gamma^\tau).$$

Notice that the solution in the bulk depends on the stochastic parameter λ only through the definition of the two subdomains Ω_1^λ and Ω_2^λ, while the analytic expression of p_Γ depends explicitly on λ. For simplicity, we will take the permeability tensor $\boldsymbol{\nu} = \mathbf{I}$. Moreover, we will set $\ell_\Gamma = 0.25$ and $\boldsymbol{\nu}_\Gamma^\tau = \nu_\Gamma^n = 1$. Finally, we impose Dirichlet boundary conditions on the whole $\partial\Omega$ and also on $\partial\Gamma$.

We choose as reference configuration the one corresponding to the fracture

$\Gamma_{ref} = \{(x, y) \in \Omega : \quad x = 0.5\}$. The aligning maps $\Phi_\lambda : \Omega_{ref} \to \Omega$ and $\Phi_\lambda^{-1} : \Omega \to \Omega_{ref}$ may then be defined explicitly as:

$$\Phi_\lambda(x) = \begin{cases} 2\lambda x & \text{if } 0 < x < \lambda, \\ 2(1-\lambda)x + 2\lambda - 1 & \text{if } \lambda < x < 1, \end{cases}$$

$$\Phi_\lambda^{-1}(x) = \begin{cases} \frac{1}{2\lambda} x & \text{if } 0 < x < \lambda, \\ -\frac{1}{2(1-\lambda)} x + \frac{2\lambda - 1}{2(\lambda - 1)} & \text{if } \lambda < x < 1. \end{cases}$$

Let us focus on the random map representing the bulk pressure $p : [a, b] \times \Omega \to \mathbb{R}$ defined in (5.5). As previously discussed, p is discontinuous with respect to the random variable λ. Indeed, if we consider the generic bulk point $x^* = (x^*(1), x^*(2))$, the random function $p(\bullet, x^*)$ will undergo a discontinuity with respect to λ when the fracture will "walk through"the point x^*, i.e., when $\lambda = x^*(1)$. This behaviour is displayed in Figure 5.6, where for several points x^*, we plot the corresponding function $p(\bullet, x^*)$ (dotted line) and its DG approximation $p_h(\bullet, x^*)$ (solid line). In particular, we consider the four bulk points

$$x_1^* = (0.2, 0.9),$$
$$x_2^* = (0.1, 0.2),$$
$$x_3^* = (0.7, 0.3),$$
$$x_4^* = (0.8, 0.8),$$

plotted in Figure 5.5 with corresponding colours. In Figure 5.6, each function $p(\bullet, x_i^*)$, $i = 1, 2, 3, 4$, is evaluated for 13 values of the parameter λ, corresponding to the Gauss-Legendre points in the interval $[a, b]$ (we refer to [31] for more details). We can clearly see that, for $i = 1, 2, 4$, the function $p(\bullet, x_i^*)$ undergoes a discontinuity for $\lambda = x_i^*(1)$ (this is not the case for x_3^* because $x_3^*(1) = 0.1 = a$). Notice that the functions $p(\bullet, x_i^*)$ are piecewise constant due to the fact that the bulk solution (5.5) depends on λ only through the definition of the two subdomains Ω_1^λ and Ω_2^λ.

Next, we show that, employing the aligning map technique, we do recover continuity with respect to the random variable. Indeed, let us now consider the function $\hat{p} : [a, b] \times \Omega_{ref} \to \mathbb{R}$. In Figure 5.7, for several points $\hat{x}^* \in \Omega_{ref}$, we plot the corresponding function $\hat{p}(\bullet, \hat{x}^*) = p(\bullet, \Phi_\bullet(\hat{x}^*))$ (dotted line) and its DG approximation $p_h(\bullet, \Phi_\bullet(\hat{x}^*))$

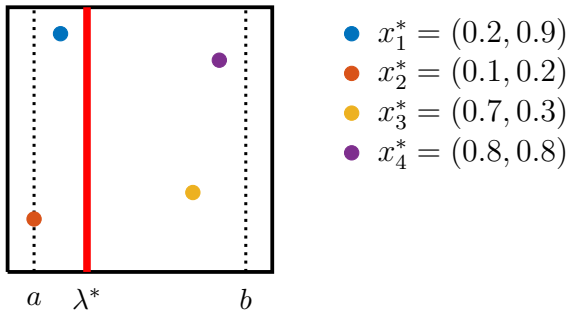

Figure 5.5: Domain corresponding to the realization of the stochastic parameter λ^* and the 4 points x_1^*, x_2^*, x_3^*, x_4^* considered in the experiments.

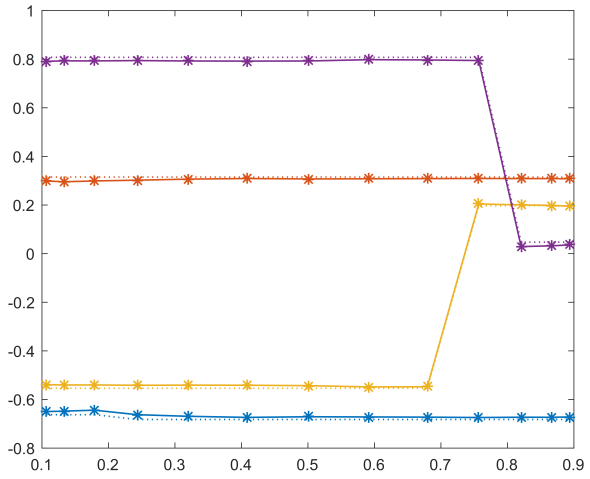

Figure 5.6: Function $p(\bullet, x_i^*)$ (dotted line) and its DG approximation $p_h(\bullet, x_i^*)$ (solid line), for $i = 1, 2, 3, 4$. Each colour is related to a different point x_i^* as shown in Figure 5.5.

(solid line). In particular, we consider the four points $\hat{x}_i^*$, $i = 1, 2, 3, 4$, obtained from the previously considered points x_i^* (see Figure 5.5) via the inverse aligning map $\Phi_{\lambda^*}^{-1}$, for $\lambda^* \in [a, b]$ (we take for example $\lambda^* = 0.3$). In Figure 5.7 we can clearly see that the functions $\hat{p}(\bullet, \hat{x}_i^*)$ are continuous (here we report their evaluation at 13 Gauss-Legendre points in $[a, b]$).

We now want to test the convergence properties of our approximation scheme (5.4) for $p : [a, b] \times \Omega \to \mathbb{R}$, with respect to the random variable. First, we consider point-wise convergence, i.e., we fix the point $(\lambda^*, x^*) \in [a, b] \times \Omega$ and measure the error as a function of the number of stochastic collocation points employed in the approximation. In the following, we take $x^* = (0.2, 0.9)$ (the point in blue in Figure 5.5) and $\lambda^* = 0.3$. We want to test the behaviour of the semi-discrete (only in λ) approximation p^{M_Λ} and of the fully-discrete (in both λ and x) approximation $p_h^{M_\Lambda}$. We recall that they are defined with

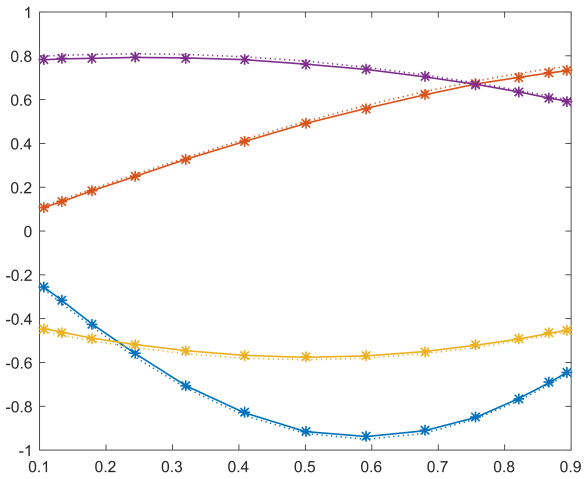

Figure 5.7: Function $\hat{p}(\bullet, \hat{x}_i^*)$ (dotted line) and its DG approximation $\hat{p}_h(\bullet, \hat{x}_i^*)$ (solid line), for $i = 1, 2, 3, 4$. Each colour is related to a different point x_i^* as shown in Figure 5.5.

the aligning map technique as

$$p^{M_\Lambda}(\lambda^*, x^*) = \sum_{i=1}^{M_\Lambda} p(\lambda_i, \Phi_{\lambda_i}(\Phi_{\lambda^*}^{-1}(x^*)))l_i(\lambda^*),$$

$$p_h^{M_\Lambda}(\lambda^*, x^*) = \sum_{i=1}^{M_\Lambda} p_h(\lambda_i, \Phi_{\lambda_i}(\Phi_{\lambda^*}^{-1}(x^*)))l_i(\lambda^*).$$

Since we are assuming an uniform distribution for the stochastic variable, we will take $\{\lambda_i\}_{i=1}^{M_\Lambda}$ equal to the Gauss-Legendre points in $[a, b]$, see [31]. Notice that, for computing the fully-discrete approximation $p_h^{M_\Lambda}$, we need to solve M_Λ DG-discrete problems, each corresponding to the domain cut by fracture Γ_{λ_i}. This implies that, for every fracture Γ_{λ_i}, with $i = 1, \ldots, M_\Lambda$, we will generate one (polygonal) mesh. We assume that all these meshes have comparable mesh-size h. We also remark that instead of the DG solution p_h, we will evaluate its continuous reconstruction $\tilde{p}_h$, see Remark 10 above.

In Figure 5.8(a) we plot, in semilogy scale and as a function of the number of the collocation points M_Λ, the following 3 quantities (with corresponding legend entry):

$$|p^{M_\Lambda}(\lambda^*, x^*) - p(\lambda^*, x^*)| \qquad \text{(ex-ex)} \qquad (5.6)$$

$$|p_h^{M_\Lambda}(\lambda^*, x^*) - p_h(\lambda^*, x^*)| \qquad \text{(DG-DG)} \qquad (5.7)$$

$$|p_h^{M_\Lambda}(\lambda^*, x^*) - p(\lambda^*, x^*)| \qquad \text{(DG-ex)} \qquad (5.8)$$

where:

(ex-ex) is the error between the exact solution $p(\lambda^*, x^*)$ and its semi-discrete approximation with respect to the stochastic variable;

(DG-DG) is the error between the DG-discrete solution computed in the domain cut by the fracture Γ_{λ^*}, namely $p_h(\lambda^*, x^*)$, and the fully-discrete approximation with respect to the stochastic variable and the spatial variable of the exact solution;

(DG-ex) is the error between the exact solution $p(\lambda^*, x^*)$ and its fully-discrete approximation with respect to the stochastic variable and the spatial variable.

The DG solution for $\lambda = \lambda^*$ and those for the collocation points λ_i were obtained with Cartesian meshes of approximately the same size (≈ 1150 elements). In Figure 5.8(a) we observe *exponential* convergence as expected from the theory of stochastic collocation methods, see Section 5.2. In particular, for the (ex-ex) case the error keeps decreasing as the number of collocation point increases, while for the (DG-DG) and (DG-ex) cases we observe a saturation of the error around the value of the error in the spatial DG-approximation.

In Figure 5.8(b), we consider the behaviour of the L^2-norm error. In particular, we compute

$$||p_h(\lambda^*, \bullet) - p_h^{M_\Lambda}(\lambda^*, \bullet)||_{L^2(\Omega)}, \tag{5.9}$$

i.e., the L^2-norm (in the spatial variable x) of the difference between the spatial DG-approximation p_h computed in the configuration Γ_{λ^*}, with $\lambda^* = 0.3$, and the fully-discrete approximation of the random solution map $p_h^{M_\Lambda}$ evaluated at $\lambda = \lambda^*$. We plot the error (5.9) (in semilogy scale) as a function of the number of collocation points M_Λ employed for computing $p_h^{M_\Lambda}(\lambda^*, \bullet)$. We consider 3 cases, where we employ different mesh-sizes h_i, $i = 1, 2, 3$, for the spatial DG-discretization. In particular, the meshes have the following sizes: $h_1 \approx 70$ elements, $h_2 \approx 195$ elements and $h_3 \approx 575$ elements. Also in this case, we observe exponential convergence.

Finally, in Figures 5.9(a) and 5.9(a) we reproduce the same results as in Figures 5.8(a) and 5.8(b), respectively, without employing the aligning map for the approximation. No kind of convergence is observed in this case, showing the effectiveness of our approach.

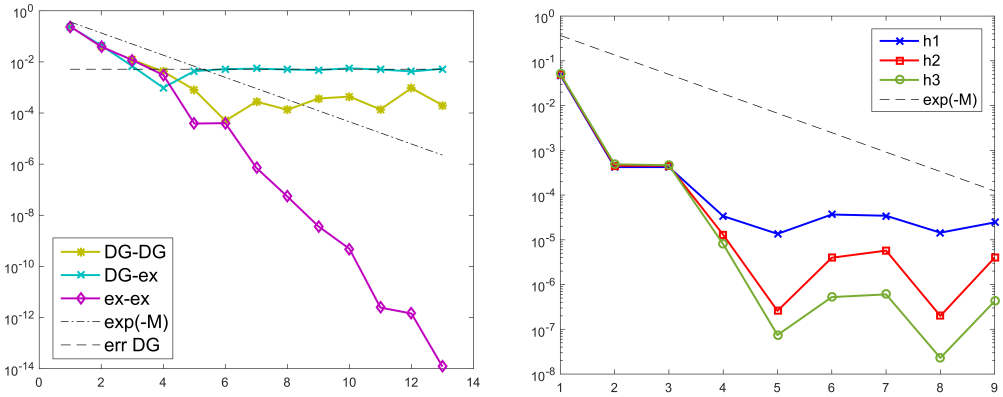

(a) Point-wise convergence (b) Convergence in the L^2-norm

Figure 5.8: (Left) Point-wise convergence in (λ^*, x^*), with $\lambda^* = 0.3$ and $x^* = (0.2, 0.9)$. The 3 errors defined in (5.6)-(5.7)-(5.8) are displayed as a function of the number of stochastic collocation points in semilogy scale.
(Right) L^2-norm (in the spatial variable) of the error between the spatial DG-solution for $\lambda = 0.3$ and the fully-discrete approximation of the random solution map evaluated at $\lambda = 0.3$. The error is presented as a function of the number of stochastic collocation points, in semilogy scale. Three curves are displayed, each corresponding to a different mesh-size employed for the spatial discretization.

5.4 Conclusions

We proposed a novel technique to deal with the flow in a porous medium cut by fractures with uncertain position. Due to the discontinuous dependence of the solution map on the stochastic parameters, standard UQ techniques may feature loss of accuracy. For this reason, taking inspiration from the approach of [73], we introduced a mapping to a reference domain, where all fractures are aligned, so that continuity with respect to the random variables may be recovered. Applied to a simple test case, where the position of the fracture is determined by a single stochastic parameter, our technique has proved to be effective to recover the convergence properties of the stochastic collocation method of [29].

The extension of our approach to more complicate configurations relies on the possibility of defining an appropriate aligning map. This is not of easy implementation even for slightly more complicated fracture geometries, for example in the case of an immersed fracture. In fact, in Figure 5.10 we display a possible procedure for defining the aligning map in the latter case. Here, the position of the fracture is determined by the realization of the stochastic vector $\boldsymbol{\lambda} = (\lambda_d, \lambda_u, \lambda_\ell)$, where λ_d is related to the position of bottom tip of the fracture, λ_u to position of the top tip and λ_ℓ to the length of the fracture. The

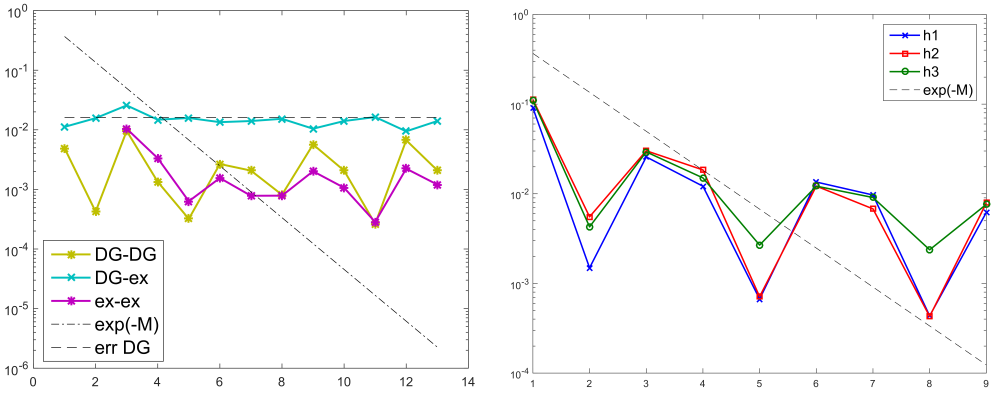

(a) Point-wise convergence (b) Convergence in the L^2-norm

Figure 5.9: Point-wise convergence and convergence in the L^2-norm without employing the aligning map in the approximation.

aligning map $\Phi_{\boldsymbol{\lambda}}$ may then be defined piecewise, by mapping each coloured subdomain of Ω into the corresponding subdomain (with the same colouring) in the reference domain Ω_{ref}. When considering more complicated configurations, especially in 3D, it is possible that the map Φ_λ may not be determined in closed form, so that we need to resort to some numerical techniques for its approximation. This aspect of our method is still under investigation and will be the object of future research, as well as the theoretical analysis of its convergence properties.

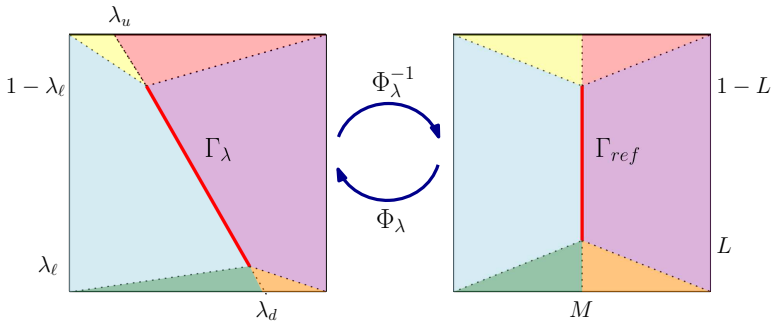

Figure 5.10: Possible aligning map to reference domain in the case of immersed fracture. The position of the fracture depends on the stochastic vector $\boldsymbol{\lambda} = (\lambda_d, \lambda_u, \lambda_\ell)$.

Conclusions and future perspectives

In this thesis we have presented a Discontinuous Galerkin approximation on polytopic grids of Darcy's flow through a fractured porous medium, where fractures are treated as a $(d-1)$-dimensional interfaces between two d-dimensional subdomains, $d = 2, 3$ [101]. We have considered the modelling, theoretical and computational aspects of the problem, with focus on the numerical discretization and its analysis. PolyDG methods have proved to be an effective tool for addressing the problem, their main advantages being: the natural way they can describe the discontinuous nature of the solution at the matrix-fracture interface; their efficiency in handling the coupling of the bulk-fracture problems, by virtue of employing jump and average operators in the formulation of the coupling conditions; their intrinsic geometric flexibility, which is very well suited to tame the geometrical complexity featured by most of applications in the computational geoscience field. The main original results contained in the chapters of the thesis can be summarized as follows.

- In Chapter 2 we have considered the simplest configuration, where one single non-immersed fracture divides the porous medium in two halves and the *primal* formulation of Darcy's law is employed for modelling the flow both in the bulk and along the fracture. We have focused on the coupling of the two problems and on the polyDG-discretization [61, 59, 6, 58, 19, 60] of the problem in the bulk employing meshes made of arbitrarily shaped elements (with edges/faces that may be in arbitrary number and whose measure may be arbitrarily small compared to the diameter of the element they belong to). We have analysed the method, proving its well-posedness and deriving a priori *hp*-error estimates in a suitable (mesh-dependent) energy norm, which we have validated with numerical experiments in a two-dimensional setting. The results of this chapter and have been published in [12].

- In Chapter 3 we have extended the results obtained in Chapter 2, designing and analysing, in the *unified* framework of [27] based on the *flux-formulation*, a polyDG approximation for all the possible combinations of primal-primal, mixed-primal, primal-mixed and mixed-mixed formulations for the bulk and fracture problems, respectively. The novelty of the method relies on the imposition of coupling conditions between bulk and fracture through a suitable definition of the numerical fluxes on the fracture faces. We have proved in an unified setting the well-posedness of all the formulations and we have derived a priori *hp*-version error estimates in a suitable (mesh-dependent) energy norm, whose validity has been assessed performing numerical experiments. The results presented in this chapter are contained in [14].

- In Chapter 4, we have extended the primal-primal formulation to the case of networks of intersecting fractures. The key instrument to obtain a polyDG approximation of the problem in the fracture network was the generalization of the concepts of jump and average at the intersection, so that the contribution from all the fractures is taken into account. We proved the well-posedness of the discrete formulation and performed an error analysis obtaining a priori *hp*-error estimates. All our theoretical results were validated performing numerical tests with known analytical solution and more realistic configurations. The results presented in this chapter are contained in [13].

- In Chapter 5 we proposed a novel technique to deal with the flow in a porous medium cut by fractures with uncertain position. Taking inspiration from the approach of [73], we introduced a mapping to a reference domain, where all fractures are aligned, so that continuity with respect to the random variables may be recovered. Applied to a simple test case, where the position of the fracture is determined by a single stochastic parameter, our technique has proved to be effective to recover the convergence properties of the stochastic collocation method of [29].

Further developments of this setting include the $3D$-implementation of the method and its validation by performing numerical simulations coming from real-world applications. Another improvement related to the implementation would be the parallelization of the algorithm, so that we can take advantage of the intrinsic high-level of parallelism featured by DG methods. From the modelling point of view, our formulation could be extended in order to take into account two-phase flows as in [91, 97] or, more in general,

multi-phase flows. Moreover, we could consider more general conditions for the flow along the intersections, for example including the angle between fractures in the model or allowing for jumps of pressure across the intersection as in [112] or [86]. Finally, the UQ results presented in Chapter 5 are very preliminary and they surely need to be extended in order to more realistic configurations. This will be the object of future research, together with the theoretical analysis of the convergence properties of the proposed method.

Bibliography

[1] C. Alboin, J. Jaffré, J. E. Roberts, and C. Serres. Modeling fractures as interfaces for flow and transport in porous media. In *Fluid flow and transport in porous media: mathematical and numerical treatment (South Hadley, MA, 2001)*, volume 295 of *Contemp. Math.*, pages 13–24. Amer. Math. Soc., Providence, RI, 2002.

[2] C. Alboin, J. Jaffré, J. E. Roberts, X. Wang, and C. Serres. Domain decomposition for some transmission problems in flow in porous media. In *Numerical treatment of multiphase flows in porous media*, volume 552 of *Lecture Notes in Phys.*, pages 22–34. Springer, Berlin, 2000.

[3] P. Angot, F. Boyer, and F. Hubert. Asymptotic and numerical modelling of flows in fractured porous media. *M2AN Math. Model. Numer. Anal.*, 43(2):239–275, 2009.

[4] P. F. Antonietti, F. Bonaldi, and I. Mazzieri. A high-order discontinuous galerkin approach to the elasto-acoustic problem. *arXiv preprint arXiv:1803.01351*, 2018.

[5] P. F. Antonietti, F. Brezzi, and L. D. Marini. Bubble stabilization of discontinuous Galerkin methods. *Comput. Methods Appl. Mech. Engrg.*, 198(21-26):1651–1659, 2009.

[6] P. F. Antonietti, A. Cangiani, J. Collis, Z. Dong, E. H. Georgoulis, S. Giani, and P. Houston. *Review of discontinuous Galerkin Finite Element Methods for partial differential equations on complicated domains*, volume 114 of *Lecture Notes in Computational Science and Engineering*, chapter 8, pages 281 – 310. Springer, 1st edition, 2016.

[7] P. F. Antonietti, L. B. da Veiga, D. Mora, and M. Verani. A stream Virtual Element formulation of the Stokes problem on polygonal meshes. *SIAM J. Numer. Anal.*, 52(1):386–404, 2014.

[8] P. F. Antonietti, L. B. da Veiga, S. Scacchi, and M. Verani. A C1 Virtual Element Method for the Cahn-Hilliard equation with polygonal meshes. *SIAM J. Numer. Anal.*, 54(1):34–56, 2016.

[9] P. F. Antonietti, A. Dedner, P. Madhavan, S. Stangalino, B. Stinner, and M. Verani. High order discontinuous galerkin methods for elliptic problems on surfaces. *SIAM J. Numer. Anal.*, 53(2):1145–1171, 2015.

[10] P. F. Antonietti, C. Facciolà, P. Houston, I. Mazzieri, G. Pennesi, and M. Verani. High–order discontinuous Galerkin methods on polyhedral grids for geophysical applications: seismic wave propagation and fractured reservoir simulations. *Submitted*, 2020.

[11] P. F. Antonietti, C. Facciolà, F. Nobile, and M. Verani. Uncertainty quantification for the approximation of flow in fractured porous media with polytopic Discontinuous Galerkin methods. *In Preparation*, 2019.

[12] P. F. Antonietti, C. Facciolà, A. Russo, and M. Verani. Discontinuous Galerkin approximation of flows in fractured porous media on polytopic grids. *SIAM J. Sci. Comput.*, 41(1):A109–A138, 2019.

[13] P. F. Antonietti, C. Facciolà, and M. Verani. Polytopic Discontinuous Galerkin methods for the numerical modelling of flow in porous media with complex networks of fractures. *In Preparation*, 2019.

[14] P. F. Antonietti, C. Facciolà, and M. Verani. Unified analysis of Discontinuous Galerkin approximations of flows in fractured porous media on polygonal and polyhedral grids. *Mathematics in Engineering*, to appear, 2020.

[15] P. F. Antonietti, L. Formaggia, A. Scotti, M. Verani, and N. Verzotti. Mimetic finite difference approximation of flows in fractured porous media. *ESAIM Math. Model. Numer. Anal.*, 50(3):809–832, 2016.

[16] P. F. Antonietti, S. Giani, and P. Houston. *hp*-version Composite Discontinuous Galerkin methods for elliptic problems on complicated domains. *SIAM J. Sci. Comput.*, 35(3):A1417–A1439, 2013.

[17] P. F. Antonietti, S. Giani, and P. Houston. Domain decomposition preconditioners for discontinuous Galerkin methods for elliptic problems on complicated domains. *J. Sci. Comput.*, 60(1):203–227, 2014.

[18] P. F. Antonietti and P. Houston. A class of domain decomposition preconditioners for *hp*-discontinuous Galerkin finite element methods. *J. Sci. Comput.*, 46(1):124–149, 2011.

[19] P. F. Antonietti, P. Houston, X. Hu, M. Sarti, and M. Verani. Multigrid algorithms for hp-version interior penalty discontinuous Galerkin methods on polygonal and polyhedral meshes. *Calcolo*, 54(4):1169–1198, 2017.

[20] P. F. Antonietti, P. Houston, and G. Pennesi. Fast numerical integration on polytopic meshes with applications to discontinuous Galerkin finite element methods. *J. Sci. Comput.*, 77:1339–1370, 2018.

[21] P. F. Antonietti, P. Houston, G. Pennesi, and E. Süli. An agglomeration-based massively parallel non-overlapping additive schwarz preconditioner for high-order discontinuous galerkin methods on polytopic grids. *arXiv preprint arXiv:1903.11357*, 2019.

[22] P. F. Antonietti, G. Manzini, and M. Verani. The fully nonconforming Virtual Element Method for biharmonic problems. *Math. Mod. Meth. Appl. Sci.*, 28(02):387–407, 2018.

[23] P. F. Antonietti and I. Mazzieri. High-order Discontinuous Galerkin methods for the elastodynamics equation on polygonal and polyhedral meshes. *Comput. Methods Appl. Mech. Engrg.*, 342:414–437, 2018.

[24] P. F. Antonietti and G. Pennesi. V-cycle multigrid algorithms for discontinuous Galerkin methods on non-nested polytopic meshes. *J. Sci. Comput.*, 78(1):625–652, 2019.

[25] P. F. Antonietti, M. Sarti, and M. Verani. Multigrid algorithms for *hp*-discontinuous Galerkin discretizations of elliptic problems. *SIAM J. Numer. Anal.*, 53(1):598–618, 2015.

[26] D. N. Arnold. An interior penalty finite element method with discontinuous elements. *SIAM J. Numer. Anal.*, 19(4):742–760, 1982.

[27] D. N. Arnold, F. Brezzi, B. Cockburn, and L. D. Marini. Unified analysis of discontinuous Galerkin methods for elliptic problems. *SIAM J. Numer. Anal.*, 39(5):1749–1779, 2001/02.

[28] B. Ayuso de Dios, K. Lipnikov, and G. Manzini. The nonconforming Virtual Element Method. *ESAIM Math. Model. Numer. Anal.*, 50(3):879 – 904, 2016.

[29] I. Babuška, F. Nobile, and R. Tempone. A stochastic collocation method for elliptic partial differential equations with random input data. *SIAM J. Numer. Anal.*, 45(3):1005–1034, 2007.

[30] I. Babuška and M. Suri. The *hp* version of the finite element method with quasi-uniform meshes. *RAIRO-Modélisation mathématique et analyse numérique*, 21(2):199–238, 1987.

[31] J. Back, F. Nobile, L. Tamellini, and R. Tempone. Stochastic spectral Galerkin and collocation methods for PDEs with random coefficients: a numerical comparison. In J. Hesthaven and E. Ronquist, editors, *Spectral and High Order Methods for Partial Differential Equations*, volume 76 of *Lecture Notes in Computational Science and Engineering*, page 43–62. Springer, 2011. Selected papers from the ICOSAHOM '09 conference, June 22-26, Trondheim, Norway.

[32] G. A. Baker. Finite element methods for elliptic equations using nonconforming elements. *Math. Comp.*, 31(137):45–59, 1977.

[33] F. Bassi, L. Botti, and A. Colombo. Agglomeration-based physical frame dG discretizations: an attempt to be mesh free. *Math. Mod. Meth. Appl. Sci.*, 24(8):1495–1539, 2014.

[34] F. Bassi, L. Botti, A. Colombo, D. A. Di Pietro, and P. Tesini. On the flexibility of agglomeration based physical space discontinuous Galerkin discretizations. *J. Comput. Phys.*, 231(1):45–65, 2012.

[35] F. Bassi, L. Botti, A. Colombo, and S. Rebay. Agglomeration based discontinuous Galerkin discretization of the Euler and Navier-Stokes equations. *Comput. & Fluids*, 61:77–85, 2012.

[36] F. Bassi and S. Rebay. A high-order accurate discontinuous finite element method for the numerical solution of the compressible Navier-Stokes equations. *J. Comput. Phys.*, 131(2):267–279, 1997.

[37] J. Bear, C. F. Tsang, and G. d. Marsily. Flow and contaminant transport in fractured rocks. *Academic Press, San Diego*, 1993.

[38] L. Beirão da Veiga, F. Brezzi, A. Cangiani, G. Manzini, L. D. Marini, and A. Russo. Basic principles of Virtual Element Methods. *Math. Models Methods Appl. Sci.*, 23(1):199 – 214, 2013.

[39] L. Beirão da Veiga, K. Lipnikov, and G. Manzini. *The Mimetic Finite Difference method for elliptic problems*, volume 11. Springer, Cham, 2014.

[40] L. Beirão da Veiga, F. Brezzi, L. Marini, and A. Russo. Virtual Element Method for general second-order elliptic problems on polygonal meshes. *Math. Models Methods Appl. Sci.*, 26(04):729–750, 2016.

[41] L. Beirão da Veiga, A. Chernov, L. Mascotto, and A. Russo. Basic principles of *hp* virtual elements on quasiuniform meshes. *Math. Models Methods Appl. Sci.*, 26(8):1567–1598, 2016.

[42] L. Beirão da Veiga, A. Chernov, L. Mascotto, and A. Russo. Exponential convergence of the *hp* virtual element method with corner singularity. *Numer. Math.*, 138(3):581–613, 2018.

[43] M. F. Benedetto, S. Berrone, A. Borio, S. Pieraccini, and S. Scialò. A hybrid mortar virtual element method for discrete fracture network simulations. *J. Comput. Phys.*, 306:148–166, 2016.

[44] M. F. Benedetto, S. Berrone, S. Pieraccini, and S. Scialò. The Virtual Element Method for discrete fracture network simulations. *Comput. Methods Appl. Mech. Engrg.*, 280:135–156, 2014.

[45] M. F. Benedetto, S. Berrone, and S. Scialò. A globally conforming method for solving flow in discrete fracture networks using the Virtual Element Method. *Finite Elements in Analysis and Design*, 109:23–36, 2016.

[46] S. Berrone, S. Pieraccini, and S. Scialò. On simulations of discrete fracture network flows with an optimization-based extended finite element method. *SIAM J. Sci. Comput.*, 35(2):A908–A935, 2013.

[47] S. Berrone, S. Pieraccini, and S. Scialò. A PDE-constrained optimization formulation for discrete fracture network flows. *SIAM J. Sci. Comput.*, 35(2):B487–B510, 2013.

[48] S. Berrone, S. Pieraccini, and S. Scialò. An optimization approach for large scale simulations of discrete fracture network flows. *J. Comput. Phys.*, 256:838–853, 2014.

[49] S. Berrone, S. Pieraccini, S. Scialò, and F. Vicini. A parallel solver for large scale DFN flow simulations. *SIAM J. Sci. Comput.*, 37(3):C285–C306, 2015.

[50] W. M. Boon, J. M. Nordbotten, and I. Yotov. Robust discretization of flow in fractured porous media. *SIAM J. Numer. Anal.*, 56(4):2203–2233, 2018.

[51] K. Brenner, J. Hennicker, R. Masson, and P. Samier. Gradient discretization of hybrid-dimensional Darcy flow in fractured porous media with discontinuous pressures at matrix–fracture interfaces. *IMA J. Numer. Anal.*, 37(3):1551–1585, 2016.

[52] F. Brezzi, B. Cockburn, L. D. Marini, and E. Süli. Stabilization mechanisms in discontinuous Galerkin finite element methods. *Comput. Methods Appl. Mech. Engrg.*, 195(25-28):3293–3310, 2006.

[53] F. Brezzi, T. J. Hughes, L. D. Marini, and A. Masud. Mixed discontinuous galerkin methods for darcy flow. *J. Sci. Comput.*, 22(1-3):119–145, 2005.

[54] F. Brezzi, K. Lipnikov, and M. Shashkov. Convergence of the Mimetic Finite Difference method for diffusion problems on polyhedral meshes. *SIAM J. Numer. Anal.*, 43(5):1872–1896 (electronic), 2005.

[55] F. Brezzi, K. Lipnikov, and M. Shashkov. Convergence of Mimetic Finite Difference method for diffusion problems on polyhedral meshes with curved faces. *Math. Mod. Meth. Appl. Sci.*, 16(2):275–297, 2006.

[56] F. Brezzi, K. Lipnikov, and V. Simoncini. A family of Mimetic Finite Difference methods on polygonal and polyhedral meshes. *Math. Mod. Meth. Appl. S.*, 15(10):1533–1551, 2005.

[57] E. Burman, P. Hansbo, M. G. Larson, and K. Larsson. Cut finite elements for convection in fractured domains. *Comput. & Fluids*, 179:726–734, 2019.

[58] A. Cangiani, Z. Dong, and E. H. Georgoulis. *hp*-version space-time discontinuous Galerkin methods for parabolic problems on prismatic meshes. *SIAM J. Sci. Comput.*, 39(4):A1251–A1279, 2017.

[59] A. Cangiani, Z. Dong, E. H. Georgoulis, and P. Houston. *hp*-version discontinuous Galerkin methods for advection-diffusion-reaction problems on polytopic meshes. *ESAIM Math. Model. Numer. Anal.*, 50(3):699–725, 2016.

[60] A. Cangiani, Z. Dong, E. H. Georgoulis, and P. Houston. *hp-version discontinuous Galerkin methods on polytopic meshes*. SpringerBriefs in Mathematics. Springer International Publishing, 2017.

[61] A. Cangiani, E. H. Georgoulis, and P. Houston. *hp*-version discontinuous Galerkin methods on polygonal and polyhedral meshes. *Math. Models Methods Appl. Sci.*, 24(10):2009–2041, 2014.

[62] A. Cangiani, G. Manzini, and O. J. Sutton. Conforming and nonconforming Virtual Element Methods for elliptic problems. *IMA J. Numer. Anal.*, 37(3):1317–1354, 2017.

[63] C. Canuto, S. Pieraccini, and D. Xiu. Uncertainty quantification of discontinuous outputs via a non-intrusive bifidelity strategy. *J. Comput. Phys.*, 398:108885, 2019.

[64] P. Castillo, B. Cockburn, I. Perugia, and D. Schötzau. An a priori error analysis of the local discontinuous Galerkin method for elliptic problems. *SIAM J. Numer. Anal.*, 38(5):1676–1706, 2000.

[65] F. A. Chave, D. Di Pietro, and L. Formaggia. A Hybrid High-Order method for Darcy flows in fractured porous media. *SIAM J. Sci. Comput.*, 40(2):A1063–A1094, 2018.

[66] A. Y. Chernyshenko and M. A. Olshanskii. An unfitted finite element method for the darcy problem in a fracture network. *arXiv preprint arXiv:1903.06351*, 2019.

[67] B. Cockburn and C. Dawson. Some extensions of the local discontinuous Galerkin method for convection-diffusion equations in multidimensions. In *The mathematics*

of finite elements and applications, X, MAFELAP 1999 (Uxbridge), pages 225–238. Elsevier, Oxford, 2000.

[68] B. Cockburn, B. Dond, and J. Guzmán. A superconvergent LDG-hybridizable Galerkin method for second-order elliptic problems. *Math. Comp.*, 77(264):1887–1916, 2008.

[69] B. Cockburn, J. Gopalakrishnan, and R. Lazarov. Unified hybridization of discontinuous Galerkin, mixed, and continuous Galerkin methods for second order elliptic problems. *SIAM J. Numer. Anal.*, 47(2):1319–1365, 2009.

[70] B. Cockburn, J. Gopalakrishnan, and F.-J. Sayas. A projection-based error analysis of HDG methods. *Math. Comp.*, 79(271):1351–1367, 2010.

[71] B. Cockburn, J. Guzmán, and H. Wang. Superconvergent discontinuous Galerkin methods for second-order elliptic problems. *Math. Comp.*, 78(265):1–24, 2009.

[72] B. Cockburn and C.-W. Shu. The local discontinuous Galerkin method for time-dependent convection-diffusion systems. *SIAM J. Numer. Anal.*, 35(6):2440–2463, 1998.

[73] I. Colombo, F. Nobile, G. Porta, A. Scotti, and L. Tamellini. Uncertainty quantification of geochemical and mechanical compaction in layered sedimentary basins. *Comput. Methods Appl. Mech. Engrg.*, 328:122–146, 2018.

[74] C. D'Angelo and A. Scotti. A mixed finite element method for darcy flow in fractured porous media with non-matching grids. *ESAIM: Mathematical Modelling and Numerical Analysis*, 46(02):465–489, 2012.

[75] A. Dedner, P. Madhavan, and B. Stinner. Analysis of the discontinuous galerkin method for elliptic problems on surfaces. *IMA J. Numer. Anal.*, 33(3):952–973, 2013.

[76] D. A. Di Pietro and A. Ern. *Mathematical aspects of discontinuous Galerkin methods*, volume 69. Springer Science & Business Media, 2011.

[77] D. A. Di Pietro and A. Ern. A Hybrid High-Order locking-free method for linear elasticity on general meshes. *Comput. Methods Appl. Mech. Engrg.*, 283:1–21, 2015.

[78] D. A. Di Pietro and A. Ern. Hybrid High-Order methods for variable-diffusion problems on general meshes. *C. R. Math. Acad. Sci. Soc. R. Can.*, 353(1):31–34, 2015.

[79] D. A. Di Pietro, A. Ern, and S. Lemaire. An arbitrary-order and compact-stencil discretization of diffusion on general meshes based on local reconstruction operators. *Comput. Meth. in Appl. Math.*, 14(4):461–472, 2014.

[80] D. A. Di Pietro, A. Ern, and S. Lemaire. A review of hybrid high-order methods: formulations, computational aspects, comparison with other methods. In G. R. Barrenechea, F. Brezzi, A. Cangiani, and E. H. Georgoulis, editors, *Building bridges: connections and challenges in modern approaches to numerical partial differential equations*, volume 114 of *Lecture Notes in Computational Science and Engineering*. Springer, Cham, 2016.

[81] J. Dolbow, N. Moës, and T. Belytschko. An extended finite element method for modeling crack growth with frictional contact. *Comput. Methods Appl. Mech. Engrg.*, 190(51):6825–6846, 2001.

[82] J. Douglas, Jr. and T. Dupont. Interior penalty procedures for elliptic and parabolic Galerkin methods. In *Computing methods in applied sciences (Second Internat. Sympos., Versailles, 1975)*, pages 207–216. Lecture Notes in Phys., Vol. 58. Springer, Berlin, 1976.

[83] J. Droniou, R. Eymard, and R. Herbin. Gradient schemes: generic tools for the numerical analysis of diffusion equations. *ESAIM Math. Model. Numer. Anal.*, 50(3):749–781, 2016.

[84] M. Dryja and P. Krzyżanowski. A massively parallel nonoverlapping additive Schwarz method for discontinuous Galerkin discretization of elliptic problems. *Numer. Math.*, 132(2):347–367, 2016.

[85] B. Flemisch, A. Fumagalli, and A. Scotti. A review of the XFEM-based approximation of flow in fractured porous media. In *Advances in Discretization Methods*, pages 47–76. Springer, 2016.

[86] L. Formaggia, A. Fumagalli, A. Scotti, and P. Ruffo. A reduced model for darcy's problem in networks of fractures. *ESAIM Math. Model. Numer. Anal.*, 48(4):1089–1116, 2014.

[87] L. Formaggia, A. Scotti, and F. Sottocasa. Analysis of a mimetic finite difference approximation of flows in fractured porous media. *ESAIM Math. Model. Numer. Anal.*, 52(2):595–630, 2018.

[88] T.-P. Fries and T. Belytschko. The extended/generalized finite element method: an overview of the method and its applications. *Internat. J. Numer. Methods Engrg.*, 84(3):253–304, 2010.

[89] N. Frih, J. E. Roberts, and A. Saada. Modeling fractures as interfaces: a model for Forchheimer fractures. *Comput. Geosci.*, 12(1):91–104, 2008.

[90] A. Fumagalli, E. Keilegavlen, and S. Scialò. Conforming, non-conforming and non-matching discretization couplings in discrete fracture network simulations. *J. Comput. Phys.*, 376:694–712, 2019.

[91] A. Fumagalli and A. Scotti. A numerical method for two-phase flow in fractured porous media with non-matching grids. *Advances in Water Resources*, 62, Part C:454–464, 2013.

[92] A. Fumagalli and A. Scotti. An efficient xfem approximation of darcy flows in arbitrarily fractured porous media. *Oil Gas Sci. Technol. Rev. IFP Energies nouvelles*, 69(4):555–564, 2014.

[93] W. Hackbusch and S. A. Sauter. Composite Finite Elements for problems containing small geometric details. Part II: Implementation and numerical results. *Comput. Visual Sci.*, 1(4):15–25, 1997.

[94] W. Hackbusch and S. A. Sauter. Composite Finite Elements for the approximation of PDEs on domains with complicated micro-structures. *Numer. Math.*, 75(4):447–472, 1997.

[95] J. S. Hesthaven and T. Warburton. *Nodal discontinuous Galerkin methods: algorithms, analysis, and applications*. Springer Science & Business Media, 2007.

[96] J. Hyman, M. Shashkov, and S. Steinberg. The numerical solution of diffusion problems in strongly heterogeneous non-isotropic materials. *J. Comput. Phys.*, 132(1):130–148, 1997.

[97] J. Jaffré, M. Mnejja, and J. Roberts. A discrete fracture model for two-phase flow with matrix-fracture interaction. *Procedia Computer Science*, 4:967 –973, 2011.

[98] O. A. Karakashian and C. Collins. Two-level additive Schwarz methods for discontinuous Galerkin approximations of second-order elliptic problems. *IMA J. Numer. Anal.*, 37(4):1800 – 1830, 2017.

[99] O. A. Karakashian and F. Pascal. A posteriori error estimates for a discontinuous galerkin approximation of second-order elliptic problems. *SIAM J. Numer. Anal.*, 41(6):2374–2399, 2003.

[100] P. Krzyżanowski. On a nonoverlapping additive Schwarz method for *hp*-discontinuous Galerkin discretization of elliptic problems. *Numerical Methods for Partial Differential Equations*, 32(6):1572–1590, 2016.

[101] V. Martin, J. Jaffré, and J. E. Roberts. Modeling fractures and barriers as interfaces for flow in porous media. *SIAM J. Sci. Comput.*, 26(5):1667–1691, 2005.

[102] L. Mascotto, I. Perugia, and A. Pichler. Non-conforming harmonic virtual element method: *h*- and *p*-versions. *J. Sci. Comput.*, 77(3):1874–1908, 2018.

[103] L. Mascotto, I. Perugia, and A. Pichler. A nonconforming Trefftz virtual element method for the Helmholtz problem. *Math. Models Methods Appl. Sci.*, 29:1619–1656, 2019.

[104] L. Mascotto, I. Perugia, and A. Pichler. A nonconforming Trefftz virtual element method for the Helmholtz problem: numerical aspects. *Comput. Methods Appl. Mech. Engrg.*, 347:445–476, 2019.

[105] A. Masud and T. J. Hughes. A stabilized mixed finite element method for darcy flow. *Comput. Methods Appl. Mech. Engrg.*, 191(39-40):4341–4370, 2002.

[106] F. Nobile, R. Tempone, and C. G. Webster. An anisotropic sparse grid stochastic collocation method for partial differential equations with random input data. *SIAM J. Numer. Anal.*, 46(5):2411–2442, 2008.

[107] I. Perugia, P. Pietra, and A. Russo. A plane wave virtual element method for the helmholtz problem. *ESAIM Math. Model. Numer. Anal.*, 50(3):783–808, 2016.

[108] I. Perugia and D. Schötzau. An *hp*-analysis of the local discontinuous galerkin method for diffusion problems. *J. Sci. Comput.*, 17(1):561–571, 2002.

[109] I. Perugia and D. Schötzau. The *hp*-local discontinuous galerkin method for low-frequency time-harmonic maxwell equations. *Mathematics of Computation*, 72(243):1179–1214, 2003.

[110] W. Reed and T. Hill. Triangular mesh methods for the neutron transport equation. *Los Alamos Report LA-UR-73-479*, 1973.

[111] B. Rivière. *Discontinuous Galerkin methods for solving elliptic and parabolic equations*, volume 35 of *Frontiers in Applied Mathematics*. Society for Industrial and Applied Mathematics (SIAM), Philadelphia, PA, 2008. Theory and implementation.

[112] N. Schwenck, B. Flemisch, R. Helmig, and B. I. Wohlmuth. Dimensionally reduced flow models in fractured porous media: crossings and boundaries. *Computational Geosciences*, 19(6):1219–1230, 2015.

[113] E. M. Stein. *Singular integrals and differentiability properties of functions*, volume 2. Princeton university press, 1970.

[114] G. Strang and G. J. Fix. *An analysis of the finite element method*, volume 212. Prentice-Hall Englewood Cliffs, NJ, 1973.

[115] N. Sukumar and A. Tabarraei. Conforming Polygonal Finite Elements. *Internat. J. Numer. Methods Engrg.*, 61(12):2045–2066, 2004.

[116] A. Tabarraei and N. Sukumar. Extended Finite Element Method on polygonal and quadtree meshes. *Comput. Methods Appl. Mech. Eng.*, 197(5):425–438, 2008.

[117] C. Talischi, G. H. Paulino, A. Pereira, and I. F. Menezes. Polymesher: a general-purpose mesh generator for polygonal elements written in matlab. *Structural and Multidisciplinary Optimization*, 45(3):309–328, 2012.

[118] T. Warburton and J. S. Hesthaven. On the constants in *hp*-finite element trace inverse inequalities. *Comput. Methods Appl. Mech. Engrg.*, 192(25):2765–2773, 2003.

[119] M. F. Wheeler. An elliptic collocation-finite element method with interior penalties. *SIAM J. Numer. Anal.*, 15(1):152–161, 1978.

[120] D. Xiu and J. S. Hesthaven. High-order collocation methods for differential equations with random inputs. *SIAM J. Sci. Comput.*, 27(3):1118–1139, 2005.